Group for High Resolution Sea Surface Temperature (GHRSST)

2009 International Users Symposium

Thursday 28th May – Friday 29th May 2009
Santa Rosa, CA USA

Conference Proceedings

Released 05 2009 (C. Gentemann/J.Vazquez/C. Donlon)

Meeting sponsored by:

Proceedings from the Group for High Resolution Sea Surface Temperature (GHRSST) 2009 International Users Symposium

Thursday 28th May – Friday 29th May 2009
Santa Rosa, CA USA

Compiled by C. L. Gentemann, J.Vazquez, and C. Donlon

Electronic copies available online at www.ghrsst-pp.org

Table of Contents

Group for High Resolution Sea Surface Temperature (GHRSST)

2009 International Users Symposium

Thursday 28th May – Friday 29th May 2009

Agenda
Version: 04

Released 05 2009 (C. Gentemann/J.Vazquez/C. Donlon)

Meeting sponsored by:

Welcome note

Hello:

...and welcome to Santa Rosa, California, USA and the International Group for High Resolution Sea Surface Temperature (GHRSST) User Symposium. On behalf of the GHRSST Science Team we would like to take this opportunity to thank Craig Donlon and the Remote Sensing Systems team for all of their help and support in preparing the workshop. We would like to specifically thank EUMETSAT's OSI-SAF for partial-sponsorship of the symposium. Thanks also to all the other sponsors and you, the participants, who make these important events possible.

The Global Ocean Data Assimilation Experiment (GODAE) High Resolution Sea Surface Temperature (SST) Pilot Project (GHRSST-PP) was initiated in 2001 at the European Commission's Joint Research Council near Lake Maggiore, Italy, by a small group of scientists who met to discuss how to take advantage of all the different satellite SSTs available to provide a higher spatial and temporal resolution SST using satellite and in situ data. At the meeting, it was decided to start an international pilot project to promote research required to better produce and use SST information, including how to test and provide observations, how to integrate and assimilate these data at operational agencies, and how to use the data in downstream applications. Now, only 8 years later, the GHRSST-PP has successfully coordinated the production of most satellite sea surface temperature datasets in a common format which are being used in a new generation of multi-sensor global interpolated SST analyses.

Although GODAE has now ended, GHRSST-PP has continued as the ***Group for High Resolution SST (GHRSST),*** dedicated to maintaining scientific and technical coordination between the international SST communities. To this end, we decided at the last science team meeting to hold a user symposium. This symposium aims to bring together the GHRSST data providers with current and future users of satellite derived SST products. Users include, but are not limited to, researchers, climate and coastal applications, and decision makers with a focus on near real time, operational applications. Bringing together the data expertise and the users provides a unique opportunity for setting the future direction of GHRSST.

The future of GHRSST is now focused on allowing for greater and more flexible access to all data products, along with reanalysis efforts that will provide the highest quality climate data records (CDRs) for use in climate models and prediction. Improved merged SSTs products from multiple sensors will maximize the temporal and spatial resolutions, while providing increased accuracy. The symposium is intended as an important step in moving GHRSST forward to meet the needs of the climate, weather forecasting, research and applications communities for the highest quality and resolution SST products.

It is with a warm heart that we thank each of you for your contributions, support and we look forward to meeting you all for a productive and stimulating workshop.

Chelle L. Gentemann & Jorge Vazquez

1 Poster Presentations

There is space for posters in the Vineyard Creek Hyatt and all participants are encouraged to bring poster presentations along to the meeting.

2 Presentations

Please allow 3-minutes time for questions and speaker-change-over. Therefore, if you have a 15-minute presentation, please plan on speaking for only 12-minutes, similarly, if you have a 20-minute presentation, plan on speaking for only 17 minutes. If early presentations run over, the chair of each session may choose to shorten later presentations at their discretion. Speakers will please follow directions of session chair.

All presentations will be given from session chair's laptop. **Please submit presentations by May 25, 2009 at 5 PM. Presentations should be named "SessionX_LastName.ppt".** To submit your presentation please go to http://www.misst.org/meetings/conference_file_upload.html and login (username=GHRSST_meet, password=sst4all).

Presenters may pre-view their talks from 8:00 AM – 8:30 AM each morning as time allows. If you are unable to provide your presentation by May 25th, please see the session chair from 8:00 AM – 8:30 AM to upload your presentation.

Each presenter should provide a **2 page summary or extended abstract** of their presentation **by May 1, 2009** for inclusion in the Symposium Proceedings. Copies of the 2-pagers will be distributed at the meeting. This will help get the proceedings published efficiently and quickly. A template for your report is provided as Document 22 https://www.ghrsst-pp.org/modules/documents/documents/Document-22-Example-paper-for%20-proceedings.doc. To submit your extended abstract please go to http://www.misst.org/meetings/conference_file_upload.html and login (username=GHRSST_meet, password=sst4all).

2.1 Session Chairs

The main tasks of a session chair are to briefly introduce each speaker, keep the presentations to the time allowed, and to **lead/moderate the discussion after each presentation**. The plenary sessions are your domain and please try to use the General discussion questions above as a guide. Finally, **the chair should work closely with the rapporteur to prepare a short summary of the session**. The report should be of a standard suitable for publication in the Workshop proceedings including appropriate figures and text concluding with the breakout session recommendations.

2.2 Rapporteurs

The purpose of the rapporteurs is **to capture important information during the session for the follow-up of the workshop by the GHRSST-PO and Science Team**. The rapporteur will be expected to present their reports to the plenary session during the science team meeting, as a basis for the general discussion and review of the symposium, and for the preparation of conclusions and recommendations for future actions of GHRSST.

In preparing your rapporteur reports, you should **avoid making lengthy summaries of the presentations and discussions**. Please try to concentrate on issues which relate directly to the objectives of the symposium, the mandate of GHRSST and the future development of GHRSST operational ocean products and services. Your presentation should be short and provide a general overview of the main session outcomes/conclusions rather than a regurgitation of each presentation made. In order to generate a representative report of the meeting, **please can you provide J.Vazquez with a soft copy of your report by the end of the meeting – what you provide will constitute the final proceedings for these sessions so please, capture as much information as you can. Your inputs will be used as the basis for the conclusions of the symposium proceedings.**

2.3 WiFi Access

WiFi access at the Hyatt Vineyard Creek has been arranged for the duration of the meeting. An access code will be available at the meeting registration table.

2.4 Poster Presentations

Rachel Weihs: Resolving the diurnal cycle in satellite derived sea surface temperatures and its significance on latent heat fluxes
Helen Beggs et al.: Enhancing ship of opportunity sea surface temperature observations in the Australian region.
Chelle L. Gentemann et al.: A new model for diurnal warming: Profiles of Ocean Heating (POSH)

Thursday, 28th May 2009

Time	Agenda item	Session leaders
08:00	Registration & Coffee: Alexander I Room	
Session 1. Invited Presentations		
08:20	Welcome and logistics: C.Gentemann and J. Vazquez	Chair: C.Gentemann Rapporteur: Ken Casey
08:30	Craig Donlon: The GHRSST Project	
08:45	Eric Lindstrom: NASA GHRSST Science	
09:00	Zdenka Willis: IOOS use of GHRSST	
09:15	Wolfgang Lengert: European SST Satellite data exploitation structure and organization	
09:30	Hans Bonekamp: EUMETSAT	
09:45	Margarita Gregg: Long Term Stewardship of GHRSST and related data at the National Oceanographic Data Center	
10:00	Olivier Arino: ESA Climate Change Initiative	
10:15	Coffee	
Session 2. GHRSST Data Products: L2P, L3P, and L4P		
10:30	Peter Minnett: GHRSST MODIS L2P	Chair: J. Vazquez Rapporteur: E. Armstrong
10:40	Helen Beggs: New Australian High Resolution Satellite SST Products from the Integrated Marine Observing System	
10:50	Emmanuelle Autret: Odyssea SST data	
11:00	Jean Tournadre: Analysis of 2 years of Ultra-high-resolution satellite SST fields	
11:10	Bruce McKenzie: GHRSST L2P and L4 data at the Naval Oceanographic Office	
11:22	Pierre Le Borgne: L2P and L3 SST data produced by EUETSAT/OSI-SAF and EC/MyOcean	
11:34	Chelle Gentemann: MW SST L2P data and blended 9km global MW+IR SSTs	
11:46	Eileen Maturi: NOAA GHRSST data: GOES L2P and blended GOES/POES L4P	
12:00	Lunch	
Session 2A. Non-GHRSST Data Products		
13:00	Akira Shibata: JAXA SST algorithm for AMSR-E	Chair: J. Vazquez Rapporteur: E. Armstrong
13:15	Yi Chao: A blended global 1-km sea surface temperature data set for research and applications	
13:30	Gary Jedlovec: An enhanced MODIS/AMSR-E composite SST product	
13:45	Bruce Brasnett: Recent changes to the CMC global real-time SST analysis	
Session 3. GHRSST Data Systems		
14:00	J Vazquez: Overview of data access GDAC and LTSRF	Chair: C.Gentemann Rapporteur: G. Wick
14:15	Martin Rutherford: GHRSST data meets ESRI ArcGIS Desktop and OGC Web Map Services	
14:30	Dave Poulter: New GHRSST HR-DDS user features	
14:45	Tess Bandon: Working with the GHRSST Data Format: Experiences of the GCOS SST Intercomparison Working Group	
15:00	Tea	
Session 3a. GHRSST data validation		
15:15	Richard Reynolds: Intercomparisons among Global Daily SST Analyses	Chair: J.Vazquez Rapporteur: G. Wick
15:30	Alexey Kaplan: Gridded SST Data Sets: How to choose a "right" one?	
15:45	Ed Armstrong: GHRSST Level 4 product comparisons in coastal regions	
16:00	Jorge Vazquez: A comparison of 1km ultra high resolution composite SST maps	
16:15	Nick Rayner: How does the (A)ATSR Reanalysis for Climate SST compare to the in situ SST record?	
16:30	Karen Veal: A Comparison of AATSR and AMSR-E Sea Surface Temperature Data	
16:45	Alec Bogdanoff: Calculation of Sea Surface Temperature using a Forward Radiative Transfer Model Approach	
17:00	NOPP Excellence in Partnering Award (Lindstrom)	
17:30	Close	
17:30	Icebreaker in the Knights Valley Garden, offered by Remote Sensing Systems. Appetizers and wine.	

Friday, 29th May 2009

Time	Agenda item	Session leaders
Session 4. GHRSST Applications		
08:00	Coffee: : Alexander I Room	
08:30	Hans Hersbach: The usage of sea-surface temperature and sea ice products at ECMWF	Chair:J.Vazquez Rapporteur: C. Merchant
08:45	Jacob Hoeyer: The Use of GHRSST data at DMI for high latitude level 4 analysis	
09:00	Peter Cornillon: Validating Ocean Circulation Models with Satellite-Derived SST Frontal Distributions	
09:15	Alexander Ignatov: The near real-time web-based SST Quality Monitor (SQUAM)	
09:30	Arthur Mariano: Motion-compensated spatio-temporal interpolation of SST fields	
09:45	Coffee	
10:00	**Invited**: David Foley: Applications of GHRSST data sets towards the stewardship of living marine resources: putting SST back in the saddle	Chair: J.Vazquez Rapporteur: C. Merchant
10:15	Dudley Chelton: The Importance of SST in Weather Forecast Models, and Coupled Ocean-Atmosphere Models	
10:30	Mark Bourassa: Impacts of High Resolution SST Fields on Objective Analyses of Wind Fields, and Practical Constraints Related to Sampling	
10:45	Suzanne Dickinson: Use of New SST Products in the CLIvar MOde water Experiment (CLIMODE)	
11:00	Françoise Orain: Impact of using Merged regional operational L3P in the operational MF Aladin model to forecast Mediterranean convective events	
11:15	Joseph Sienkiewicz: Application of GHRSST L4P analyses product at the NOAA Ocean Prediction Center	
11:30	Gang Liu: NOAA Coral Reef Watch's Current Application of Satellite Sea Surface Temperature Data in Operational Near Real-Time Global Monitoring and Experimental Outlook of Coral Health and Potential Application of GHRSST	
11:45	Lewis Gramer and Jim Hendee: Integration of SST and other Data for Ecological Forecasting on Coral Reefs	
12:00	Lunch	
13:00	Matt Martin: Use of SST and sea-ice data in operational analysis and assimilation systems at the UK Met Office	
13:15	Dimitris Menemenlis: Towards the utilization of GHRSST data for improving estimates of the global ocean circulation	
Session 5. GHRSST Science		
13:30	Ajoy Kumar: Application of satellited derived SSTs along the Delmarva region	Chair: C.Gentemann Rapporteur: C. Donlon
13:45	Chris Halle: Investigating the Coastal Ocean using HF Radar and Remotely Senses Sea Surface Temperature	
14:00	Dale Kiefer: Satellite Monitoring of Links between ENSO and Tropical Tuna	
14:15	Steinar Eastwood: SST warm spots in the Arctic Ocean	
14:30	Sara Purca: Seasonal to decadal variability of the SST front off the Peruvian coast: connection with the intraseasonal equatorial Kelvin wave activity	
14:45	Changming Dong: Mesoscale and Submesoscale Eddy Detection Using GHRSST Data	
15:00	Tea	
15:15	Peter Cornillon: An Atlas of SST Fronts in the North and South Atlantic	Chair: C.Gentemann Rapporteur: C. Donlon
15:30	Subrahmanya Bulusu: Detection of Rossby Waves in SST and salinity	
15:45	Holger Brix: GHRSST and ECCO2: SST Variability and Mixed Layer Heat	
16:00	Christopher Jeffery: Using GHRSST L4 products to calculate bulk estimates of air-sea heat fluxes	
16:15	Chris Merchant: Diurnal warming analysis for GHRSST products	
16:30	Chelle Gentemann: Multi-satellite measurements of large diurnal warming	
16:45	Closing summary: C.Gentemann & J. Vazquez	
17:00	Dinner in Santa Rosa, meet in lobby at 18:00	

2.4 Hotel Map and Conference Rooms

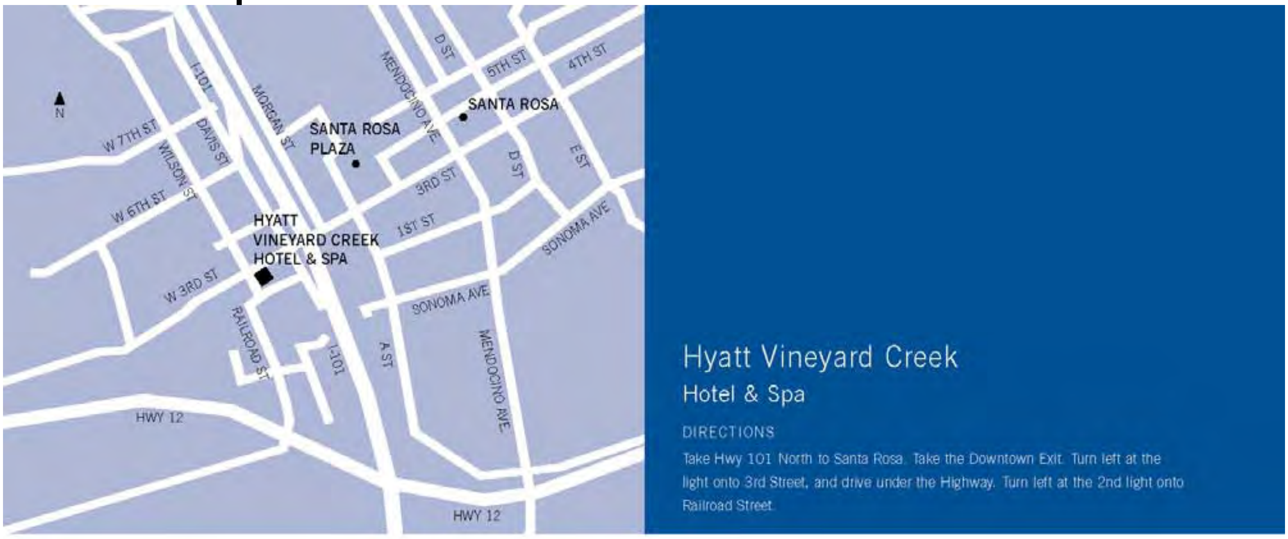

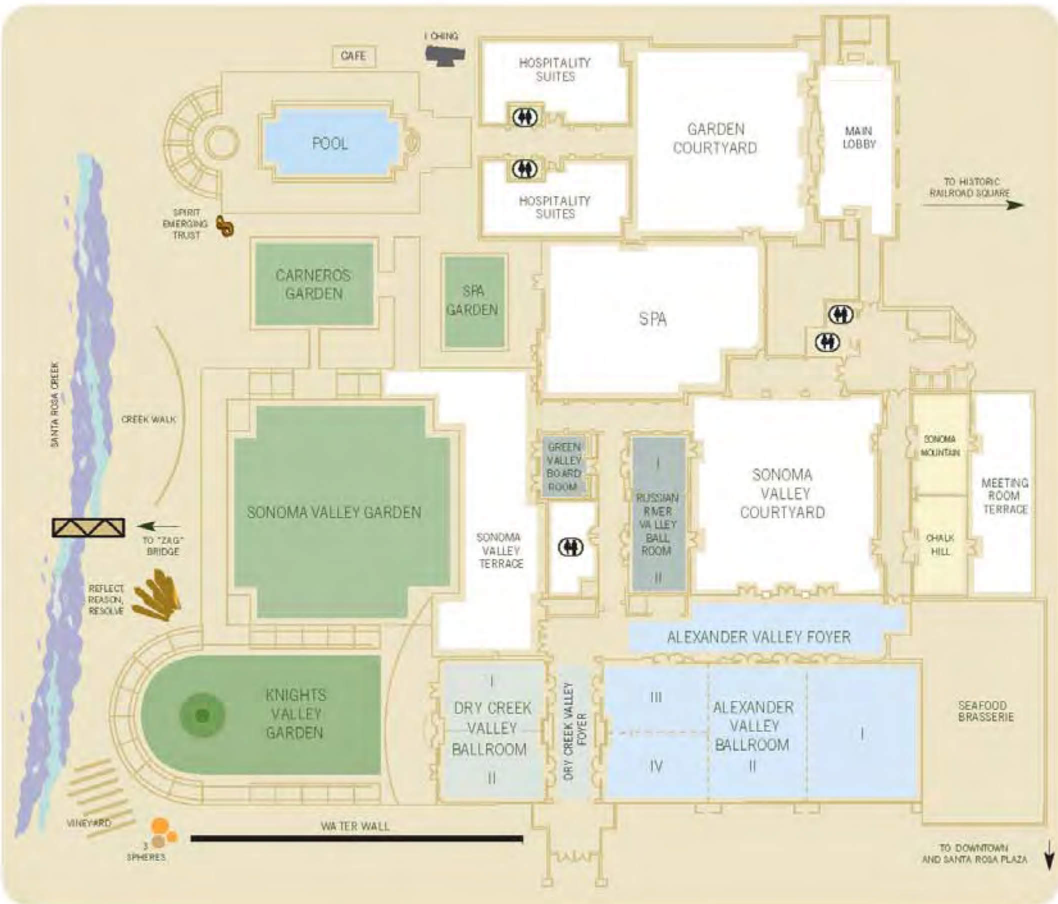

Appendix-I Provisional attendance list

(Please pass corrections to the GHRSST-PO for update)

Arino, Olivier
ESA/ESRIN
Via Galleleo Gallili
Frascati
Italy
Fax: +39 06 94180552/80942
E-mail: olivier.arino@esa.int

Armstrong, Edward
Jet Propulsion Laboratory/California Institute of Technology PO.DAAC
300/320 4800 Oak Grove Dr.
Pasadena, California
United States
Phone: +1 818 393-6710
Fax: +1 818 393 6720
E-mail: Edward.armstrong@jpl.nasa.gov

Autret, Emmanuelle
IFREMER
Technopôle Brest Iroise
29280 Plouzané
France
Phone: +33 (0)2 98 22 45 32
E-mail: Emmanuelle.autret@ifremer.fr

Beggs, Helen
Ocean Prediction Group,
Centre for Australian Weather and Climate Research,
Bureau of Meteorology
PO Box 1289,
Melbourne, Vic 3001
Australia
Tel: +61 (0)3 9669 4394
Fax: +61 (0)3 9669 4660
E-mail: h.beggs@bom.gov.au

Bingham, Andrew
Jet Propulsion Laboratory PO.DAAC
4800 Oak Grove Dr.
Pasadena, California
Mobile: 818-687-0626
E-mail: andrew.bingham@jpl.nasa.gov

Bogdanoff, Alec
Florida State University
Phone: 954-609-3854
E-mail: abogdanoff@fsu.edu

Bonekamp, Hans
EUMETSAT
Phone: +49 6151 807 7357
Fax: 496151807838
E-mail: hans.bonekamp@eumetsat.int

Bourassa, Mark
Florida State University / COAPS
Phone: (850) 644-4841
Fax: 850-644-4841
E-mail: bourassa@coaps.fsu.edu

Brandon, Tess
NOAA National Oceanographic Data Center
Phone: +1 301 713 3272 x181
Fax: +1 301 713 3302
E-mail: tess.brandon@noaa.gov

Brasnett, Bruce
Canadian Meteorological Centre
E-mail: Bruce.Brasnett@ec.gc.ca
Mobile: 5144214665

Brix, Holger
UCLA-JIFRESSE
Phone: 310-825-4526 (UCLA) or
818-393-1018 (JPL)
E-mail: hbrix@ucla.edu
Bulusu, Subrahmanya
University of South Carolina
Fax: (803) 777 6610
Mobile: (803) 777 2572
E-mail: sbulusu@geol.sc.edu

Bulusu, Subrahmanya
University of South Carolina
Fax: (803) 777 6610 Mobile: (803) 777 2572
E-mail: sbulusu@geol.sc.edu

Casey, Kenneth S.
NOAA/NESDIS
National Oceanographic Data Center
1315 East-West Highway
Silver Spring, MD 20910,
USA
Phone: +1 301-713-3272 x133
Mobile: +1 410-507-5902
Fax: +1 301-713-3300
E-mail: Kenneth.Casey@noaa.gov

Castro, Sandra
University of Colorado,
Boulder, Colorado
USA
Phone: +1 303 492 1241
Fax: +1 303 492 2825
E-mail: sandrac@colorado.edu

Chao, Yi
Jet Propulsion Laboratory
Phone: 818-354-8168
E-mail: Yi.Chao@jpl.nasa.gov

Chelton, Dudley
Oregon State University
Fax: 5417372064
Mobile: 5417374017
E-mail: chelton@coas.oregonstate.edu

Chin, T. Mike
Jet Propulsion Laboratory
Mobile: +1 818-393-2510
E-mail: mike.chin@jpl.nasa.gov

Corlett, Gary
Univ. of Leicester
Space Research Centre
University Road
Leicester, LE17RH UK
Tel:+44 116 2522465
Fax: +44 116 2522464
Mobile: +44-116-2525250
E-mail: gkc1@le.ac.uk

Cornillon, Peter
University of Rhode Island
Phone: (401) 742-2911
Fax: (401) 742-6728
E-mail: pcornillon@gso.uri.edu

Cummings, James A.
Oceanographer
Marine Meteorology Division, Code 7533
Naval Research Laboratory
Monterey, California 93943
U.S.A.
Phone: (831) 656 1935
Fax: (831) 656 4769
Email: cummings@nrlmry.navy.mil

Dickinson, Suzanne
University of Washington
Fax: 206-543-6785
Mobile: 206-543-1380
E-mail: suzanne@apl.washington.edu
Dong, Changming
IGPP, UCLA
Mobile: 310-794-5899
E-mail: cdong@atmos.ucla.edu

Dong, Changming
IGPP, UCLA
4855 Slichter Hall,
405 Hilgard Ave,
Los Angeles, CA 90095
USA
Tel: 310-794-5899
E-mail: cdong@atmos.ucla.edu

Donlon, Craig
Principal Scientist for Oceans and Ice
ESA/ESTEC (EOP-SME)
Keplerlaan 1, 2201 AZ Noordwijk
The Netherlands
Phone: +31 (0)715 653687
Fax: +31 (0)715 655675
Email: craig.donlon@esa.int

Eastwood, Steinar
Norwegian Meteorological Institute
Mobile: +47 98682042
Fax: +47 22963050
E-mail: s.eastwood@met.no

Escudero, Luis
Marine Institute of Peru
Fax: 5114291858
Mobile: 511992013291
E-mail: lescudero@imarpe.gob.pe

Foley, Dave
Joint Institute for Marine and Atmospheric Science, U. Hawaii
Email: dave.foley@noaa.gov
Fax: 8316488440
Mobile: 8316480632

Franz, Bryan
NASA GSFC
Phone: 301 2865429
Fax: 301 2860268
E-mail: bryan.a.franz@nasa.gov

Gentemann, Chelle
Remote Sensing Systems
438 First St. Suite 200;
Santa Rosa, CA 95401
USA
Phone: +1 707-545-2904x14
Fax: +1 707-545-2906
E-mail: gentemann@remss.com

Lewis Gramer
University of Miami, CIMAS
4600 Rickenback Cswy
Miami, FL 33149
Mobile: 305-561-1735
E-mail: lew.gramer@noaa.gov

Gregg, Margarita
NOAA/NESDIS/NODC
Phone: (301) 713-3300
Fax: 301-713-3300
E-mail: margarita.gregg@noaa.gov

Halle, Chris
Bodega Marine Laboratory, UC Davis
Fax: 7078752009
Mobile: 7078751928
E-mail: cmhalle@ucdavis.edu

Harrison, Daniel
University of Southern California
Phone: 2135951806
E-mail: dpharris@usc.edu

Hersbach, Hans
ECMWF
Fax: +44 118 986 9450
Mobile: +44 118 949 9476
E-mail: hans.hersbach@ecmwf.int

Hoeyer, Jacob
Danish Meteorological Institute
Denmark
Phone: +45 2627 8990
Mobile: +45 39157203
E-mail: jlh@dmi.dk

Houghton, Nigel
European Space Agency (ESA)
Phone: +39 06 941 80667
Fax: +39 06 941 80632
E-mail: nigel.houghton@esa.int

Ignatov, Alexander
DOC/NOAA/NESDIS
Phone: (301) 763-8572
Fax: 301-763-8572
E-mail: Alex.Ignatov@noaa.gov

Islam, M. Zahirul
Marinelife Alliance
Phone: +88 0171 6624310
E-mail: marinelife_al@yahoo.com

Jedlovec, Gary
NASA/MSFC
Mobile: 256-961-7966
Email: gary.jedlovec@nasa.gov

Jeffery, Christopher
NOAA/ National Oceanographic Data Center
1315 East-West Highway
Silver Springs, MD 20910
Phone: 301 713-3272 Ext 102
Fax: 301 713-3302
E-mail: christopher.d.jeffery@noaa.gov

Ji, Ming
NOAA/NCEP/Ocean Prediction Center
Email: ming.ji@noaa.gov
Mobile: 301-763-8000x7400

Kaplan, Alexey
Lamont-Doherty Earth Observatory of
Columbia University
Phone: (845) 365-8689
Fax: (845) 365-8736
E-mail: alexeyk@ldeo.columbia.edu

Kiefer, Dale
University of Southern California
Phone: 213-740-5814
Fax: (213) 740-8123
E-mail: kiefer@usc.edu

Kumar, Ajoy
Millersville University
Mobile: 717-871-2432
Fax: 717-871-4725
E-mail: ajoy.kumar@millersville.edu

LaFontaine, Frank
NSSTC/Raytheon
USA
Mobile: 256-961-7796
E-mail: frank.j.lafontaine@nasa.gov

Lam, Chi H.
University of Southern California
USA
Phone: 2137405813
E-mail: chihinl@usc.edu

Lavender, Samantha
University of Plymouth
Plymouth
United Kingdom
Phone: +44 1752 232460
Fax: +44 1752 232406
E-mail:s.lavender@plymouth.ac.uk

Le Borgne, Pierre
Météo-France/Centre de Météorologie Spatiale
Avenue de Lorraine, BP 50747
22307 Lannion Cedex
France
Phone: +33 (0)2 96 05 67 52
Fax: +33 (0)2 96 05 67 37
E-mail:Pierre.LeBorgne@meteo.fr

Lengert, Wolfgang
ESA / ESRIN
Phone: +39 06 94180642
E-mail: Wolfgang.Lengert@esa.int

Lindstrom, Eric
NASA Headquarters
Fax: 2023582770
Mobile: 2023584540
Email: eric.j.lindstrom@nasa.gov

Liu, Gang
NOAA-IMSG
Mobile: 703-380-8981
Email: gang.liu@noaa.gov

Mariano, Arthur
University of Miami, RSMAS
Phone: 305-421-4193
E-mail: amariano@rsmas.miami.edu

John Marra
NOAA IDEA Center
John A. Burns Hall (JAB4092)
1601 East-West Rd.
Honolulu, HI 96848
E-mail : john.marra@noaa.gov

Marsouin, Anne
Météo-France/Centre de Météorologie Spatiale
Avenue de Lorraine, BP 50747
22307 Lannion Cedex France
Phone: +33 (0)2 96 05 67 46
Fax: +33 (0)2 96 05 67 37
E-mail: anne.marsouin@meteo.fr

Martin, Matt
Met Office, Fitzroy Road
Exeter,EX1 3PB United Kingdom
Phone: +44 (0)1392 885681
Mobile: +44(0)1392 886465
E-mail: matthew.martin@metoffice.gov.uk

Maturi, Eileen
NOAA/NESDIS/ORA
Silver Springs, MD USA
Phone: +1 301 763-8102 x 172
Fax: +1 301 763-8572
E-mail: Eileen.Maturi@noaa.gov

McKenzie, Bruce
Naval Oceanographic Office
Mississippi, USA
Phone: 228-688-4586
Fax: 228-688-5577
E-mail: bruce.mckenzie@navy.mil

Merchant, Chris
Institute for Meteorology
The University of Edinburgh
Mayfield Road
Edinburgh EH9 3JZ
United Kingdom
Phone: +44 (0)131 650 5097
Fax: +44 (0)131 662 0478
E-mail:c.merchant@ed.ac.uk

Menemenlis, Dimitris
Jet Propulsion Laboratory
California Institute of Technology
Mail Stop 300-323
4800 Oak Grove Dr.
Pasadena CA 91109
USA
Phone: 818-354-1656
Email: menemenlis@jpl.nasa.gov

Minnett, Peter
Rosenstiel School of Marine and Atmospheric Science
University of Miami
4600 Rickenbacker Causeway
Miami, FL 33149-1098,
USA
Phone: +1 305 421 4104
Fax: +1 305 421 4622
E-mail: pminnett@rsmas.miami.edu

Orain, Françoise
Météo-France
Centre de Météorologie Spatiale
Avenue de Lorraine, BP 50747
22307 Lannion Cedex,
France
Fax: +33 2 96 05 67 37
Mobile: +33 2 96 05 67 85
Email: francoise.orain@meteo.fr

Poulter, David
School of Ocean and Earth Science
University of Southampton
Southampton Oceanography Centre
European Way Southampton SO14 3ZH,
United Kingdom
Phone: +44 02380596107
Fax: +44 02380593059
E-mail: djsp@soc.soton.ac.uk

Purca, Sara
IMARPE
Phone: 51-1-4296069
Fax: +51-1-4296069
E-mail: spurca@imarpe.gob.pe

Rayner, Nick
Met Office Hadley Centre
Met Office, Fitzroy Road
Exeter,EX1 3PB
United Kingdom
Phone: +44 (0)1392 884291
E-mail: nick.rayner@metoffice.gov.uk

Reynolds, Richard W.
NOAA/NCDC
Phone: (828) 271-4302
Fax: (828) 271-4328
E-mail: Richard.W.Reynolds@noaa.gov

Roberts-Jones, Jonah
Met Office, Fitzroy Road
Exeter,EX1 3PB
United Kingdom
Phone: (+44)1392 886441
E-mail: jonah.roberts-jones@metoffice.gov.uk

Roquet, Hervé
Météo-France/Centre de Météorologie Spatiale
Avenue de Lorraine, BP 50747
22307 Lannion Cedex
France
Phone: +33 (0)2 96 05 67 64
Mobile: +33 (0)6 80 34 11 14
Fax: +33 (0)2 96 05 67 37
E-mail: Herve.Roquet@meteo.fr

Rutherford, Martin
Royal Australian Navy
Phone: +61 2 93593139
Fax: +61 2 93593120
E-mail: tdom@metoc.gov.au

Ryan, Edward
University of Miami, RSMAS
4600 Rickenback Cswy
Miami, FL 33149
USA
Phone: 305-421-4109
E-mail: eryan@rsmas.miami.edu

Sapper, John
NOAA/NESDIS
5200 Auth Rd
Camp Springs, Maryland 20746
USA
Phone: 301-763-8142 x103
E-mail: john.sapper@noaa.gov

Shibata, Akira
Meteorological Research Institute
Japan
Phone: +81-29-853-8621
Fax: +81-29-855-7240
E-mail: ashibata@mri-jma.go.jp

Sienkiewicz, Joseph M.
NOAA Ocean Prediction Center
5200 Auth Rd
Camp Springs, Maryland 20746
USA
Phone: +1 3017638000 ext. 7302
Fax: +1 3017638085
E-mail: joseph.sienkiewicz@noaa.gov

Tournadre, Jean
IFREMER
Technopôle Brest Iroise
29280 Plouzané
France
Phone: +33 (0)2 98 22 44 97
Fax: +33 (0)2 98 22 45 33
E-mail: jean.tournadre@ifremer.fr

Vazquez, Jorge
Jet Propulsion Laboratory/California Institute of Technology
300/323 4800 Oak Grove Drive
Pasadena, CA 91109,
USA
Phone: 818-354-6980
Mobile: 626 862 3771
Fax: 818-393-6720
E-mail: jorge.vazquez@jpl.nasa.gov

Veal, Karen
University of Leicester
Phone: +44 116 252 5264
E-mail: klv3@le.ac.uk

Weihs, Rachel
Florida State University / COAPS
Phone: 941-376-0410
Fax: 850-644-4841
E-mail: weihs@met.fsu.edu
Wentz, Frank
Remote Sensing Systems
438 First St. #200
Santa Rosa, CA 95401 USA
Phone: 707-545-2904
Fax: 707-545-2906
E-mail: frank.wentz@remss.com

Wentz, Frank
Remote Sensing Systems
438 First St. Suite 200;
Santa Rosa, CA 95401
USA
Phone: +1 707-545-2904x16
Fax: +1 707-545-2906
E-mail: frank.wentz@remss.com

Wick, Gary
NOAA Environmental Technology Laboratory
R/ET6 325 Broadway
Boulder, CO 80305 USA
Phone: 303-497-6322
Fax: 303-497-6181
E-mail: Gary.A.Wick@noaa.gov

Willis, Zdenka S.
NOAA Integrated Ocean Observing System
Program Office
Phone: 301 427 2420
E-mail: Zdenka.Willis@noaa.gov

Steven J. Worley
National Center for Atmospheric Research
Fax: 303-497-1291
Mobile: 303-497-1248
Email: worley@ucar.edu

How to find out more about the GHRSST:

A complete description of the GHRSST together with all project documentation can be found at the following web spaces:

GHRSST	http://www.ghrsst-pp.org
Medspiration	http://www.medspiration.org
BLUElink>	http://www.bluelink.au
MISST	http://www.misst.org
NGSST	http://www.ocean.caos.tohoku.jp
GHRSST GDAC	http://ghrsst.jpl.nasa.gov
GHRSST LTSRF	http://ghrsst.nodc.noaa.gov
ESA	http://www.esa.int
Met Office	http://www.metoffice.gov.uk

GHRSST International Project Office

MetOffice
FitzRoy Road
Exeter, EX1 3PB
United Kingdom

Tel: +44 (0)1392 886622
Fax: +44 (0)1393 885681
E-mail: craig.donlon@esa.int
http://www.ghrsst-pp.org

The GHRSST International Project Office is sponsored by the European Space Agency and the Met Office, United Kingdom.

THE GROUP FOR HIGH RESOLUTION SEA SURFACE TEMPERATURE (GHRSST)

Craig Donlon[(1)]

[(1)] *ESA/ESTEC (EOP-SME), Keplerlaan 1, 2201 AZ Noordwijk, The Netherlands. Email: craig.donlon@esa.int*

ABSTRACT

This paper provides a summary review of the GHRSST Project.

1. INTRODUCTION

Sea Surface Temperature (SST) is required by a variety of scientific and operational ocean and atmospheric applications. The Global Ocean Data Assimilation Experiment (GODAE) is an international collaboration for ocean forecasting activities which, in 2002, initiated a GODAE High Resolution SST Pilot Project (GHRSST-PP) to address an emerging need for more accurate high resolution sea surface temperature (SST) products. At the 9th GHRSST-PP Science Team meeting (2008) the GHRSST Pilot Project was closed and a new collaboration was developed which is called the Group for High Resolution Sea Surface Temperature (GHRSST) which will continue to manage the user/producer need to collaborate and learn from each other. Today, GHRSST s a truly international project with over $30 million US invested across all of the project activities. It orchestrates the harmonisation of a wide variety of different yet complementary SST data streams from many sources as input to a coherent set of GHRSST specified products having a common format and set of ancillary contents. These are shared, indexed, processed, quality controlled, analyzed and documented within a Regional/Global Task Sharing (R/GTS) framework implemented in an internationally distributed manner. Large volumes (currently over 25Gb per day) of data and data services are harnessed together to deliver the new generation of global coverage high resolution SST data sets together with meaningful error estimates for each observation or analysis grid point to meet the SST community User Requirements. The main successes of GHRSST include:

- Wide and open access in near real time to many satellite SST data products has been established in an operational-like manner using existing data user-driven distribution protocols, tools and services. Over 26 Gb of data are provided in NRT every day by GHRSST Services, and over 30,000 international users have accessed GHRSST products (Donlon et al., 2009).
- International agreement on the definition of different SST parameters in the upper layer of the ocean that distinguish between measurements made by infrared radiometers, passive microwave radiometers, in situ sub-surface observations and SST merged analysis outputs. These definitions have been registered in the Climate Forecast (CF) standard name table for wide application (Donlon et al., 2008).
- Diverse satellite SST data product formats and product content have been homogenized according to international consensus and user requirements to include measurement uncertainty estimates for each derived SST value and supporting auxiliary data sets to facilitate their use by data assimilation systems.
- A significant increase in the number of in situ SST measurements from a variety of complementary sources are now available including Argo, drifting buoys, moored buoys and ships. In situ operators (VOS-Clim) are now reporting observation depth with SST measurements.
- 10 international GHRSST SST community workshops have been held attended by an average of 45 delegates to ensure that the SST user-producer community has been involved at all stages of GHRSST service and product development and evolution.
- GHRSST technical advisory groups have successfully conducted extensive research to ensure that SST diurnal variability (DV) is properly flagged within observational data, developed methods to correct for bias in different satellite data sets, provided uncertainty estimates on a measurement by measurement basis, developed high resolution sea ice data sets and accurate SST products in the marginal ice zone.
- New SST analysis products using new methods to merge in situ data with complementary microwave and infrared satellite data have been developed and implemented operationally.
- Inter-comparison frameworks (e.g., the GHRSST Multiproduct Ensemble (GMPE) have been developed at resolutions of 10km or better for the global ocean and other regions of interest. An operational high Resolution Diagnostic Data Set (HR-DDS) has been established for real time inter-comparisons and validation/verification of GHRSST products allowing real time monitoring of satellite and in situ SST data streams.

- A delayed-mode inter-comparison framework has been established in conjunction with the GCOS SST and Sea Ice Working Group to understand the linkages between the modern era satellite-based SST record and historical primarily ship-based SST reconstructions (see http://ghrsst.nodc.noaa.gov).
- Methods to convert between radiometric 'skin' SST and the SST at depths measured by ships and buoys have been developed (e.g., Donlon et al, 2002) that are now used by operational SST analysis systems (e.g., Stark et al., 2007).
- An internationally distributed suite of user focused services are now provided in a sustained Regional/Global Task Sharing (R/GTS) framework that addresses international organizational challenges and recognizes the implementing institutional capacities, capabilities and funding prospects. Long term stewardship, user support and help services including standards-based data management and interoperability have been developed that are manned and operated within the R/GTS on a daily basis.
- Methods to manage long-term satellite SST data sets for use in a reanalysis program that considers SST data for the entire satellite era have begun.

GHRSST has earned broad recognition as the international authority for modern-era SST activities because it has successfully built and nurtured a framework in which the exchange of satellite SST data has flourished and given new life to the study and application of high-resolution SST using satellite and in situ data. Applications have demonstrated positive impact in ocean and atmospheric forecasting systems and a new generation of data products and services to serve these and other users have been built and are operated on a day-to-day basis. The success of GHRSST stems from the Agencies and Offices that have supported the activities of the Pilot Project allowing a dedicated group of scientists and operational entities to successfully work together and bridge the gap between operations and science. All good operational systems are underpinned by excellent science and GHRSST has endeavored to provide a forum in which operational systems and scientists can meet and discuss problems and solutions to address the real-world challenges associated with the application of high-resolution SST data sets.

2. GHRSST Data products and services

GHRSST provides two major types of near-real time SST products (Level 2 pre-processing and Level 4 analysis products) supported by user support, data delivery, data management and quality control services. Together these make up a consistent system through which any satellite SST measurements can be channeled, conditioned and evaluated against in situ measurements and other satellite data, easily used by operational forecasting systems, used in the construction of real time SST analyses and contribute to the construction of a long term climate record of global SST distribution.

The L2P product is designed to provide all SST data from various agencies and different sensors in a common format and with the addition of ancillary information to assist interpretation. For every L2 file (defined as geo-referenced SST products) of input data, GHRSST produces a matching L2P (L2 pre-processed) product that contains identical SST values in the same geographical layout (swath or lat/long co-ordinates) as those in the source L2 products. The difference is that each data record (corresponding to a pixel) is augmented with an estimate of the bias error and standard deviation of error derived from statistical databases of in situ and satellite data on a sensor by senor basis (called Single Sensor Error Statistics, SSES), surface wind speed, aerosol optical depth, sea ice concentration, the time of observation and a set of quality control flags.

The GHRSST L4 analysis products provide merged, gridded and gap-free SST data sets produced by analysis of several complementary inputs. The objective in generating L4 products is to provide the best available estimate of the SST from a combined analysis of all available L2P (and other) SST data.

A dedicated Re-analysis (RAN) Program is a GHRSST service that is now developing a long term satellite-derived SST data set at high resolution building on the operational data streams and off-line delayed mode SST data sets not available to the real time system. Other services include

- A High Resolution Diagnostic Data Set (HR-DDS, see http://www.hrdds.net) that allows users to interactively view, compare and analyze SST data products, ocean model data sets and auxiliary data sets from the various data streams within GHRSST,
- A Match-up Database (MDB) of co-located satellite and in situ SST required for quality control of satellite SST datasets, in particular for deriving or verifying SSES using in situ SST observations from ships, buoys and profiling floats.
- A GHRSST Multi-Product Ensemble (GMPE) uses ensemble techniques to investigate SST analysis differences using both analyses and observational products.

3. GHRSST REGIONAL/GLOBAL TASK SHARING FRAMEWORK (R/GTS)

At the core of GHRSST success is the international collaboration on which it is based. In eight years of discussion, debate and planning the main agencies responsible for operating satellite SST sensors and for producing the primary SST datasets have worked with ocean scientists familiar with the processes affecting remote sensing of SST, and with key operational users of SST data, to lay down the rule base for the sharing, indexing, processing, quality control, archiving, analysis and documentation of SST data from diverse sources. This is specified in the GHRSST Data Processing Specification document (Donlon et al., 2006) which defines clearly the input and output data specifications, data processing procedures, algorithms and data product file formats that are common to each GHRSST sub-system.

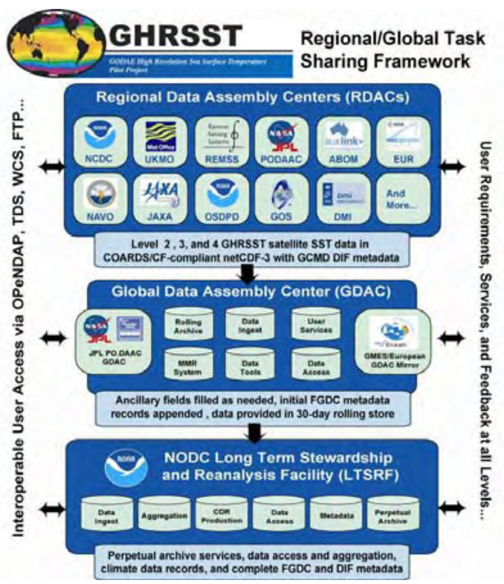

Figure 1 *The GHRSST Regional/Global Task Sharing (R/GTS) framework. The R/GTS establishes an international set of RDACs, each of which delivers data to a GDAC (online at http://ghrsst.jpl.nasa.gov) and the regional user community. Data are served from the GDAC to near-real-time users and applications for 30 days before the data are sent to the GHRSST LTSRF (at http://ghrsst.nodc.noaa.gov) for long-term archive, stewardship, provision to delayed mode users, and future CDR production.*

The project is currently developing a GDS-v2.0 incorporating lessons learned and preparing for the future. In order for the GHRSST Regional/Global Task Sharing (R/GTS) framework to function, all GHRSST products, must strictly follow the common Data Processing Specification when generating L2P and L4 data. As a result, users with tools to read data from one RDAC can draw data from any of the others and/or the GDAC and should find it is immediately readable by their systems having uniformity within the limits of flexibility permitted by the GHRSST Data Processing Specification.

GHRSST was able to move rapidly from defining the Processing Specification to the present situation in which global L2P and L4 products are being generated in large numbers and beginning to be used operationally, because it established by consensus an implementation framework in which the new data products and services are provided. No attempt was made to impose a top-down structure for commissioning data production. Instead, agreement and commitment to the GHRSST Data Processing Specification facilitated the existing agencies each to contribute a part of the necessary international effort through the Regional/Global Task Sharing system that is illustrated in Figure 8. This is a distributed modular model with a hierarchical distinction between RDAC, GDAC and the Long Term Stewardship and Re-analysis Facility (LTSRF).

4. TRANSITION TO OPERATIONS AND THE FUTURE

There is much ‘unfinished business’ in terms of the challenges that GHRSST has begun to tackle – particularly in the area of uncertainty estimation for SST products. Furthermore, the R/GTS framework is now a framework that is relied upon by many users and one that has evolved from a need as a bottom-up development. GHRSST will continue to manage the R/GTS, the GDS-v2.0 and the user/producer need to continually collaborate and learn from each other. GHRSST will also focus more attention toward the production of SST Climate Data Records as part of the Reanalysis project in order to satisfy the needs for a merged long term SST data set through the satellite era. Collaboration with GCOS in this respect has led to exciting new developments that are studying differences between comparable data sets using dedicated tools (see http://ghrsst.nodc.noaa.gov/intercomp.html for more information). New cost effective approaches to an integrated and optimized SST measurement system have been developed (e.g., Zhang et al., 2009) and are now used operationally to reduce bias error in AVHRR data using targeted global deployment strategies for drifting buoys. A future vision for the work of GHRSST in the next 10 years has recently been developed as a community white paper for the OceanObs 09 conference which is available at http://www.ghrsst-pp.org/modules/documents/documents/OO-ModernEraSST-v3.0.pdf.

5. CONCLUSION

The GODAE High Resolution SST Pilot Project has harnessed the attention and contribution of many international users and producers of satellite SST. It has successfully built and nurtured a framework in which the exchange of satellite SST data has flourished and given new life to the study of high-resolution SST using satellite and in situ data. Applications have demonstrated positive impact in ocean and atmospheric forecasting systems and a new generation of data products and services to serve these and other users have been built and are operated on a day-to-day basis. The GODAE Pilot Project has successfully demonstrated that the requirements of GODAE can be met and has concluded. A new collaboration established called the Group for High Resolution SST (GHRSST) that will build on the lessons learned during the pilot has been initiated that will continue the evolution of high resolution SST data sets in near real time, serve the needs of data assimilation systems and develop SST climate data records. Full information can be found at http://www.ghrsst-pp.org.

6. REFERENCES

Donlon, C. J., P. J. Minnett, C. Gentemann, T. J. Nightingale, I. J. Barton, B. Ward, and J. Murray, 2002: Toward improved validation of satellite sea surface skin temperature measurements for climate research. *Journal of Climate*, **15,** 353-369

Donlon C, Robinson I S, Reynolds M, Wimmer W, Fisher G, Edwards R, Nightingale T J., 2008. An Infrared Sea Surface Temperature Autonomous Radiometer (ISAR) for Deployment aboard Volunteer Observing Ships (VOS). Journal of Atmospheric and Oceanic Technology 25 (1): 93-113.

Donlon, C. J., I. Robinson, K. S Casey, J. Vazquez-Cuervo, E Armstrong, O. Arino, C. Gentemann, D. May, P. LeBorgne, J. Piollé, I. Barton1, H Beggs, D. J. S. Poulter, C. J. Merchant, A. Bingham, S. Heinz, A Harris, G. Wick, B. Emery, P. Minnett, R. Evans, D. Llewellyn-Jones, C. Mutlow, R. Reynolds, H. Kawamura1 and N. Rayner. The Global Ocean Data Assimilation Experiment (GODAE) high Resolution Sea Surface Temperature Pilot Project (GHRSST-PP), 2009: Oceangraphy Magazine in press.

Donlon, C. J., I. Robinson, K. S Casey, J. Vazquez-Cuervo, E Armstrong, O. Arino, C. Gentemann, D. May, P. LeBorgne, J. Piollé, I. Barton1, H Beggs, D. J. S. Poulter, C. J. Merchant, A. Bingham, S. Heinz, A Harris, G. Wick, B. Emery, P. Minnett, R. Evans, D. Llewellyn-Jones, C. Mutlow, R. Reynolds, H. Kawamura1 and N. Rayner. The Global Ocean Data Assimilation Experiment (GODAE) high Resolution Sea Surface Temperature Pilot Project (GHRSST-PP), 2007: *Bull. Am. Meteorol. Soc*., 88 (8), 1197-1213, (DOI:10.1175/BAMS-88-8-1197)

Donlon, C.J. and the GHRSST-PP Science Team, 2006: *The GHRSST-PP data processing specification version 1.6*., 241 pp. [Available online at www.ghrsst-pp.org.]

Stark, J. D., C. J. Donlon, M. J. Martin and M. E. McCulloch, 2007, OSTIA : An operational, high resolution, real time, global sea surface temperature analysis system., Oceans '07 IEEE Aberdeen, conference proceedings. Marine challenges: coastline to deep sea. Aberdeen, Scotland. IEEE.

Zhang, H.M., R.W. Reynolds, R. Lumpkin, R. Molinari, K. Arzayus, M. Johnson, and T.M. Smith, 2009: An Integrated Global Observing System For Sea Surface Temperature Using Satellites and in Situ Data: Research to Operations. *Bull. Amer. Meteor. Soc.*, **90**, 31–38.

IOOS® USE OF GHRSST

Zdenka Willis[(1)]

[(1)] *NOAA IOOS Program, Silver Spring MD, USA. Email: Zdenka.Willis@noaa.gov*

1. INTRODUCTION

The Integrated Ocean Observing System (IOOS®) is a multidisciplinary system designed to enhance our ability to collect, deliver, and use ocean information. The goal is to provide continuous data on our open oceans, coastal waters, and Great Lakes in the formats, rates, and scales required by scientists, managers, businesses, governments, and the public to support research and inform decision-making. NOAA is leading interagency and regional efforts to build the U.S. IOOS. Since GHRSST is similarly focused on integrating satellite-based observations of sea surface temperature (SST), natural synergies exist between the two programs and should be further explored.

2. THE U.S. IOOS

The U.S. IOOS consists of both Federal and regional contributions of ocean observations, products, and services. Currently, this partnership consists of 17 U.S. federal and 11 regional partners, each of which consists of numerous organizations within those regions. IOOS may be viewed as having two interdependent pieces: a national coastal component and a global component. By working across the Federal agencies and with the regional partners to integrate data, IOOS partners are able to provide a more comprehensive, detailed view of coastal, Great Lakes, and ocean environments. The result is a coordinated system that allows resource managers, emergency responders, scientists, policy makers, and many others quick and easy access to a range of information on-demand and in formats useful for everyday decisions. The range of observations these components are working to integrate is illustrated in Figure 1.

3. THE NATIONAL COASTAL COMPONENT

The national coastal component of IOOS includes U.S. observations, products, and services provided by a number of Federal agencies to monitor and manage the Great Lakes and entire U.S. ocean environment. The coastal component also includes the network of 11 non-Federal Regional Associations that allow these Federal agencies to expand their measurements to issues and geographic areas of particular interest to local communities.

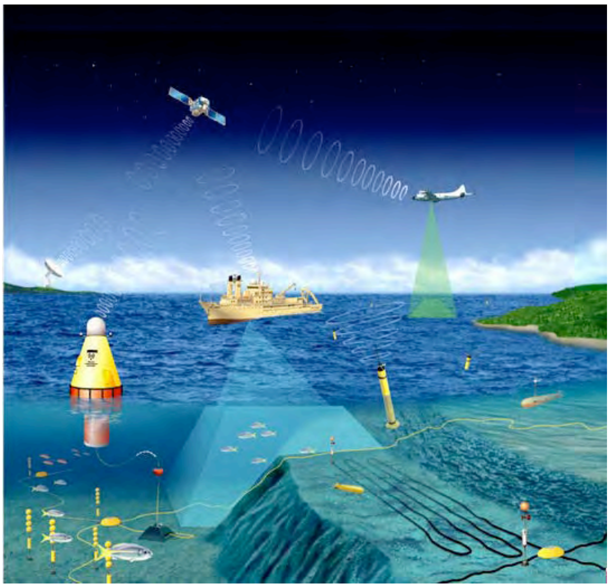

Figure 1. The above image provides a graphical depiction of many types of observing systems used to collect data describing our oceans, coasts, and Great Lakes.

4. THE GLOBAL COMPONENT

IOOS is the U.S. contribution to the Global Ocean Observing System, or "GOOS." GOOS is a global system for sustained ocean observations designed to improve weather forecasts and climate predictions. GOOS is also the ocean component of an even larger system, known as the Global Earth Observation System of System (GEOSS). GEOSS will work with and build upon these other national, regional, and international systems to provide comprehensive, coordinated Earth observations from thousands of instruments worldwide, transforming the data they collect into useful information for society.

5. IOOS SUBSYSTEMS

According to the U.S. IOOS Development Plan, the process of linking observations to the development of useful, environmental information requires "a managed, efficient, two-way flow of data and information among three essential sub-systems." These sub-systems include:

- Measurements: Ocean observations collected from systems in the water, as well as land-based, airborne, or satellite platforms;

- Data Management and Communications (DMAC): The primary mechanism to integrate collected IOOS data so that they are compatible with one another and accessible to users; and

- Modeling and Analysis: Products and services delivered to users, including related socio-economic research, outreach, training, and education.

Through these sub-systems, IOOS links observations to modeling and predictions to provide data and information needed to improve the nation's ability to achieve seven societal goals:

- Improve predictions of climate change and weather and their effects on coastal communities and the nation;

- Improve the safety and efficiency of maritime operations;

- Allow more effective mitigation of the effects of natural hazards;

- Improve national and homeland security;

- Reduce public health risks;

- Allow more effective protection and restoration of healthy coastal ecosystems; and

- Enable the sustained use of ocean and coastal resources.

6. THE IOOS DATA INTEGRATION FRAMEWORK

The NOAA IOOS program initiated development of a Data Integration Framework (DIF) to improve management and delivery of an initial subset of ocean observations. The DIF is establishing the technical infrastructure, standards, and protocols needed to improve delivery of at least six of 20 IOOS core oceanographic variables defined in the U.S. IOOS Development Plan, as well as marine winds.

The following services are the first to be established by the NOAA IOOS program and its partners to provide access to data. These services are now undergoing beta-test and should still be considered experimental. The services will be modified and enhanced during the course of the DIF project.

NDBC Sensor Observation Service (SOS): This server provides in-situ temperature, salinity, currents, water level, waves and winds data from National Data Buoy Center (NDBC) moorings, IOOS Regional Coastal Ocean Observing Systems, Deep-ocean Assessment and Reporting of Tsunamis (DART) buoys, and Tropical Atmosphere Ocean (TAO) buoys. The server is operated by the NOAA National Weather Service (NWS) NDBC. SOS is an Open Geospatial Consortium (OGC) standard. [http://sdf.ndbc.noaa.gov/sos/]

CO-OPS SOS: This server provides in-situ temperature, conductivity, currents, water level, and waves data from the National Water Level Observing Network (NWLON) and the Physical Oceanographic Real-Time System (PORTS). The server is operated by the NOAA National Ocean Service (NOS) Center for Operational Oceanographic Products and Services (CO-OPS). [http://opendap.co-ops.nos.noaa.gov/ioos-dif-sos/]

NDBC THREDDS Data Server (TDS): This server provides gridded surface currents derived from high-frequency radar (HFR) installations along the coasts. The server supports Web Coverage Service (WCS) and Open-source Project for a Network Data Access Protocol (OpenDAP) and is operated by NDBC. WSC is an OGC standard. [http://sdf.ndbc.noaa.gov/wcs/]

SECOORA SOS: This server provides a variety of in-situ parameters from a collection of data providers. Server is operated by SECOORA (Southeast Coastal Ocean Observing Regional Association). Software documentation on creating this service from the supporting database is at http://code.google.com/p/xenia/wiki/XeniaSOS. [http://nautilus.baruch.sc.edu/obskml/scripts/difSOS.html]

CoastWatch TDS: This server provides access to chlorophyll concentrations derived from satellite ocean color observations. This server is operated by NOAA National Environmental Satellite, Data, and Information Service (NESDIS) CoastWatch program. http://coastwatch.noaa.gov/

The DIF currently focuses on in-situ IOOS variables, but the full US IOOS DMAC subsystem calls for remote sensed information as well. GHRSST provides this integration for the remote sensed SST. As the DIF expands to provide additional DMAC capabilities the two programs should develop an implementation plan that will provide specific next steps for the integration of the two programs

7. CONCLUSION

NOAA IOOS recently published a business case regarding data integration. We found that between 25-50% of a forecaster's time is spent discovering, getting access to and reformatting data before it can be used. This is a lost opportunity. Furthermore, there are a wide variety of data types that we need to describe our oceans, coasts and Great Lakes but limited resources. Therefore is it incumbent on us to coordinate to the maximum extent possible national and international programs. GHRSST and US IOOS, with their similar efforts related to integrated data, services, and standards, could each benefit from closer coordination and linkages.

ESA SST Satellite data exploitation structure and organization

Wolfgang Lengert

The ESA (A)ATSR missions were funded by the UK Department of Energy and Climate Change (DECC) and ATSR-1 / ATSR-2 were funded by the UK Natural Environment Research Council (NERC). By investing in the (A)ATSR missions all funding bodies, including ESA are interested in ensuring that the investments are utmost exploited.

During 2009 a new (A)ATSR exploitation plan will be released providing full transparency on the mission of the past, presents, and future also considering SLSTR activities. Furthermore it provides an overview, beside the science, also of the applications and operational activities performed on these data. This exploitation plan shall become a tool for scientists, users and funding bodies allowing quickly visibility on which activities are, or have been funded by whom, or which projects might be funded in the future. For the funding bodies this plan is an essential document since it shows easily which projects will help in achieving their policy or science objectives.

To ensure that the document will be a living document and therewith remains a tool for all (A)ATSR partners, input from the SST community (GHRSST user, science and Quality Working Group) is required.

The presentation gives an overview of ESA SST Satellite (ATSR-1, ATSR-2, AATSR, SLSTR) data exploitation structure and organization around the new (A)ATSR exploitation plan. It also encourages to use this document as a tool to get new science or application ideas funded.

LONG TERM STEWARDSHIP OF GHRSST AND RELATED DATA AT THE NATIONAL OCEANOGRAPHIC DATA CENTER

Margarita Gregg (1)

(1) *NOAA National Oceanographic Data Center, Silver Spring MD, USA. Email: Margarita.Gregg@noaa.gov*

ABSTRACT

The National Oceanographic Data Center (NODC) is operated by the U.S. National Oceanic and Atmospheric Administration (NOAA) to provide long-term, scientific stewardship of a wide range of marine data and information. NODC preserves and provides access to model simulations and satellite, in situ, and video-based observations of physical, biological, chemical, and ecosystem parameters. Working with the international community, NODC serves as the Group for High Resolution SST (GHRSST) Long Term Stewardship and Reanalysis Facility (LTSRF). The significant contributions made by NODC span a range from fundamental archive functions of preservation and access, to higher levels of scientific data stewardship involving reprocessing and intercomparison, to application of the data for societal benefit. These contributions are summarized here and demonstrate the importance of active archive involvement in international activities like GHRSST.

1. INTRODUCTION

NODC is one of three National Data Centers operated by the National Oceanic and Atmospheric Administration (NOAA) of the U.S. Department of Commerce. NODC was chartered to "acquire, process, preserve, and disseminate oceanographic data" and its primary mission is to ensure that global oceanographic data sets collected at great cost are maintained in a permanent archive that is easily accessible to the world science community and to other users. The main NODC facility is located in Silver Spring, Maryland. NODC also has field offices collocated with major government and academic oceanographic laboratories in Mississippi, Florida, California, Washington, and Hawaii.

NODC has been actively participating in GHRSST since its inception as the GODAE High Resolution SST Pilot Project (GHRSST-PP), and established archive procedures in 2006. It also leads the GHRSST Reanalysis Technical Advisory Group (RAN-TAG), supports the GHRSST/Global Climate Observing System (GCOS) SST and Sea Ice Working Group's SST intercomparison facility, provides AVHRR Pathfinder SST data to the GHRSST community, and serves GHRSST data to a range of users around world. The NODC GHRSST web site is available at http://ghrsst.nodc.noaa.gov.

2. FUNDAMENTAL ARCHIVE SERVICES

Thirty days after observation, NODC receives all GHRSST data sets processed through the GHRSST Global Data Assembly Center (GDAC), located at the NASA Jet Propulsion Laboratory's Physical Oceanography Distributed Active Archive Center (PO.DAAC). Using automated procedures, NODC acquires the data, processes it into the archive, builds additional metadata, and makes it available to the international user community via http, ftp, and OPeNDAP. The NODC archive meets rigorous national and international standards for digital archives, including the provision of multiple, geographically distributed copies and failover capabilities in the event the primary facility in Silver Spring becomes unavailable.

These routines bring to NODC approximately 1000 netCDF files each day, with a volume of about 25 GB. As of 01 May 2009, the archive contains nearly 20 Terabytes of compressed data and nearly one million netCDF files conforming to GHRSST conventions (Figure 1). Working together, the PO.DAAC GDAC and NODC LTSRF have served over 28,000 unique users more than 46 Terabytes of data contained in 13.5 million netCDF files. In the first 3 months of 2009, NODC has already served more data than in all of 2008 in terms of both volumes and number of files, and is on pace to double the number of users accessing the data.

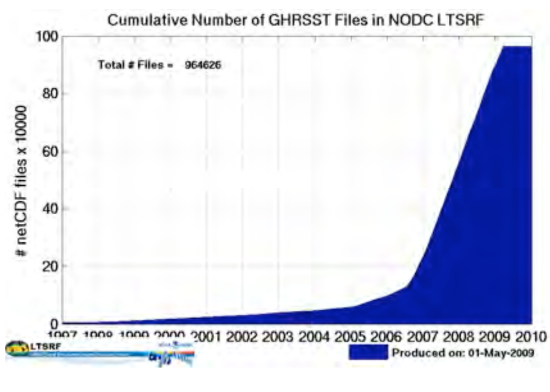

Figure 1: Cumulative number of netCDF files as of 01 May 2009 in the GHRSST LTSRF at NODC. Approximately 1000 additional data files are archived each day, and the archive currently holds nearly one million files.

3. SCIENTIFIC DATA STEWARDSHIP

The NODC GHRSST LTSRF provides not only the essential functions of ingest, archival storage, and data access, but also a range of enhanced scientific data stewardship services. Collaborating with the activities of the GCOS SST and Sea Ice Working Group, NODC hosts the GHSST/GCOS SST Intercomparison system as part of its LTSRF operations. This intercomparison facility computes a standard suite of diagnostic statistics and graphics from modern, satellite-era SST data sets as well as historical, ship-based SST reconstruction data sets. Figure 2 illustrates an example cross-comparison between the satellite-based Pathfinder SST data and the UK Met Office Hadley Centre HadSST2 in situ SST product. All of the SST products within the facility have been converted to and are available in GHRSST format. These data along with the suite of intercomparison statistics and diagnostic images are available at http://ghrsst.nodc.noaa.gov/intercomp.html.

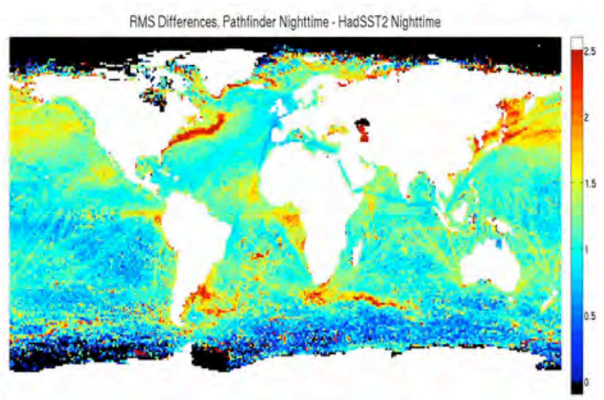

Figure 2: Example intercomparison graphic showing the nighttime RMS SST difference in (degrees C) between NODC's AVHRR Pathfinder and the in situ HadSST2 product from the Hadley Centre, UK Met Office. The GHRSST/GCOS system computes standard diagnostic metrics for modern and historical era SST reconstructions and provides access to the data in GHRSST-compliant format.

NODC also provides enhanced scientific stewardship services through its AVHRR Pathfinder SST reprocessing effort. Pathfinder attempts to provide the longest, most accurate, and most consistent global climate data record of AVHRR-based SST. Pathfinder Version 5 currently serves as the baseline to GHRSST reanalysis efforts, and the Version 6 product under development now is working toward full integration and compliance with GHRSST formats and standards. The AVHRR Pathfinder SST data are available at http://pathfinder.nodc.noaa.gov.

4. APPLICATIONS FOR SOCIETAL BENEFIT

In addition to providing critical archive and scientific data stewardship services, NODC works with its national and international partners to apply the SST data it stewards for societal benefit. By applying the data to a broad range of applications, its true value can be achieved.

A recent example of this application of SST data to societal benefit is illustrated in Figure 3, which depicts the first-ever global map of human impacts of marine ecosystems (Halpern et al., 2008). The SST data stewarded at NODC were used in this large synthesis study to represent anthropogenic warming of the world ocean. When coupled with more than a dozen other human induced threats, a global picture emerged of threatened ecosystems, providing critical information to marine resource managers, scientists, and policy makers.

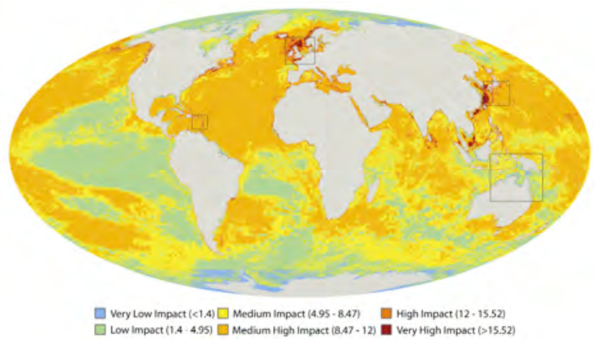

Figure 3: Global display of impacted marine ecosystems, with cooler shades (blue to green) representing areas with lower levels of human impact. Warmer shades (yellow to red) represent areas with higher levels of human impact. From Halpern et al., (2008).

5. RELATED DATA AND INFORMATION

NODC also manages the world's largest collection of publicly available oceanographic data. NODC holdings include in situ and remotely sensed physical, chemical, and biological oceanographic data from coastal and deep ocean areas. With this large and diverse collection of data and information, NODC contains numerous other datasets related to GHRSST scientific and data production efforts. For example, NODC produces the World Ocean Database (WOD), which contains an extensive quality-controlled collection of profile data. The WOD near surface observations, along with NODC's archive of Argo profiling float data, can prove useful to GHRSST efforts to study the foundation SST layer just below the influence of diurnal variations. Many other useful and related data sets are also available in NODC's oceanographic data collections.

6. CONCLUSION

Through its broad spectrum of GHRSST-related activities, from providing essential archive services, to enhanced scientific data stewardship, to application of the data for societal benefit, NODC is demonstrating the importance of the archives to scientific data collection and integration efforts like GHRSST. Working with its international partners, NODC is working to ensure that the full value of the global SST observation network is realized.

REFERENCES

Halpern, Benjamin S., S. Walbridge, K.A. Selkoe, C.V. Kappel, F. Micheli, C. D'Agrosa, J.F. Bruno, K.S. Casey, C. Ebert, H.E. Fox, R. Fujita, D. Heinemann, Hunter S. Lenihan, E.M.P. Madin, M.T. Perry, E.R. Selig, M/ Spalding, R. Steneck, and R. Watson (2008). A global map of human impact on marine ecosystems. *Science*, vol. 319, no. 5865, pp. 948-952 (DOI: 10.1126/science.1149345).

MODIS SEA SURFACE TEMPERATURES.

Peter J Minnett[(1)] & Robert H Evans[(1)]

[(1)] *Rosenstiel School of Marine and Atmospheric Science, University of Miami,4600 Rickenbacker Causeway, Miami, Florida (USA), Email pminnett@rsmas.miami.edu*

ABSTRACT

The MODerate-resolution Imaging Spectroradiometer (MODIS) is a complex visible and infrared radiometer that includes many innovative features that result in the potential to improve the accuracies of the retrievals of sea-surface temperature (SST). The approaches to deriving increasingly more accurate atmospheric correction algorithms, and the methods to demonstrate these accuracies and contributing the Climate Data Records of SST are described.

1. INTRODUCTION

The sea-surface temperature (SST) is an “essential climate variable,” being an important parameter in the global climate system: it is a controlling variable in the ocean-atmosphere exchange of heat, moisture and gases; its patterns reveal subsurface oceanic variability; and long-term evolution of its global, regional and seasonal averages are potential indicators of climate change. The difficulty in making adequate measurements of SST can only be resolved by using satellite radiometers which provide the capability of self-consistent, global measurements on repeat cycles of hours to days. The potential of this long series of satellite measurements in climate research is great (e.g. Allen et al., 1994; Good et al., 2007), but, as expounded in the National Research Council Report on Climate Data Records (CDR; NRC, 2000), to make full use of such measurements requires a clear understanding of the residual uncertainties in the derived SST fields. This can be accomplished by ensuring the characteristics of the spacecraft radiometers are well determined, and the algorithms used to process the data to retrieve SST are accurate and their shortcoming well understood.

In this presentation we will discuss the contributions of the MODIS (MODerate-resolution Imaging Spectro-radiometer – Salomonson et al., 1989; Guenther et al., 1996; Barnes et al., 1998;Esaias et al., 1998) to the generation of an accurate SST CDR, and the approach developed to determine the characteristics of the uncertainties in the derived SST fields. There are two MODIS’s in operation, one on the NASA satellite *Terra*, launched in late 1999, and the other on *Aqua*, launched in 2002.

In this paper we present a new Operational SST and Sea Ice Analysis system (OSTIA) which has been developed at the Met Office, discuss the source data, and show the impact of Envisat AATSR data.

2. MODIS OVERVIEW

For the measurement of SST, MODIS includes the standard “split-window” pair of bands in the 10-13 µm atmospheric transmission window (Band 31, λ = 11.03 µm and Band 32, λ = 12.02 µm) and, for the first time, three bands in the 3.5-4.1 µm window. Of these, Band 20 has a relatively wide band pass and is comparable to Channel 3b of the AVHRR (λ = 3.75 µm); the other two, Bands 22 (λ = 3.96 µm) and 23 (λ = 4.05 µm) are much narrower and less susceptible to contamination by the effects of the atmosphere. In addition to the new spectral bands, there are several aspects of the design of MODIS that are innovative developments that extend beyond the capabilities of the heritage instruments. These include a double-sided “paddle-wheel” scan mirror and ten detectors for each spectral band. The measurements of MODIS in the infrared are calibrated on-orbit using an internal black-body target and a view of deep, cold space in a fashion similar to that used for the AVHRR. However, the black-body calibration target is of novel design, and unlike the base-plate target of AVHRR, it is internal to the instrument and thereby avoids the temperature excursions experienced in the AVHRR calibration procedure around the orbit (Brown et al., 1985). The complexity of the instrument meant that the pre-launch calibration and characterization measurements had to be rigorous and exacting. However, the requirements of some of the characterization measurements were at the limit or beyond the accuracies achievable in the laboratory and it was recognized that some residual instrumental artifacts would be present in the post-launch data and would have to be corrected empirically or with the assistance of specific on-orbit exercises.

3. MODIS ATMOSPHERIC CORRECTION ALGORITHM

The form of the MODIS atmospheric correction algorithm is based on that refined over many years, based on the so-called Non-Linear SST (Walton, 1988), and modified in the AVHRR SST Pathfinder Project (Kilpatrick et al., 2001).

The algorithm using measurements in the 10-12µm atmospheric window, suitable for both daytime and night-time use, is:

$$SST = c_1 + c_2 * T_{11} + c_3 * (T_{11}-T_{12}) * T_{sfc} + c_4 * (\sec(\theta)-1) * (T_{11}-T_{12})$$

where T_n are brightness temperatures measured in the channels at n μm wavelength, T_{sfc} is a 'first guess' estimate of the SST in the area, and θ is the satellite zenith angle. Alternative forms of the algorithm, some excluding the use of T_{sfc} were investigated, but were found less effective.

The night-time algorithm, using two bands in the 4μm atmospheric window is:

$$SST4 = c_1 + c_2 * T_{3.9} + c_3 * (T_{3.9}-T_{4.0}) + c_4 * (\sec(\theta)-1)$$

Note, the coefficients in each expression are different. There coefficients are derived by analysis of collocated and contemporaneous match-ups with *in situ* measurements.

The MODIS Matchup Data Base (MDB) is a compilation of the MODIS brightness temperatures collocated with in situ measurements from the radiometers and buoys. Each record is augmented with values of the ancillary atmospheric variables (e.g. aerosol characteristics, water vapor concentration, and surface wind speed) and of the geometrical and instrumental characteristics, which provide the mechanism for improving insight into the sources of uncertainty. The MDB is the basis of determination of the error characteristics of the MODIS SST retrievals (Evans et al., 2006).

The in situ measurement in the MDB comprise a large number of subsurface temperature measurements from drifting and moored buoys, and from a smaller number of skin SST measurements made from radiometers mounted on ships. One such radiometer, is the Marine-Atmospheric Emitted Radiance Interferometer (M-AERI; Minnett et al., 2001), which is a Fourier Transform InfraRed (FTIR) interferometric spectro-radiometer that includes very accurate internal calibration. It was developed specifically for the validation of MODIS skin SST retrievals. To ensure traceability to NIST standards, an infrared calibration facility has been established at RSMAS, including a water-bath black body calibration target, built to a NIST design (Fowler, 1995) and characterized by the NIST Transfer Radiometer (TXR; Rice and Johnson, 1998), which is the infrared radiometric standard for the EOS program (Rice and Johnson, 1996). This facility has become the reference standard for other ship-board radiometers (Rice et al., 2004; Barton et al., 2004). The 3rd International Infrared Radiometry Workshop took place in Miami in May 2009.

4. DISCUSSION

With the passage of time, corrections for the instrumental artifacts in the MODIS infrared data, derived primarily by the MODIS Characterization Support Team led by Dr Jack Xiong, have improved and resulted in smaller noise levels in the infrared brightness temperature measurements. These improvements have triggered periodic reprocessing of the MODIS global SST time series. Each reprocessing has been accompanied by a new generation of the MDBs and revised coefficients for the atmospheric correction algorithm. The Version 6 reprocessing, anticipated for later in 2009, marks a new threshold in the development of more accurate SST fields, with the instrumental artifacts being reduced to a sufficiently low level that a new approach to the algorithm has been facilitated with the result that markedly improved accuracies can be demonstrated.

5. ACKNOWLEDGEMNTS

These results are the product of many years of effort and the support of Dr Eric Lindstrom at NASA HQ is gratefully acknowledged.

6. REFERENCES

Allen, M. R., C. T. Mutlow, G. M. C. Blumberg, J. R. Christy, R. T. McNider, and D. T. Llewellyn-Jones, 1994: Global change detection. *Nature*, **370,** 24-25.

Barnes, W. L., T. S. Pagano, and V. V. Salomonson, 1998: Prelaunch characteristics of the moderate resolution imaging spectroradiometer (MODIS) on EOS-AM1. *IEEE Transactions on Geoscience and Remote Sensing*, **36,** 1088-110.

Barton, I. J., P. J. Minnett, C. J. Donlon, S. J. Hook, A. T. Jessup, K. A. Maillet, and T. J. Nightingale, 2004: The Miami2001 infrared radiometer calibration and inter-comparison: 2. Ship comparisons. *Journal of Atmospheric and Oceanic Technology*, **21,** 268-283.

Brown, O. B., J. W. Brown, and R. H. Evans, 1985: Calibration of Advanced Very High Resolution Radiometer infrared observations. *Journal of Geophysical Research*, **90,** 11667-11677.

Esaias, W. E., M. R. Abbott, I. Barton, O. B. Brown, J. W. Campbell, K. L. Carder, D. K. Clark, R. H. Evans, F. E. Hoge, H. R. Gordon, W. M. Balch, R. Letelier, and P. J. Minnett., 1998: An Overview of MODIS Capabilities for Ocean Science Observations. *IEEE Transactions on Geoscience and Remote Sensing*, **36,** 1250-1265.

Evans, R. H., K.Kilpatrick, P. J. Minnett, S. Walsh, V. Haliwell, and W. Baringer, 2006: Error Hypercube - a Novel Method to Characterize Bias and Uncertainty for Satellite Infrared Measurements of Sea Surface Temperature. *13th Ocean Sciences Meeting*.

Fowler, J. B., 1995: A third generation water bath based blackbody source. *Journal of Research of the*

National Institute of Standards and Technology, **100,** 591-599.

Good, S. A., G. K. Corlett, J. J. Remedios, E. J. Noyes, and D. T. Llewellyn-Jones, 2007: The global trend in sea surface temperature from 20 years of Advanced Very-High Resolution Radiometer data. *Journal of Climate*, **20,** 1255-1264.

Guenther, B., W. Barnes, E. Knight, J. Barker, J. Harnden, R. Weber, M. Roberto, G. Godden, H. Montgomery, and P. Abel, 1996: MODIS calibration: A brief review of the strategy for the at-launch calibration approach. *Journal of Atmospheric and Ocean Science*, **13,** 274-285.

Kilpatrick, K. A., G. P. Podestá, and R. H. Evans, 2001: Overview of the NOAA/NASA Pathfinder algorithm for Sea Surface Temperature and associated Matchup Database. *Journal of Geophysical Research*, **106,** 9179-9198.

Minnett, P. J., R. O. Knuteson, F. A. Best, B. J. Osborne, J. A. Hanafin, and O. B. Brown, 2001: The Marine-Atmospheric Emitted Radiance Interferometer (M-AERI), a high-accuracy, sea-going infrared spectroradiometer. *Journal of Atmospheric and Oceanic Technology*, **18,** 994-1013.

NRC, 2000: *Issues in the Integration of Research and Operational Satellite Systems for Climate Research: II. Implementation*. National Academy of Sciences, 82 pp.

Rice, J. P. and B. C. Johnson, 1996: A NIST Thermal Infrared Transfer Standard Radiometer for the EOS Program. *The Earth Observer*, **8,** 31.

Rice, J. P. and B. C. Johnson, 1998: The NIST EOS Thermal-Infrared Transfer Radiometer. *Metrologia*, **35,** 505-509.

Rice, J. P., J. J. Butler, B. C. Johnson, P. J. Minnett, K. A. Maillet, T. J. Nightingale, S. J. Hook, A. Abtahi, C. J. Donlon, and I. J. Barton, 2004: The Miami2001 Infrared Radiometer Calibration and Intercomparison: 1. Laboratory Characterization of Blackbody Targets. *Journal of Atmospheric and Oceanic Technology*, **21,** 258-267.

Salomonson, V. V., W. L. Barnes, P. W. Maymon, H. E. Montgomery, and H. Ostrow, 1989: MODIS: Advanced facility instrument for studies of the earth as a system *IEEE Transactions on Geoscience and Remote Sensing.*, **27,** 145–153.

Walton, C. C., 1988: Nonlinear multichannel algorithms for estimating sea surface temperature with AVHRR satellite data. *Journal of Applied Meteorology*, **27,** 115-124.

NEW AUSTRALIAN HIGH RESOLUTION AVHRR SST PRODUCTS FROM THE INTEGRATED MARINE OBSERVING SYSTEM

Helen Beggs[1], Leon Majewski[2] and George Paltoglou[1]

[1] *Centre for Australian Weather and Climate Research, Bureau of Meteorology, GPO Box 1289, Melbourne, VIC 3001, Australia*
[2] *Bureau of Meteorology, GPO Box 1289, Melbourne, VIC 3001, Australia,*
Email : H.Beggs@bom.gov.au or ghrsst@bom.gov.au

ABSTRACT

The Australian Bureau of Meteorology (the Bureau) is producing 1 km resolution sea surface temperature (SST) products in real time from Advanced Very High Resolution Radiometer (AVHRR) sensors on board NOAA Polar Orbiter platforms received at the Bureau's satellite reception facilities. As part of the Australian Integrated Marine Observing System (IMOS: http://www.imos.org.au) the Bureau has recently upgraded its SST processing system to comply with the GHRSST-PP (now Group for High Resolution SST) Data Processing Specification v1.6 (Donlon et al., 2005) and up-to-date processing practices. The significant components include the use of regional rather than global buoy SSTs for satellite SST calibration, noise resistance methods of SST coefficient estimation, the development of a match-up database (MDB), calculation of single sensor error statistics (SSES), an analysis of cloud proximity confidence in terms of km rather than pixels, stitching of overlapping raw AVHRR data from several groundstations and the generation and distribution of SST products in GHRSST L2P and L3P format. This paper provides an overview of these advances and the new high-resolution products which will shortly become publicly available through IMOS and the GHRSST Global Data Assembly Centre.

1. INTRODUCTION

The Bureau has calculated SST from High Resolution Picture Transmission (HRPT) AVHRR since the early 1990's using McIDAS (http://www.ssec.wisc.edu/mcidas/). The native format of McIDAS satellite products (e.g. AREA files) has proved a barrier for many user groups to gain access to Bureau generated SST. The GHRSST format allows users to access SST data through the well described and often familiar netCDF interface. In recent years the Bureau has, where possible and practical, adopted the GHRSST format for storing and distributing SST products.

Previously, there have been no single day and single night HRPT AVHRR composite SST products available for the Australian region. The IMOS Satellite SST Products Sub-Facility now produces not only real-time, single-swath, 1 km resolution, HRPT AVHRR SST L2P files, but also near real-time, single sensor, composite, GHRSST format L3P SST products, gridded at 0.01° x 0.01° over the region 90°E to 180°E, 0°N to 55°S for a single night and a single day of data (Figure 1).

(a)

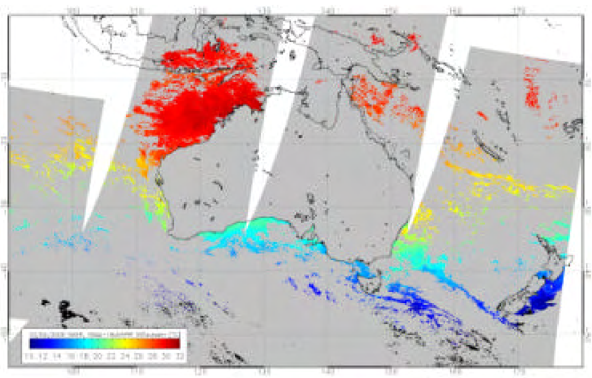

(b)

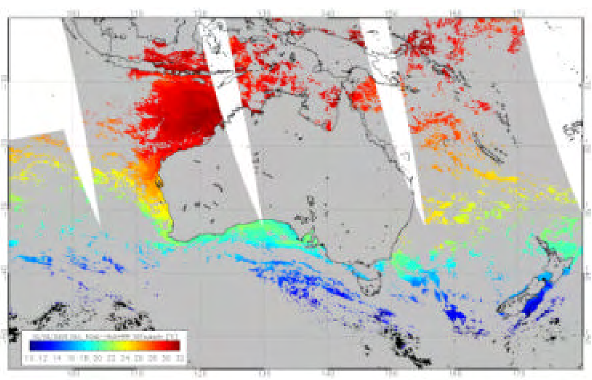

Figure 1. Example of (a) night and (b) day 0.01° x 0.01° L3P composites from locally received NOAA-18 AVHRR SST data for 10 April 2009. The grey areas represent sensor coverage and sensor view angle was less than 60°. SST is plotted for cloud-free pixels (proximity confidence flag = 5).

The aim over 2009 and 2010 is to reprocess archives of raw HRPT AVHRR data to produce these L2P and L3P files from NOAA polar-orbiting satellites back to around 1990.

2. PROCESSING SYSTEM OVERVIEW

The Bureau, in conjunction with a number of consortia, receives HRPT AVHRR data generated from NOAA-17, NOAA-18 and NOAA-19 satellites from six ground stations located around Australia (Melbourne, Perth, Darwin, Townsville, Alice Springs and Hobart) and one in Antarctica (Casey). The raw data is stitched using a method developed by Edward King of CSIRO Marine and Atmospheric Research (King, 2003) and SST is calculated and distributed using the processing system outlined in Figure 2.

AVHRR and associated ancillary data are used to calculate a SST product and an associated cloud mask. A non-linear SST (NLSST) algorithm [*Walton et al.*, 1998] is used in operational processing of daytime AVHRR data. For night-time AVHRR data the MCSST triple window algorithm is used. Regression coefficients for these day/night algorithms were calculated using SST measurements from drifting and moored buoys in the Australian region (75°E to 185°E, 15°N to 65°S). The Regression method used is a Singular Value Decomposition with aggressive zeroing of the weighting matrix. Cloud masks for each data set are determined using the CLAVR-1 algorithm [*Stowe et al.*, 1999].

To comply with the GHRSST L2P and L3P formats, data providers need to supply an uncertainty with the SST product. Uncertainty estimates for valid SST retrievals are determined by comparing the satellite derived SST measurement with quality controlled *in situ* temperature measurements following the Medspiration guidelines [Piolle and Prevest, 2006]. The *in situ* temperature measurements are obtained from a network of drifting buoys and are essential inputs into our Matchup Database and SSES algorithms.

As the cloud contamination scale length has not been well defined for the AVHRR system, the Bureau analysed the matchup error between buoys and AVHRR SST as a function of cloud patterns as defined by the cloud mask. Numerous estimators of cloud contamination scale length were examined and the most efficient was determined as the distance in km to the nearest cloudy pixel. These were then related to the cloud proximity confidence ordinal scale.

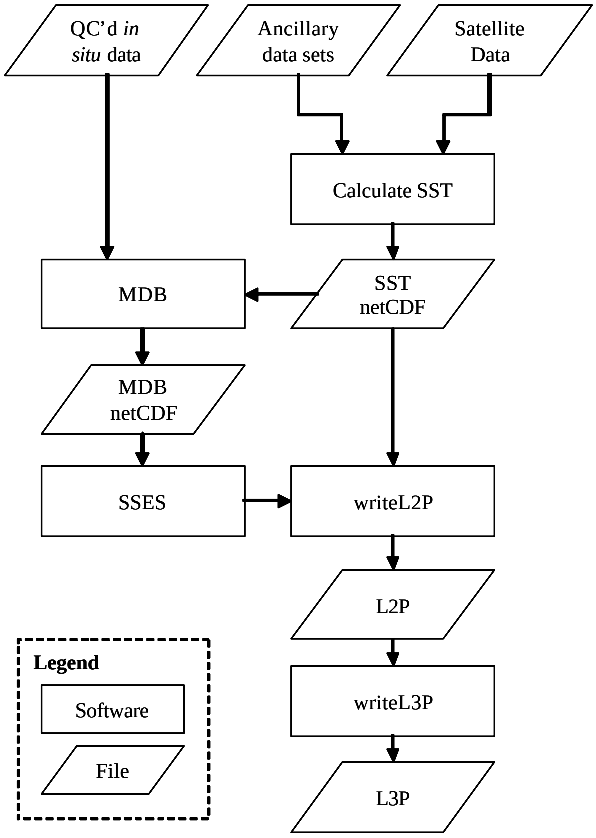

Figure 2. Block diagram of the Bureau of Meteorology new IMOS stellite SST processing system.

In the final stage of the processing system the SST data is packaged with ancillary data (e.g. wind speed) into the GHRSST-PP v1.6 L2P format (Donlon et al., 2005). The L2P file is then distributed to internal and external users and gridded using the mapx library developed at NSIDC (http://geospatialmethods.org/mapx) to produce single day and single night composite GHRSST v2.0 L3P files following the format outlined in Piolle and Casey (2008).

3. MATCHUP DATABASE (MDB)

The Bureau has developed software to compare satellite SST and temperature observations from collocated and contemporaneous drifting buoys. The Bureau have implemented a MDB following the Medspiration MDB guidelines [*Piolle and Prevest*, 2006]. For *each in situ* measurement:

1) Find the closest satellite pixel (valid or not) to *the in situ* measurement.

2) Find the neighbouring pixels that are within a specified spatial and temporal distance to the satellite image pixel identified in step 1. For

example, get all satellite image pixels that are ±12 km and ±2 hours from the *in situ* measurement.

3) Select the closest valid pixel in time then distance. This is the matchup.

4) Calculate the following statistics for the neighbour box identified in step 2:

   a) percentage of valid pixels;

   b) mean sea surface temperature;

   c) standard deviation sea surface temperature;

   d) percentage of pixels having proximity confidence values equal to 0, 1, 2, 3, 4, 5.

Brute force searching across high resolution imagery is computationally intensive. Therefore a failsafe iterative processs was employed to reduce total CPU usage by a factor of 20 over a brute force method. The MDB software allows the temporal and spatial search constraints to be specified via XML.

An analysis of NOAA-17 and 18 data indicated that proximity confidence values based on a 3D lookup table of distance to nearest cloud, satellite zenith angle, and day/night pass could be used advantageously and was therefore implemented.

4. CALCULATION OF SSES

Results from the MDB are used to calculate SSES, following the GHRSST-PP Data Processing Specification v1.6 (Donlon et al., 2005). Currently a spatial search size of ±12 km and a time difference threshold of 2 hours are used within the MDB to generate matches to be used in SSES calculation. Matchups from the preceding three weeks are sorted into groups by proximity confidence value. For each proximity confidence group the difference between satellite and *in situ* SST is calculated. From this difference a bias and standard deviation is obtained and used to fill the SSES fields. Figure 3 shows the matchup statistics for NOAA-17 and NOAA-18 for a proximity confidence of 5 (best) for the Australian region covering the period 17 December 2008 to 4 April 2009.

For NOAA-17 nighttime standard deviation was 0.22°C and daytime was 0.42°C. For NOAA-18 nighttime standard deviation was 0.32°C and daytime was 0.40°C. These values compare very favourably with the Bureau's pre-existing level 2 HRPT AVHRR SST products of 0.53°C and 0.59°C for nighttime matchups over the same period for NOAA-17 and NOAA-18 respectively.

(a)

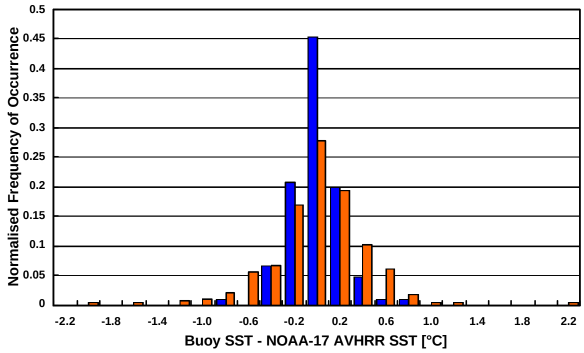

(b)

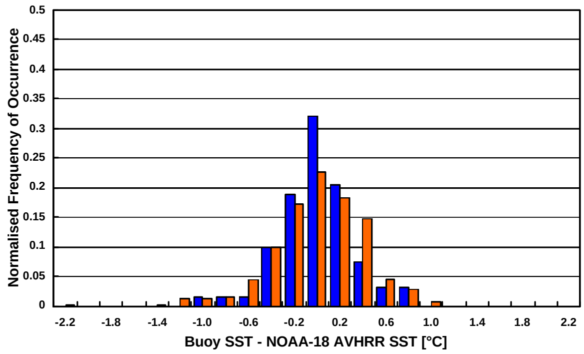

Figure 3. Histogram of matchup statistics for HRPT AVHRR SST from (a) NOAA-17 and (b) NOAA-18 for proximity confidence=5 for the Australian region pver the period 17 December 2008 to 4 April 2009. Blue bars represent nighttime data and orange represents daytime.

Much of this improvement to the errors has been achieved by taking care when determining the high class data in the L2P and L3P files (ie. proximity confidence = 5). Therefore, by analysing matchups versus distance to nearest cloud, it was determined that it is necessary to be 6 km away from cloud to have minimal chance of cloud contamination. The HRPT AVHRR data has also been restricted to satellite zenith angles < 50°. Other improvements to the processing have been to stitch the overlapping raw data from a number of groundstations, use regional rather than global buoy observations in producing the regression coefficients for the SST NLSST algorithms and to optimise the fit of the HRPT AVHRR radiances to the *in situ* SST data.

5. DATA DISTRIBUTION AND ACCESS

These GHRSST formatted HRPT AVHRR L2P and L3P data files are being made available to the IMOS Australian Oceans Distributed Active Archive Centre

(AO-DAAC) to increase awareness and access to the Bureau's data. The AO-DAAC is designed to make various remotely sensed ocean products available to researchers through an OPeNDAP interface, associated metadata database and web interface (King *et al*., 2008).

A web-based interface to the AO-DAAC system has been provided at http://www.eoc.csiro.au/aodaac, where the spatial extent of the requested data can be specified using a Google-Maps interface. The requested data can be returned as a set of OPeNDAP URLs, ASCII text, or extracted into a single HDF file.

Later in 2009, it is planned to also make the same L2P and L3P files available to a wider audience via the GHRSST Global Data Assembly Centre hosted by JPL's PO.DAAC (http://ghrsst.jpl.nasa.gov) and the GHRSST Long-Term Stewardship and Reanalysis Facility hosted by NODC (http://ghrsst.nodc.noaa.gov).

6. CONCLUSION

As part of the IMOS Project the Bureau of Meteorology has recently commenced producing HRPT AVHRR SST level 2 and level 3 products in the GHRSST-PP v1.6 L2P and GHRSST v2.0 L3P formats. These files will be made available through an IMOS OPeNDAP server accessible via http://imos.org.au/srs_data.html by July 2009 and through the GHRSST GDAC by December 2009.

The new IMOS HRPT AVHRR L2P SSTs are significantly more accurate than the Bureau's pre-existing HRPT AVHRR level 2 SST data from NOAA-17 and NOAA-18 satellites, with standard deviations of night-time matchups with drifting and moored buoys approximately halved through improved processing techniques.

By late 2009 it is planned that the AVHRR L2P products will be incorporated into the Regional Australian Multi-Sensor SST Analysis [RAMSSA; *Beggs*, 2007] that produces 1/12° resolution, daily SST analyses over the Australian region (20°N - 70°S, 60°E - 170°W). They will also be used in diurnal warming studies of the oceans near Antarctica and the Tropical Warm Pool north of Australia. The single day and single night HRPT AVHRR SST L3P data will be used by researchers at the University of Western Australia in the Transient Coastal Upwelling Along Ningaloo Reef Project. This project is all ready using the Bureau's legacy HRPT AVHRR SST 14-day, 0.01° x 0.01° resolution, Mosaic L3P products, and the enhanced accuracy and smaller temporal resolution is expected to significantly benefit this coral reef study.

7. ACKNOWLEDGMENTS

This work is supported by the Integrated Marine Observing System (IMOS) – an initiative of the Australian Government being conducted as part of the National Collaborative Research Infrastructure Strategy.

8. REFERENCES

Beggs, H. (2007), *A high-resolution blended sea surface temperature analysis over the Australian region*, *BMRC Research Report, RR130,* Bur. Met. Australia. 43 pp. (http://www.bom.gov.au/bmrc/pubs/researchreports/RR130.pdf)

Donlon, C. and the GHRSST-PP Science Team (2005) The Recommended GHRSST-PP Data Processing Specification GDS (Version 1 revision 1.6), *GHRSST-PP Report Number 17*, http://www.ghrsst-pp.org/documents.htm?parent=50

Donlon, C. and the GHRSST Science Team (2008) GHRSST Data Specification v2.0, 9 December 2008 Draft, http://www.ghrsst-pp.org/documents.htm?parent=76

King, E.A. (2003) The Australian AVHRR Data Set at CSIRO/EOC: Origins, Processes, Holdings and Prospects, *CSIRO Earth Observation Centre Report 2003/04, Canberra, Australia.* http://www.eoc.csiro.au/cats/caps/capshome.html

King, E. (2008) eResearch Australasia 2008, Melbourne, Australia.

Piolle, J., and C. Prevest (2006), Match-up database user manual, [online] Available from: http://www.medspiration.org/tools/mdb/ (Accessed 3 July 2008)

Piolle, J. and K. Casey (2008) The Recommended GHRSST Data Specification (GDS) L3 Product Specification, [online] Available from: http://www.ghrsst-pp.org/modules/documents/documents/GDS-v2.0-rev0.1-core-L3-product-format-specification_003.doc, 30 October 2008.

Stowe, L. L., P. A. Davis, and E. P. McClain (1999), Scientific basis and initial evaluation of the CLAVR-1 global clear /cloud classification algorithm for the Advanced Very High Resolution Radiometer, *Journal of Atmospheric and Oceanic Technology*, *16*(6), 656-681.

Walton, C. C., W. G. Pichel, J. F. Sapper, and D. A. May (1998), The development and operational application of nonlinear algorithms for the measurement of sea surface temperatures with the NOAA polar-orbiting environmental satellites, *J Geopyhs Res*, *103*(C12), 2799-28012.

HIGH RESOLUTION SST FIELDS: THE MEDSPIRATION PROJECT

Jean Tournadre, Jean-François Piollé, Emmanuelle Autret, and Pierre Tandéo

IFREMER, Laboratoire d'Océanographie Spatiale, Plouzané, France. email:jeant@ifremer.fr j

ABSTRACT

The GODAE High Resolution SST Pilot Project (GHRSST-PP) aims to combine all the available Sea Surface Temperature data from across the globe to form a high resolution, high accuracy and high availability SST product for applications in short, medium and decadal/climate time scales. The Medspiration project, sponsored by the European Space Agency is a component of the GHRSST-PP whose goal is the production of near real time ultra high resolution (2km) SST fields for the Mediterranean Sea. The first processing task is the generation of so-called L2-P single satellite SST products. The second is to collate the data from different sensors and to produce an analyzed L4 SST field (through objective analysis). The system is operational since mid-2005. The processing chain is presented as well as a first assessment of the first two years of data.

1. INTRODUCTION

In 2002, GODAE (Global Ocean Data Assimilation Experiment) initiated the GODAE High Resolution SST Pilot Project, GHRSST-PP to address an emerging need for accurate high resolution sea surface temperature (SST) products (1). SST is required by operational ocean and atmospheric forecasting systems to constrain the modeled upper ocean circulation thermal structure and for exchange of energy between the ocean and atmosphere. The goal is to combine all the available SST data from across the globe to form a high resolution, high accuracy and high availability SST product. It is organized as a partnership between regional groups responsible for generating SST products, to a common specification, within a limited geographical area. The primary task of the Regional Data Assembly Centers is to collate all level 2 satellite SST measurements within their region, perform quality assessment and reissue the data in a common format (GHRSST L2P data) including a measure of the quality of every measurement. Some centers also use the L2P data to produce global or regional analyzed SST products (called GHRSST L4 data), using well defined procedures. Medspiration has been created by ESA in 2004 to serve as a European DAC for GHRSST-PP, generating L2P and MDB products for the Atlantic Ocean and its adjoining seas (2). Medspiration has also the task of producing an ultra-high resolution (2 km) analyzed SST product for the Mediterranean Sea. The Medspiration system is operational for the European Seas since 2005 and after a test period the processing chain has been stabilized beginning of 2006. Two years of data (2006-2007) have been produced with only minors processing changes. This archive provides a good opportunity to evaluate and to analyzed the interest of ultra high resolution analyzed SST fields.

2. ANALYZED L4 SST MEDSPIRATION PRODUCTS

The concept of SST concept is by itself not trivial and it requires a definition as precise as possible to allow a pertinent inter-comparison of the different measurements. The definition we used is the one defined within GHRSST (1). Without going into the details of the measure of SST from space (see for ex. (3)), the basic principle is the measurement of brightness temperature of the sea surface by space borne radiometers.

The Medspiration analyzed (L4) SST are produced at ultra-high resolution on a 2x2 km² grid for the Mediterranean Sea. Optimal interpolation (OI) techniques are used to combine all coincident L2P SST data and to fill gaps where no observations are available. Whereas L2P data essentially represent the skin or sub-skin SST, the L4 SST product is defined to represent SST foundation as defined by the GHRSST-PP team and is updated only once every 24 hr. As the parametrization of the diurnal cycle is up to now not fully operational, the analysis is conducted on nighttime data (from 8 pm to 6 am) only to eliminate any possible diurnal warming. The analysis is produced every day around 18:00 for the day before. It is centered at 00:00 UTC. The first step of the L4 processing aims at reducing the number of observations involved in the analysis by selecting the best possible observations in the neighborhood of the grid points and to create for each sensors and each day a collated data file (called L3 products) . The L2P SST data are thus checked and the best estimate, i.e. valid and closer to the analysis time, is then selected using the solar zenith angle. The resulting collated files, which contain one L2P observation per grid point, per sensor and per day, constitute the base of the Optimal Interpolation. The configuration used for the Mediterranean SST fields is the following; Latitude : 30.0 N to 46.5 N; Longitude: 18.0W to 36.5 E, Grid step: 0.02; Grid points : 825x2750; Processing hour : 00:00 UT; Zonal and meridional correlation lengths : 50 km;Time correlation scale: 5 days.

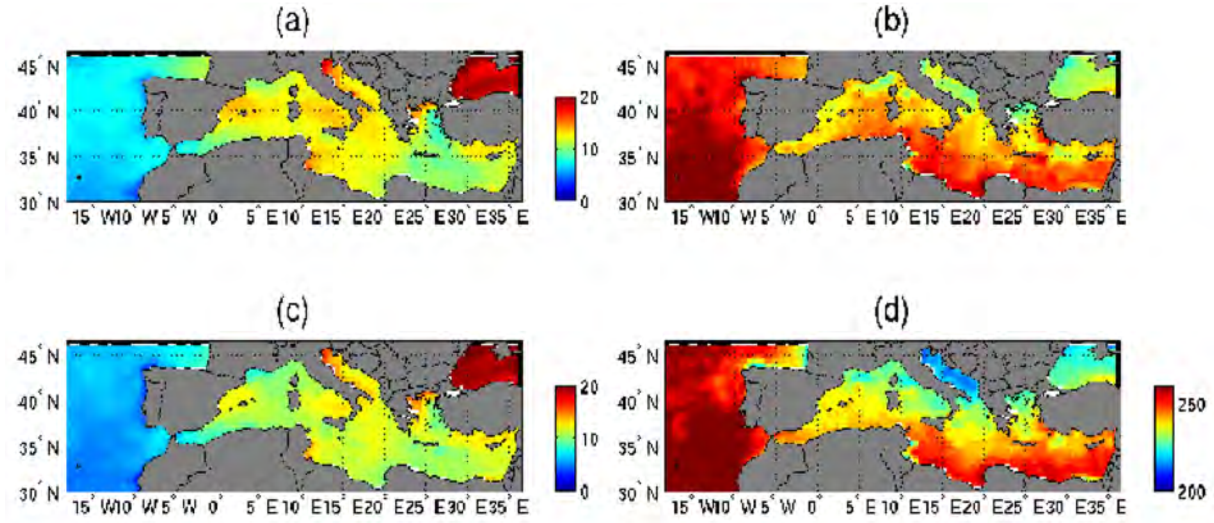

Figure 1: Amplitude (a) and phase (b) of the SST seasonal cycle for 2006 and (c) and (d) for 2007.

The L2P and L4 SST data sets are available in netcdf format at http://www.medspiration.org. The L4 archive covers the whole 2006 and 2007 years except for 3 missing days in 2006.

3. EXAMPLE OF APPLICATION THE MEDITERRANEAN SEASONAL CYCLE.

The SST seasonal cycle of the Mediterranean sea has been computed by sinusoidal fitting and analyzed for 2006 and 2007 . The amplitude and phase are presented in Figure 1. The figure shows the large variability of the cycle between the Atlantic and the Mediterranean Sea. as well as the large differences between 2006 and 2007 especially in the western Med. In 2006, the Near Atlantic is characterized by a weak seasonal cycle of about 7K, while in the Western and Central basins, which experienced very high summer temperatures, the amplitude reached 15 to 20 K; In the Eastern Med. where Etesian winds limited the summer maximum the amplitude remained between 12 and 17 K. The phase of the cycle represented here by the day of the maximum SST clearly delineates three main zones: the near Atlantic where the maximum is reached at the end of summer (September), the northern Med. (north of 37 N) basin where it is reached in early August and the Southern Med. where it is reached in late august. In 2007, the picture changed dramatically. While there are little changes in the Near Atlantic (amplitude between 5 and 10 K) and in the Eastern Med. the amplitude of the seasonal cycle in the Central and Western Med. decreases by about 3-5 K while the phase of the cycle occurs about 20 days later than in 2006.

4. CONCLUSION

The Medspiration project has been successful in producing ultra high resolution daily SST fields complying with the L4 format specification of GHRSST-PP. The archive covers more than two years with the same processing scheme. The main problem encountered during operation, apart from the technical data transmission one, concerns the inter-calibration of the different L2P SST's. New analysis systems such as the one developed for Mersea Project includes operational inter-calibration algorithm that were build on the Medspiration experience. The L4 data set also opens for new scientific studies of the Mediterranean sea dynamic at very resolution that were not possible from single SST images.

5. REFERENCES

1. C. Donlon et al., “The Global Ocean Data Assimilation Experiment High-resolution Sea Surface Temperature Pilot Project,” Bull. Amer. Meteor. Soc., vol. 88, pp. 1197--1213, 2007.
2. O. Arino, C. Donlon. I. S. Robinson, J-F. Piolle, and P. Leborgne, “Medspiration : A Precursor to the GMES Marine Core Service Sea-Surface Thematic Assembly Centre,” E.S.A bulletin ISSN 0376-4265, vol. 132, pp. 50--56, 2007.
3. I. S. Robinson, Measuring the Ocean from space. *The principles and methods of satellite oceanography*, Springer-Praxis Pub. Ltd, Chichester, UK, 2004.

L2P and L3 SST data produced by EUMETSAT/OSI-SAF and EC/MyOcean

Pierre Le Borgne, Gérard Legendre, Anne Marsouin, Francoise Orain and Hervé Roquet
Meteo France CMS
22302 Lannion, France

Contact: Pierre.leborgne@meteo.fr

ABSTRACT

The EUMETSAT Ocean and Sea Ice Satellite Facility (OSI SAF) have officially adopted The GHRSST L2/L3P format for all their SST products. The OSI SAF SST production system is based on two processing chains: one dedicated to polar orbiter AVHRR data, the second to geostationary satellite data.

The OSI SAF AVHRR chain is now fully operational and is producing SST L2P and L3P from METOP at full resolution on a global scale (see figure 1) and from NOAA-18 on a regional (European seas, figure 2) scale.

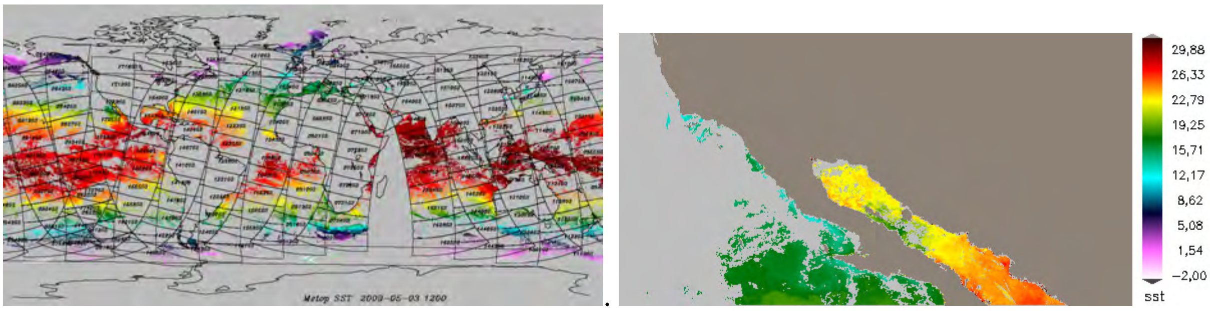

Figure 1; left: global L3P on the 03/05/09 centered at 1200 UTC showing the contribution of the 3minute granules and right: 1 km resolution granule over California on the same day.

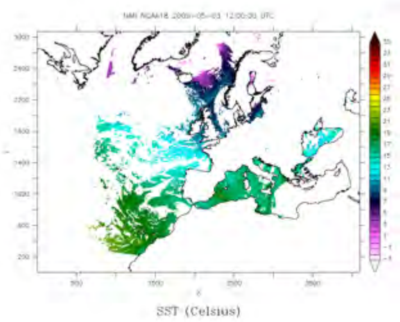

Figure 2: 2 km resolution NOAA18 SST over Europe (NAR area)

The future OSI SAF geostationary SST chain is expected to be operational in 2010: A prototype has been developed and has been producing routinely SST fields over the MSG SEVIRI globe at full resolution every 15 minutes since January 2009. Compared to the present OSI SAF Atlantic product coverage, the MSG/ Seviri zone will be extended to 60E to include the western Indian Ocean (figure 3). Diurnal warming and front maps will be delivered as experimental products aside from the SST L3P (figure 3).

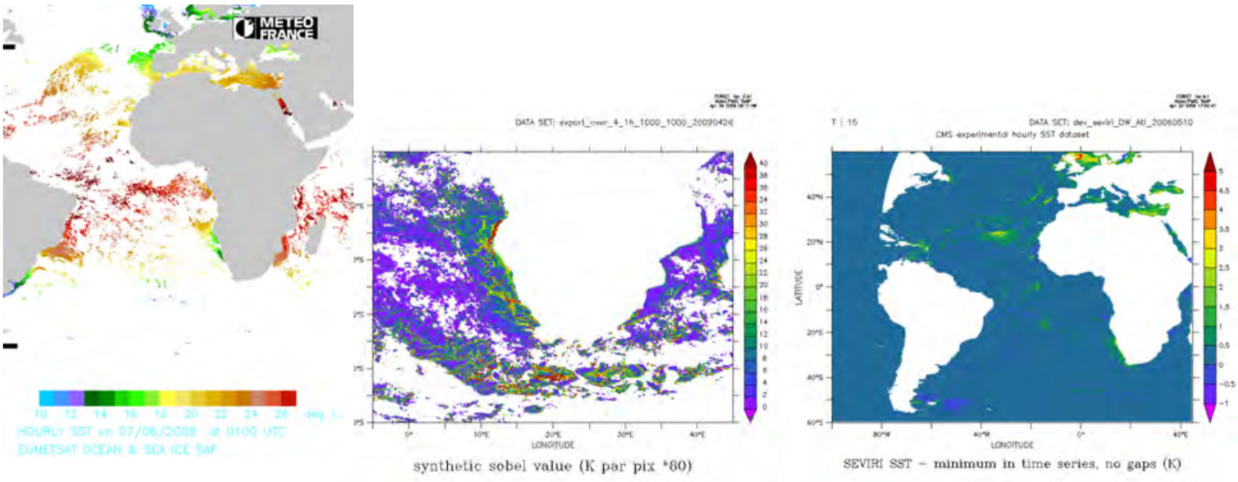

Figure 3; left: new coverage of the EUMETSAT/OSISAF MSG SST products; middle: front maps over south Africa; right: diurnal warming over the Atlantic.

In the framework of the EC/MyOcean project, L3 (collated) products (figure 6) as well as L4 (analyses, see also E. Autret's presentation) will be soon delivered on an operational basis.

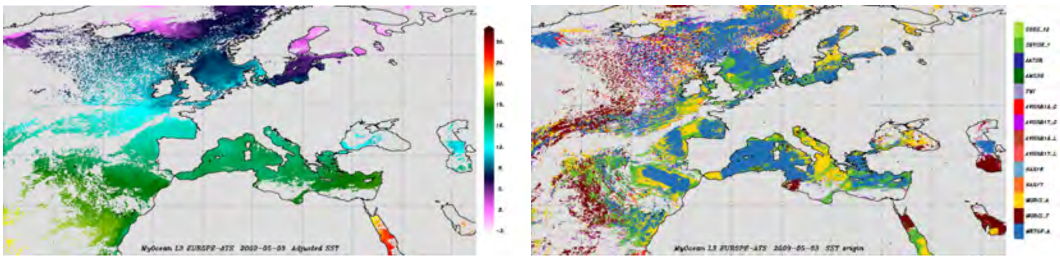

Figure 6; left: EC/MyOcean collated L3 on the 3rd of May 2009 and right: origin of the data.

The presentation will detail the characteristics of the products and present validation results.

MW SST L2P DATA

Chelle L. Gentemann[1]

[1] *Remote Sensing Systems, 438 First St. #200, Santa Rosa, CA 95401 (USA), Email: Gentemann@remss.com*

ABSTRACT

The complete time series of SST data from the Tropical Rainfall Measuring Mission's (TRMM) Microwave Imager (TMI) and AQUA's Advanced Microwave Scanning Radiometer – Earth observing system (AMSR-E) have been produced in the Group for High Resolution Sea Surface Temperature (GHRSST) Level-2 Pre-processed (L2P) fomat. These data, and others, are then used to produce a global 9 km SST product, output in GHRSST Level-4 (L4) format.

1. INTRODUCTION

Inclusion of satellite sea surface temperatures (SSTs) in data fusion analyses or numerical models requires accurate estimates of retrieval errors in near real-time (NRT). The primary error sources of satellite SST retrievals are due to errors in spacecraft navigation, sensor calibration, sensor noise, and the retrieval algorithm. Comparisons to in situ data and interpolated satellite SSTs products are utilized to investigate errors in the microwave (MW) SSTs. Individual retrieval errors are calculated, assuming that errors are independent and additive in a root-sum-squared sense. These new GHRSST files include time of measurement, MW SST, estimated bias, and estimated standard deviation.

2. TMI AND AMSR-E L2P DATA

The Tropical Rainfall Measuring Mission (TRMM) Microwave Imager (TMI) was launched in December 1997. Orbiting at an altitude of about 400 km, this sun-asynchronous satellite is in an equatorial orbit retrieving data within 39 degrees latitude. The orbit precesses through the diurnal cycle, measuring a complete cycle every 23 days (Kummerow et al., 1998). National Aeronautics and Space Administration's (NASA) Aqua satellite, launched May 4 2002, carries the Japan Aerospace eXploration Agengy (JAXA)'s Advanced Microwave Scanning Radiometer – Earth Observing System (AMSR-E) microwave radiometer. This is the first polar orbiting microwave radiometer capable of accurate global SSTs since the poorly calibrated Scanning Multichannel Microwave Radiometer (SMMR) was launched in 1978 (Wentz et al., 2000).

3. IN SITU DATA FOR VALIDATION

Errors are determined using co-locations with *in situ* data. NRT *in situ* measurements are downloaded daily from the Global Ocean Data Assimilation Experiment (GODAE) Monterey server, which is sponsored by the Office of Naval Research (ONR) and hosted by the Fleet Numerical Meteorology and Oceanography Center (FNMOC). These measurements are obtained by FNMOC from the GTS and processed for the GODAE server. Measurements from ship engine room intakes, fixed (moored) buoys, drifting buoys, ship hull sensors, and CMAN stations are included in the dataset. Each measurement is assigned a probability of random error based on comparisons with climatology and forecast fields (Cummings).

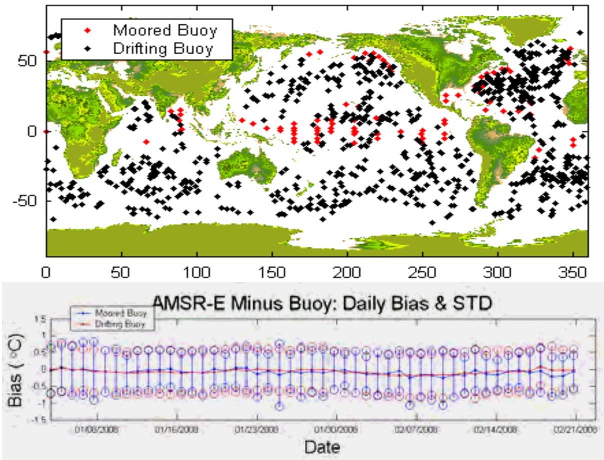

Figure 1. Top panel: AMSR-E and in situ data co-locations, 6 February 2008. Bottom panel: Daily bias and standard deviation from co-locations.

Errors are determined in a NRT sense by using collocations with buoys from the GTS network to calculate a 'global' daily mean bias and standard deviation (STD) (Figure 1). These are then adjusted using static lookup tables based on a priori knowledge of other error sources. The static tables are derived through extensive inter-comparison of MW SSTs with moored buoys and interpolated satellite SSTs (Figure 2).

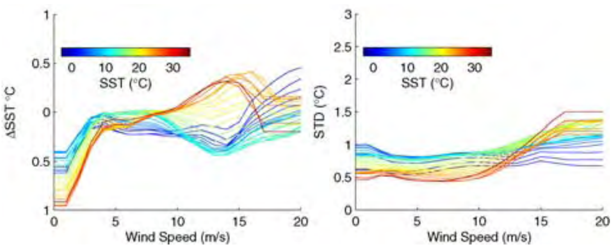

Figure 2. Nighttime AMSR-E minus Reynolds as a function of SST and wind speed.

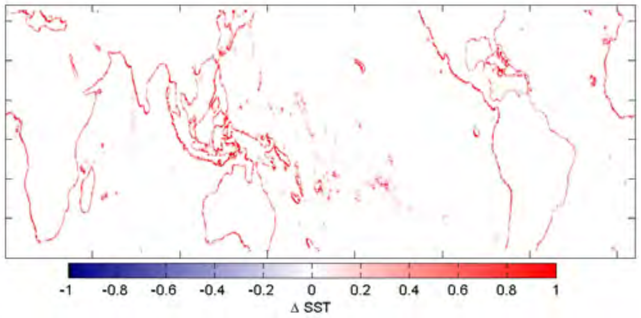

Figure 3. Estimate of bias due to sidelobe contamination near land.

4. ADDITIONAL DATA QUALITY

Rejection and confidence flags are assigned to each pixel. Most users should simply utilize data with a proximity confidence value equal to 4 (Table 1). For advanced users, the confidence flag value contains information on which quality tests were failed. For TMI, land contamination is a problem in the SSTs (Figure 3). Using either a proximity confidence value equal to 4 or examining the bit 5 confidence flag will remove most land contaminated data.

Table 1. Microwave Proximity confidence value (MWPCV) definitions.

Value	Definition
1	Bad: Data has been rejected
2	Suspect: Data that may be contaminated, (any confidence flags thrown except DW)
3	Unprocessed: Data that have not been classified by confidence flags. This data should be fine.
4	Excellent: Data that we think are good

Table 2. Microwave confidence flags definitions.

Bit	Definition
0	rain present within 50km and difference from yesterday's OI SST greater than 0.6 K
1	rain present within 100km and difference from yesterday's OI SST greater than 0.8 K
2	ice present within 150 km and difference from yesterday's OI SST greater than 0.6 K
3	difference from yesterday's OI SST greater than 5 K
4	STD and Mean calculated from yesterday's OI SST from data within 250 km of pixel. SST at pixel required to be within 3*STD of mean
5	land present within 125 km and difference from yesterday's OI SST greater than 0.6 K
6	diurnal warming calculated from model greater than 1 K
7	diurnal warming calculated from model greater than 0.3 K

5. ANCILLARY DATA

The microwave SSTs are considered a sub-skin measurement. To compare them to infrared skin SSTs, a correction for the cool skin layer, usually 0.1 to 0.3 K, is necessary. Below the skin layer, thermal stratification established by solar heating is referred to as a diurnal warm layer or diurnal thermocline. Surface temperature deviations greater than 3.0 K, referenced to subsurface temperatures below the extent of surface heating, are not uncommon and may persist for hours (Kawai and Wada, 2007; Minnett, 2003; Yokoyama et al., 1995). Even larger amplitudes of diurnal warming (up to 4 – 6 K) have been reported in several studies (Flament et al., 1994; Gentemann et al., 2008; Merchant et al., 2008).

Since both the cool skin and diurnal warming may affect the measured sub skin SST provided by TMI and AMSR-E, these are provided as ancillary data in the orbital and gridded L2P files. Cool skin is estimated using the Wick skin model. The Gentemann et al. diurnal (2003) model determines diurnal warming as a function of wind speed, daily average solar insolution, and local time of day. This is used to determine the diurnal warming for each measurement.

6. CONCLUSION

The TMI and AMSR-E L2P dataset is available from 1998 – present (TMI) and 2002 – present (AMSR-E). Ancillary data, such as estimates of measurement error, diurnal warming, and the cool skin improve the usefulness of the data.

7. REFERENCES

1. Flament,P., M.Firing, M.Sawyer, and C.Trefois. 1994. Amplitude and horizontal structure of a large diurnal sea surface arming event during the coastal ocean dynamics experiment. *Journal of Physical Oceanography* 24(1):124-139.
2. Gentemann,C.L., C.J.Donlon, A.Stuart-Menteth, and F.J.Wentz. 2003. Diurnal signals in satellite sea surface temperature measurements. *Geophysical Research Letters* 30(3):doi:10.1029/2002GL016291.
3. Gentemann,C.L., P.J.Minnett, P.Le Borgne, and C.J.Merchant. 2008. Multi-satellite measurements of large diurnal warming events. *Geophysical Research Letters* 35(L22602):doi:10.1029/2008GL035730.
4. Kawai,Y. and A.Wada. 2007. Diurnal sea surface temperature variation and its impact on the atmosphere and ocean: a review. *Journal of Oceanography* 63(5):721-877.
5. Kummerow,C.D., W.Barnes, T.Kozu, J.Shieu, and J.J.Simpson. 1998. The tropical rainfall measuring mission (TRMM) sensor package. *Journal of*

Atmospheric and Oceanic Technology 15(3):809-817.

6. Merchant,C.J., M.J.Filipiak, P.Le Borgne, H.Roquet, E.Autret, J.-F.Piollé, and S.Lavender. 2008. Diurnal warm-layer events in the western Mediterranean and European shelf seas. *Geophysical Research Letters* 35:doi:10.1029/2007GL033071.
7. Minnett,P.J. 2003. Radiometric measurements of the sea-surface skin temperature - the competing roles of the diurnal thermocline and the cool skin. *International Journal of Remote Sensing* 24(24):5033-5047.
8. Wentz,F.J., C.L.Gentemann, D.K.Smith, and D.B.Chelton. 2000. Satellite measurements of sea surface temperature through clouds. *Science* 288(5467):847-850.
9. Yokoyama,R., S.Tanba, and T.Souma. 1995. Sea surface effects on the sea surface temperature estimation by remote sensing. *International Journal of Remote Sensing* 16:227-238.

NOAA GHRSST data: GOES/MTSAT/MSG L2P and blended GOES/POES Analysis

Eileen Maturi [(1)], John Sapper [(1)], Jonathan Mittaz [(2)] and Andy Harris [(2)]

(1) NOAA/NESDIS, (2) University of Maryland, Cooperative Institute for Climate Studies (CICS)
Email : eileen.maturi@nesdis.noaa.gov

1. INTRODUCTION

The National Oceanic and Atmospheric Administration's (NOAA) office of National Environmental Satellite Data and Services (NESDIS) generates operational geostationary Level-2P (L2P – "P" stands for preprocessed) and a blended geostationary and polar orbiting Level 4 SST analysis to satisfy the requirements of the GHRSST users.

2. NOAA LEVEL-2P SST PRODUCTS

Background

The accuracy of the sea surface temperature for each pixel is important for user's applications. This is important for many marine applications, numerical weather predication (NWP) and also for monitoring the global climate. The L2P format provides this user information by appending the single-sensor error statistics (SSES) to the standard SST value at each pixel plus a number of ancillary data records which include latitude, longitude, time, cloud proximity, aerosol optical depth, wind speed, surface solar irradiance, and sea ice fraction. The single-sensor error statistics parameters are the primary means of providing end-users with quantitative information on data accuracy.

Single Sensor Error Statistics (SSES) Methodology

Retrieval errors have been characterized for the GOES SST retrievals using NCEP forecast fields and fast radiative transfer modeling. Since the CRTM (Community Radiative Transfer Model) fast model is already run for the Bayesian probabilistic cloud detection as part of the processing this information is readily available and are written out to intermediate files for use in calculation of retrieval bias and standard deviation. The retrieval errors are assumed to depend on clear-sky transmittance (the main cause of non-linearity in linear retrieval methods) and air-sea temperature difference (ASTD). The dependence of bias on ASTD itself is assumed to be a function of clear-sky transmittance, since the sensor receives less signal from the surface in lower transmittance atmospheres and the success of the retrieval is therefore more dependent on being close to the mean state used to derive the linear retrieval coefficients in such cases.

While the current GOES SSESs are derived from buoy matchup data selected with a single clear sky probability range of greater than 95%, the MTSAT1R

and MSG-2 SSESs are derived in 4 separate clear sky probability bands of 0.8-0.95, 0.95-0.99, 0.99-0.999 and greater than 0.999. The appropriate SSES for each probability band is then derived in a similar manner to that for GOES, *i.e.* is a function of clear-sky transmittance and ASTD. The division of the SSES into separate clear sky probability bands allows for a more accurate parameterization of the SSES taking into account the possible presence of clouds within any given pixel.

GOES E/W L2P SST Products

NOAA provides full L2P SST products for GOES E/W as part of its operational processing. The L2P products are derived from ½-hourly GOES-East & West North & South sectors in native satellite projection and include the full L2P ancillary fields.

MTSAT/MSG L2P SST Products

Again, NOAA provides full L2P SST products for MTSAT1R and MSG as part of routine operations. For MTSAT1R1 the L2P product is produced every hour in native satellite projection whereas for MSG-2 the L2P product is produced every 15 minutes. Both the MTSAT1R and MSG-2 L2P products contain the full L2P ancillary field

3. NOAA SST ANALYSIS PRODUCTS

Background

Since the SST has a strong influence on many air-sea exchange processes it is a key parameter in many environment and process models. Although there are many in situ observations from moored and drifting buoys and ships, a truly global coverage is only obtainable from an analysis incorporating satellite borne instruments. Each instrument has its own strengths and weaknesses, depending on the sensor type, platform, orbit and so on. The production of an accurate SST is dependent on merging the data from these sources, accounting for the differing measurement methods and accuracies, while maintaining as much of the information in the observations as possible. In order to capture the best of each sensor, a blended SST analysis has been implemented.

NOAA's POES-GOES Blended product

Operational SST retrievals from NOAA's GOES and POES satellites are used to produce a daily global, high-resolution SST Analysis. The method employs a recursive estimation algorithm which emulates the Kalman filter, with a very fast multiscale OI algorithm used for the update step (Fieguth et al., 1998, 2002). This approach preserves fine-scale structure in SST estimates, and allows geophysical realistic treatment of land-sea boundaries. The sequential estimation technique enables observations from different times to contribute appropriately to the SST estimate, and realistic error estimates based on both old and new SST observations are propagated. The approach is to divide and conquer; statistics are sought to conditionally decorrelate spatial subsets of observations so that each can be processed independently. In physical terms, this corresponds to assuming that for each subset, the influence of the external SST field can be completely represented by knowledge of the SST around the boundary. Completely sampling the boundary would result in an optimal solution. However a useful approximation can be achieved by sub-sampling the boundary, offering a computationally efficient method for interpolation of extremely large datasets. Square artifacts in estimates can sometimes result from inadequate sampling of the boundary, but recent improvements to the boundary sampling method have minimized this problem.

A prior model which captures the inherent spatial variability of the SST field must be determined. Investigation with model data has demonstrated that it is necessary to use non-stationary anisotropic models which adapt to the measurement density of the SST observations. This is achieved using a multi-pass approach in which a range of fixed correlation lengths are used to generate stationary estimates which are then interpolated to produce the desired, non-stationary estimates and errors, that is, we are using a mixture of stationary models to accurately mimic the effect of a non-stationary prior (see Khellah et al., 2003).

In the prediction step, the system dynamics are used to predict both the new SST estimate and the associated error information. We assume that the ocean dynamics are very slow so that a very simple dynamic model --- each pixel independently evolving randomly --- is appropriate. This model implies the following simple estimate prediction: $T(t|t-1) = T(t-1|t-1)$, *i.e.* no climatological drift is applied to the previous day's analysis. The prior is modified implicitly by introducing new measurements; that is, we consider that the measurement at any time t consists of two independent components; the new SST observations, and the predicted estimate from the previous time step. The new SST estimate is simply obtained by adding the estimated anomaly field to the previous SST estimate. Propagation of error statistics is achieved by appropriately down weighting the impact of the previous SST estimate by increasing the associated error variance and calculating error estimate based on both this error and the observational error associated with the new observations.

Observational noise is empirically determined from each dataset, (this may be constant or spatially varying) as this is vital in ensuring appropriate SST and error estimates in the analysis. The observational SST data are quality-controlled using a spatio-temporally varying consistency check with the previous day's SST analysis and individual dataset bias estimates (the thresholds vary according to both the error estimate in the analysis and the estimate of SST variability). Data are then averaged into the 0.1 degree spatial resolution used in the analysis.

The RTG SST (Real Time Global Sea Surface Temperature) product has been chosen as the reference dataset, as the quality of the SST retrieval is good in terms of low noise and cloud contamination. The use of physical retrieval methodology in the RTG SST estimation helps to reduce retrieval biases *c.f.* more traditional regression-based AVHRR SSTs. Data from each of the GOES instruments are averaged separately into day and night. NOAA-18 nighttime, MetOp-A daytime and NOAA-18 nighttime are each considered as separate datasets.

An appropriate spatially-varying bias correction with respect to the RTG analysis is estimated and applied to each of the other contributing datasets. This bias is updated by taking a weighted average of the bias estimate and the observed bias of the observations with the RTG analysis for the current day. The resulting SST analyses exhibit realistic evolution of SST anomalies and good estimation of coastal SST gradients (http://www.orbit2.nesdis.noaa.gov/sod/mecb/blended_validation/test/index.html).

Fieguth, P.W. et al., ``Mapping Mediterranean altimeter data with a multiresolution optimal interpolation algorithm'', J. Atmos. Ocean Tech, 15 (2): 535-546, 1998.

Khellah, F., P.W. Fieguth, M.J. Murray and M.R. Allen, ``Statistical Processing of Large Image Sequences'', IEEE Transactions on geoscience and remote sensing 14 (1), 80-93, 2005

JAXA SST Algorithm for AMSR-E

Akira Shibata
Japan Aerospace Exploration Agency
shibata.akira@jaxa.jp
(phone) +81-29-868-2724

The Advanced Microwave Scanning Radiometer for EOS (AMSR-E) aboard the National Aeronautics and Space Administration (NASA) Aqua has been providing sea surface temperature (SST) in global oceans since June 2002 up to the present. SST retrieving algorithm for AMSR-E in Japan was developed at the Earth Observation Research Center (EORC) of the Japan Aerospace Exploration Agency (JAXA), and it has been used to produce the AMSR-E SST operationally.

The JAXA SST algorithm is based on a physical model as described in the followings. The first step is to make adjustments to the AMSR-E 6GHz brightness temperature (Tb) at vertical (V) polarization (6V) to take into account the following corrections: (a) salinity correction, (b) incidence angle correction, (c) atmospheric corrections using 23V and 36V data, which are also used to mask rainy areas, and (d) wind effect correction using the horizontal data at 6GHz (6H). The corrected 6V is then converted to SST using the Fresnel formula, assuming calm ocean condition, ocean salinity of 35 psu and an incidence angle of 55.0 degree.

Among several corrections on 6V, the wind effect correction is most difficult and needs several attentions. The first attention is that a correction on 6V, inc_6V, varies with a wind speed condition as shown in eq.(1).

$$\begin{aligned} \text{inc\_6V} &= 0 && \text{for 6H* less than z0,} \\ &= (\text{6H*} - \text{z0}) \times \text{sp} && \text{for 6H* greater than z0,} \end{aligned} \qquad (1)$$

where 6H* is defined by eq.(2) and represents the wind speed condition.. Both z0 and sp are constants.

$$\begin{aligned} &\text{6H*} = \text{AMSR\_6H} - \text{atmos\_effect\_6H} - \text{calm\_ocean\_6H}, \\ &\text{atmos\_effect\_6H)} = \text{simu\_6H} - \text{calm\_ocean\_6H}, \end{aligned} \qquad (2)$$

where AMSR_6H is the AMSR-E Tb at 6H, atmos_effect_6H is the atmospheric correction on 6H, calm_ocean_6H is the ocean microwave emission for 6H under calm ocean conditions, and simu_6H. is a simulated Tb of 6H at a satellite height.

The second attention is that a value of sp varies with a relative wind direction (RWD), which is defined by the AMSR-E viewing angle and wind direction. The estimation of the RWD is made by a graphical method using 6H* and s36 defined by eq. (3).

$$s36=(AMSR\_36H-(a\times(AMSR\_36V-208)+b))/fac,$$

$$fac= 1 - (AMSR\_36V-200)\times 0.0045 \qquad (3)$$

where AMSR_36H/V are the AMSR-E TBs at 36H/V, and constants a, b are dependable on SST.

The relating function for 6H* with s36 was obtained from a data combination between AMSR and the NASA scatterometer SeaWinds both aboard on the Advanced Observation Satellite-II (ADEOS-II), which was launched in December 2002 by JAXA.

The third attention is that a value of sp also varies with an air-sea temperature difference (ASD). This reflects that the microwave Tb increments are induced probably by ocean foam and/or whitecaps under a condition of wind speed above 6-7m/s. It has been known that the appearance of ocean foam (or whitecap) depends on the ASD. The air temperature used in the JAXA SST algorithm is adopted from a weather forecast model operated by the Japan Meteorological Agency.

The retrieved AMSR-E SST was compared with buoy SST in global oceans. Root mean square (rms) of differences of two SSTs was calculated as 0.561°C using data in the year 2003. Cross talks of the AMSR-E SST were also checked against the AMSR-E water vapor and AMSR-E liquid water, and their differences were limited within 0.1°C in almost ranges. As for dependencies on the relative wind direction, they were checked using the wind direction retrieved from the ADEOS-II/SeaWinds, and their differences were limited within 0.2-0.3°C between upwind and downwind directions.

Finally, several rms were calculated for three different cases: case (1) sp does not vary with either RWD or ASD, rms=0.629°C: case (2) sp varies with the RWD but does not vary with the ASD, rms= 0.601°C: case (3) sp varies with both RWD and ASD, rms=0.563°C. Those results were obtained using the collocated data in February in 2003.

A BLENDED GLOBAL 1-KM SEA SURFACE TEMPERATURE DATA SET FOR RESEARCH AND APPLICATIONS

Yi Chao, Zhijin Li, Peggy Li, Benyang Tang, Quoc Vu

Jet Propulsion Laboratory, California Institute of Technology
Yi.Chao@jpl.nasa.gov

ABSTRACT

A global Sea Surface Temperature (SST) data set at 1-km (also known as ultra-high resolution) is produced daily and distributed to the research and application communities. The input SST data sets are derived from the Global High-Resolution Sea Surface Temperature (GHRSST) L2P products with a spatial resolution ranging from 1-km to 25-km. In situ SST measurements are also used to blend with these satellite SST data sets with a goal to produce a blended data (with all gap filled) at the highest possible resolution (i.e., 1-km). We have developed a multi-scale two-dimensional variational (MS-2DVAR) blending algorithm, which is characterized by inhomogeneous and anisotropic background error covariance specifically developed for regional applications. Currently, images can be accessed from http://ourocean.jpl.nasa.gov/SST. A subset interface is also provided to produce regional images over any part of the world ocean. Our blended global SST can also be visualized using Google Earth by downloading the daily KML file from our web site. We are in the process of setting up a OpenDAP/THREDDS server where users can download the digital data. Future plans to improve the blending algorithm and data quality will also be discussed.

1. INTRODUCTION

Global sea surface temperature is a critical variable in both the research and application communities. The production of an accurate SST is dependent on merging the data from both in situ and satellite platforms, taking into account the differing sampling patterns and measurement accuracies, while maintaining the highest resolution possible.

Many blended SST products have been developed to address either the climate variability with a spatial resolution larger than 25-km or the synoptic weather fluctuations with a spatial resolution between 5-km and 25 km (see http://www.ghrsst-pp.org/L4-Gridded-SST.html for a complete list of these L4 SST products). While these high-resolution SST data are important for numerical weather predication (NWP) and climate applications, there are increasing needs for an ultra high-resolution (UHR) SST on the order of 1-km, the highest resolution resolved by the satellite infrared sensors.

G1SST is designed to meet the needs of regional and coastal applications requiring the highest spatial resolution (i.e., 1-km) possible that is resolved by the satellite sensors. This blended data is of particular importance to the emerging Integrated Ocean Observing System (IOOS) and operational oceanography.

In this paper we present a new blended SST product that has been processed in near real-time since September 1, 2008. Our preliminary experiences in developing and distributing this global 1-km SST (G1SST) data set will be described. Technical challenges in the production of G1SST will be described and include (1) gridding very large data files at 1-km spatial resolutions, (2) blending more than a dozen different satellite data sets at variable spatial resolutions, and (3) workflow management to enable near real-time data processing and interactive visualization. Future plans to improve the blending algorithm and data quality will also be discussed.

2. G1SST PRODUCT OVERVIEW

The G1SST product builds on the GHRSST-PP (http://www.ghrsst-pp.org). The input data are obtained from the GHRSST GDAC and include twelve L2P products as listed in Table 1:

- Infra-red sensors on polar orbiting satellites (e.g., AVHRR on NOAA 17 & 18, MODIS on Aqua and Terra with two channels on each satellite, AATSR on EnviSat) with ultra high resolutions of 1-2 km
- Infra-red sensors on geostationary satellites (e.g., GOES 11 & 12 and SEVIRI) with a resolution of 6-km and 10-km, respectively.
- Microwave sensors (e.g., AMSR-E on Aqua, TMI on TRMM) with a resolution of 25-km

We also use thousands of *in situ* SST measurements available daily from ships, drifting and moored buoys.

3. BLENDING ALGORITHM: 2DVAR

The G1SST uses a 2-dimensional variational (2DVAR) algorithm. Using all the available SST data products, the blending process can be formulated to seek the optimal SST by minimizing the cost function with respect to T*:*

Sensor (Platform)	Sensor Type	Resolution	Coverage
AATSR (EnviSat)	Infra-red	1-km	Global
AMSR-E (Aqua)	Microwave	25-km	Global
AVHRR (NOAA 17 & 18)	Infra-red	2-km	Global
GOES (11 & 12)	Infra-red	6-km	Pacific & Atlantic
In situ	Ships, drifting & moorings	Single-point	Global
MODIS (Aqua & Terra)	Infra-red	1-km	Global
SEVIRI (MSG)	Infra-red	10-km	Atlantic
TMI (TRMM)	Microwave	25-km	Tropics (40S-40N)

Table 1. A list of input data sets used to produce G1SST.

$$J(T) = \frac{1}{2}(T - T^b)^T B^{-1}(T - T^b) + \frac{1}{2}\sum_{s=1}^{N}(H_s T - T_s^o)^T R_s^{-1}(H_s T - T_s^o)$$

where T^b is the background, T_s^o the observations, N the number of the types of SST observations, $\boldsymbol{B}$ the error covariance matrix of T^b, and R_s the observational error covariance of T_s^o. H_s is the observational operator, which maps the blended SSTs to the observation locations.

In practice, it is difficult to directly minimize the above define cost function numerically. Generally, some transformations are applied to improve the performance of the numerical minimization. In this study, we calculate the cost function using the increment $\delta T = T - T_b$.

4. G1SST PRODUCTION AND DISTRIBUTION

The G1SST data processing runs daily using a window of 24 hours. The previous day G1SST data are available in the morning of the California local time since September 1, 2008. Because of the large data volume, only images are currently available through the following web site: http://ourocean.jpl.nasa.gov/SST. We provide the global ocean image (Figure 1) as well as six selected regions: U.S. East Coast (Figure 2), U.S. West Coast, Gulf of Mexico and Caribbean Sea, Hawaii Islands, Peru Coastal Ocean, and South China Sea. Our blended global SST can also be visualized using Google Earth by downloading the daily KML file.

5. CONCLUSION

A global 1-km SST (G1SST) data have been developed and distributed daily to the research and application communities. G1SST builds upon data provided by the GHRSST-PP L2P data products. We are in the process of generating a long time series of SST prior to September 1, 2008. In the meantime, we are also conducting a systematic evaluation of the G1SST product. The Argo data are not used in our blending, and therefore will serve as an independent data set to quantify the accuracy of G1SST. Future improvements in our data processing and blending algorithm are also planned to take into account issues such as bias correction, diurnal cycle adjustment, and a better representation of the input data error and error covariance are also anticipated in the near future.

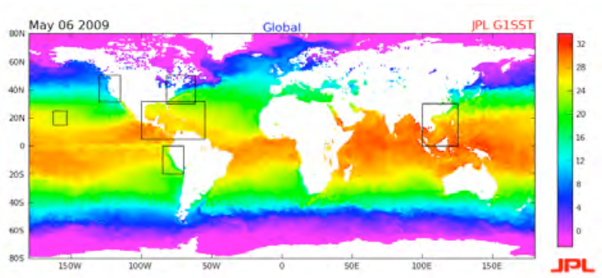

Figure 1. A sample G1SST image over the world ocean.

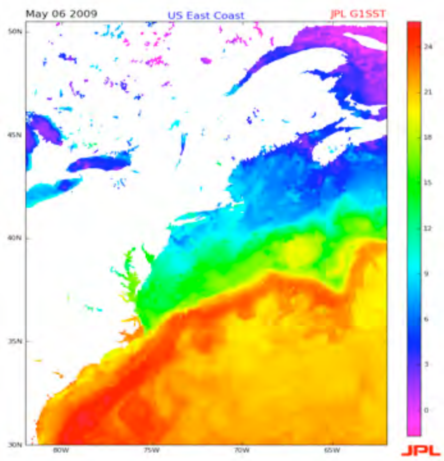

Figure 2. A sample G1SST image for the Gulf Stream.

6. REFERENCES

Chao, Y., Z. Li, J. Farrara, P. Huang, 2009, Blending sea surface temperatures from multiple satellites and in-situ observations for coastal oceans, *J. Atmos. Ocean. Tech.*, (in press).

Acknowledgements

All the input data are obtained from the JPL PO.DAAC GHRSST GDAC (http://ghrsst.jpl.nasa.gov/). Technical discussions with Ed Armstrong, Craig Donlon, Dave Foley, Chelle Gentemann, and Jorge Vazquez are greatly appreciated.

AN ENHANCED MODIS / AMSR-E SST COMPOSITE PRODUCT

Gary Jedlovec [(1)], Frank LaFontaine[(2)], Jaclyn Shafer[(3)],

Jorge Vazquez[(4)], Edward Armstrong [(4)] , Mike Chin [(4)]

(1) *Earth Science Office, Marshall Space Flight Center, 320 Sparkman Drive, Huntsville, AL 35805*
Email: Gary.Jedlovec@nasa.gov
(2) *Raytheon Information Solutions, 320 Sparkman Drive, Huntsville, Alabama 35805*
(3) *Earth System Science Center, University of Alabama Huntsville, 320 Sparkman Drive, Huntsville, Alabama 35805*
(4) *Jet Propulsion Laboratory, California Institute of Technology, 2800 Oak Grove, Pasadena, CA 91109*

ABSTRACT

A combined MODIS / AMSR-E SST composite product was developed using the GHRSST L2P data set and an enhanced algorithm to reduce latency and improve the quality and accuracy of the SST data for weather forecasting applications.

1. INTRODUCTION

Accurate high resolution specification of sea surface temperature (SST) is important for regional weather forecasting studies and coastal ocean applications. Chelton et al. (2007) and Lacasse et al. (2008) showed that the use of coarse resolution SST products such as from the real-time global (RTG) SST analysis (Thiebaux et al. 2003) in regional weather forecast models do not properly portray the fluxes of heat and moisture from the ocean that drive the formation of low level clouds and precipitation over the ocean. Case et al. (2008) presents a detail analysis of the impact of the composite SST product in coast regions. Regional coverage of accurate SST variability is also important for hurricane track and intensity forecasts and verification of ocean circulation models.

Haines et al. (2007) described a polar orbiting data compositing technique which provides spatially continuous, accurate, high-resolution SST fields using data from the Moderate-resolution Imaging Spectrometer (MODIS) on NASA's Terra and Aqua satellites. The compositing technique generates four daily maps of SST using data from the previous days to augment and fill in for clouds and missing data in the current days / times MODIS orbital swath. The approach was limited during periods of long-term cloud cover where latency of past data reduced the accuracy of the data presented in the composites.

The research discussed in this paper is in collaboration with and a companion to the work of Vazquez et al. (2009) reported on in this symposium to develop an enhanced SST composite product for regional weather applications. The enhancements come from the addition of AMSR-E data to reduce the latency of the MODIS due to prolonged cloud cover, and by incorporating a more sophisticated temporal weighting scheme which includes observational errors for each data set. The enhanced SST composite product will be integrated into NASA's Short Term Prediction and Research Transition (SPoRT) program (Jedlovec et al. 2006) and distributed to the NWS, other government agencies, and the public for use in regional weather forecast applications. This paper describes the methodology used to overcome several limitations of the MOSID / AMSR-E L2P data set in order to produce the SST composite product. The companion paper provides a comparison between SST maps produced using these methodologies, as well as direct comparisons with gridded maps of SST derived from the Advanced-Along Track Scanning Radiometer (AATSR).

The previous approach of Haines et al. (2007) calculated high-resolution (1km) SST composites based on finding a minimum of three cloud free pixels at each location for a given collection period (up to 30 days). The two warmest pixels were then averaged and the value was used to represent the SST at that pixel. A latency map was generated for each composite that provided information on how many days were necessary to find the minimum three cloud free pixels. With the availability of GHRSST L2P data, several enhancements were add to the composite methodology:

- include passive microwave SST data into the compositing process,
- implement a straightforward strategy for using the error characteristics in GHRSST L2P data in the calculation of the composites,
- extend the compositing region to the entire West and East Coasts of the United States,
- use the proximity flags in the GHRSST L2P data to remove cloud and erroneous pixels.

2. METHODOLOGY AND DATA

The methodology used here and in Vazquez et al. (2009) are similar to each other andis highlighted below. SST composites are produced over a given region at four times each day corresponding to Terra and Aqua equator crossing times (i.e., Terra day, Aqua day, Terra night, and Aqua night). Day-time (night-time) AMSR-E SST data from Aqua are used with both Terra and Aqua MODIS day-time (night-time) SST data sets. For a given day and region, the data from the previous seven days form a collection used in the compositing. At each 1km pixel, cloud-free SST values (as determined by the L2P confidence flags) from the collection (both AMSR-E and MODIS) are used to form a weighted average based on their latency (number of days from the current day) and quality (also from the L2P data stream). In this way recent SST data are given more weight than older data. One of the primary issues involved in incorporating the AMSR-E microwave data in the composites is the tradeoff between the decreased spatial resolution of the AMSR-E data (25km) and the increased coverage due to it's near all weather capability. Currently, the AMSR-E is given a weight of around 20% compared to MODIS data. In this way the spatial structure observed in the 1km MODIS data is preserved.

3. COMPOSITE LIMITATIONS CAUSED BY THE L2P DATA

Several limitations surfaced in the adaptation of this enhanced compositing approach. The use of a seven day collection period was initially thought to be sufficient to provide complete data coverage over the ocean regions in the MODIS / AMSR-E composite product. This turned out not to be the case because of AMSR-E constraints and MODIS cloud detection problems. The use of the AMSR-E reduced the latency of the data in the collection and produced a better (still needs to be quantified) SST composite product, however, missing data within 125km of land (coastal regions or islands) created some seemingly artificial gradients in these regions. In addition,, the confidence flags in the MODIS L2P data stream consistently rejected data in high SST gradient regions (along the Gulf stream) despite the lack of cloud cover.

4. RESULTS

The figure below presents an example of the MODIS / AMSR-E SST composite product for June 1, 2007 using the above methodologies. The use of MODIS data preserves much of the detailed structure in the 1km data as can be seen in the various thermal features such as the loop current in the Gulf of Mexico and details of the Gulf Stream off the east coast of the

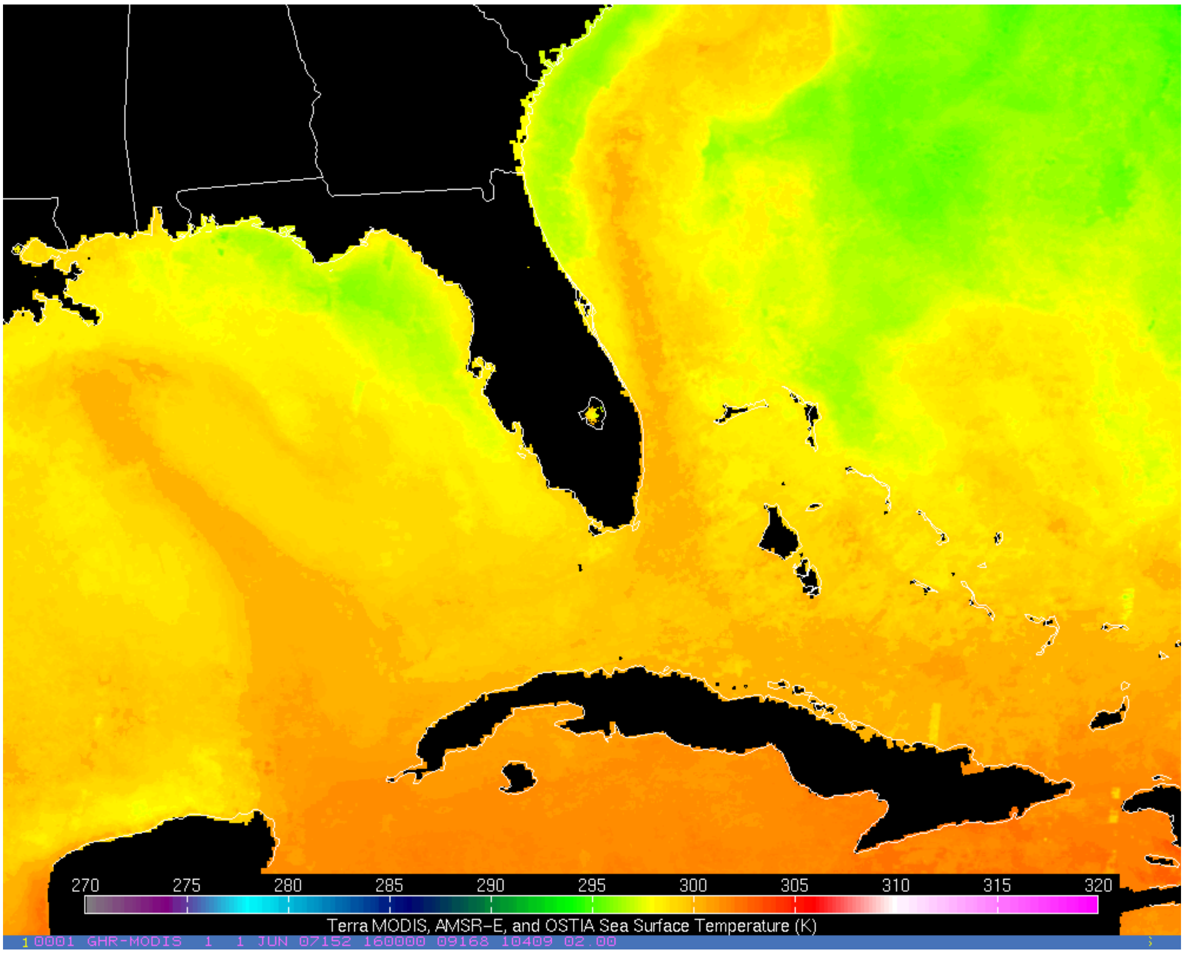

United States. To overcome the limitations of the L2P data set described above, the Operational Sea Surface Temperature and Sea Ice Analysis (OSTIA) SST product (Stark et al., 2007) was introduced as an "observation" along with MODIS and AMSR-E and subsequently was included in the temporal weighted average composite. In this way, when no AMSR-E or MODIS data are present in the seven day collection, composite SST values are represented by the OSTIA values. The regions where this occurs are not readily apparent because of the blending provided by the weighted compositing approach.

This collaborative work will produce the enhanced MODIS / AMSR-E composite data set for use in weather forecasting over four regions:

-90W to -70W and 20N to 35N – Florida
-100W to -50W and 10N to 40N - Hurricane
-110W to -45W and 10N to 52N - Atlantic
-140W to -90W and 20N to 50N - Pacific

These data sets will be made available in real-time via a public ftp site.

5. ACKNOWLEDGEMENTS

This research was funded by Dr. Tsengdar Lee of the NASA Science Mission Directorate's Earth Science Division through NASA's research to operations proposal solicitation, a part of NASA's Research Opportunities in Space and Earth Science (ROSES) program.

6. REFERENCES

Case, J. L., P. Santos, M. E. Splitt, S. M. Lazarus, K. K. Fuell, S. L. Haines, S. R. Dembek, and W. M. Lapenta, 2008: A multi-season study of the effects of MODIS sea-surface temperatures on operational WRF forecasts at NWS Miami, FL. Preprints, *12th Conf. on Integrated Observing and Assimilation Systems for Atmosphere, Oceans, and Land Surface*, New Orleans, LA, Amer. Meteor. Soc., 14.1. [Available online at http://ams.confex.com/ams/pdfpapers/131892.pdf]

Chelton, D. B., M. G. Schlax, and R. M. Samelson, Summertime Coupling between Sea Surface Temperature and Wind Stress in the California Current System, *J. Phys. Oceano*, **37** (3), 495-517, 2007.

Haines, S. L., G. J. Jedlovec, and S.M. Lazurus, 2007: A MODIS Sea Surface Temperature Composite for Regional Applications, Trans. Geosci. Rem. Sens., **45**, No. 9, IEEE, 2919-2927.

Jedlovec, G., S. Goodman, M. Goodman, and B. Lapenta, 2006: Use of Earth Observing System Data in Weather Forecasting. IGARSS 2006, Denver.

LaCasse, K. M., M. E. Splitt, S. M. Lazarus, and W. M. Lapenta, 2008: The impact of high resolution sea surface temperatures on short-term model simulations of the nocturnal Florida marine boundary layer. *Mon Wea. Rev*., **136**, 4, 1349-1372.

Stark, J. D., C. J. Donlon, M. J. Martin, and M. E. McCulloch, OSTIA: An operational, high resolution, real time, global sea surface temperature analysis system. Oceans '07 IEEE Aberdeen, conference proceedings. Marine challenges: coastline to deep sea. Aberdeen, Scotland .IEEE.

Thiebaux, J., E. Rogers, Q. Wang, and B. Katz, 2003: A new high-resolution blended real-time global sea surface temperature analysis. *Bull. Amer. Met. Soc*, **84**, 5, 645-656.

Vazquez, J, T. M. Cvidhin, E. Armstrong, and G. Jedlovec, 2009: A comparison of 1km ultra high resolution composite SST maps. Symposium proceedings from the GHRSST User Symposium, May 28-29, 2009, Santa Rosa, CA.

RECENT DEVELOPMENTS IN THE CANADIAN METEOROLOGICAL CENTRE GLOBAL SST ANALYSIS

Bruce Brasnett

Canadian Meteorological Centre, 2121Trans-Canada Highway, Dorval, Quebec, H9P 1J3, Canada. E-mail: Bruce.Brasnett@ec.gc.ca

Several changes have been made to the CMC analysis since a detailed description of the analysis was published (1). These include conversion to the GHRSST L2P datasets for NOAA17, NOAA18 and METOP-A, increase in resolution and addition of ice information.

1. MIGRATION TO GHRSST DATASETS

Although retrievals from AVHRR aboard NOAA17 have been used for some time, the CMC analysis now uses the GHRSST L2P format for these retrievals, and retrievals from NOAA18 and METOP-A in the same format have been added. A/ATSR (ATS_NR__2P) retrievals continue to be obtained from ESA in BUFR format while AMSR-E retrievals continue to be obtained from RSS as daily binary data files. SSES bias estimates are applied to the L2P retrievals prior to use. A thinning algorithm is applied to all retrievals to create a manageable dataset for assimilation and maintain a balance between the different sources. Figure 1 shows the mean spacing for infrared and AMSR-E retrievals. It was found by varying the spacing of retrievals that infrared retrievals contribute more information to the analysis than AMSR-E at high latitudes while the opposite is true in the tropics. The spacing of the retrievals reflects this experience.

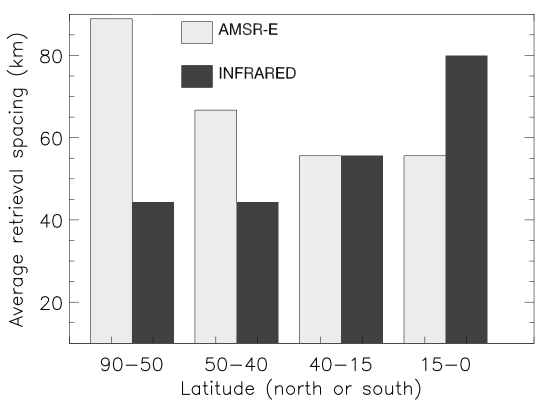

Figure 1. Latitudinal variation of the spacing of retrievals used in the CMC analysis.

The spacing shown in fig. 1 is an average value. The actual spacing is non-uniform. The algorithm used to select retrievals is illustrated in fig. 2. The globe is divided into grid cells with sides measuring approximately 55 km (at this latitude). From all retrievals in a given cell, the retrieval associated with the median SST is selected for use. The location of the median is nearly random, which accounts for the clustering and gaps in fig.2. Selection of the median reduces the risk of choosing an outlier and should therefore yield a more representative result than either a grid cell average or a selection based on location rather than value.

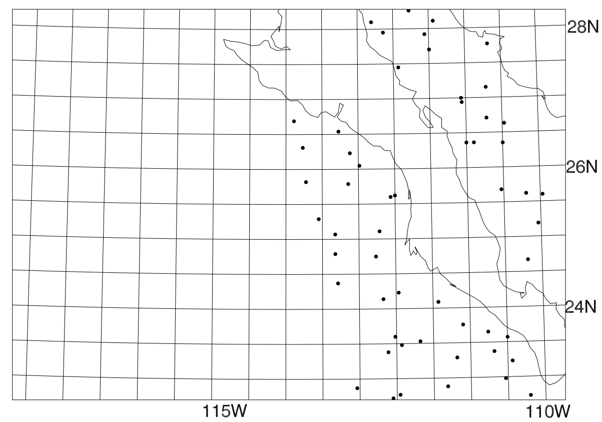

Figure 2. Grid cells used in retrieval thinning algorithm and the sample of METOP-A retrievals selected for use for 1 Feb. 2008.

Although the clustering and gaps in fig. 2 appear problematic, a different view emerges when examining the distribution of observations over several days. Figure 3 shows a 10-day sample of selected METOP-A retrievals. In fig. 3, few gaps remain as virtually every grid cell contains multiple retrievals. This sampling appears adequate for resolving small scale features and, provided information from prior observations is preserved on the analysis grid, a detailed high-resolution analysis should be possible.

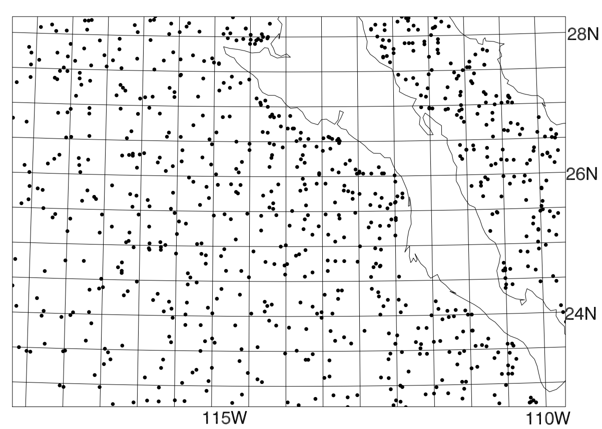

Figure 3. Distribution of METOP-A retrievals used from Feb. 1-10, 2008.

2. INCREASE IN ANALYSIS RESOLUTION

The analysis is now produced on a 0.2 degree lat-long grid rather than the 1/3 deg grid used in (1). This corresponds to a reduction in the grid length from 37 km to 22 km in the north-south direction. Background error correlation length scales have been revised downward as well as shown in fig. 4.

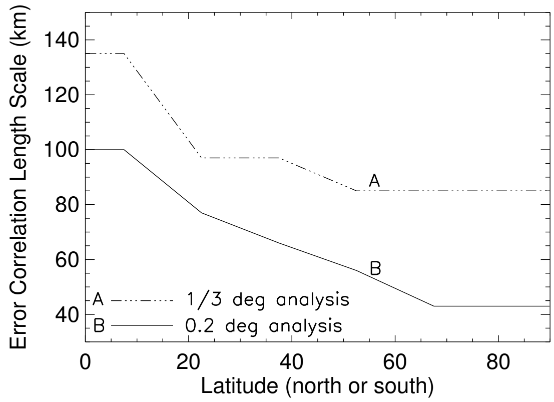

Figure 4. Background error correlation length scales (e-folding distances) for the 1/3 degree analysis (A) and the new analysis (B)

The revised background error correlation length scales in fig. 4 were found by an empirical process guided by analysis error estimates using independent data. The increase in resolution of the analysis grid alone gave almost no gain in accuracy. As shown in fig. 5, the combination of a higher resolution analysis grid and smaller correlation length scales produced a modest gain in accuracy for the mid-latitudes and high latitudes, but little improvement in the tropics.

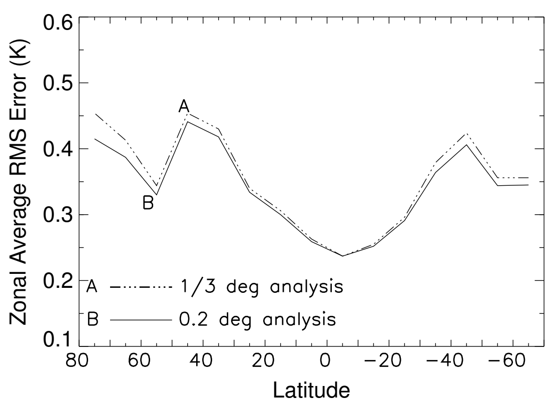

Figure 5. Zonal average analysis RMS error estimates using independent, quality controlled ARGO float data as truth. Data are from the period Nov. 1, 2007 to Oct. 31, 2008. The results labeled B include smaller correlation lengths.

Many small scale features in the SST field are not adequately sampled by ARGO floats or other in situ data sources. An example of such a feature is a cold water column that occurs at the southeastern tip of the Grand Banks, near 43N, 50W. The Canadian department of fisheries and oceans routinely measures profiles of temperature and salinity in this area at least twice per year as part of the Atlantic Zone Monitoring Program (AZMP). Data are available for download at http://www.meds-sdmm.dfo-mpo.gc.ca/isdm-gdsi/azmp-pmza/hydro/index-eng.html. Figure 6 shows the temperatures nearest the surface for the AZMP section collected April 21-22, 2008. The observations show an area of significantly colder water between 450 km and 500 km from shore. The higher resolution analysis combined with the smaller correlation length scales (solid line) produce an improved analysis in this area compared to the lower resolution product (dashed line). Work is continuing to try to further improve the analysis of this feature.

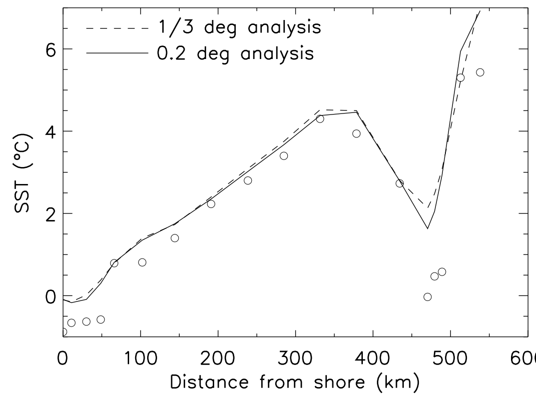

Figure 6. SST from an AZMP section April 21-22, 2008 (circles). The dashed line shows the corresponding values from the 1/3 degree analysis and the solid line the values from the 0.2 degree analysis.

3. ADDITION OF ICE INFORMATION

As part of its NWP program, CMC produces daily global analyses of fractional ice cover on a lat-long grid with grid length 1/3°. The primary data source for this analysis is the SSM/I microwave sensor aboard DMSP satellites (currently F13 and F15). These retrievals cannot be used within about 100 km of land necessitating the use of climatology in this zone. Over Canadian waters, the SSM/I data is supplemented by data from the Canadian Ice Centre, where ice is mapped using data from a variety of sources including MODIS, AVHRR and RADARSAT.

The ice cover product is used to generate proxy SST "observations" at each point of the 1/3° grid where ice cover exceeds 60%. The proxy value most frequently used here is -1.8℃. However, this value is not particularly appropriate when ice is melting, as commonly occurs during the latter half of polar day. In order to identify these situations, analyses of surface air temperature for the past 24-hour period are consulted. These analyses are produced every 6 hours using a 6-hour forecast from the global forecast model as background, and incorporate all available air temperature reports from drifters, ships and land stations. If, at a given grid point, the air temperature remained above freezing over the previous 24 hours, a proxy SST of 0℃ is used instead of -1.8℃.

The proxy SST data generated from ice are thinned to a spacing of 55 km, typically resulting in between 6000 and 9000 values. An algorithm that varies the location from day to day of the selected proxy SST within a grid cell is employed to improve sampling over time. The proxy SSTs are then assimilated with an ascribed observation error of 1.0℃, higher than the error ascribed to any other observation type.

Figure 7 shows the impact ice information has on analysis error estimates. It should be remembered that the ARGO float data used here only sample ice-free regions. Clearly, fig. 7 indicates that the ice information improves the analysis even beyond the ice edge.

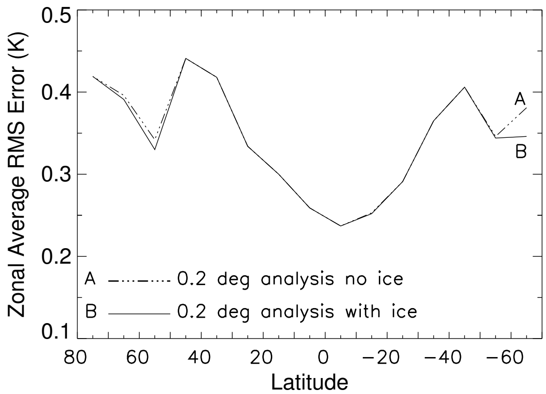

Figure 7. Zonal average analysis errors (K) for the new analysis (B) and the same analysis but with ice information excluded (A).

4. CHOICE OF ANALYSIS VARIABLE

One unconventional aspect of the CMC analysis is the use of SST anomaly from climatology as the analysis variable. This choice offers several advantages over analyzing SST directly. The anomaly field is not dominated by the north-south gradient that appears in the SST field, making the anomaly more isotropic than SST. This is helpful given that it is assumed in the method used here that the background error correlations are isotropic. Also, the magnitudes of anomaly gradients are usually much less than those of SST. Figure 8 illustrates this for the analysis of Mar. 30, 2009. The north Pacific, in particular, has significantly diminished gradients in the anomaly field (lower panel). Since an error in the location of a gradient translates into an analysis error that is proportional to the magnitude of the gradient, it is appealing to analyse a field with smaller magnitude gradients. Perhaps the most important property of the anomaly is that it typically evolves very slowly, a property that fits well with the persistence model used in the present analysis scheme. Finally, an anomaly analysis includes a climatological trend implicitly, unlike most schemes which must explicitly add a climatological trend, typically by adding the difference in the climatology over one day to the background. The latter approach makes it more difficult to preserve the information contained in the background.

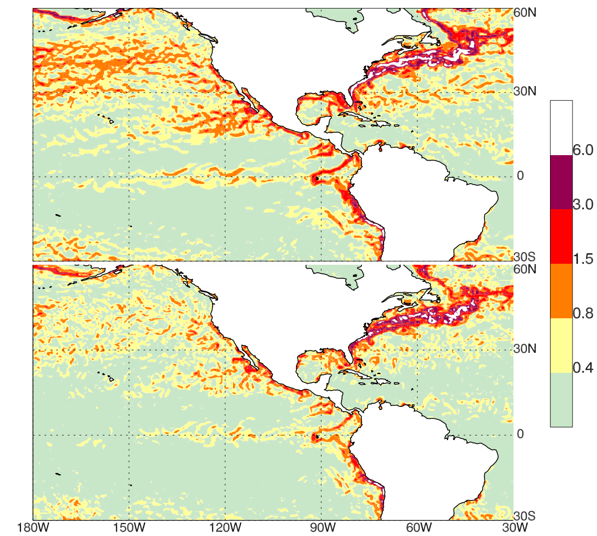

Figure 8. Magnitude of the SST gradient (upper panel) and the anomaly gradient (lower panel) for the 0.2 deg resolution analysis on Mar. 30, 2009.Units are K (100 km)$^{-1}$.

Acknowledgment

A/ATSR retrievals were supplied by ESA. AMSR-E data are produced by Remote Sensing Systems and sponsored by the NASA Earth Science REASoN DISCOVER project and the AMSR-E Science Team. Data are available at www.remss.com. AVHRR data were supplied by NASA-JPL under the GHRSST collaborative framework.

Reference

[1] Brasnett B. 2008. The impact of satellite retrievals in a global sea-surface-temperature analysis. *Q. J. R. Meteorol. Soc.* **134**: 1745-1760, DOI: 10.1002/qj.319.

Overview of data access GDAC and LTSRF

Jorge Vazquez[(1)], Kenneth S. Casey [(2)], Edward Armstrong[(1)], Tess Brandon [(2)],

(1) *Jet Propulsion Laboratory, California Institute of Technology, 2800 Oak Grove, Pasadena, CA 91109, Email: jorge.vazquez@jpl.nasa.gov*

(2) *National Oceanographic Data Center, National Oceanographic and Atmospheric Administration, 1315 East-West Highway*, Maryland,

)

ABSTRACT

Data from the Group for High Resolution Sea Surface Temperature (GHRSST) is distributed as a collaborative effort between the Global Data Assembly Center (GDAC) at NASA's Physical Oceanography Distributed Active Archive Center (PO.DAAC) and the Long Term Stewardship and Reanalysis Facility (LTSRF) at the National Oceanographic and Atmospheric Administration's (NOAA) National Oceanographic Data Center (NODC). The GDAC has the primary responsibility as a clearinghouse and rolling store for all products that are less than 30 days from satellite acquisition. After 30 days all products are sent to NODC for permanent archive and access. All products are available through http access (**HTTP://GHRSST.JPL.NASA.GOV**; **HTTP://GHRSST.NODC.NOAA.GOV**) as well as FTP access and OPeNDAP. A metadata master repository search capability is available at the GDAC for retrieving data files within specific time and space windows.

1. INTRODUCTION

The Group for High Resolution Sea Surface Temperature (GHRSST) currently distributes sea surface temperature products from a wide variety of satellite sensors. Near real time products (less than 30 days) are distributed through NASA's Global Data Assembly Center (GDAC) at the Physical Oceanography Distributed Active Archive Center (PO.DAAC). After 30 days products are sent to NOAA's National Oceanographic Data Center (NODC) Long Term Stewardship and Reanalysis Facility (LTSRF) for long-term archive and storage. Level 2 Preprocessed (L2P) products are available from several sensors including:

1) NOAA's polar orbiting Advanced Very High Resolution Radiometer (AVHRR)
2) European Space Agency's (ESA) Advanced Along-Track Scanning Radiometer (AATSR)
3) NASA's Moderate Resolution Imaging Spectroradiometer (MODIS) on board the Aqua and Terra spacecrafts
4) NASA's Advanced Microwave Scanning Radiometer –Earth Observing System (AMSR-E) on board the Aqua spacecraft
5) NASA's Tropical Microwave Imager (TMI) on board the Tropical Rainfall Measuring Mission (TRMM)
6) NOAA's Geostationary Operational Environmental Satellite (GOES) Imager
7) The European Spinning Enhanced Visible and Infrared Imager (SEVIRI) on board the Meteosat Second Generation (MSG) Satellites

GHRSST also produces Level 4 (L4) datasets. The L4 products are gridded, gap-free, and created by blending SST from difference satellite and in situ sources. Several Level 4 products are currently available and include:

1. UK Met Office's OSTIA
2. European RDAC's ODYSSEA
3. REMSS MW + IR OI
4. NCDC Daily OI
5. NAVO K10 Analysis
6. ABOM's GAMSSA

A complete list of these products may also be found at:

http://ghrsst.jpl.nasa.gov/GHRSST_product_table.html. These products are all available through the POET interface at: http://poet.jpl.nasa.gov.

2. ACCESSING DATA

All products are available through http access (HTTP://GHRSST.JPL.NASA.GOV; HTTP://GHRSST.NODC.NOAA.GOV) as well as FTP access and OPeNDAP. A metadata master repository search capability is available at the GDAC for retrieving data files within specific time and space windows.

At NODC files may be accessed through OPeNDAP. At the GDAC data may be accessed through the OPeNDAP server at:
http://dods.jpl.nasa.gov/

3. DATA STATISTICS

Since 2006 dramatic increases in the usage and distribution of GHRSST data have occurred. Both the GDAC/PODAAC and LTSRF/NODC maintain statistics on data users, volume of data distributed, and number of files distributed.

Figure 1 shows the number of users from 2006-2008 and the total. Between the NODC and GDAC over 25000 unique users have been served, with dramatic increases seen in successive years.

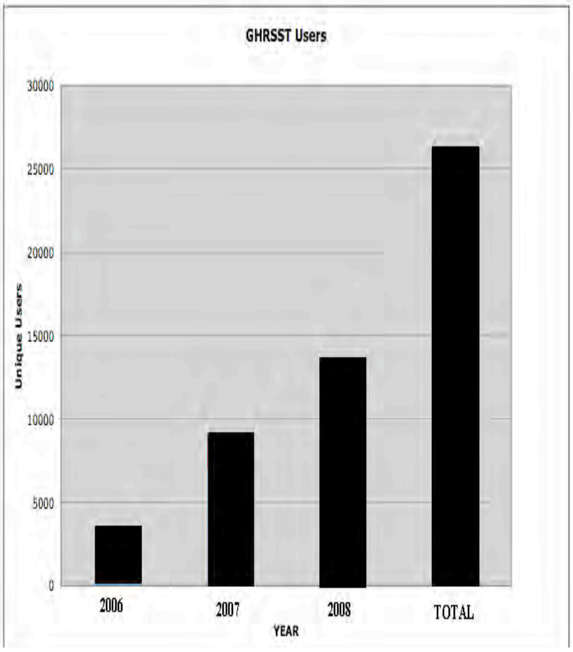

FIGURE 1: Total Usage

Figure 2 shows the total volume of data distributed in gigabytes. Jointly, NODC and the GDAC/PODAAC have distributed close to 40 terabytes of data.

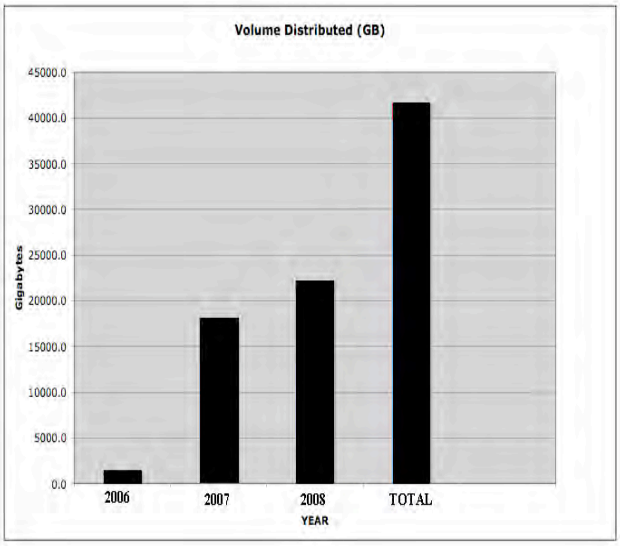

FIGURE 2: Total Volume Distributed

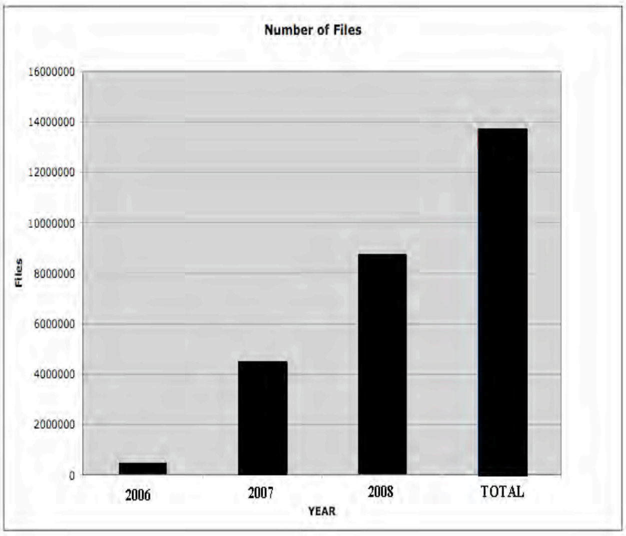

FIGURE 3: Total Files Distributed

Figure 3 shows the total number of files distributed from 2006 through 2008. Close to 14 million files have been distributed between NODC and the GDAC/PODAAC.

All these statistics indicate a dramatic increase in GHRSST usage since 2006. The number of unique data users has increased by a factor of 5. As the project continues to implement new methodologies for accessing data, along with future reanalysis efforts, it is anticipated that these numbers will continue to increase dramatically. Working together NODC and PO.DAAC are serving up more and more customers, along with more and more data every year!

DISPLAYING GHRSST DATA USING ESRI ARCGIS DESKTOP

Martin Rutherford

Royal Australian Navy Directorate of Oceanography and Meteorology, Garden Island, Potts Point
Email: tdom@metoc.gov.au

ABSTRACT

Two 'tutorial like' User Guides detailing how to process and display GHRSST L2P and L4 data using ESRI ArcGIS Desktop software have been developed by the Royal Australian Navy and published through the GHRSST Web site. The first User Guide takes the novice Desktop user through the steps to download, display, and contour GHRSST data in ArcMap and ArcGlobe. For the more advanced user, the second Guide describes how to code the same steps using ESRI ModelBuilder and Python geo-processing scripts, to automate the majority of the keystrokes. The automated geo-processing scripts are used by the Royal Australian Navy to process L4 data and publish it as a Web Map Service.

1. INTRODUCTION

Geographic Information Systems (GIS) describe the family of software applications and supporting databases that capture, store, manage and present data with a spatial context, i.e. having a location on earth. With a global market share of over 30%, the suite of GIS software products marketed by ESRI, particularly ArcGIS Desktop, are the most widely used; by a user group estimated at around one million across 300,000 organisations in over 150 countries. Although not a format traditionally supported by GIS systems, ESRI has recently added tools to ingest netCDF data, which can then be analysed, displayed and published using the core GIS functionality. The availability of these netCDF tools now allows GHRSST data to be used natively by the suite of ESRI software applications, including ArcGIS Desktop.

This paper describes how to use ArcGIS Desktop to display GHRSST L2P and L4 data and the scripting tools available to automate the processing.

2. User Guide 1 - Displaying GHRSST Products in ESRI ArcGIS Desktop

2.1. Getting Started

Displaying GHRSST data in ArcGIS Desktop (Version 9.3 Service Pack 1) requires the user to have the ArcGIS Desktop Spatial Analyst Extension installed. The tools to ingest netCDF data are found in the Multi-dimension toolbox which must be loaded into the ArcToolbox window. The software does not currently support connections to remote data servers hence the data to be displayed must be held locally. Users should refer to the GHRSST Data Access Tutorial for instructions on how to access the data via ftp or http connections.

2.2. Displaying GHRSST L4 Products

A schematic diagram of the steps required to display GHRSST L4 products is given in Fig. 1. L4 netCDF data is on a regular equal interval grid, hence can be read by ArcGIS Desktop as a raster layer. Many users will want to see the data displayed in degrees Celsius or Fahrenheit and the ESRI Raster Calculator allows formulae to be applied to all pixels to change units.

The resolution and fine detail of GHRSST L4 products makes contours appear pixcellated and smoothing may be required to produce a clearer map. Smoothing is done on a copy of the raster using neighbourhood statistics and contours of the smoothed raster created at 1 degree, 2 degree and 5 degree intervals. The smoothed raster is then discarded and the contours displayed over the original full resolution raster.

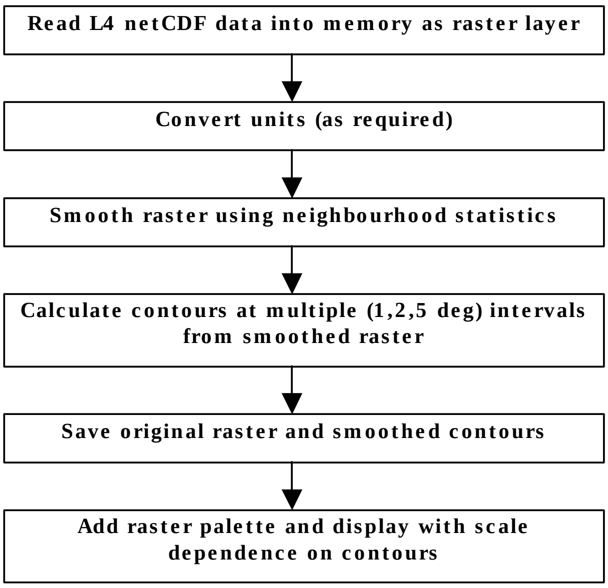

Figure 1- GHRSST L4 processing work flow

The multiple contours are used with scale dependence when displaying the data. At the global scale, a one degree contour interval would result in over 35 contours, obscuring the image below in high gradient regions. The ArcGIS Desktop display properties allow different contours to be displayed at different map scales, for example 5 degrees intervals for the globe, 2 degrees at basin scale and one degree at regional scale.

Figure 2 shows the typical output of a GHRSST L4 global product displayed in ArcGIS Desktop.

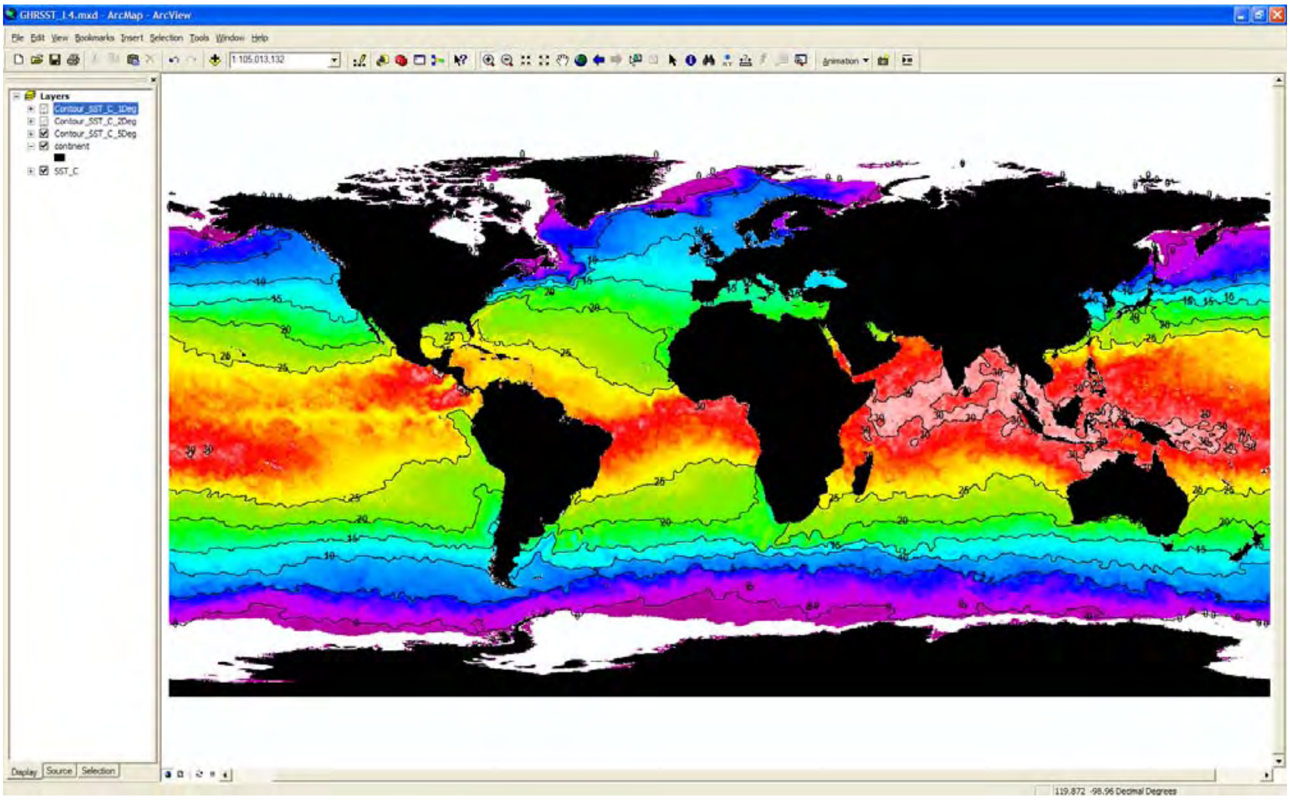

Figure 2 - GHRSST L4 product processed and displayed in ArcGIS Desktop

2.3. Displaying GHRSST L2P Products

In contrast to the L4 products which are regularly gridded, the L2P swathe products are in 'satellite projection' and can not be ingested directly into ArcGIS Desktop as a raster. Instead, a separate ingest tool that allows netCDF files to be input as points is used. Every point in the file is added to a table and calculations such as changing units must now be performed on the table. This firstly requires a query to identify the non-null values, which are saved into a new table. In contrast to raster calculations where a formula can be applied to each pixel, when working with tables a new field must be created and its values calculated by applying a formula to values in another field. For example, a new field of SST_C is created and its values calculated using the Kelvin to degrees Celsius conversion formula. The original field can then be deleted.

The field containing the converted units can be converted to a raster at a user selectable grid resolution using data conversion tools. Thereafter it can be contoured and displayed as described earlier for the L4 products. Figure 3 shows a schematic of the work flow for L2P products up to and including its conversion to a raster.

A typical output of L2P processing in ArcGIS Desktop is shown in Figure 4.

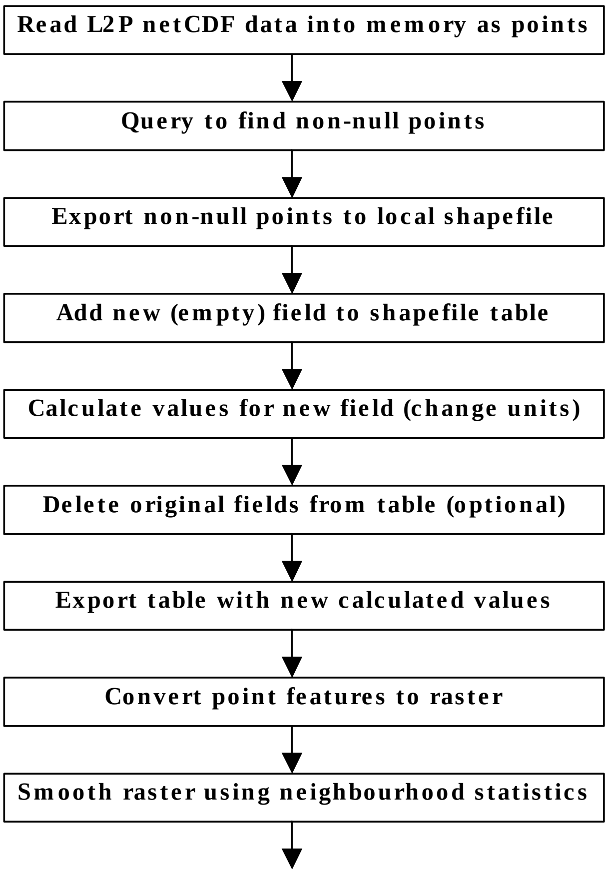

Figure 3- GHRSST L2P work flow

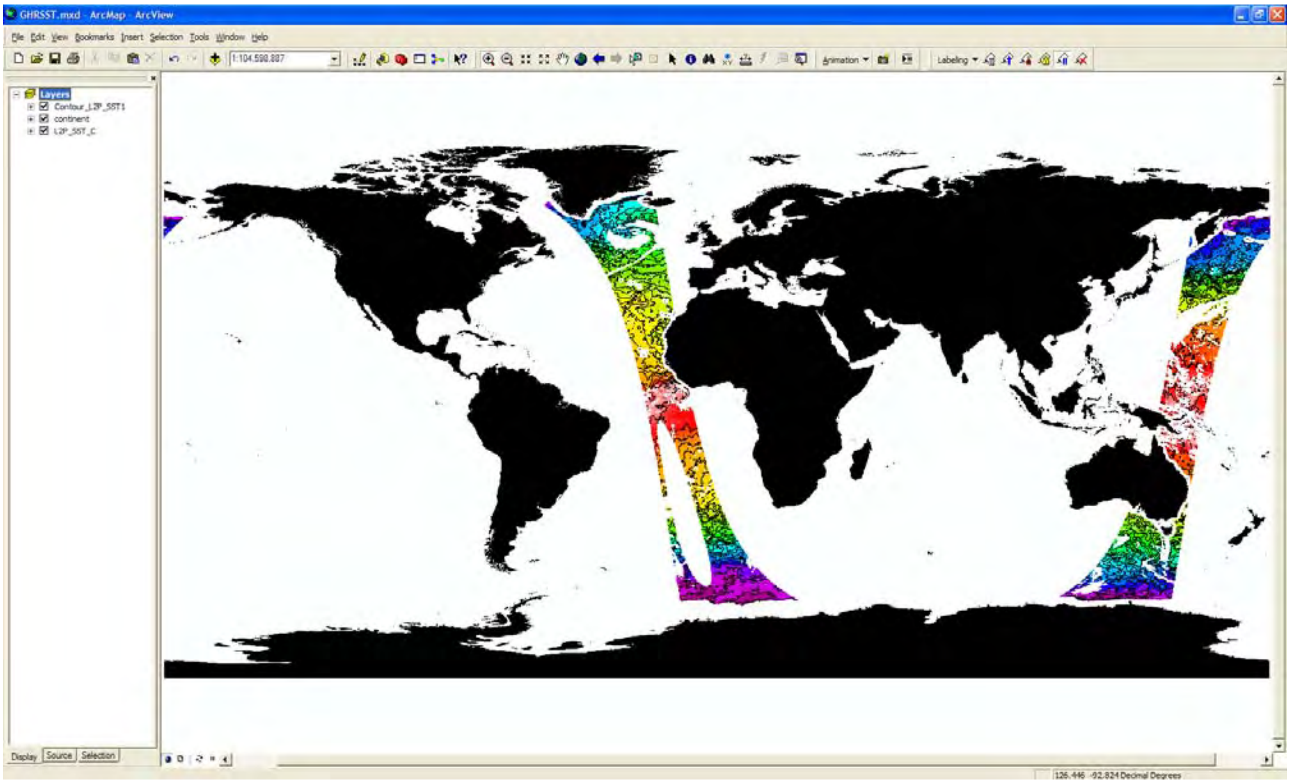

Figure 4 - GHRSST L2P product processed and displayed in ArcGIS Desktop

3. USER GUIDE 2 - Geo-processing GHRSST Products using ArcGIS Desktop

The process outlined in paragraph 2 above and detailed in User Guide 1 is lengthy, at times tedious and requires a large number of keystrokes. Fortunately, all of the steps can be chained together, with the output from one process providing the input to the next, and run in a single command using the ESRI ModelBuilder tool, which is built in to ArcGIS Desktop.

The geo-processing User Guide provides a step by step tutorial that assists the user in building models that replicate exactly the steps taken in the first User Guide. The models can also be exported as a Python script and run from a command line or as a UNIX cron or Windows scheduled task. Figure 5 shows the geo-processing model for GHRSST L4 products.

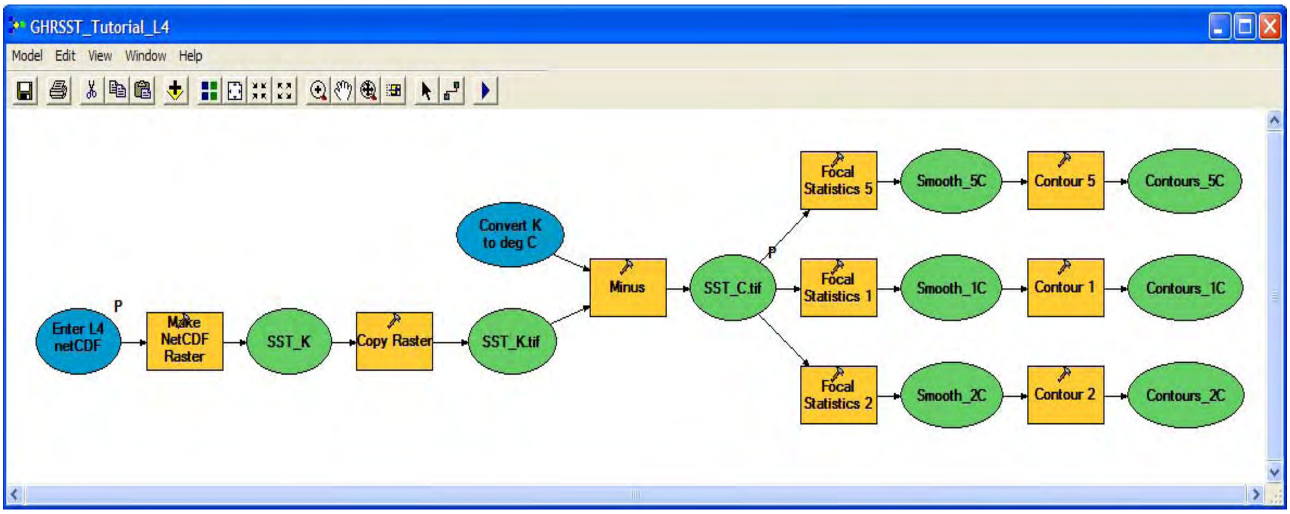

Figure 5- GHRSST L4 Geo-processing model

4. WEB MAP SERVICES

The geo-processing models can also be run in batch mode. Daily global L4 processing is undertaken by the Royal Australian Navy, using python scripts built around the model shown in Figure 5. The resulting images are then published as Open GIS Consortium (OGC) compliant Web Map Services on the Directorate of Oceanography and Meteorology home page (www.metoc.gov.au). Figure 6 shows a GHRSST L4 product that was published as a web map service displayed in ESRI ArcGlobe. The ArcGlobe application, like other ESRI ArcGIS Desktop products, allows users to connect to web services published and broadcast by other sites.

5. CONCLUSION

GIS applications are now in widespread use throughout the potential GHRSST user community. The commonly used ESRI ArcGIS Desktop application provides users with a rich tool set that can be used to process and display GHRSST L2P and L4 data in both interactive and automated modes. The ability to extend the geo-processing models to Python scripts, run as scheduled tasks, allows batch processing and publishing of GHRSST products as standards compliant web map services, thus satisfying the requirements of user communities that wish to view and interact (zoom, pan, compare) with the products without downloading the raw data.

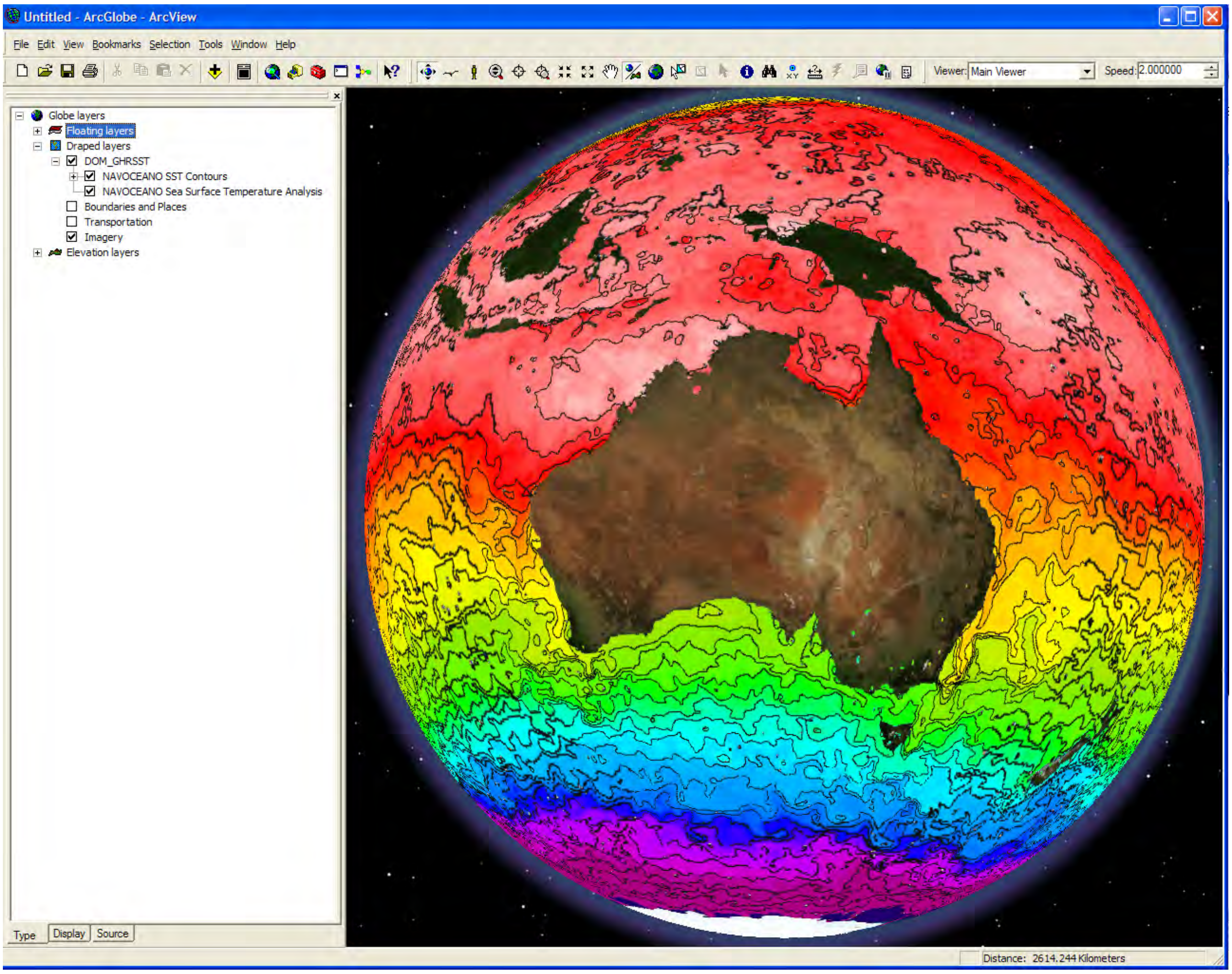

Figure 6 - Web Map Service of GHRSST L4 Product displayed in ESRI ArcGlobe

WORKING WITH THE GHRSST DATA FORMAT: EXPERIENCES OF THE GCOS SST INTERCOMPARISON WORKING GROUP.

Tess Brandon(1)

(1) *NOAA National Oceanographic Data Center (NODC), 1315 East West Highway, Silver Spring, Maryland (USA)*
Email : tess.brandon@noaa.gov

ABSTRACT.

The GCOS SST intercomparison facility is an online resource at NODC that provides access to a suite of SST datasets and standard intercomparison diagnostics. As part of the GHRSST Reanalysis effort, the datasets are reformatted to Matlab and netCDF formats following the GHRSST format specification. Although GCOS datasets are unique in the context of the GHRSST convention, use of the format specification is largely successful and user statistics demonstrate a preference for netCDF over Matlab formats. However, additional formats such as ASCII must be made available to fully understand the needs of the SST user community for GCOS intercomparison products.

1. INTRODUCTION.

Global and near-global SST analysis products are created using a wide range of statistical reconstructions and interpolations that are applied to datasets from a variety of input platforms. These datasets are subjected to quality control processes, bias corrections, and input from sea ice data as well as *a priori* assumptions. The result of these different analysis routines is a collection of products that can say subtly or significantly different things about the changing climate. The Global Climate Observing System (GCOS) Sea Surface Temperature (SST) and Sea Ice (SI) Working Group (WG) was created with the goal of understanding the origin and nature of the differences between these analyses.

As part of that effort, the NODC has undertaken a project to record and evaluate differences among SST/SI analyses. Working within the context of the GHRSST Reanalysis effort, the NODC established an online intercomparison facility, through which all GCOS datasets are available for download in Matlab and netCDF formats, following the GHRSST convention[1]. This paper describes the experiences of the GCOS SST WG in working with the GHRSST format, and netCDF in general, in terms of file creation, file dissemination and use.

2. CONVERTING TO GHRSST FORMAT.

A major goal of the intercomparison facility is to maximize access: the intended audience of the site includes both working group members and general users of SST products. However, the collection of SST products being intercompared spans a wide range of temporal and spatial resolutions, as well as data formats (Figure 1). Thus, to maximize user compatibility, all GCOS datasets were reformatted to adhere to one standard format at two resolutions in GHRSST-compliant netCDF and Matlab formats.

Data Set Name	Satellite Era (1981-2007)	Historical Era (1850-2008)	Original Format
AVHRR Pathfinder V5[2]	X		HDF
Operational AVHRR	X		text
Hadley Centre SST V2[3]	X	X	netCDF
NOAA OISSTv2[4]	X		text
NOAA ¼-deg. DOISSTv1[5]	X		netCDF
Hadley Centre ISSTv1[6]	X	X	netCDF
NOAA ERSSTv3[7]	X	X	text
Kaplan Reconstructed[8]	X	X	netCDF
International COADS v2.4[9]		X	netCDF
COBE Analysis[10]		X	text

Figure 1: GCOS SST/SI Intercomparison Products

This reformatting was performed in Matlab using open source netCDF tools. GCOS datasets are unique in the context of the GHRSST format specification for several reasons, but overall the format specification was found to be flexible enough to accommodate them. For one thing, each GCOS dataset consists of a "data cube" (time dimension >1) rather than a two-dimensional map of SST at a single timestep. More challenging differences include the current lack of a Level 3 format specification for the several GCOS datasets that fall under L3 processing classification. In all cases, the Level 4 specification was used in favor of its reduced requirements.

Also, although certain GCOS datasets contain fields of standard deviation or uncertainty that do not exactly comply with the GHRSST "analysis_error" field, all datasets use this standard variable name for lack of more specific options within the GHRSST convention.

In addition to netCDF, a Matlab format was designed that mimics the GHRSST format in terms of variable names, dimensions and attributes.

3. USER REPORTS.

In addition to the SST datasets, the intercomparison facility provides access to a large collection of standard intercomparison diagnostics calculated for each dataset, browse graphics of these diagnostics, and the software used to reformat the original SST analysis products. Figure 2 shows all downloads from the intercomparison facility since January 2008, separated by file type.

File Type	Number of Requests	% Bytes	% Available files of that type
.nc.gz	72	53	514
.nc	857	13	92
.mat	201	31	287
.jpg	2905	4	497
.fig	96	0	84

Figure 2: User statistics for all GCOS intercomparison site files downloaded since January 2008.

Of the files available through the site, only the datasets themselves are represented in GHRSST-compliant netCDF. Of these, the weekly, one degree satellite era data sets are compressed (extension .nc.gz), and are the most frequently downloaded file type in this report period. Upon further analysis, approximately 60% of the GHRSST-style files (including Matlab imitations) were netCDF. All other data files are available either in netCDF or both netCDF and Matlab formats. In general these numbers show a preference for netCDF files over Matlab files. This is not surprising given the wide range of tools able to read netCDF files, compared with the commercial software-specific Matlab files.

Working group members were asked to speak anecdotally about their experience using the GHRSST format specification in the context of this project. Responses varied greatly according to the format of choice already being employed by each member for his or her own data set. One netCDF user had abandoned Climate Forecast conventions (CF – a component of the GHRSST convention) due to a lack of simple documentation for the standard, its best practices, and any explanation of rationale. Another user preferred formatted text accompanied by a format statement, citing the steep learning curve and time required upfront to read netCDF for the first time. He uses simple text so that “anyone with any computer could most easily use the data.” Ironically, simple text can be the most challenging format to work with for Matlab users.

4. FUTURE WORK.

In general, users will choose formats that allow them to work with software and scientific analysis tools they already employ. NetCDF can be read by a wide array of tools, and in the case of GCOS SST products, is preferred over the Matlab format. The GCOS intercomparison facility does not currently provide access to its products in any other format. However, the original plan drafted by the working group includes ASCII as a third format in the interest of possible future uses. Thus a new goal of the intercomparison facility is to provide all GCOS SST datasets in ASCII with accompanying format statements, and to revisit user statistics after a year for comparison to netCDF and Matlab formats. This will more completely address the current needs of the SST user community, in addition to providing insight into those needs for future improvements to format specifications and standards.

5. REFERENCES.

1. The GHRSST-PP Science Team and GDS-TAG working group, 2008: The Recommended GHRSST-PP Data Processing Specification GDS (Version 2.0 revision 0.1) L4 product specification.
2. 4 km AVHRR Pathfinder Version 5 SST Project, http://pathfinder.nodc.noaa.gov.
3. Rayner, N. A. et al., 2006: Improved analyses of changes and uncertainties in sea surface temperature measured *in situ* since the mid-nineteenth century: the HadSST2 data set. *J. Climate*, 19(3) 446-469.
4. Reynolds, R.W., 1988: A real-time global sea surface temperature analysis. *J. Climate*, 1, 75-86.
5. Reynolds, R.W. et al., 2002: An improved in situ and satellite SST analysis for climate. *J. Climate*, 15, 1609-1625.
6. Rayner, N.A. et al., 2003: Global analyses of sea surface temperature, sea ice, and night marine air temperature since the late nineteenth century. *J. Geophys. Res.*, 108 (D14), 4407 10.1029/2002JD002670.
7. Smith, T.M. et al., 2008: Improvements to NOAA’s historical merged land-ocean surface temperature analysis (1880-2006). *J. Climate*, 21, 2283-2296.
8. Kaplan, A. et al., 1998: Analyses of global sea surface temperature 1856-1991. *J. Geophys. Res.*, 103, 18.567-18.589.
9. Woodruff, S.D. et al., 2005: ICOADS Release 2.1 data and products. Int. J. Climatol. (CLIMAR-II Special Issue), 25, 823-842 (DOI: 10.1002/joc.1166).
10. Ishii, M. et al., 2005: Objective Analyses of SST and Marine Meteorological Variables for the 20th Centure using ICOADS and the KOBE Collection. Int. J. Climatol., 25, 865-879.

COMPARISONS OF DAILY SEA SURFACE TEMPERATURE ANALYSES FOR 2007-08.

Richard W. Reynolds [(1)], Dudley B. Chelton [(2)] and Qingtao Song [(3)]

[(1)] *NOAA National Climatic Data Center, Asheville, North Carolina (USA), Email: Richard.W.Reynolds@noaa.gov*
[(2)]*College of Oceanic and Atmospheric Sciences and Cooperative Institute for Oceanographic Satellite Studies, Oregon State University, Corvallis, Oregon (USA)*
[(3)] *National Satellite Ocean Applications Service, Beijing (China)*

ABSTRACT

Six different sea surface temperature (SST) analyses have been compared with each other and with buoy data for the period: 2007-08. All analyses used different sets of satellite data with different algorithms, spatial resolution, etc. Most analysis procedures and weighting functions differ. Thus, differences among analyses could be large in high gradient and data sparse regions. To help quantify SST analysis differences, wavenumber spectra were computed at several locations. Furthermore statistical comparisons made using collocated buoys showed that grid resolution does not always correlate with analysis resolution. The results also indicate that changes in satellite instruments over time can impact SST analysis resolution.

1. INTRODUCTION

Sea surface temperature (SST) analyses have increased in recent years along with an increase in the number of satellite instruments. Many of these analyses are part of the Group for High-Resolution Sea Surface Temperature (GHRSST) (1, and http://www.ghrsst-pp.org/, see in particular "Data Access"). The analyses use in situ and remotely sensed data from a variety of geostationary and polar satellites and are computed over different regions and time periods with different spatial and temporal resolutions. Most of these products tend to cover roughly the last five years when satellite instruments such as the microwave (MW) Advanced Microwave Scanning Radiometer (AMSR) and the infrared (IR) Moderate Resolution Imaging Spectroradiometer (MODIS), joined two longer time series of IR instruments: the Advanced Very High Resolution Radiometer (AVHRR), since November 1981, and the Along Track Scanning Radiometer (ATSR), since August 1991, as sources of global SST observations.

2. ANALYSES

Analyses were selected that were global with at least daily resolution and available for a two year period, 2007-08. Analyses from GHRSST Jet Propulsion laboratory (JPL) web site were preferred (see table at http://ghrsst.jpl.nasa.gov/GHRSST_product_table.html). These selection criteria resulted in 5 analyses. One additional analysis from the National Oceanic and Atmospheric Administration's (NOAA) National Centers for Environmental Prediction (NCEP) was added because it is used at two forecast centers. The analyses are discussed by increasing grid resolution.

Analyses 1 and 2: Two of the analyses are produced daily on a 1/4° grid at NOAA's National Climatic Data Center and described by (2). One analysis (AVHRR-only) uses in situ and AVHRR data, the second analysis (AMSR+AVHRR) adds AMSR data. Both analysis procedures are the same. In situ data from ships and buoys are used to provide a large-scale bias correction of the satellite data.

Analysis 3: The US Navy Coupled Ocean Data Assimilation (NCODA) analysis (3) is computed operationally using in situ data and AVHRR, AMSR, and Geostationary Orbiting Environmental Satellite (GOES) data. The analysis is performed on a 1/9° grid on the equator with gradual reductions in latitudinal intervals to keep the size of the grid boxes nearly square between 80°S and 80°N.

Analysis 4: The Remote Sensing System (RSS) analysis is computed on a ~1/11° grid using AMSR, Tropical Rainfall Measuring Mission Microwave Imager (TMI) and MODIS data. This analysis is unpublished, although some details are available at http://www.ssmi.com/sst/microwave_oi_sst_browse.html. The RSS is the only analysis that does not use in situ data directly.

Analysis 5: The NCEP Real Time Global High Resolution (RTG-HR) is operationally computed daily using in situ and AVHRR data on a 1/12° grid (4). Only the most recent year of analyses is available for download at ftp://polar.ncep.noaa.gov/pub/history/sst/ophi/.
Analyses are not available on the JPL GHRSST data web site.

Analysis 6: The UK Met Office has a 1/20° Operational SST and Sea Ice Analysis (OSTIA) analysis on a 1/20° grid that uses in situ, AVHRR, AMSR, TMI, Advanced ATSR (AATSR), and geostationary Spinning Enhanced Visible and Infrared Imager (SEVIRI) data. A paper is under preparation. Further details can be found at http://ghrsst-pp.metoffice.com/pages/latest_analysis/ostia.html.

3. PRELIMINARY DIFFERENCES

Figure 1 shows a region in the western tropical Pacific for 1 January 2007. The results show that the features are smoothest in the RTG-HR analysis. The RSS analysis has considerable small-scale detail that is derived from MODIS 1 km data. However, because MODIS data are limited by swath width and clouds, they are not available every day for the region shown in the figure. Thus, some of the RSS small scale details may be several days old or older.

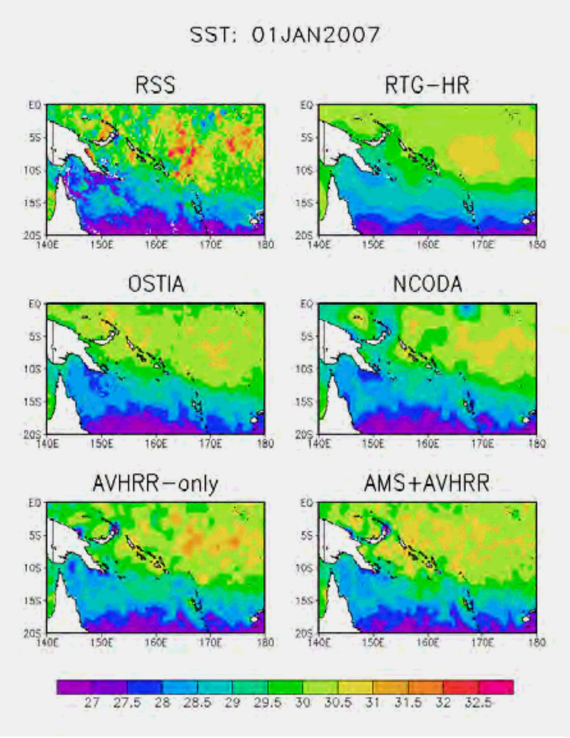

Figure 1. Six daily SST analyses for 1 January 2007. Highest details are evident in RSS, lowest in RTG-HR.

4. WAVE NUMBER SPECTRA

The resolutions of the six SST analysis products considered in this study are evident from the zonal wavenumber spectra in Fig. 2. Spectra are shown for a Southern Hemisphere mid-latitude region (the Agulhas Return Current in the South Indian Ocean). Each spectrum is the ensemble average of 31 individual zonal wavenumber spectra computed from daily SST fields over the months of January 2007 and July 2007.

A consistent feature in Fig. 2 is that the RSS SST fields have much higher spectral energy than any of the other SST products at wavelengths shorter than about 300 km owing to the effects of the small-scale energy discussed previously. The RSS spectra roll off with zonal wavenumber, k, as approximately k^{-2} in all cases. In comparison, the wavenumber dependence of the OSTIA spectra ranges from k^{-4} to k^{-5}. The NCODA, AVHRR-only and AMSR+AVHRR spectra are somewhat steeper. The spectral energy in the RSS fields is more than 2 orders of magnitude higher than any of the other SST analyses at the highest wave numbers, thus quantifying the noisy character of the RSS SST fields evident from their speckled appearance in the example map in Fig. 1. Another consistent feature is that the RTG-HR SST fields have significantly lower resolution than any of the other SST products, as evident from the steep roll off of the spectra at wavelengths shorter than about 250 km. This roll off indicates that the analysis procedure evidently attenuates the shorter-scale variability.

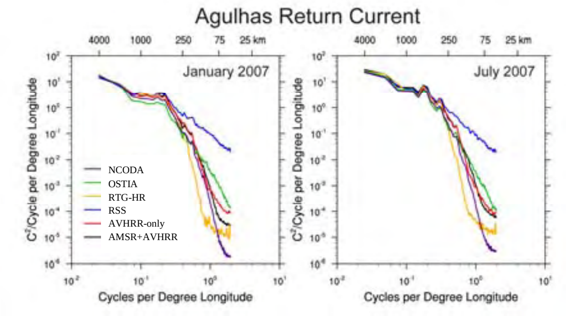

Figure 2. Zonal wavenumber spectra for January 2007 (left) and July 2007 (right) for the Agulhas Return Current (45ºE to 85ºE, 47ºS to 38ºS)

5. COMPARISONS WITH BUOYS

To further quantify these results, comparisons were carried out using buoy data. As noted above, buoys are used in all analyses except the RSS analysis. Thus, the buoys are not independent data. The extent to which the buoy SSTs were replicated in any particular SST product depends on how heavily they were weighted compared to other data used in the analysis procedure.

In the AMSR+AVHHR and AVHRR-only analyses, buoy data were averaged onto a daily 1/4° grid after climatological outliers were removed. Over the 2007-08 period, the gridded buoy data were screened for locations with at least one daily observation for 90% of the days (722 days out of 731). The resulting 92 locations were grouped into ten regions. Time series from the analyses were constructed by spatial linear interpolation to the buoy locations. Missing data in all time series (both data and analysis) were filled by temporal linear interpolation.

Auto spectra were computed at each buoy location. The individual spectra were averaged over each region. If each spectrum were based on independent analyses or data, the spectral degrees of freedom for the average would be multiplied by the number of buoy locations used. The increase in the degrees of freedom would reduce the confidence limits. To avoid over reduction in the confidence limits, the number of independent time series in each average spectrum was estimated to be equal to half the total number of buoy locations in each region.

Figure 3 shows the auto spectra in the Aleutians Region. At low frequencies (< 0.02 cpd) the RTG-HR significantly differs from the other analyses and the buoys at the 95% confidence limit. This difference is due to a 2007 winter bias offset which may be due to bad sea ice data. At middle frequencies (between 0.02 and 0.2) the RSS and RTG-HR analyses have significantly greater variability than the buoys and the other analyses. In addition, the RTG-HR has highest variability at the highest frequencies while the AVHRR-only has the lowest. These high frequency differences are significant and that implies that the RTG-HR is too noisy and that the AVHRR-only is too smooth.

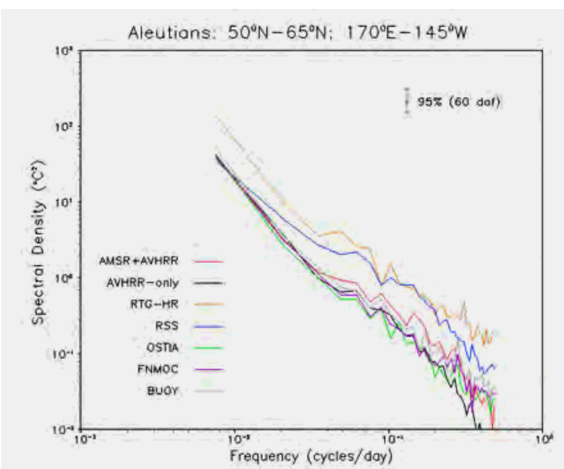

Figure 3. Average auto spectra for the buoys and the 6 analyses for the Aleutian Region. Note the RTG-HR difference at low frequencies.

Figure 4 shows the auto spectra in the Western Tropical Pacific Region. All spectra agree with each other within the confidence limits at low frequencies (< 0.02 cpd). However, the RSS analysis has significantly larger variance than the other spectra at middle and high frequencies. Furthermore, over these frequencies the RSS SST variance is roughly half an order of magnitude larger than any of the other SST spectra. A similar RSS difference also occurs in the other tropical regions and was the most dramatic difference among the analyses. The RSS difference is consistent with the wavenumber spectral analysis in Section 4 and suggests that the RSS analysis needs more spatial smoothing.

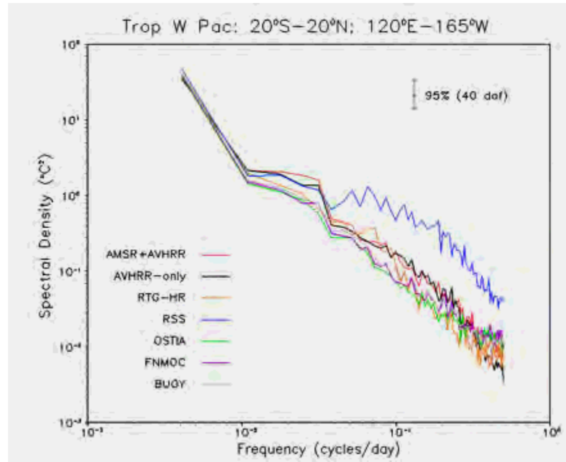

Figure 4. Average auto spectra for the buoys and the 6 analyses for the Tropical West Pacific Region. Note the high values for the RSS analysis for high frequencies (>0.02cpd).

Because the spectra are 'red' as shown in Figs 3 and 4, the correlation between buoys and analyses will be dominated by the lowest frequencies. Thus, the correlations presented here were computed using filtered time series. The filtering was done at a cutoff frequency of 0.2 cpd (a 5 day period) to separate low and high frequencies for both frequency bands. Cross correlations were computed between the buoys and analysis time series for each region.

The analysis-to-buoy correlations for each region are shown in Fig. 5 for the high frequency correlations (> 0.2 cpd). These are much lower and show more differences among analyses than the low frequency correlations (not shown). The NCODA correlations are the highest (between 0.70 and 0.86); the analyses with the next higher correlations vary with region among the AVHRR-only, AMSR+AVHRR and OSTIA with OSTIA more often the largest. The RTG-HR and RSS are almost always lower that the others except in the Gulf Stream Extension Region, where the RTG-HR has a slightly higher correlation than the AMSR+AVHRR analysis. The AVHRR-only and AMSR+AVHRR correlations are very similar (within 0.10) except in the Gulf Stream Extension Region where the AVHRR-only is higher than the AMSR+AVHRR (0.61 and 0.37, respectively). The difference may be related to the cloud cover in this region. If the AVHRR data are restricted due to clouds, the buoy data will be relatively more important in the AVHRR-only analysis than the AMSR+AVHRR analysis.

6. CONCLUSION

Six different SST analyses have been compared with each other and with buoy data for the period: 2007-08. To help determine SST analysis resolution, wavenumber spectra were computed at several locations. These results suggested that the RSS is too noisy and the RTG-HR analysis is too smooth. Further comparisons were made using collocated buoys for ten regions using time series, auto-spectra and low and high pass filtered correlations between the buoy data and the analyses. These result showed that RSS is too noisy in the tropics and that RTG-HR had winter biases in the Aleutians Region during January and February 2007. The correlation results showed that analysis-to-buoy correlations at high frequencies (> 0.2 cpd) were best with the NCODA and OSTIA analyses and worst with the RTG-HR and RSS analyses. The high correlation indicates that NCODA, and to a somewhat lesser extent, OSTIA were strongly tuned locally to buoy data, where they exist. The AVHRR-only analysis is useful for climate studies because it is the only daily SST analysis that extends back to September 1981.

The grid resolution is a lower limit of the final analysis resolution. A grid scale that is consistently smaller than the actual analysis resolution becomes computationally inefficient. The expected analysis resolution is determined by analysis parameters such as error correlation scales. However, the actual analysis resolution is limited by input observation resolution and coverage over the temporal period of the analysis. In the examples shown here the OSTIA analysis has the smallest grid size and yet does not show the smallest analysis scales. If the analysis resolution was made too small, as it was for the RSS analysis, the analysis will appear to have high resolution, but the features will represent noise rather than signal. Consider for example a region with 1 km IR data and 50 km MW data. During cloudy periods the IR data will be limited while the MW data will not be impacted. Thus, any analysis which attempts to obtain the highest resolution possible based on IR data must reduce this resolution in regions where the IR data are missing or the coverage is reduced. This change in IR coverage can result in apparent temporal inhomogeneity in the small-scale variance that could wrongly be interpreted as real and may be problematic for some applications.

7. REFERENCES

1. Donlon, C. and others, "The Global Ocean Data Assimilation Experiment High-resolution Sea Surface Temperature Pilot". *Bull. Amer. Meteor. Soc.*, **88**, 1197-1213, 2007.
2. Reynolds, R. W., T. M. Smith, C. Liu, D. B. Chelton, K. S. Casey, and M. G. Schlax, "Daily high-resolution blended analyses for sea surface temperature", *J. Climate*, **20**, 5473-5496, 2007.
3. Cummings, J. A., Operational multivariate ocean data assimilation, *Q. J. R. Meteorol. Soc.*, **131**, 3583-3604, 2005.
4. Gemmill, William, Bert Katz and Xu Li, "Daily Real-Time Global Sea Surface Temperature - High Resolution Analysis at NOAA/NCEP", NOAA / NWS / NCEP / MMAB Office Note Nr. 260, 39 pp, 2007 (Available at: http://polar.ncep.noaa.gov/sst/).

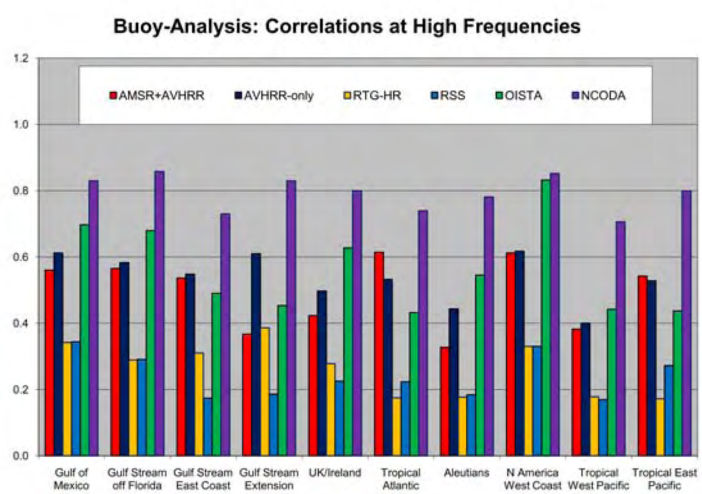

Figure 5. Correlations for high frequencies (>0.2cpd) for 2007-08. Note that the NCODA – buoy high frequency correlations are the largest.

GRIDDED SST DATA SETS: HOW TO CHOOSE A "RIGHT" ONE?

Alexey Kaplan(1)
Lamont-Doherty Earth Observatory of Columbia University, Palisades, NY (United States)
Email: alexeyk@ldeo.columbia.edu

ABSTRACT
As Global High-Resolution Sea Surface Temperature (GHRSST) Pilot Project matured, its variety of operational gridded analyses, Level 4 (L4) products, started growing very fast. At this time there are no less than ten global SST analyses produced on daily or 6-hourly basis, with spatial grid resolutions varying from 5 to 25 km; there are also regional products, some with the spatial grid resolution down to 2 km. While having a systematic intercomparison system for all these products and a uniform description of their uncertainties is an important priority, from the point of view of most users a practical problem in need of a quick solution is how to choose the "best" data set for each application?

1. INTERCOMPARISON APPROACH

In every analysis scheme the SST data entering the analysis, upon passing the quality control, is getting reconciled and interpolated into the gridded analyzed field. Results depend both on the data used in the analysis, its bias-correction procedures, and on the assumed covariance structures. This dependency is complicated: if data coverage is dense and observations are assumed to be of good quality, the covariance structures almost do not matter, neither for the solution, nor for error estimates. But if the data coverage is sparse and/or they are assumed to be of poor quality, the OI solution takes the form of the assumed covariance structure in most places. Among two analyses using precisely the same data, the one that specifies larger observational error and larger-scale covariance will produce a smoother solution. But the one which specifies these parameters to be closer to the truth will produce a solution with the smaller actual error.

Since the list of GHRSST L4 products is currently growing quite fast (Donlon et al. 2007), the primary focus of this paper is on the intercomparison on the following representative data sets,

- Operational SST and Sea Ice Analysis (OSTIA) produced daily by the U.K. Met Office, with 6 km spatial resolution, applying multiscale OI to all GHRSST input satellite data sets and in situ observations (Stark et al. 2007),
- Microwave and infrared "fusion" (MW-IR) OI SST from Remote Sensing Systems, 9 km spatial resolution (hereafter RSS),
- NCDC Daily OI combining AMSR and AVHRR, observations with in situ data on 0.25^o spatial grid (Reynolds et al. 2007),

with the addition of others as needed, e.g.,

- FNMOC 10-km high resolution SST and sea ice analysis updated every 6 hours,
- High resolution version of the NCEP RTG analysis (RTG-HR) with $1/12^o$ spatial resolution,
- Regional Mediterranean Sea analysis from Medspiration, with 2km spatial resolution.

Figure 1 illustrates the basic utility of such comparisons: three data sets (OSTIA, RSS, and NCDC) of quite different nominal resolution (6, 9, and 25 km) are intercompared in terms of their mean differences and standard deviations of these differences around their means. Comparison was done for the period January 2 - June 24, 2008; OSTIA and RSS data sets were averaged on the 25 km NCDC Daily analysis grid. In terms of mean bias pattern there is significantly more similarity between RSS and OSTIA than between them and NCDC. The patterns of standard deviation of time-varying differences are quite similar for all three pairs and can be tracked to the pattern of small-scale and short-term variability in the SST.

Along with intercomparison of L4 products, a similar intercomparison of major input streams into these analyses can be performed as well, e.g. AVHRR Pathfinder product, as well as L2P GHRSST data sets for AATSR, MODIS, AMSR-E, TMI, and in situ SST data sets from International Comprehensive Ocean–Atmosphere Data Set (ICOADS, Woodruff et al., 1987; Worley et al., 2005) and the U.K. Met Office Hadley Centre data set of bias corrected in situ SST observations (HadSST2, Rayner et al., 2006). These will be separated by day vs night, by observational platforms (buoy vs ship), and, if needed, by measurement type (e.g. buckets vs engine intake room measurements on ships). The usefulness of such comparisons is illustrated here by the AVHRR Pathfinder SST compared with ICOADS $1^o \times 1^o$ summaries (Figure 2). The comparison covered 2000-2005 period and found AVHRR on average cooler than in situ measurements. Both data sets are probably biased: AVHRR data can be too cool because of residual cloud contamination (Reynolds et al. 2007), and various inter-platform biases in 0.1-0.3^{o}C range are now being identified in in situ data (Reynolds, Rayner, 9th GHRTSST-PP Science Team meeting presentations; Kenedy, Kent, CLIMAR-III presentations). The most striking one is obvious in Figure 2, left panel: SST data from ship routes between Hawaii and the Western U.S is clearly too cold.

2. EFFECTIVE RESOLUTION VS ANALYSIS ERROR

It is important to characterize effective spatial and temporal resolution of GHRSST L4 products and to analyze the distribution of their error over different time and space scales. Figure 3 illustrates the differences between nominal and actual resolution in the analyzed fields of three GHRSST L4 products, for January 2, 2008, in the California Coastal System.

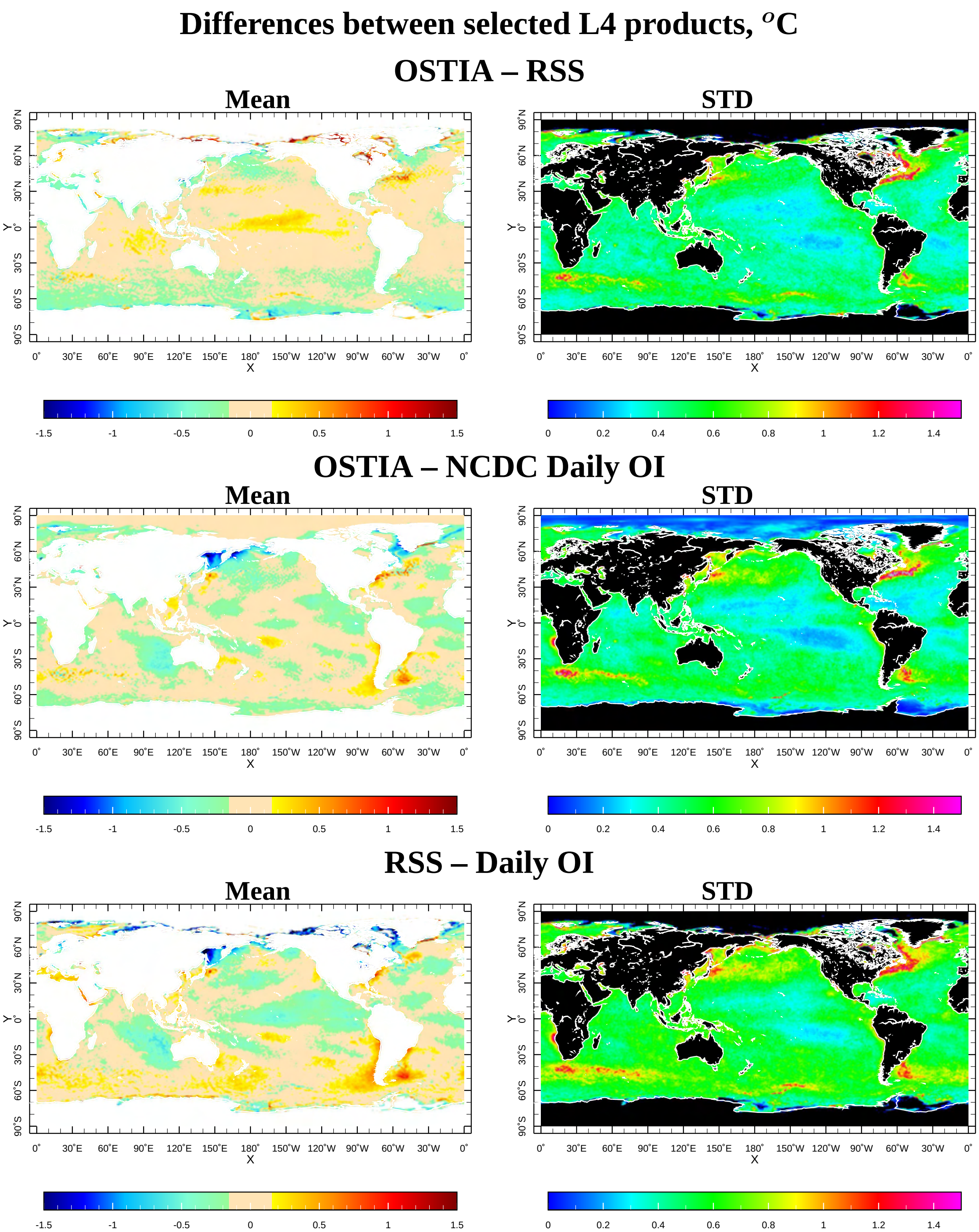

Figure 1: Mean and standard deviation differences between OSTIA, RSS, and NCDC Daily OI products, ^{o}C. Period of comparison is January 2 – June 24, 2008; higher resolution data sets are averaged on 0.25^{o} grid.

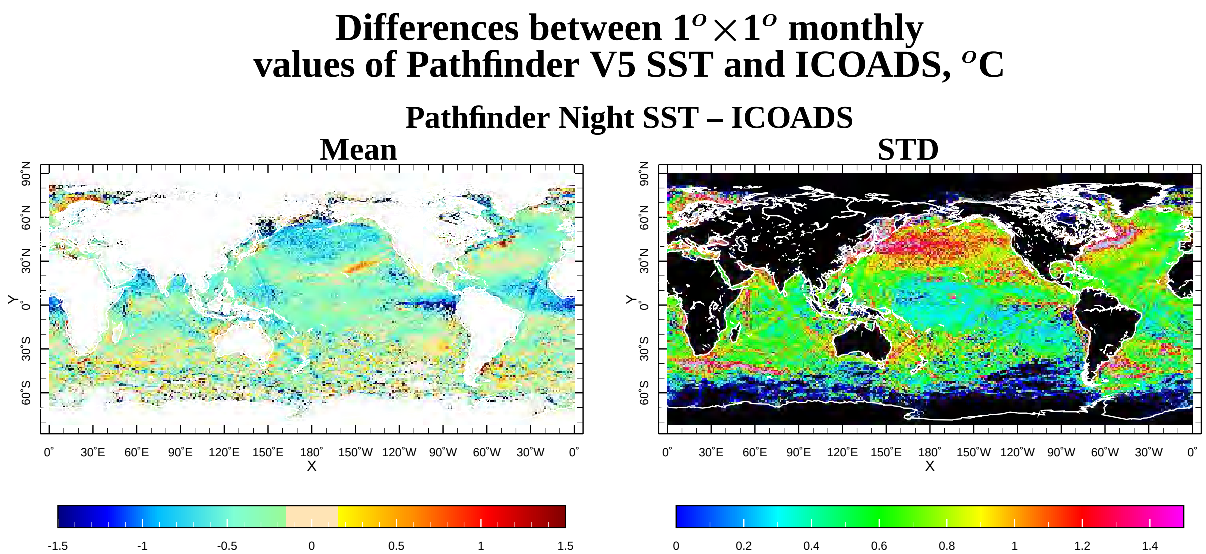

Figure 2: Difference between $1^o \times 1^o$ monthly summaries of Pathfinder V5 SST values and ICOADS. Left panels show mean difference for 2000-2005 period, and right panels show standard deviations of the differences between the two data sets. Daily differences were averaged into monthly bins before calculating means and standard deviations. Units are ^{o}C. ICOADS observations were not separated for day and night.

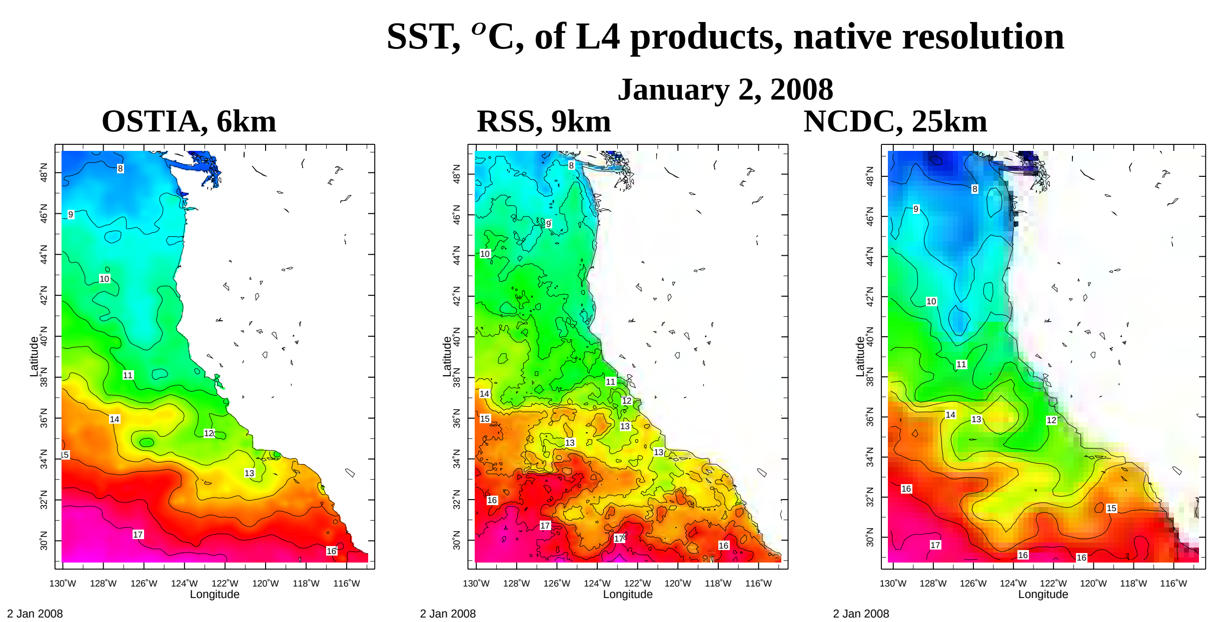

Figure 3: SST, ^{o}C, on January 2, 2008, in the California Coastal System from three GHRSST L4 products.

$|\nabla T|$, ^{o}C/100km, of L4 products, native resolution

January 2 – June 24, 2008

OSTIA, 6km **RSS, 9km** **NCDC, 25km**

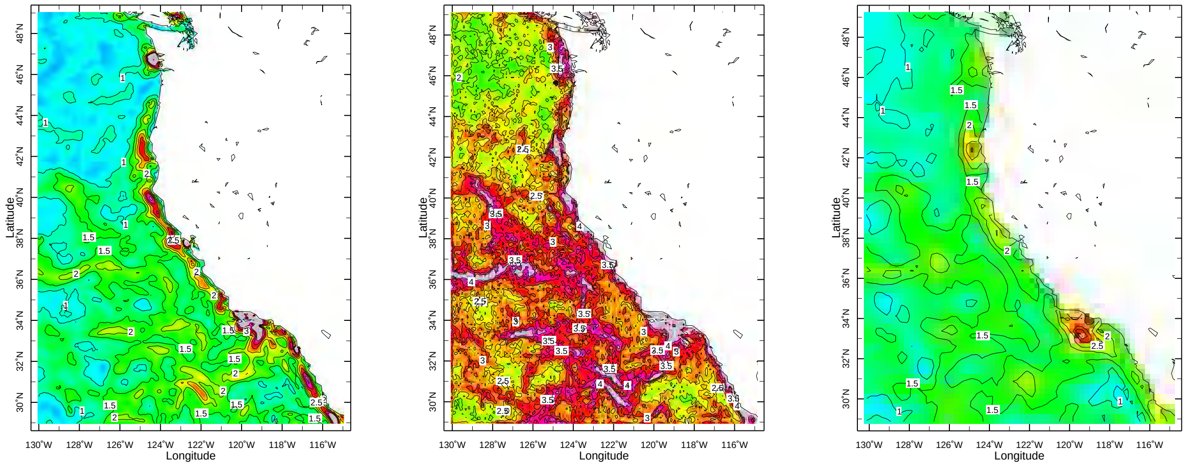

Figure 4: $|\nabla T|$, ^{o}C/100km, averaged over January 2 – June 24, 2008, period in the California Coastal System, according to three GHRSST L4 products.

In terms of relatively large scales, OSTIA and NCDC Daily OI look almost similarly smooth, while the RSS fields, of intermediate nominal resolution, has a seemingly weaker separation of large-scale and small-scale variability. When the magnitude of daily horizontal SST gradient is averaged for the period January 2 - June 24, 2008 (Figure 4), the OSTIA representation of the gradient field looks much closer to the GOES-based pattern derived by Castelao et al. (2006) than the representations by other analyses do. (A similar point, but with an additional emphasis on temporal variability, was made by R.W.Reynolds in his presentation at the 9th GHRSST-PP Science Team Meeting).

3. CONCLUSIONS

While the truly best data set might not even exist among available products, I recommend the following. From all data sets satisfying a given user's requirements of spatial and temporal coverage that also have spatial and temporal grid resolutions as fine as absolutely necessary to be used in a given application, at this time the highest weight should be given simply to the amount and types of input data that come into the candidate L4 products. Indeed, the nominal resolution of the product's grid does not necessarily reflect its actual resolution, because the latter can be and often is reduced by the analysis scheme to the extent that a product on a nominally finer grid can have lower actual resolution. The resolution characteristic is partially independent of the error: while the error of optimal analyses based on the same complete suite of the input data always increases with increasing resolution, for suboptimal analyses based on different sets of inputs, this relationship does not have to hold.

4. REFERENCES

Castelao, R.M., T.P.Mavor, J.A.Barth, L.C.Baker, 2006: Sea surface temperature fronts in the California Current System from geostationary satellite observations, *J. Geophys. Res.*, **111**, doi: 10.1029/ 2006JC003541.

Donlon, C., et al., 2007: The Global Ocean Data Assimilation Experiment High-Resolution Sea Surface Temperature Pilot Project, *Bull. Amer. Meteorological Soc.*, **88**, 1197-1213.

Rayner, N.A., P.Brohan, D.E.Parker, et al., 2006: Improved analyses of changes and uncertainties in sea surface temperature measured in situ sice the mid-nineteenth century: The HadSST2 dataset, *J. Climate*, **19**, 446-469.

Stark, J.D., C.J.Donlon, M.J.Martin, and M.E.McCulloch, 2007: OSTIA – An operational, high resolution, real time, global sea surface temperature analysis system., *Oceans '07 IEEE*, Aberdeen, Conference Proceedings, 061214-029.

Reynolds, R.W., T.M. Smith, C.Liu, D.B.Chelton, K.S.Casey, and M.G.Schlax, 2007: Daily High-Resolution-Blended Analyses for Sea Surface Temperature, *J. Climate*, **20**, 5473-5496.

Worley, S.J., S.D. Woodruff, R.W. Reynolds, S.J. Lubker, and N. Lott, 2005: ICOADS Release 2.1 data and products. *Int. J. Climatol.*, **25**, 823-842.

GHRSST Level 4 product comparisons in coastal regions

Edward Armstrong[1] and Jorge Vazquez[1]
[1]*Jet Propulsion Laboratory, California Institute of Technology, Pasadena, CA, USA*
edward.m.armstrong@jpl.nasa.gov

Abstract
The Group for High Resolution SST (GHRSST) Project has produced several sea surface temperature (SST) products based on a wide variety of infrared and microwave sensors. These include Level 4 global products that are typically produced at a 6-27 km spatial resolution with a daily temporal frequency. The Level 4 products are based on a statistical blend or merging of the Level 2 input data (e.g., through optimal interpolation) and result in globally gap free data. Before such data can be used in coastal ocean model initialization or assimilation, it is necessary to assess their accuracy and validation in the region of interest to determine under what conditions they can be used in confidence. In this investigation, we analyze four GHRSST Level 4 products over a period of one year (June 2007-June 2008) in the Gulf of Mexico, and western and eastern US coastal regions. The in situ sources of SST for the assessments were more than 30 moored buoys from the NOAA National Data Buoy Center. These buoys were used for daily comparisons with the SST satellite sources that allowed us to spatially discriminate from very near shore to offshore locations where the dynamic oceanographic conditions can substantially change. The hourly SST measurements from the buoys were also used to temporally separate the validation into both a 24-hour daily comparison as well as a nighttime only comparison to assess the confidence of a "foundation" temperature in the Level 4 SST products. The reasoning here is that L4 products should compare more favorably to nighttime only in situ data. Initial comparisons indicate the GHRSST products perform very well with accuracies of about 0.5-0.8 °C although there are locations and products where larger errors exist.

Data Sources and Methods
The investigation compared four unique GHRSST Level 4 products known by their product identifications as AVHRR_OI and AVHRR_AMSR_OI from the NOAA National Climatic Data Center (NCDC), OSTIA from the UK. Met Office, and mw_ir_OI from Remote Sensing Systems. Both products from the NCDC are considered a "blended" L4 product using IR radiometer data (AVHRR and AMSRE) and in situ data from ships and buoys. The OSTIA product also contains these data sources in addition to TMI, SEVIRI and AATSR and is considered a "foundation" temperature. The mw_ir_OI product uses only satellite sources from AMSRE, TMI and MODIS and also represents a "foundation" temperature. All these GHRSST products were acquired from the GHRSST Global Data Assembly Center (http://ghrsst.jpl.nasa.gov).

Buoy observations were acquired from the NOAA National Data Buoy Center (NDBC; http://ndbc.noaa.gov) for automated coastal buoys within the study regions.

For the one year comparison period, matchups between the buoys and locations of nearest satellite SST pixels were performed over a 24 hour daily and separate 12 hour nighttime and daytime periods based on local sunrise and sunset times.

Discussion

Over 30 buoys were compared in the three study regions over a one-year period with the results summarized in Figure1 and Table 1.

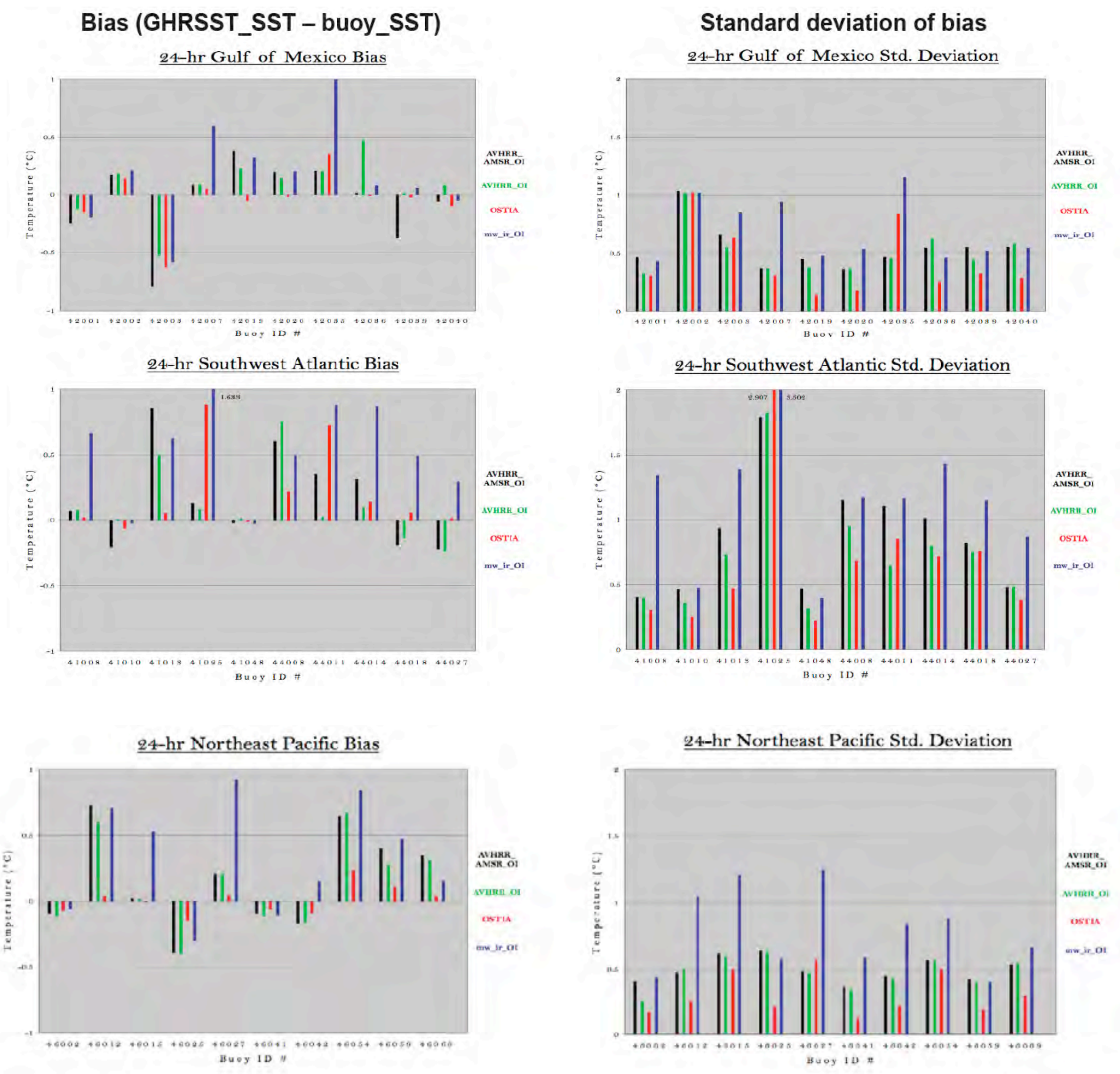

Figure 1. Bias and standard deviation of bias comparisons for four GHRSST Level 4 products (shown in different colors) in three US coastal regions. X-axis represents individual NDBC buoy locations (based on NDBC identification number.) These figures represent the matchups of 24-hour averaged buoy data to the daily GHRSST level 4 products.

24 hour/night bias summary statistics for all matchups

Gulf of Mexico		24 Hour		Nighttime	
		mean Bias	Std. Dev.	mean Bias	Std. Dev.
L4 Product	AVHRR_AMSR_OI	-0.041	0.548	0.011	0.566
	AVHRR_OI	0.077	0.514	0.129	0.531
	OSTIA	-0.042	0.430	0.009	0.446
	mw_ir_OI	0.163	0.695	0.216	0.696

Northeast Pacific		24 Hour		Nighttime	
		mean Bias	Std. Dev.	mean Bias	Std. Dev.
L4 Product	AVHRR_AMSR_OI	0.103	0.501	0.116	0.525
	AVHRR_OI	0.085	0.463	0.099	0.488
	OSTIA	-0.025	0.276	-0.012	0.305
	mw_ir_OI	0.278	0.744	0.292	0.760

Southwest Atlantic		24 Hour		Nighttime	
		mean Bias	Std. Dev.	mean Bias	Std. Dev.
L4 Product	AVHRR_AMSR_OI	0.140	0.780	0.196	0.824
	AVHRR_OI	0.107	0.702	0.163	0.750
	OSTIA	0.092	0.587	0.149	0.635
	mw_ir_OI	0.515	1.175	0.570	1.193

Table 1. Bias and standard deviation regional summary statistics for matchups between satellite products and all available regional buoys. Matchups were performed using a buoy 24-hour period and a nighttime only period (sunset to sunrise).

While the one-year sample size of buoy-to-satellite matchups was small considering the multi-year length of these satellite products, even this short time series reveals several features. Most apparent is that these coastal regions represent challenging areas for fusing satellite data due to ocean variability related to shelf breaks, eddies, strong currents and shear, upwelling and other dynamic processes. Thus, in many cases matchups to the in situ data are no better than 1.0 °C, although in general they are better than that. A caveat here is that except for the mw_ir_OI product, the Level 4 products assimilate some buoy data in their optimal interpolation schemes. Unfortunately, the buoys used are not documented, so it is impossible to determine which comparisons are truly independent. However, it is very likely that in locations where the mw_ir_OI SST product has large errors in contrast to the other products this is due to the non-assimilation of buoy data. A further characteristic of these comparisons is that for products that claim to be a "foundation" temperature (mw_ir_OI and OSTIA), there does not appear to be a significant reduction in their biases when compared to nighttime only SST buoy observations as shown in Table 1. Thus, in these coastal regions they must be treated with more caution in their representation of the "foundation" temperature.

In conclusion, these results have a mixed message. In general, the Level 4 products performed well, with errors (bias + standard deviation) of around 0.5-0.8 °C as compared to in situ data from fixed buoys in these coastal regions. However, given the dynamic nature of these regions, it appears unlikely that all products will meet or improve upon this level of error unless additional refinements and data are added to the OI schemes including more satellite data, more buoys, and motion and diurnal warming compensation. In the future we intend to carry out more of these comparisons regionally and globally at seasonal and interannual scales with a more complete suite of L4 products including ODYSSEA and RAMSSA using an automated matchup program based on OPeNDAP access to both satellite products and in situ data from fixed and drifting buoys, and ships.

Acknowledgement
The research described in this paper was carried out at the Jet Propulsion Laboratory, California Institute of Technology, under a contract with the National Aeronautics and Space Administration.

COMPARISONS OF ULTRA-HIGH RESOLUTION 1KM SEA SURFACE TEMPERATURE DATA SETS

Jorge Vazquez(1), Toshio M. Chin (1), Edward Armstrong (1), Gary Jedlovec (2)

(1) *Jet Propulsion Laboratory, California Institute of Technology, 2800 Oak Grove, Pasadena, CA 91109, Email:* jorge.vazquez@jpl.nasa.gov

(2) *Gary J. Jedlovec, Short Term Prediction Research and Transition Center SPoRT, Marshall Space Flight Center,* 320 Sparkman Drive Huntsville, AL 35805 *Email: Gary.Jedlovec@nasa.gov*

ABSTRACT

In a collaborative effort with the Short Term Prediction adn Research Cener (SPoRT) methodologies have been developed and compared to produce 1km ultra-high resolution sea surface temperatures (SSTs) in a test region defined by :

-100°W TO -49°W AND 15°N TO 50°N.

Composites are calculated for both daytime and nighttime fields and compared directly with SSTs from the Advanced Along-Track Scanning Radiometer (AATSR). Biases were close to zero and RMS différences less than 0.4°C.

1. INTRODUCTION

In a collaborative effort with the Short Term Prediction and Research Center (SPoRT) methodologies have been implemented to produce 1km ultra-high resolution SST data sets. This paper should be considered as a companion to the one presented by Jedlovec et al. (2009). Comparisons between SST maps produced using different methodologies, as well as direct comparisons with gridded maps of SST derived from the Advanced-Along Track Scanning Radiometer (AATSR) are presented.

- The methodology essentially builds on the work of: (Jedlovec et al. 2004) with additional enhancements that include the calculation of weighted SST averages from the (Advanced Microwave Scanning Radiometer-Earth Observing System) AMSR-E and the Moderate Resolution Imaging Spectroradiometer (MODIS_ data. The primary approach to generating the composites is based on the methodology described in Haines et al. (2007).
- The approach calculates high-resolution Sea Surface Temperature (SST) composites based on finding a minimum of three cloud free pixels for a given collection area. The two warmest pixels are then averaged and the value used to fill the collection area. A latency map is generated for each composite that provides information on how many days were necessary to find the minimum three cloud free pixels.

With the availability of the Group for High Resolution Sea Surface Temperate (GHRSST) Level 2 Preprocessed (L2P) data several enhancements were added to the composite methodology:

- Microwave data from AMSRE is used in the compositing.
- A straightforward strategy was implemented to use the error characteristics in the GHRSST L2P data in the calculation of the composites.
- The compositing region was extended to the entire West and East Coasts of the United States
- Proximity flags in the GHRSST L2P data were implemented to remove cloud and erroneous pixels.

2. METHODOLOGY AND DATA

One of the primary issues involved in incorporating the AMSRE microwave data in implementing composites is the tradeoff between the decreased spatial resolution of the AMSRE data (25km) and the increased coverage due to it's near all weather capability. Several approaches are implemented and compared.

Test data from the GHRSST L2P data sets for MODIS Aqua, MODIS Terra, and AMSR-E were extracted for a period from January 1 2009 to March 31, 2009 in a region between -100°W to -49°W and 15°N to 50°N. Weights were calculated for MODIS Terra, MODIS Aqua, and the AMSRE data. These weights were based on two factors: the time latency from the analysis time and the RMS value as contained in the single sensor error characteristics (SSES) in the GHRSST L2P data. Maps were generated separately for MODIS Terra Day, MODIS Terra Night, MODIS Aqua Day and MODIS

Aqua Night. It was decided to initially maintain the day and night maps separately until a methodology was implemented for the diurnal cycle.

After the determination of the weights and gridding the following methodology is implemented for calculating the composite.

A collection period is defined over a one-week period. Separate weights are assigned to the AMSR-E data and MODIS databased on both the time in days from the analysis day and the RMS value that is part of the GHRSST L2P data. The following is a step-by-step description of the approach:

1) Week one

All weights in the 7-day period lagging the analysis time are calculated such that the total weight is a combination of the RMS and TIME weights:

Weight (ix,iy,it)=timeweight(it)*rmsweight(ix,iy,it)

Where "it" varies from 1 to 7 and "ix" and "iy" varies over the spatial domain for each latitude and longitude point. In most cases it=1 means the "analysis time".

The MODIS AQUA and TERRA weights become a combination of two weights, a latency period and the RMS error.

TIMEweight(ix,iy)=1./(analysis time – data time)

Where "data time" is always less than the "analysis time". If "analysis time" = "data time" the timeweight is simply set to a value of "2".

RMSweight(ix,iy,it)=1./RMS(ix,iy,it) where RMS(ix,iy,it) is the "RMS" value taken directly from the GHRSST L2P data.

MODISweight(ix,iy,it)=TIMEweight(ix,iy)*RMSweight(ix,iy,it)

The AMSRE weights are calculated as above but given a lower weight by 0.25 because of their reduced spatial resolution. Thus

AMSREweight(ix,iy,it)=

TIMEweight(ix,iy)*RMSweight(ix,iy,it)*0.25

A weighted SST value is calculated for the first week such that:

SST(ix,iy,analysistime)= $\sum_{it=1}^{it=7}$ MODISSST(ix,iy,it)*MODISweight(ix,iy,it)/ $\sum_{it=1}^{it=7}$ MODISweight(ix,iy,it +

$\sum_{it=1}^{it=7}$ AMSRESST(ix,iy,it)*AMSREweight(ix,iy,it))/ $\sum_{it=1}^{it=7}$ AMSREweight(ix,iy,it) (1) where AMSRESST is the SST from GHRSST L2P AMSR-E data and MODISSST is the SST from the GHRSST L2P MODIS data.

2) Step one is repeated for successive weeks lagging the "analysistime" until all non land values of (ix,iy) are filled. Only those values not filled in step 1) are used in step 2).

Biases are removed from AMSRESST and MODISSST based on the values contained within the GHRSST L2P data. Two approaches were taken based on equation (1) and later compared.

- An average SST value was derived by summing over AMSRE and MODIS SST for the first week. Successive weeks are filled in only were data is missing (Version 1.0 of the algorithm) V10

- An average SST value was derived for week one over only MODIS data. AMSRE data was only used in first week where MODIS data does not fill in pixel (Version 2.0 of the algorithm) V20.

3. VALIDATION WITH AATSR DATA

Comparisons are done between the composites and the AATSR data. Biases and RMS differences were calculated between each of the maps. Figure 1 shows

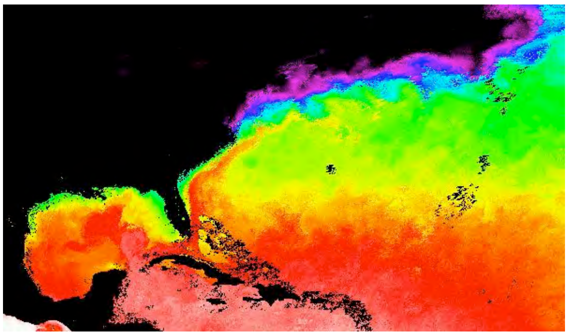

examples of the two approaches (V10 and V20) for day 89 of 2009. Figure 2 shows the biases and RMS differences between V10 for the daytime and nighttime data versus AATSR for day 70 of 2009.

A

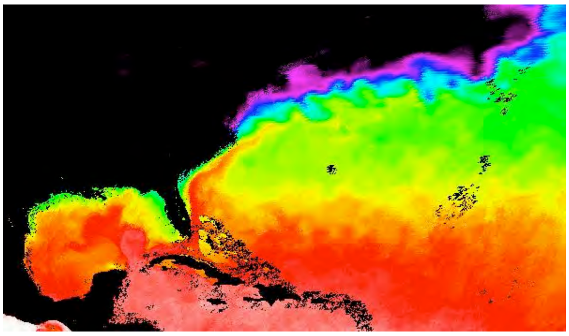

B

Figure 1(A,B): Composites using V10 (A) and V20 (B) of the algorithm.

A

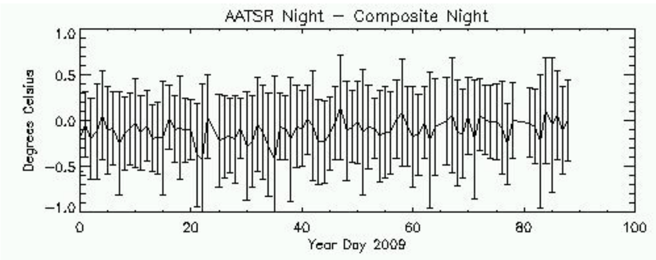

B

:

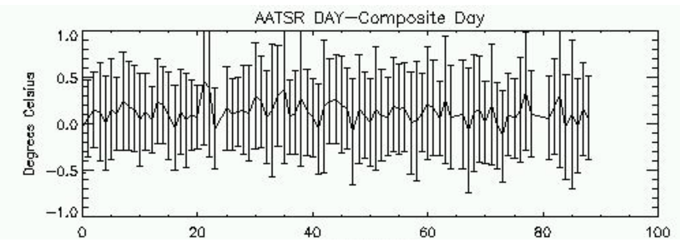

Figure 2(A,B): Differences between AATSR-Composite for V10 for Nighttime and Daytime fields.

In both cases overall biases were less than 0.1°C with RMS values around 0.4°C. Nighttime AATSR data was cooler than the composite and daytime AATSR data warmer than the composite.

4. CONCLUSIONS

A methodology is presented to produce 1km ultra-high resolution SSTs using MODIS and AMSR-E GHRSST L2P data and the SSES bias and RMS fields. Initial results are encouraging and show biases close to zero when compared directly with AATSR data. RMS differences between the daytime and nighttime composites and the AATSR data are around 0.4°C.

Acknowledgements

This research was funded by Dr. Tsengdar Lee of the NASA Science Mission Directorate's Earth Science Division through NASA's research to operations proposal solicitation, a part of NASA's Research Opportunities in Space and Earth Science (ROSES) program.

REFERENCES

Haines, S. L., G. J. Jedlovec, and S.M. Lazurus, 2007: A MODIS Sea Surface Temperature Composite for Regional Applications, accepted IEEE Transactions in Geosciences and Remote Sensing.

Jedlovec, G. J., S. L. Haines, R. J. Suggs, T. Bradshaw, C. Darden, J. Burks, 2004: Use of EOS Data in AWIPS for Weather Forecasting. 20th Conference on Interactive Information Processing Systems (IIPS), AMS, Seattle, CDROM.

A Comparison of AATSR and AMSR-E Sea Surface Temperature Data

By Karen L Veal and Gary Corlett

Sea-surface temperature (SST) is designated an "Essential Climate Variable" and is used in the quantitative monitoring of global change. Satellite SST datasets are now of sufficient duration to provide useful time series in which the presence, or otherwise, of global and regional trends in SST can be investigated. The majority of satellite SSTs are retrieved from measurements at infrared wavelengths (the Advanced Along-Track Scanning Radiometer (AATSR), for example) and can only be obtained using clear-sky radiances. The impact upon global and regional average SST averages of using only clear-sky radiances has not yet been determined. Satellite microwave radiometers, such as the Advanced Microwave Scanning Radiometer for EOS (AMSR-E), have the advantage of being able to retrieve SST through clouds, although not in the presence of precipitation. However, the relative uncertainty between the infrared and the microwave clear-sky SST data must be understood before an assessment of the differences between clear-sky and 'all-sky' SST trends can be made.

This work aims to identify and quantify the differences between the AATSR SST version 2.0 and the AMSR-E SST version 5 datasets. Global and regional time series of monthly average AATSR SST anomaly and AMSR-E SST anomaly, for 2002 to 2008, were compared and regional biases in SST anomaly were determined. Such comparisons of SST datasets are facilitated by the Group for High-Resolution Sea Surface Temperature which provides different SST datasets in a common format. The SST anomalies were calculated using the NCEP climatology for 1971-2000.

Initial findings indicate good agreement between the two datasets is found in the tropics but seasonally varying biases are seen in the higher latitudes.

CALCULATION OF SEA SURFACE TEMPERATURE USING A FORWARD RADIATIVE TRANSFER MODEL APPROACH

Alec Bogdanoff[1], Carol Anne Clayson[1] , Brent Roberts[1]

[1] Florida State University, Department of Meteorology, Tallahassee, FL
Email : abogdanoff@fsu.edu

ABSTRACT

Many retrieval schemes for sea surface temperatures (SSTs) use empirically based techniques to relate brightness temperatures (BTs) to ship and buoy SSTs and thus may be biased towards those areas where in situ measurements are abundant. These schemes calculate weights from BTs, and adjust the weights to produce appropriate comparisons with the in situ data. A forward model approach using a radiative transfer model (RTM) as described by Merchant and Le Borgne (2004), specifically using the RTTOV fast RTM, allows for improvement in the accuracy of weighting coefficients. This increases confidence in SSTs in areas sparse in in situ data and provides a more physical approach to the derivation of BT coefficients.

1. INTRODUCTION

Merchant and Le Borgne (2004) applied the forward model approach using the Along-Track Scanning Radiometer (ATSR). In this study we use the same approach but with Advanced Very High Resolution Radiometer (AVHRR) data. In addition, we explore the use of neural networks for providing the weighting coefficients, and evaluate the gains in computational efficiency as compared to differences in error characteristics with respect to the use of the full RTM. Nonlinear approaches to the calculation of SSTs are a common methodology (e.g. Walton et. al. 1998).

2. AVHRR/BUOY MATCH UP

Pierre Le Borgne at Météo-France created the AVHRR/buoy match up dataset. The satellite passes are matched to the location of the buoys. The maximum temporal gap between satellite pass and in situ measurement is three hours. Only the MetOp-A AVHRR data is used in the match up from April 2007 to March 2008. The data has been cloud cleared and quality checked, leaving 236,704 match up points. For more information on the match up database, see Merchant et. al. (2008). Figure 2 shows a spatial distribution of the match up data points. Each tick mark represents the location of the buoy.

To allow for uncontaminated use of the 3.7 μm AVHRR channel, only nighttime matches were used. Therefore, all three channels of the AVHRR (3.7, 10.8, 12.0 μm) can be used. Nighttime further allows a correction to the buoy SST to estimate the skin temperature without also requiring adjustment due to warm diurnal daytime layer. Moreover, using a nighttime temperature minimized the SST change during the temporal measurement gap.

A correction of 0.2°C is subtracted from the in situ buoy observation to adjust to a skin temperature. All neural networks and the multiple linear regression are trained to a corrected skin temperature.

3. NEURAL NETWORK APPROACH

Neural networks are a multi-layer perceptron technique. They are a formalism for non-linear regressions. The basis of the technique is the individual weighted calculation of the inputs to an output. Using a biological reference, the neurons are the colored circles in Figure 1 and the interconnecting lines are the synapses. Signals are transformed using hyperbolic tangent. The technique is further described in Rumelhart et. al. (1986).

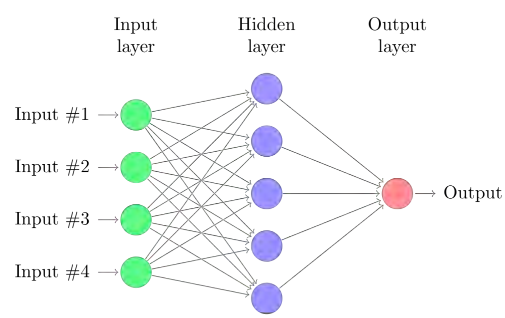

Figure 1. An example schematic of a Neural Network with four input neurons, one hidden layer with five neurons, and one output neuron.

Figure 1 shows an example neural network. This schematic is similar to the direct BT to SST neural network approach followed here (MLR – NO RTM, described below); however, there are seven hidden

	MLP – NO RTM	MLP – RTM	MLR	O&SI SAF	MLP – O&SI
RMS (K)	0.425	0.403	0.614	0.390	0.284
Mean Bias (K)	0.350	0.310	0.487	0.329	0.220

Table 1. Root mean square error and mean bias of the five methods.

neurons instead of five. All neural nets in this study have one hidden layer. The number of hidden neurons is based on the number of inputs and outputs.

Chris Merchant of the University of Edinburgh ran the Radiative Transfer for TOVS (RTTOV) model using matched numerical weather prediction model (NWP) profiles (provided by Pierre Le Borgne). Details of the RTM can be found in Merchant et al. (2008). These NWP profiles and RTTOV outputs are used to train the neural network described in this work.

100,000 randomly selected matchups are used to train the neural network. This allows for the validation of the network with the remaining matchups not used to train the network. Two neural nets were trained using the 100,000 data points, and a multiple linear regression (MLR) was trained using all 236,704 matchup points.

The first neural net (MLP-NO RTM) does not use any of the RTM data. It contains only the observed BTs and satellite zenith as inputs and only outputs an SST. The corrected SST is used to train the model. The second neural net (MLP-RTM) uses all the data of the NWP, the observed BTs, longitude, latitude, satellite zenith angle, and solar zenith angle as inputs. The network is trained using the outputs of the RTM and the corrected SST.

It is important to note that the neural nets are the initially trained networks. They have not been bias corrected, and multiple runs have not occurred. Future work will increase the accuracy of the neural network approach. Varying the inputs can substantially change the accuracy of the network, as well, if the initial fields are not rigorously evaluated for representativeness.

For comparison, the Ocean and Sea Ice Satellite Application Facility of EUMETSAT's algorithm (O&SI SAF Algorithm) for nighttime estimation of AVHRR SSTs is used (O&SI SAF 2009). A third neural network is trained using the inputs of the O&SI SAF algorithm to show the ability of the neural network to emulate the algorithm (MLP-O&SI).

4. RESULTS

Table 1 shows the root mean square error and mean bias of the five approaches. The simple MLR approach has the largest bias and rms errors of all the methods, with the least Gaussian distribution of

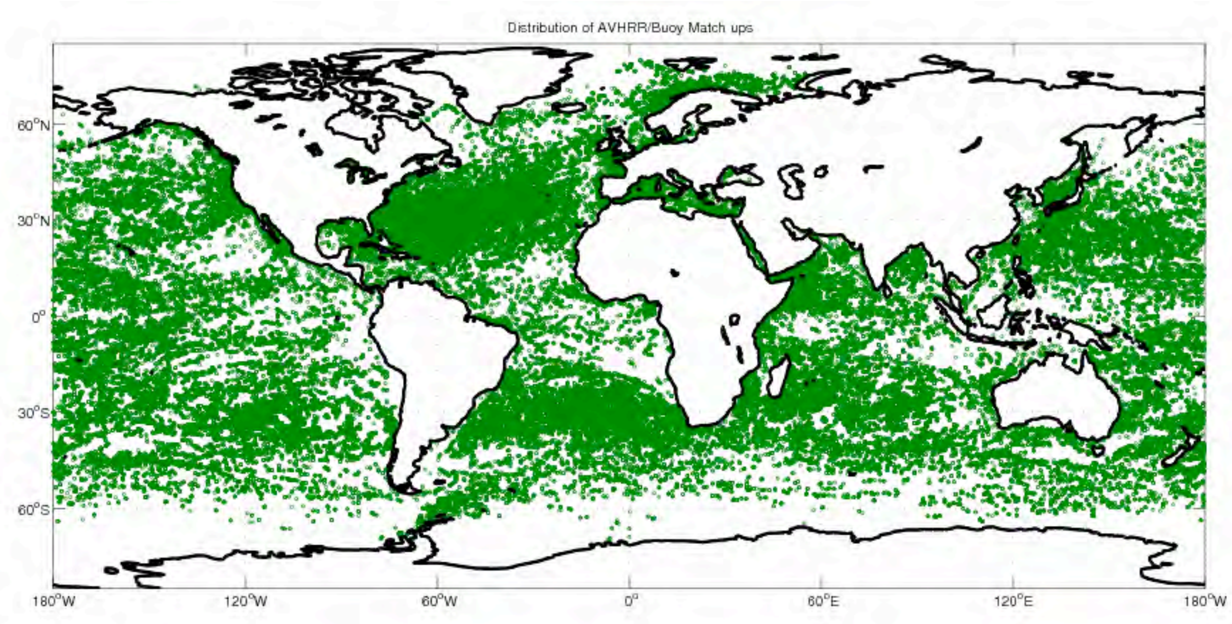

Figure 2. Distribution of AVHRR/buoy match ups.

errors (see from the histogram of the residuals shown in Figure 3). The neural network emulation of the O&SI SAF algorithm performs the best overall. The O&SI SAF algorithm performs very well as well. As a first guess model, the neural networks do an exceptional job, with the inclusion of the RTM increasing the accuracy of the modeled approach.

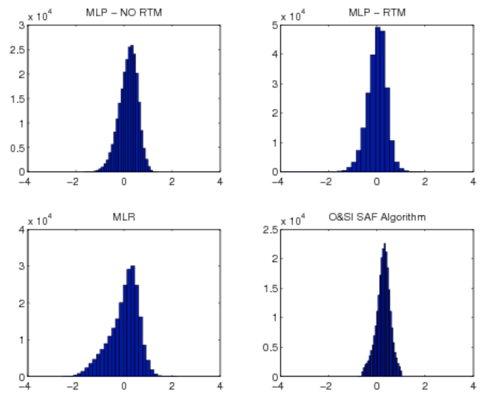

Figure 3. Distribution of residuals.

Plotting the residuals versus corrected in situ SST allows for the examination of systematic errors of the SST calculation approaches. Figure 4 shows the MLR approach performs more poorly at higher SSTs. The MLP-RTM generally has randomly scattered residuals, with some increase in distribution spread at higher SSTs. It is the authors' opinion that these residuals can be greatly decreased by further optimization of the neural networks. The quality assurance procedures of the O&SI SAF algorithm have successfully restricted the range of outliers.

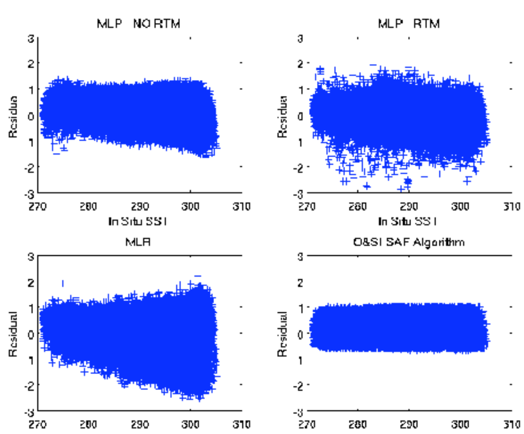

Figure 4. Histogram of residuals.

5. FUTURE WORK

1. Neural networks are statistically based and many more runs are required to determine the best regression. Further optimization of the networks will increase the accuracy of the approach.

2. Expand beyond clear sky at night. The effect of using a RTM approach will be greater during daytime and cloudy sky conditions. Chavallier et. al. (1998) successfully used neural networks to emulate an RTM.

3. Expand beyond MetOp-A satellite to allow for better global coverage of satellite derived SSTs.

4. The error characteristics of the resulting SST datasets will be compared to GHRSST products.

6. ACKNOWLEDGEMENTS

The authors would like to acknowledge the collaborators who made this project possible and provide continuing support and ideas. Chris Merchant of the University of Edinburgh provided the RTM data and Pierre Le Borgne of Météo-France provided the AVHRR/buoy match up dataset.

The dataset is from EUMETSAT's Ocean and Sea Ice Satellite Application Facility. We would like to thank the NASA PO Program for their support of this research.

7. REFERENCES

Chevallier, F., F. Chéruy, N. A. Scott, and A. Chédin, 1998: A neural network approach for a fast and accurate computation of a longwave radiative budget. *J. Appl. Meteor.*, ***37***, *1385–1397.*

Merchant, C. J. and P. Le Borgne, 2004: Retrieval of Sea Surface Temperature from Space, Based on Modeling of Infrared Radiative Transfer: Capabilities and Limitations. *J. Atmos. Oceanic Technol.*, **21,** 1734-1746.

_____ , P. Le Borgne, A. Marsouin, and H. Roquet, 2008: Optimal estimation of sea surface temperature from split-window observations. *Remote Sens. Environ.*, **112,** 2469-2484, doi:10.1016/j.rse.2007.11.011.

Ocean & Sea Ice SAF Project Team, 2009: MetOp/AVHRR Sea Surface Temperature Product User Manual Version 1.5. O&SI SAF Product User Manual. SAF/OSI/CDOP/M-F/TEC/MA/127, 48 pp.

Rumelhart, D. E., G. E. Hinton, and R. J. Williams, 1986: Learning internal representations by error propagation. *Parallel Distributed Processing: Exploration in the Macrostructure of Cognition 1*, D. E. Rumelhart and McClelland, Eds., MIT Press, 318-362.

Walton, C. C., W. G. Pichel, J. F. Sapper, and D. A. May, 1998: The development and operational application of nonlinear algorithm for the measurement of sea surface temperatures with the NOAA polar-orbiting environmental satellites. *J. Geophys. Res.*, **103(C12),** 27999-28012.

USAGE OF SEA-SURFACE TEMPERATURE AND SEA-ICE COVER AT ECMWF.

Hans Hersbach[(1)] and Matthias Drusch[(2)]

(1) European Centre for Medium-Range Weather Forecasts, Shinfield Park,Reading RG2 9AX (United Kingdom), Email: hans.hersbach@ecmwf.int

(2) Current affiliation: European Space Agency, ESTEC, P.O. Box 299, 2200 AG Noordwijk (The Netherlands)

1. INTRODUCTION

The integrated assimilation and forecast system (IFS) at the European Centre for Medium-Range Weather Forecasts (ECMWF) does not perform an in-house analysis for sea-surface temperature (SST) and sea-ice cover (CI). These fields are required as boundary conditions in the operational atmospheric ten-day forecast. The gridded analysis fields are imported from elsewhere, and are interpolated to the ECMWF model grid. An analysis step is performed, in which SST and CI are adjusted for a limited number of grid points to enforce consistency. Over land, values are set to missing, while over those lakes where the external analysis field is not expected to contain information, climatological values are used. For regions where CI is below 20% it is reset to zero, and a lower limit of 271.46K is set to SST. For points where CI is above 20%, SST is reset to 273.16K. CI is reset to zero whenever SST is above 274.16K.

Between 10 May 2001 and 30 September 2008, SST and CI analysis fields have been taken from the Real-Time-Global (RTG) product of the National Centers for Environmental Prediction (NCEP) . This 0.5x0.5-degree product [1,2] was used over the global oceans and seas, the Caspian Sea, and the Great Lakes.

On 30 September 2008, the RTG NCEP product was replaced by the Operational Sea-surface Temperature and sea Ice Analysis (OSTIA) as produced by the UK Met Office [3,4]. This product is delivered at a much enhanced grid of 0.05x0.05 degrees. It is used over the global oceans and seas, and over the Caspian Sea. Over the Great Lakes, the usage of the RTG products is continued, since OSTIA does currently not contain information for this region.

This presentation will focus on differences between the usage of SST and CI products from RTG and OSTIA, respectively. Two sets of ECMWF analysis suites at full model resolution (horizontal resolution of around 25km) were conducted for the months February 2008 and August 2008. For these test periods some consistent large differences in SST up to 10K are observed. A few details are described in Section 2. Differences in sea-ice cover will be the subject of Section 3. The document ends with some concluding remarks (Section 4).

2. SEA-SURFACE TEMPERATURE.

In the ECMWF SST analysis, the external product is interpolated onto the ECMWF model grid (25km). This means that potential differences in intrinsic resolution between OSTIA (gridded at 0.05 degrees) and RTG (gridded at 0.5 degrees) will be smoothed out to 25km. At this level, a comparison of SST analyses based on RTG and OSTIA does not expose clear differences in small-scale variability or resolution. In most areas around the globe, differences between the two products are found to alternate and averaging out over time.

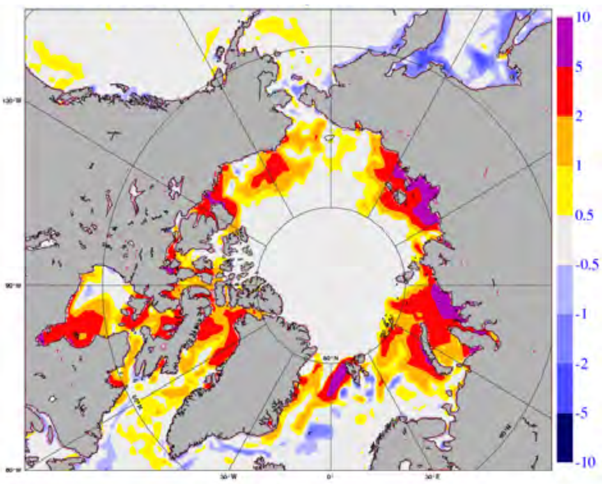

Figure 1. Average difference (Kelvin) over August 2008 in ECMWF SST analyses of OSTIA – RTG.

In polar regions, however, large consistent differences are observed. Most striking differences occur in (Northern Hemispheric) Summer in the Arctic region, where at some locations (e.g. the Kara Sea) the monthly-mean SST from OSTIA may be up to 10K warmer than RTG. An example for August 2008 is presented in Figure 1. A comparison with sea-temperature from buoy and ship data north of 70N, as obtained via the Global Telecommunication System (GTS), indicates that OSTIA provides the more accurate product (see Figure 2). In addition, near-surface air temperature from the analysis suite based on OSTIA compares slightly better to air temperature from these in situ data as well (not shown). One reason for large differences in SST in polar regions may be that OSTIA uses data from both microwave and infra-red sensors, while RTG only utilised infra-red data. This inhibits RTG from a frequent observation of persistently clouded areas, such as encountered in polar areas.

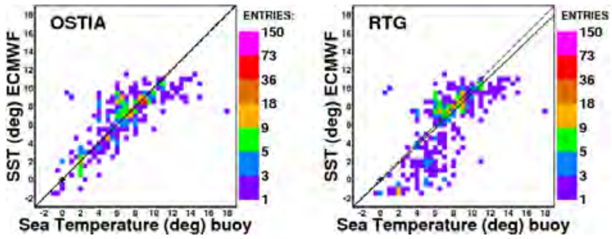

Figure 2. Collocation between ECMWF SST analysis (left: based on OSTIA, right: based on RTG) and buoy data north of 70N, for August 2008.

3. SEA-ICE COVER

The sea-ice product from OSTIA originates from the EUMETSAT Ocean and Sea Ice Satellite Facility (OSI-SAF), which embraces a Baysian analysis method for SSM/I data [4]. In general it is found that the extent of OSTIA sea-ice, as used at ECMWF, is somewhat lower than for RTG. A higher SST may be partially responsible for this. In areas of considerable sea ice, the cover tends to be highest for OSTIA. As a result, OSTIA shows a sharper transition from zero to full ice cover. An example is given in Figure 3, which displays the situation for August 2008 over the Antarctic.

Due to a difference in surface roughness length (typically 0.1 mm over water and 1 mm over sea ice), surface wind is affected by the extent of sea-ice cover. For August 2008, for instance, surface wind is found higher by 0.5m/s to 1m/s over the Ross Sea for the analysis suite that had used OSTIA.

At ECMWF, surface wind from scatterometer data is assimilated routinely. Due to a high sensitivity, data is screened on the presence of sea-ice. The suite based on OSTIA appears less effective in the screening of affected scatterometer data (not shown). This indicates that the sea-ice extent from OSTIA may be somewhat under estimated.

4. FINAL REMARKS

Since 30 September 2008, the SST and CI analysis at ECMWF is based on OSTIA over the global oceans, and the Caspian Sea, while information from RTG is used over the Great Lakes. Availability of these surface quantities over smaller lakes would be desirable, since at present climatology is used. Compared to RTG, the higher OSTIA SST in the Arctic Summer is supported by ship and buoy data. The issue on the smaller extent of OSTIA sea ice would need some attention.

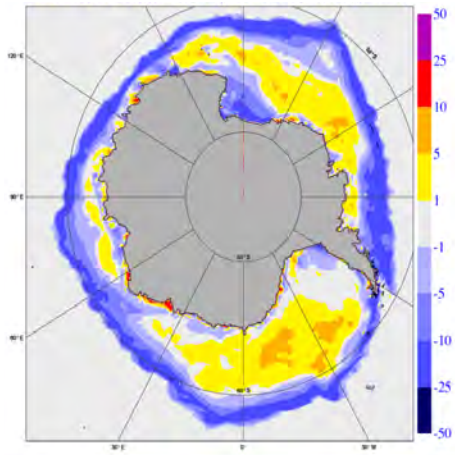

Figure 3: Average difference (Percent) over August 2008 in ECMWF CI analyses of OSTIA – RTG.

The ingestion of SST and CI is monitored at ECMWF. For each analysis cycle increment maps are created, while time series provide information on trends or sudden shocks. Up to date, the system is found to behave nominally.

5. ACKNOWLEDGMENTS

We would like to thank Elias Holm for the development and implementation of the area-averaged interpolation scheme, Jean Bidlot for the ship and buoy comparison, and Ioannis Mallas for the setup of the acquisition of OSTIA data at ECMWF.

6. REFERENCES

1. J. Thiebaux, E. Rogers, W. Wang. and B. Katz (2003), "A new High-Resolution Blended Real-Time Global Sea Surface Temperature Analysis", Bull.of.Ame.Soc., 84, 645-656.
2. R. W. Grumbine (1996), "Automated passive microwave sea-ice concentration at NCEP", NOAA NCEP Tech. Note.
3. J. D. Stark, C. J. Donlon, M. J. Martin and M. E. McCulloch (2007), "OSTIA: An operational, high resolution, real time, global sea surface temperature analysis system.", available from http://ghrsst-pp.metoffice.com/pages/latest_analysis/ostia.html.
4. S. Anderson, L-A. Breivik, S. Eastwood, O. Godoy, M. Lind, M. Porcires and H. Schyberg (2007), "OSI SAF Sea Ice Product Manual", available from http://saf.met.no/docs/.

THE USE OF SST DATA AT DMI FOR HIGH LATUITUDE LEVEL 4 ANALYSIS

Jacob L. Høyer

Center for Ocean and Ice, Danish Meteorological Institute,
Lyngbyvej 100, København Ø, email : jlh@dmi.dk

ABSTRACT

DMI is currently producing several regional level 4 Sea Surface Temperature (SST) analysis. The Arctic Ocean Level 4 product is the focus of this paper. The interpolated SST products are based upon the same multiplatform optimal interpolation analysis scheme that: pre-process the available GHRSST-pp L2P SST products, perform quality control, bias adjust, interpolate and generate monitoring and validation statistics. Local covariance statistics empirically derived from the satellite data, are used for the analysis and the performance of the two products is validated against drifting buoys. Issues and areas of developments for the Arctic Ocean analysis are presented in the end.

1. INTRODUCTION

The sea surface temperature (SST) is an important parameter, that is used in both oceanic models and Numerical Weather Prediction systems. The temperature of the sea surface can be observed from space using both infrared and microwave sensors from satellites in geostationary and polar orbit. The infrared sensors typically have the best spatial resolution and highest accuracy but they are limited by cloud cover. In the microwave part of the spectrum, the SST can be observed in the presence of cloud cover, but the spatial resolution is not as good as for the infrared satellite sensors. The different sampling characteristics of the satellites and the model demand for high resolution SST fields without gaps, makes it very relevant to perform an analysis of the SST observations, whereby the different satellite observations are referenced to each other and interpolated to produce a daily high resolution field without gaps. For this purpose, DMI has developed an optimal interpolation algorithm that uses statistics derived from the data itself to produce level 4 fields for the Arctic Ocean and several other regions around the world (see http://ocean.dmi.dk/satellite/). The analysis system for the Arctic Ocean is used in this paper as an example on how the DMI level 4 products are produced.

2. THE DMI ANALYSIS SYSTEM

The DMI analysis system consists of several different steps. The major tasks are:

1. Retrieval of the satellite L2P observations
2. Pre-processing: quality control, collating the satellite observations
3. Optimal Interpolation, including ice masking
4. Generation of monitoring and validation statistics

A fundamental part of the scheme is the ingestion of the satellite data. All the satellite observations that are used to produce the SST fields are obtained via ftp from the GHRSST-pp project as level 2P observations (Donlon et. al, 2007). The different sensors and their characteristics are listed in table 1

Sensor	Satellite	Sensor	Resolution
AATSR	ENVISAT	IR	1 km
MODIS	Aqua	IR	1km
Modis	Terra	IR	1km
AVHRR	NOAA 17+18	IR	1, 2 and 9 km
AVHRR	METOP_A	IR	1 km
Seviri	MSG-1	IR	5 km
AMSR-E	Aqua	MW	25 km

Table 1: Satellite observations that are currently included in the DMI level 4 analysis system for the Arctic Ocean. IR stands for infrared and MW stands for Microwave.

In addition to the satellite SST observations, ice information is included from the Ocean and Sea Ice SAF project. The ice product is the Northern Hemisphere ice edge product in a 0.1 degrees resolution.

The individual L2P data products are being quality controlled, corrected for biases and averaged to the analysis grid before they are being used in the analysis. All satellite observations within 24 hours from the analysis time is included in the Arctic analysis. Both day and night time observations are included and all observations are referenced to subskin observations.

In the analysis step, the collated files are ingested and anomalies are generated by subtracting the previous days analysis as a guess field. All grid points with ice present are treated as satellite observations with an SST of -1.8ºC. If more that one satellite observation is available in a grid point, a weighted average is calculated for the given point using the individual error values. Optimal interpolation is performed on the resulting collated grid to produce the SST analysis and error estimates. After the interpolation, monitoring statistics is generated and figures produced about e.g. the number of satellite observations included, anomalies of the individual satellite products, the size of the increments etc.

The analysis system has been running for the Arctic Ocean in a 0.05 degrees resolution. Analysis fields are available from January 2006 up to present. Figure 1 shows an example of the SST field for May 5th 2009.

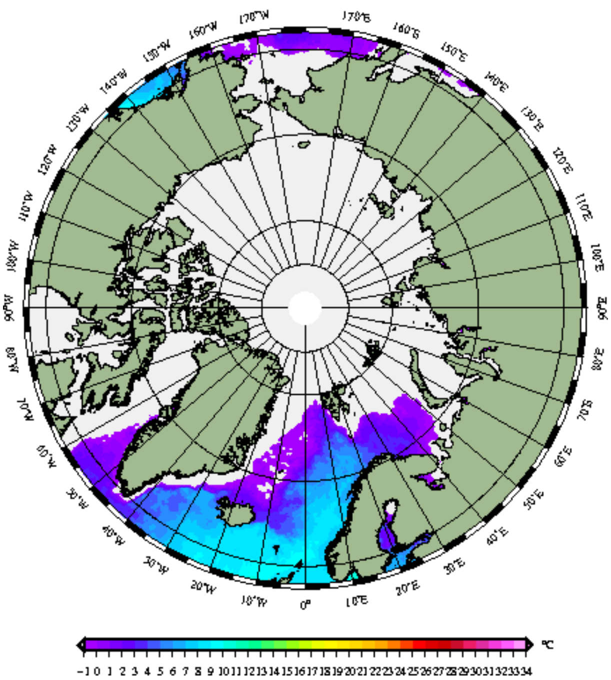

Figure 1 Example of the DMI Arctic Ocean level 4 SST product for May 5th, 2009.

3. ON LINE VALIDATION

As a part of the operational system, validation statistics are being produced every day by comparing the data against drifting buoys. The results are displayed for the last 60 days and both the individually pre-processed satellite Level 3 as well as the Level 4 products are validated. Figure 2 shows the positions and anomalies of the drifting buoys and figure 3 and 4 show the time series of the comparisons.

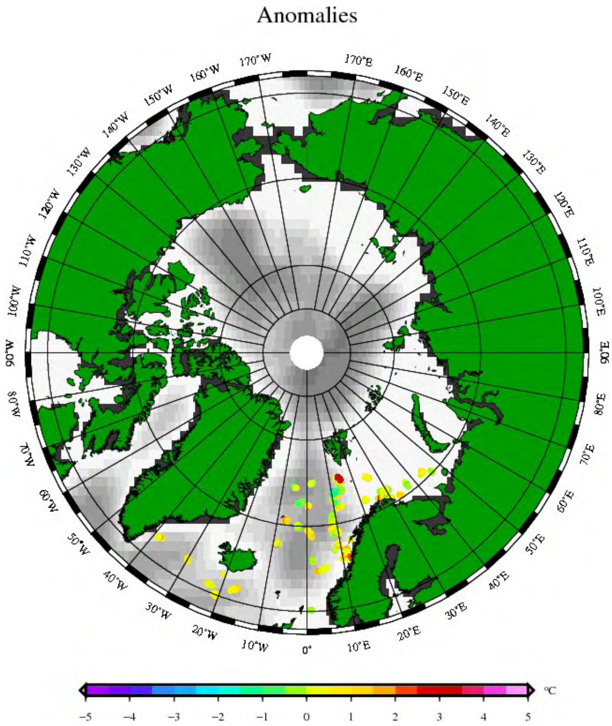

Figure 2: Positions of the drifting buoy observations used for validation. The colors indicate the differences between the in situ observations and the analysis (DMI analysis – in situ).

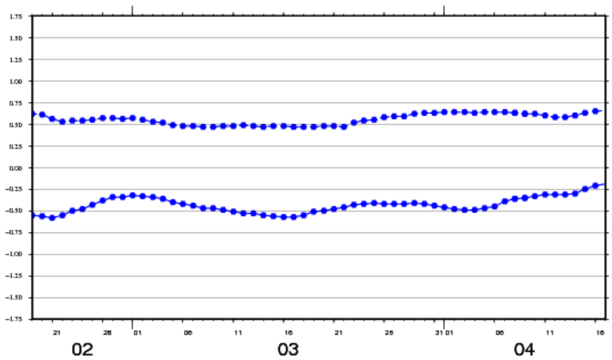

Figure 3: 7 days averages of differences between drifting buoy observations and the Arctic level 4 SST products.

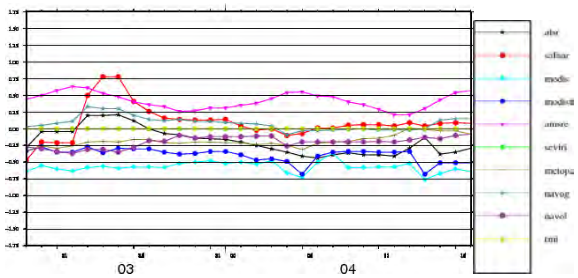

Figure 4: Online validation (bias) of the individual pre-processed level 3 satellite products.

It is clear from the figure that the performance of the Arctic Level 4 SST product is good in terms of standard deviation, whereas the bias seems to be to low at the moment. Figure 4 shows that the cold bias of the Level 4 product arises from the a cold bias on the individual pre-processed satellite observations. This indicates that additional correction for satellite biases is needed in the Arctic, besides the applications of the SSES supplied with the L2P data.

4. APPLICATIONS

The DMI level 4 analysis is being used in a wide range of applications. It is e.g., being assimilated in to the operational hydrodynamic models at DMI, hereby increasing the model skill substantially. In addition, the SST fields for the Greenland area are used in the operational ice charting section, that are responsible for producing ice charts for the Greenland waters. Figure 5 shows an example of how the SST data are integrated in the GIS system to aid the analyser that are producing the weekly ice charts.

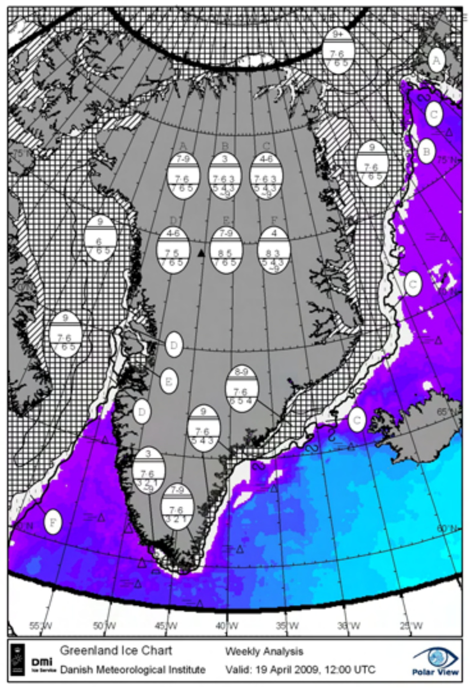

Figure 5 Example of an application of the SST data in the operational ice charting division at DMI. The weekly ice chart has been overlaid the SST field.

5. CONCLUSION

The DMI analysis system ingests all available GHRSST-pp L2P products to produce daily high resolution SST products for the Arctic Ocean. The validation of the SST product against drifting buoys shows a standard deviation of around 0.5ºC and a negative bias at the moment. The negative bias arises from the individual satellite products, that show consistent negative biases. The exception if the AMSR-E data, that show pronounced positive biases. The consistency of the regional biases suggests that additional bias corrections can improve the data in high latitudes, and this is the topic of ongoing work. In addition to the bias issues, there are several other factors that complicate the production of an accurate SST analysis product, such as marginal ice zone SST retrievals, and altered statistics close to the ice edge. These issues will be included in the future work in order increase the quality of the DMI Arctic Ocean SST analysis.

6. REFERENCES

1. Donlon et al, 2007, The GODAE High Resolution Sea Surface Temperature Pilot Project (GHRSST-

PP), Bulletin of the American Meteorological Society, 88, (8) (august 2007).

Validating Ocean Circulation Models with Satellite-Derived SST Frontal Distributions

Andy Eichmann and Peter Cornillon

The probability of finding SST fronts in HYCOM (an ocean general circulation model) output is compared with that of finding fronts in MODIS SST fields. The comparison identifies several regions of significant difference, regions in which HYCOM finds substantially less fronts than MODIS. These regions are also shown to correspond to regions in which the surface to 50m temperature difference in HYCOM is larger than the surface to 50m temperature in the World Ocean Atlas (WOA) and in which the WOA shows very little upper ocean stratification; i.e., the paucity of fronts in HYCOM appears to result from a problem in the parameterization of the mixed layer in HYCOM. This is a significant finding in that the upper ocean is important in air-sea exchange processes so, if these processes are incorrectly parameterized in portions of the ocean, it is likely that atmospheric forcing of the model is in error.

THE NEAR REAL-TIME WEB-BASED SST QUALITY MONITOR (SQUAM)

Alexander Ignatov[1], Prasanjit Dash[1,2], John Sapper[3], Yury Kihai[1,4]

[1] *NOAA NESDIS, Center for SaTellite Applications and Research (STAR), 5200 Auth Road, Camp Springs, MD 20746, USA, Alex.Ignatov@noaa.gov*

[2] *Cooperative Institute for Research in the Atmosphere (CIRA), Colorado State University, Foothills Campus, Fort Collins, CO 80523, USA, Prasanjit.Dash@noaa.gov*

[3] *NOAA NESDIS, Office of Satellite Data Processing and Distribution (OSDPD), 5200 Auth Road, Camp Springs, MD 20746, USA, John.Sapper@noaa.gov*

[4] *Perot Systems Government Services, 4500 Forbes Boulevard, Lanham, MD 20705, USA, Yury.Kihai@noaa.gov*

ABSTRACT

A web-based SST Quality Monitor (SQUAM) was designed to quality control (QC) operational AVHRR products and to monitor them for stability and cross-platform consistency in near real-time (NRT). Currently SQUAM monitors NESDIS SST products from NOAA-16, -17, -18, and MetOp-A. The methodology is based on statistical analyses of anomalies in satellite SST (T_S) with respect to several global reference SST fields (T_R). Empirical histograms of SST anomalies (T_S-T_R) are analyzed for proximity to a Gaussian shape. Fraction of outliers and the first four moments of a Gaussian distribution are trended as a function of time. A double-differencing (DD) technique is employed to monitor SST products for cross-platform consistency. The results are automatically posted in NRT at http://www.star.nesdis.noaa.gov/sod/sst/squam.

1. METHODOLOGY

NESDIS operational AVHRR SSTs (T_S) are customarily validated against *in situ* SSTs (T_R) from collocated buoys. Global distribution of buoys is sparse and geographically biased, and the quality of their SSTs is non-uniform and sub-optimal. Attaining reliable validation statistics requires months of data.

SQUAM complements the "golden standard" validation against *in situ* SSTs by employing several global analysis SST fields as reference, including weekly Reynolds OI.v2 and six daily SST products: two Reynolds's (AVHRR and AVHRR+AMSR-E based), two RTG (low and high resolution), OSTIA, and ODYSSEA. The global fields cover the world's oceans much more fully and uniformly than *in situ* data. As a result, the number of "match-ups" is much larger, and their quality is more uniform than (and yet anchored to) the *in situ* SSTs. This allows monitoring of satellite SST on much shorter time scales approaching NRT. Using multiple reference fields facilitates separating artifacts in satellite data from those in the reference fields.

2. HANDLING OUTLIERS

Examples of SST anomaly histograms from SQUAM are shown in Fig. 1. Median and robust standard deviation (RSD) are used to identify and remove outliers falling outside the "median ± 4×RSD" range.

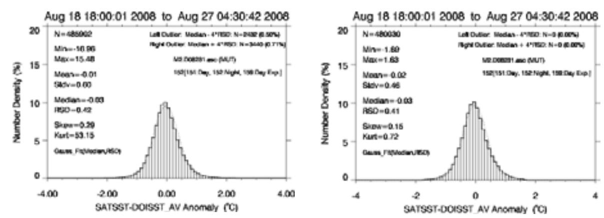

Figure 1. Example night-time MetOp-A SST anomaly histograms with respect to daily Reynolds AVHHR-based SST: (left) outliers retained; (right) outliers removed.

Typically, NESDIS heritage satellite SST product has ~0.5% low, and ~1% high outliers. Removing outliers brings SST anomalies closer to a Gaussian shape.

3. PRODUCT STABILITY

Gaussian parameters are further trended to check satellite SSTs for stability. Fig. 2 shows sample time series (outlier removed) of the median global night-time SST anomalies from four satellites. SSTs from NOAA-17 and -18 are consistent whereas MetOp-A SST is biased ~+0.10K high and NOAA-16 SST is unstable.

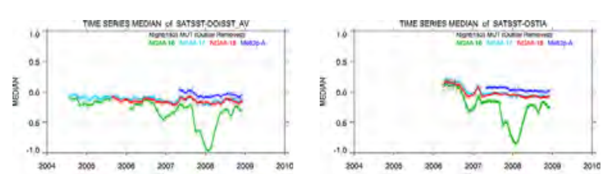

Figure 2. Time series of median night-time SST anomalies with respect to two reference SSTs: (left) daily Reynolds (AVHRR based); (right) OSTIA.

Fig. 3 shows time series of RSDs corresponding to medians in Fig. 2. All products are stable, except NOAA-16. The RSDs are better than 0.5 K for both reference SSTs, but are somewhat larger for Reynolds than for OSTIA (recall that neither Reynolds nor OSTIA use NESDIS SST as input). An abrupt change in RSDs with respect to Reynolds occurred in January 2006 when the Reynolds product switched from Pathfinder to NAVO SST input.

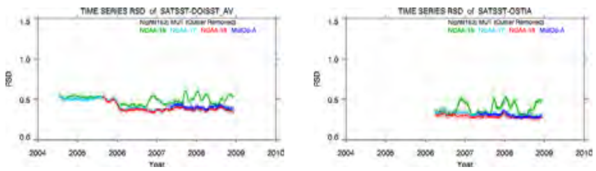

Figure 3. Time series of robust standard deviations (RSD) corresponding to Fig. 2.

4. CROSS-PLATFORM CONSISTENCY USING DOUBLE-DIFFERENCES (DD)

Double differences (DD) of SST anomalies are employed to more accurately quantify cross-platform consistency (Fig. 4). NOAA-18 and -17 agree to within several hundredths of a Kelvin, whereas MetOp-A is biased high by ~+0.1 K.

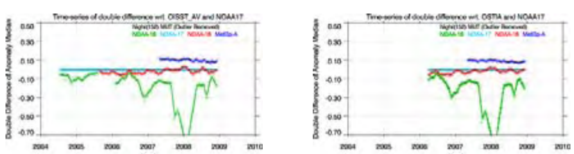

Figure 4. Night-time double-differences (with respect to NOAA-17 product).

5. USING DD TECHNIQUE TO CROSS-COMPARE REFERENCE SST'S

The DD technique can be "inverted" to monitor cross-consistency of different reference SSTs (Fig. 5). The "NOAA-17 - RTG_LR" was selected as a reference and subtracted from the other NOAA-17 anomalies.

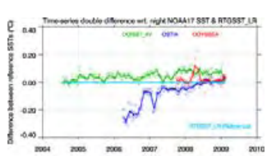

Figure 5. Double-differences (with respect to RTG-LR).

Globally, daily Reynolds is warmer than RTG SST, by several hundredths of a Kelvin. In its first year, OSTIA was biased cold by ~-0.3K. The bias has reduced in late 2006 to ~-0.1K, but then spiked again to ~-0.2 K in early 2007. The ODYSSEA has been largely consistent with RTG SST, except it spiked by ~+0.1 K in early 2008. OSTIA, ODYSSEA and RTG have been consistent since mid-2008, while the daily Reynolds remains biased warm by several hundredths of a Kelvin.

6. CONCLUSION

Heritage AVHRR SSTs from NOAA-16, -17, -18, and MetOp-A from 2004 to present are stable and cross-platform consistent. The remaining differences are largely attributed to different temporal sampling from different platforms, and to the diurnal variability in the satellite SST, which is not captured in the global reference fields. The exception is NOAA-16, whose sensor calibration likely experiences problems in the terminator zone. The double-differencing technique is instrumental in checking for consistency between different satellite and SST analysis products. The ultimate objective is achieving their convergence into a high-resolution and higher quality global SST product.

Future work will include continuous near-real time processing and web monitoring of NESDIS operational SST products, including the heritage product and the newly developed Advanced Clear Sky Processor over Oceans (ACSPO) products. Special emphasis will be on identifying and resolving the observed inconsistencies and anomalies (such as NOAA-16). SQUAM will also be adapted to test SST products derived from other existing (MSG SEVIRI, NOAA-19) and future (NPOESS/VIIRS and GOES-R/ABI) sensors. Accounting for diurnal variation in reference SSTs will be explored. The SQUAM will be instrumental for quality control of climate data records and for establishing reliable links between the past, present, and next generation SST products.

7. ACKNOWLEDGEMENT

This work was supported by NESDIS PSDI, NPOESS Integrated Program Office; and by the GOES-R Algorithm Working Group. The views, opinions, and findings contained in this report are those of the authors and should not be construed as an official NOAA or US Government position, policy, or decision.

8. REFERENCES

1. P. Dash, A. Ignatov, Y. Kihai and J. Sapper, "The near real-time SST Quality Monitor: Application to NESDIS heritage AVHRR products", *Remote Sensing of Environment*, March 2009 (submitted). http://www.star.nesdis.noaa.gov/sod/sst/squam/documents/SQUAM_MUT_RSE_2009.pdf

Motion-compensated spatio-temporal interpolation of SST fields

Arthur J. Mariano[1] **T. Mike Chin**[2] **Ed H. Ryan**[1] **Jorge Vazquez**[2] **Edward Armstrong**[2]

[1] *RSMAS / University of Miami*
[2] *JPL / California Institute of Technology*
Email: `amariano@rsmas.miami.edu`

Abstract

Introduction

Satellite-based SST data are irregularly sampled, in space and time, from different sensors with different error and sampling characteristics. In particular, SST data from the microwave (MW) sensors have typically much coarser resolution than the infra-red (IR) sensors that can have a nominal 1 km resolution. However, the IR-based measurements are prone to much larger data voids than MW-based measurements due to cloud contamination. Fusion of such multi-resolution measurements require an optimal methodology for spatio-temporal interpolation and statistical consistency of the results. The Parameter matrix Objective Analysis (PMOA) method for spatio-temporal interpolation of heterogeneous, non-stationary, and large data sets has been formulated and applied to multi-platform SST data.

The PMOA allows each data file, as well as each data point, to have its own error level and segments the data into space-time bins. The PM is the set of nine parameters that can vary between the space-time bins for a general 3-D correlation function, $Cor(dx, dy, dt)$

$$Cor = C(1)[1. - (DX/C(4))^2 - (DY/C(5))^2]$$

$$* \exp^{-[(DX/C(6))^2 + (DY/C(7))^2 + (dt/C(8))^2]},$$

$$DX = dx - C(2) * dt \quad DY = dy - C(3) * dt$$

These parameters are, in general, space- and time-dependent, but for brevity are denoted as $C(1) = C(0,0,0) = 1.0$-error level; $C(2)$ and $C(3)$ are the zonal and meridional feature displacement velocities; $C(4)$ and $C(5)$ are the zonal and meridional zero-crossing scales; $C(6)$, $C(7)$, and $C(8)$ are the zonal, meridional, and temporal e-folding scales, and $C(9)$ is the rotation angle. Bins size are on the order of the twice the e-folding scales in space and time. Data are sequentially put into bins and the array locations of the first and last data into each bin is stored for efficient identification of influential data points for the OA.

The PMOA uses a bi-cubic smoothing spline fit to a sliding time window of usually $1 - 3$ weeks worth of data centered about the estimation time to produce a first guess field for detrending the data. The OA at each estimation location uses $O(10 - 20)$ influential data points that are most correlated, in the absolute value sense, with the estimation point. Identifying these points is done by first searching the space-time bin of the estimation bin for influential data points and then nearby bins if not enough data are found in the first search.

A preliminary study by Mariano and Brown (1992) showed that the most critical correlation parameters in the PMOA are the Feature Displacement Velocities (FDVs) that are needed to propagate the data to a common estimation time. Inaccurate FDVs are equivalent to having bad position data for your observations. (SST estimates are not sensitive to the space and time scales as long as they are the right order of magnitude.) Of course, the FDVs are the most difficult to estimate. Almost all FDV estimation methods can simply be categorized into two sets; one set based on conservation equations, called optical flow methods ; and the another set based on regional feature matching between two images, usually by maximizing cross-correlation or some other region matching metric, and differencing the center locations of the matched regions. The conservation equation methods differ in the addition constraints, such as zero divergence and smoothness constrains formulated in terms of temporal and/or spatial derivatives. Marcello et al (2008) evaluated a dozen different region matching metric and a few simple optical flow methods with simulated and real images and FDV estimation errors ranged from 20% and 50%. Our estimation problem, because of large data gaps, is much harder than the more ideal cases studied by Marcello et al (2008). Experience in engineering applications have shown that these methods work the best for complete fields.

Consequentially, our approach for motion-compensated spatio-temporal interpolation is multi-scale. Low resolution FDVs will first be calculated from the gappy data by a contour approach detailed in the next paragraph. The PMOA will be used to produce SST estimates on a regular grid. The resulting high resolution SST fields will then be used to calculate higher resolution FDVs using an optical flow method from a sequence of images. Our optical flow method will also incorporate temporal smoothness. Experiments with FDVs calculated by Yang *et al.* (2001) from 18 km resolution SST data using an optical flow method that only incorporated spatial smoothness and a soft, divergence-free constraint clearly showed that temporal smoothness in the FDVs estimates from SST data is needed. The set of higher resolution FDVs will be used to produce a new set of SST estimates from the original gappy data. The error bars from the first OA will also be used to further edit the data.

Mariano and Chin (1996) used a contour-based approach to estimate the nine correlation parameters from SST data in the tropical Pacific. This approach was more robust than traditional nonlinear fitting techniques for finding the nine correlation parmeters but not perfect. This approach first calculates the 3-D correlation function for each PM space-time bin, and then locates the correlation maximum, the zero-crossing contour, and the spatial e-folding contour are found for each temporal lag. The error level is one minus the maximum correlation value for the zero temporal lag. The FDVs are presently calculated by fitting two straight lines to the center location, in correlation lag space, of the set of e-folding scales. The spatial scales are determined by finding the eigenvalues of the covariance matrix of positions for both the e-folding and zero-crossing scale contours. The temporal e-folding scale is found by fitting an exponential function to the set of maximum values for each temporal lag. Outliers in the parameter estimates are removed and replaced by a value interpolated from surrounding estimates.

One of the key analysis parameters is the inverse-smoothing parameter, ρ, defined by Inoue (1986) that is used in the bic-cubic smoothing spline that is used for the mean field in the PMOA. Our analysis shows that too small a value for ρ lead to a very smooth trend surface and the resulting SST fields are too smooth in regions with siginificant cloud cover for a few days. Values of $\rho \geq 0.1$ lead to better interpolation across these data gaps. However, the larger values of ρ ”whiten” the residuals about the mean field and lead to poor estimates of the correlation function and its parameters.

We have applied the PMOA to MODIS A-, MODIS T-, and AMSREA-based SST data and have produced 1 km resolution SST maps with error maps.

Acknowledgement

The work described here was carried out at the Jet Propulsion Laboratory, California Institute of Technology, and the University of Miami Rosenstiel School of Marine and Atmospheric Science under a contract with the National Aeronautics and Space Administration (NASA).

References

Inoue, H., 1986: A Least-Square Smooth Fitting for Irregularly Spaced Data: Finite-Element Approach Using the Cubic B-Spline Basis. *Geophysics*, **51** (11), 2051-2066.

J. Marcello, F. Eugenio, F. Marqus, A. Hernndez-Guerra, and A. Gasull, 2008. Motion Estimation Techniques to Automatically Track Oceanographic Thermal Structures in Multisensor Image Sequences. *IEEE Trans. on Geosci. & Remote Sensing*, **46 (9)**, 2743-2762.

Mariano and O. Brown, 1992: Efficient objective analysis of dynamically heterogeneous and nonstationary fields via the parameter matrix. *Deep-Sea-Res.*, **39** (7/8), 1255-1271.

Mariano, A. J., and T. M. Chin, 1996. Feature and Contour based data analysis and assimilation in physical oceanography. *Stochastic Modelling in Physical Oceanography*, (Adler, Muller and Rozovskii, eds.), Birkhauser, 311-342.

Yang, Q., B. Parvin and A. J. Mariano, 2001. Detection of vortices and saddle points in SST data. *Geophysical Research Letters*, Jan 15, **28** (2), 331-334.

Applications of GHRSST data sets towards the stewardship of living marine resources: putting SST back in the saddle.

David G. Foley

Joint Institute for Marine and Atmospheric Research, University of Hawai`i at Manoa

Environmental Research Division, Southwest Fisheries Science Center, National Marine Fisheries Service, NOAA, 1352 Lighthouse Ave., Pacific Grove, CA 93950 USA

In the past decade there has been a proliferation of publicly available sea surface temperature (SST) data sets derived from a variety of satellite platforms and sensors. Federal, State, County and municipal researchers and managers who are not necessarily expert in the production and distribution of oceanographic satellite data often face a bewildering, and seemingly contradictory, array of options when choosing data for use in their applications. The standardization of methods promoted by the Group for High Resolution Sea Surface Temperature (GHRSST) provides a pathway by which many of the issues surrounding the use of SST data might be resolved. Specifically, the characterization of localized error for each data set provides much needed reassurance for data users who are skeptical about the quality of satellite-based SST measurements. This error characterization also allows for more effective integration of the various SST products into blended fields that provide a better overall description of the marine environment. Finally, having provided a more compelling final product, the GHRSST standardized format allows for uniform access using tools compliant with those recommended by the US Integrated Ocean Observing System and its international counterparts.

THE IMPORTANCE OF SST IN WEATHER FORECAST MODELS AND COUPLED CLIMATE MODELS

Dudley B. Chelton

College of Oceanic and Atmospheric Sciences, Oregon State University, Corvallis, OR
Email: chelton@coas.oregonstate.edu

1. INTRODUCTION AND BACKGROUND

Satellite observations of sea-surface temperature (SST) from the Advanced Microwave Scanning Radiometer (AMSR) and surface winds from QuikSCAT have revealed a remarkably strong coupling between surface winds and SST (see review by Small et al., 2008). This coupling becomes clear after averaging over periods of a month or longer to reduce the effects of synoptic weather variability on surface winds that are unrelated to SST. It is found throughout the World Ocean wherever there are strong SST fronts. The Agulhas Return Current (ARC) region of the southwest Indian Ocean is shown as an example in Fig. 1a. On scales smaller than about 1000 km, the wind stress magnitude is linearly related to SST with locally higher winds over warmer water and lower winds over cooler water. A key aspect of the dynamics is that vertical mixing is enhanced over warmer water, which increases surface winds through downward mixing of momentum. Diminished vertical mixing over cooler water decouples the surface winds from the stronger winds aloft, resulting in decreased surface winds.

The observed SST influence on surface winds is clearly evident in the wind fields from the forecast models run operationally at the European Centre for Medium-Range Weather Forecasts (ECMWF) and the NOAA National Centers for Environmental Prediction (NCEP) (Figs. 1b and c, respectively) but with coupling coefficients that are only about half of the observed values (right panels of Figs. 1b and c).

The observed SST influence on surface winds is also evident in coupled climate models that have sufficient grid resolution. The coupling is shown in Fig. 2 for two versions of the NCAR Community Climate System Model. CCSM3.0 has a 1.4° grid for the atmospheric component and a 1° grid for the ocean component. The atmosphere and ocean components of the CCSM3.5 model have higher grid resolutions of 0.25° and 0.1°, respectively. The spatial scales of the SST-induced perturbations are much too large in CCSM3.0 (Fig. 2a), but are nonetheless visually apparent. The scales of the coupled SST and wind stress patterns in CCSM3.5 (Fig. 2b) are much smaller than in CCSM3.0, and are in fact smaller than in the QuikSCAT observations and the ECMWF model. The coupling coefficients (right panels of Fig. 2) are nearly the same for both coupled climate models and are comparable to those for the ECMWF

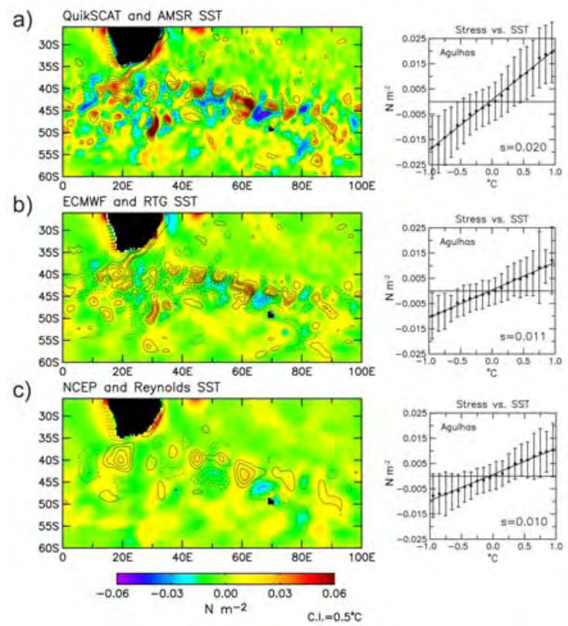

Fig. 1. Maps of spatially high-pass filtered wind stress magnitude and SST over the 4-month period November 2002-February 2003 from a) satellite observations (QuikSCAT and AMSR); b) the operational ECMWF model with RTG SST; and c) the operational NCEP model with Reynolds SST. The fields were filtered with half-power filter wavelength cutoffs of 30° of longitude by 10° of latitude. Binned scatter plots of wind stress magnitude dependence on SST constructed from monthly mean fields are shown on the right. The slopes of the least-squares fit lines through the binned averages are referred to here as the coupling coefficients.

and NCEP models, i.e., smaller than the observed coupling by a factor of 2-3.

The importance of the resolution of the SST boundary condition to atmospheric models is readily apparent from the time series of small-scale variance of surface wind speed in the ECMWF model shown in Fig. 3. There was an abrupt increase immediately after the 9 May 2001 change of the SST boundary condition in the ECMWF model from the low-resolution Reynolds SST analyses (Reynolds et al., 2002) to the higher-resolution RTG SST analyses (see also Chelton, 2005; Chelton and

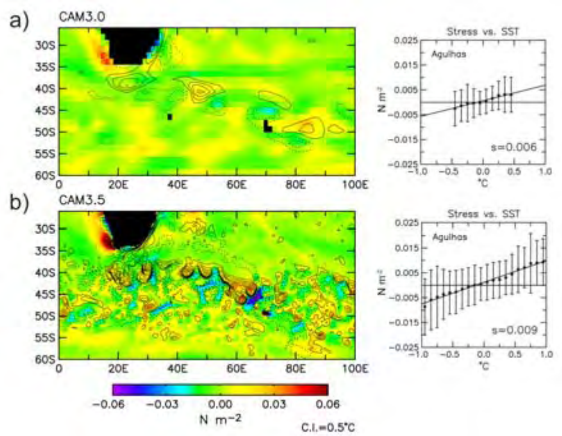

Fig. 2. The same as Fig. 1, except for a representative November-February averaging period from two versions of the NCAR Community Climate System Model: a) CCSM3.0 with 1.4° atmospheric grid and 1.0° oceanic grid; and b) CCSM3.5 with 0.25° atmospheric grid and 0.1° oceanic grid.

Wentz, 2005; Song et al., 2009). The coarse ~900 km zonal by ~600 km meridional smoothing inherent in the Reynolds SST analyses severely limit the accuracy of the surface wind response to SST. The NCEP model continues to use Reynolds SST as the surface boundary condition, thus explaining the much smoother structure of the NCEP surface wind field in Fig. 1c.

2. MESOSCALE MODEL SIMULATIONS OF SURFACE WIND RESPONSE TO SST

The under-representation of surface wind response to SST in the ECMWF model (and, by inference, the NCEP model and the CCSM3.0 and CCSM3.5 coupled models) has been investigated by Song et al. (2009) from sensitivity studies conducted with the Weather Research and Forecasting (WRF) mesoscale atmospheric model. The WRF simulations were for the ARC region, which is well suited to studies of SST influence on surface winds because of its isolated location far from continental influence and because of the strong, meandering SST front that is present year-round in association with the eastward flowing Agulhas Return Current.

The details of the WRF model simulations can be found in Song et al. (2009). The SST boundary condition for the model runs was specified as the July 2002 average from three different sources and was held constant throughout each model integration. The model runs also included a variety of grid resolutions and horizontal and vertical mixing parameterizations.

For each configuration, the surface wind field was averaged over 28 days and compared with QuikSCAT and ECMWF wind fields averaged over the same

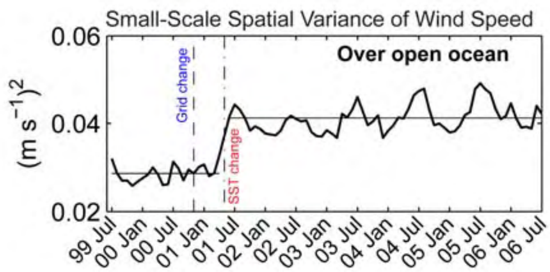

Fig. 3. Time series of the spatial variance of 10-m wind speeds in monthly averages from the operational ECMWF model over the strong midlatitude SST frontal regions of the ocean. The vertical dashed lines correspond to times of major changes of the ECMWF model: The grid resolution was changed from TL319 to TL511 (i.e., from about 60 km to about 40 km) on 21 November 2000 and the SST boundary condition was changed from the Reynolds SST analyses to the RTG SST analyses on 9 May 2001. (From Song et al., 2009.)

period. The 28-day wind fields were spatially high-pass filtered with half-power filter cutoffs of 30º of longitude by 10º of latitude to isolate the SST influence on surface winds. The WRF model simulations were then assessed by comparing the coupling coefficient for wind speed response to SST deduced from each model run with the coupling coefficients derived from QuikSCAT observations and the ECMWF model.

2.1. Sensitivity to SST Boundary Condition

The influence of the SST boundary condition is shown in Fig. 4 from WRF simulations with three different SST boundary conditions (Reynolds, RTG and AMSR), but with otherwise identical model configurations. The surface wind fields are highly correlated spatially with whichever SST field was used as the boundary condition. The presence or absence of small-scale structure in the WRF surface wind field is therefore dependent on the presence or absence of small-scale structure in the SST field. This is also evident from the direct correspondence between the wavenumber spectra of SST and wind speed for the three model runs (bottom two panels of Fig. 4).

The coupling coefficients from the WRF simulations differ only slightly for the three SST boundary conditions (right panels of Fig. 4). A given change in SST thus produces essentially the same wind speed response, regardless of the detailed accuracy and resolution of the SST field that is used for the ocean surface boundary condition. The coupling coefficient is therefore a robust measure of the low-level wind response to SST, and hence of the ability of the model to represent the air-sea interaction phenomenon that is of interest here.

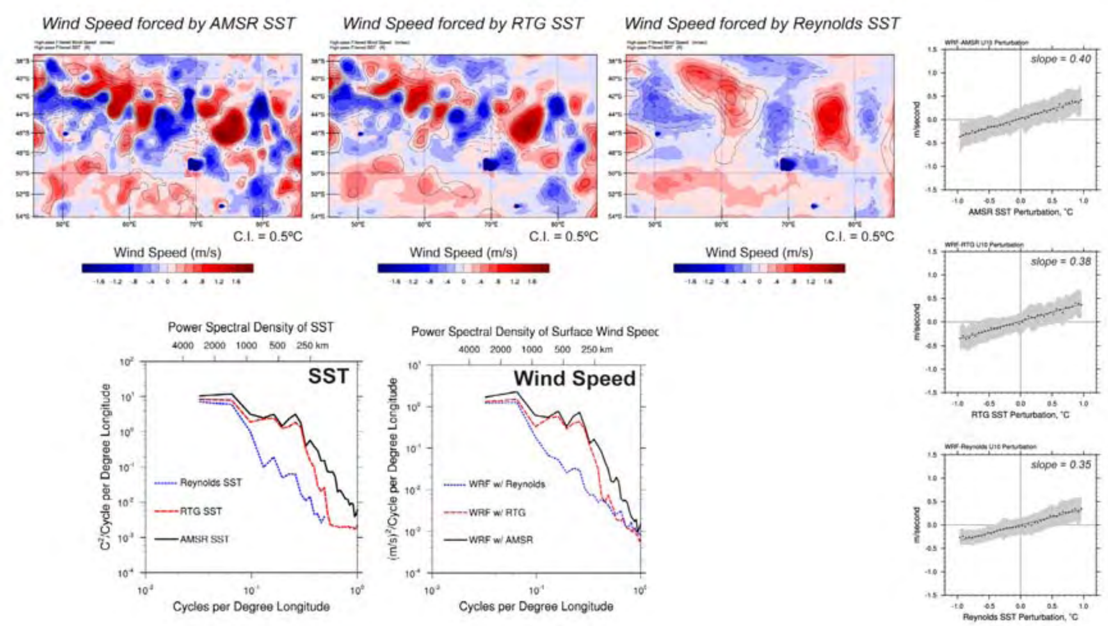

Fig. 4. Monthly average maps of SST and 10-m wind speed from the WRF mesoscale model with three different July 2002 SST boundary conditions: AMSR satellite observations, the RTG SST analyses, and the Reynolds SST analyses. Spatially high-pass filtered wind speed and SST are shown in the top panels as color and contours, respectively, with a contour interval of 0.5°C. Binned scatter plots of 10-m wind speed as a function of SST are shown in the right panels for each model run and wavenumber spectra of the three SST fields and the associated three surface wind speed fields are shown in the bottom panels. (After Song et al., 2009.)

While the spatial structures of the small-scale variability in the ECMWF surface wind fields forced with the RTG SST analyses are in good agreement with QuikSCAT observations (left panels of Figs. 1a and b), their intensity is visually too small by about a factor of two, consistent with the approximate factor-of-two underestimation of the coupling coefficients (right panels of Figs. 1a and b; see also Maloney and Chelton, 2006). From the WRF simulations in Fig. 4, resolution limitations of the RTG SST analyses affect the accuracy of surface winds only on wavelength scales shorter than about 250 km (see the wavenumber spectra of wind speed in the bottom right panel of Fig. 4; see also Song et al. 2009), which is the approximate resolution of the RTG SST analyses (see the wavenumber spectra of SST in the bottom left panel of Fig. 4; see also Chelton and Wentz, 2005).

Horizontal mixing in the WRF model was similarly found to be a limiting factor only on wavelength scales shorter than about 250 km. Moreover, the WRF simulations also found that the ~40 km grid resolution of the TL511 spectral dynamical core used in the ECMWF operational model from 21 November 2000 to 31 January 2006 is a limiting factor only on scales shorter than about 250 km. Song et al. (2009) thus conclude that the approximate factor-of-2 underestimation of variance of surface winds in the ECMWF model on wavelength scales of 250–1000 km is due primarily to inadequacies in the parameterization of vertical turbulent mixing (see section 2.2 below).

It is clear from Fig. 2a and analogous figures for the other coupled climate models analyzed by Maloney and Chelton (2006) that grid resolution becomes a more limiting factor when it is too coarse. The feature resolution in numerical models is generally about a factor of 5 coarser than the model grid (Walters, 2000). The 100–1000 km scales of SST-induced perturbations of the surface wind field are therefore not adequately resolved by the 1.4° grid spacing of the atmospheric component of the CCSM3.0 model. The improved grid resolution of 0.25º in CCSM3.5 allows resolution of scales down to about 250 km (Fig. 2b).

2.2. Sensitivity to Vertical Mixing

The importance of vertical mixing has been investigated by Song et al. (2009) from the WRF model by considering a wide range of parameterizations of the vertical mixing sensitivity to atmospheric stability. Results from two of the simulations are discussed here. To mimic the ECMWF model formulation for the time period 9 May 2001 through 31 January 2006, the grid spacing for these simulations was 40 km and RTG SST was used as the surface boundary condition.

The mixing parameterization used for the WRF simulation in Fig. 5 is the Mellor and Yamada (1982) formulation. This mixing yields a monthly average wind speed field very similar to that from the ECMWF model (left panels of Fig. 5) with a coupling coefficient essentially identical to that derived from the ECMWF model (right panels of Fig. 5). This suggests that the vertical mixing in the ECMWF model is comparable to that in the WRF model with Mellor-Yamada mixing.

The mixing parameterization used for the WRF simulation in Fig. 6 is the Grenier and Bretherton (2001) formulation that has a dependence on atmospheric stability that is 5 times stronger than the Mellor-Yamada formulation. The Grenier-Bretherton mixing yields a monthly average wind speed field very similar to the QuikSCAT observations (left panels of Fig. 6) with coupling coefficient essentially identical to that derived from QuikSCAT (right panels of Fig. 6).

It is clear from Figs. 5 and 6 that the dependence of the Mellor-Yamada mixing on atmospheric stability is too weak by approximately the factor-of-5 difference between the Mellor-Yamada and Grenier-Bretherton formulations. Fig. 5 thus suggests that the

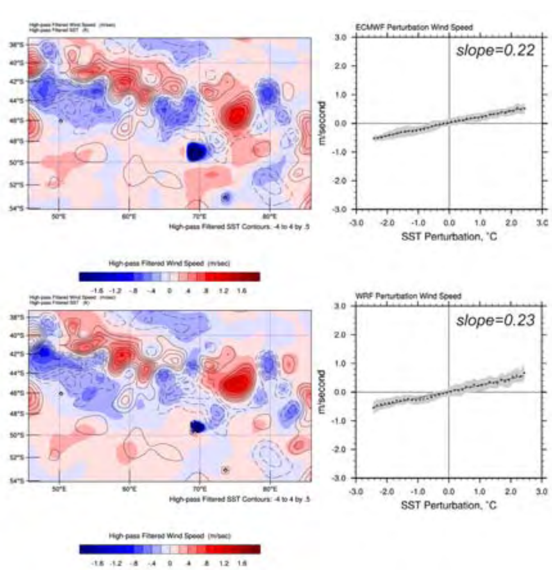

Fig. 5. Monthly averages of 10-m wind speed from (top) the ECMWF operational model and (bottom) the WRF model with 40-km grid spacing and the Mellor-Yamada parameterization of vertical mixing. Spatially high-pass filtered wind speed and SST are shown in the left panels as color and contours, respectively, with a contour interval of 0.5°C. Binned scatter plots of wind speed as a function of SST are shown in the right panels. (After Song et al., 2009.)

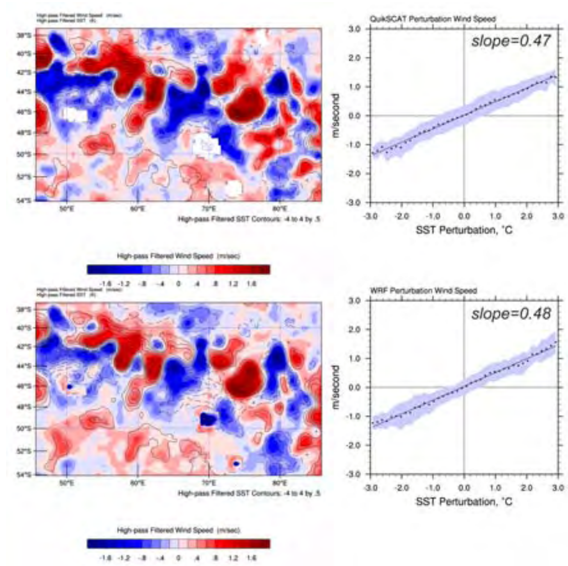

Fig. 6. The same as Fig. 5, except 10-m equivalent neutral stability wind speed from (top) QuikSCAT observations and (bottom) the WRF model with 25-km grid spacing and the Grenier-Bretherton parameterization of vertical mixing. (After Song et al., 2009.)

underestimation of variance in the ECMWF model on scales smaller than ~1000 km is likely due to the model having a vertical mixing parameterization that is comparable to the Mellor-Yamada formulation.

3. CONCLUSIONS

The observational evidence that SST exerts a strong influence on surface winds is unequivocal. Winds are locally stronger over warmer water and weaker over cooler water. Spatial variations in the SST field thus result in spatial variations in the surface wind field, resulting in wind stress curl structures that generate open-ocean upwelling and drive the large-scale ocean circulation (Chelton et al., 2004). This ocean-atmosphere interaction likely has important feedback effects on the ocean circulation, as well as on air-sea heat fluxes and ocean biology. It is therefore crucial that this SST influence on surface winds be accurately represented in the wind fields that are used to force ocean circulation models. Most ocean models are forced by the surface wind analyses or reanalyses from the ECMWF or NCEP models. As shown in Figs. 1, 5 and 6, these models underestimate the SST influence on surface winds by a factor of 2 or more. Likewise, this ocean-atmosphere coupling is underestimated by a factor of 2 or more in coupled climate models (Fig. 2).

Surface convergence and divergence associated with spatial variations in the SST field (Chelton et al., 2004) generate vertical motion in the atmosphere. This SST influence is evident throughout the troposphere over the Gulf Stream (Minobe et al., 2008). SST influence has also been detected throughout the troposphere in the Agulhas Return Current region (Liu et al., 2007). The ocean-atmosphere interaction identified from the satellite observations may therefore be important to the general circulation of the atmosphere, again emphasizing the importance of accurate representation of the SST influence on surface winds in operational forecast models and coupled climate models.

The conclusions from the WRF simulations summarized in section 2 are that the primary factors responsible for underestimation of SST-induced small-scale variability in the surface wind field are: 1) the resolution of the SST boundary condition in uncoupled models (and presumably the resolution of the ocean component of coupled models); and 2) parameterization of vertical mixing sensitivity to atmospheric stability.

In the case of the ECMWF model, we conclude that it is likely that the approximate factor-of-2 underestimation of the surface wind response to SST is attributable primarily to underestimation of the dependence of vertical mixing on atmospheric stability. The resolution of the SST boundary condition is a secondary issue in the ECMWF model, but is the most limiting factor in the NCEP model that presently continues to use the Reynolds SST analyses as the ocean boundary condition.

For coupled climate models, the representation of SST influence on surface winds depends also on the grid resolution. While the observed SST influence is adequately resolved on scales longer than about 250 km by the grid resolutions of present operational forecast models, the grid resolutions of many coupled models are too coarse to represent this ocean-atmosphere interaction accurately.

4. REFERENCES

Chelton, D. B., 2005: The impact of SST specification on ECMWF surface wind stress fields in the eastern tropical Pacific. *J. Climate*, **18**, 530-550.

Chelton, D. B., and F. J. Wentz, 2005: Global microwave satellite observations of sea-surface temperature for numerical weather prediction and climate research. *Bull. Amer. Meteor. Soc.*, **86**, 1097-1115.

Chelton, D. B., M. G. Schlax, M. H. Freilich, and R. F. Milliff, 2004: Satellite measurements reveal persistent small-scale features in ocean winds. *Science*, **303**, 978-983.

Grenier, H., and C. S. Bretherton, 2001: A moist PBL parameterization for large-scale models and its application to subtropical cloud-topped marine boundary layers. *Mon. Wea. Rev.*, **129**, 357-377.

Liu, W. T., X. Xie, and P. Niiler, 2007: Ocean-atmosphere interaction over Agulhas Extension meanders. *J. Clim*., **20**, 5784—5797.

Maloney, E. D., and D. B. Chelton, 2006: An assessment of the sea surface temperature influence on surface wind stress in numerical weather prediction and climate models. *J. Climate*, **19**, 2743-2762.

Mellor, G. and T. Yamada, 1982: Development of a turbulent closure model for geophysical fluid problems. *Rev. Astrophys. Space Phys.*, **20**, 851-875.

Minobe, S., A. Kuwano-Yoshida, N. Komori, S.-P. Xie, and R. J. Small, 2008: Influence of the Gulf Stream on the troposphere. *Nature*, **452**, 206-209.

Reynolds, R. W., N. A. Rayner, T. M. Smith, D. C. Stokes, and W. Wang, 2002: An improved in situ and satellite SST analysis for climate. *J. Climate*, **15**, 1609-1625.

Small, R. J., and Coauthors, 2008: Air-sea interaction over ocean fronts and eddies. *Dyn. Atmos. Oceans*, doi:10.1016/j.dynatmoce.2008.01.001.

Song, Q., D. B. Chelton, S. K. Esbensen, N. Thum, and L. W. O'Neill, 2009: Coupling between sea surface temperature and low-level winds in mesoscale numerical models. *J. Clim.*, **22**, 146-164.

Walters, M. K., 2000: Comments on “The differentiation between grid spacing and resolution and their application to numerical modeling”. *Bull. Amer. Meteor. Soc.*, **81**, 2475-2477.

Impacts of High Resolution SST Fields on Objective Analysis of Wind Fields, and Practical Constraints Related to Sampling

Mark A. Bourassa and Paul J. Hughes
COAPS & Department of Meteorology
Florida State University
Tallahassee, FL 32306-2840
E-Mail: bourassa@coaps.fsu.edu

***Abstract*— High resolution SSTs are used to add information to an overly smooth vector wind field. The key diagnostic for this study is the spectra density (spatial) of wind vector components. Wind fields are derived from a reanalysis pressure field without SST information, and the finer spatial scales are shown to be limited by smoothing. The winds are determined through the UWPBL model, which can also use air temperature information to consider additional physics. For simplicity, it is assumed that the air temperature is equal to the SST in Reynolds 0.25° GHRSST product. The wind fields derived with this temperature information are smoothing limited at much smaller spatial scales. Knowledge of these scales can also be used to determine the averaging scales used in determining tuning parameters in objective analyses.**

I. INTRODUCTION

With one or two wide swath scatterometers (e.g., SeaWinds on QuikSCAT and/or ADEOS2) the key limiting factor in producing useful gridded wind products is the temporal sampling. Winds can change rapidly in time relative to many other surface variables; therefore, sampling is critical. Consequently, daily averaged wind fields based largely on satellite data, and with crudely homogeneous error characteristics (Schlax et al. 2001), have spatial resolutions limited by smoothing. The resolution can arguably be improved by including data from other sources: satellites (Atlas 1996), numerical weather prediction (Liu et al, 1998), reanalyses (Chin et al. 1998; Morey et al. 2006), or several of these (Yu and Weller 2007). However, inconsistencies between QuikSCAT and the other products limit the effectiveness of these approaches, perhaps requiring increased smoothing.

A key issue for users of satellite derived data sets is the actual resolution of the product. In many cases the resolution is variable in space and time, but is described only by the grid spacing, which is arbitrary. An average resolution or a resolution as a function of latitude would help potential users of these products determine if the product is suitable for their needs. Spectral density of wind speed or wind components can be used to identify the length scale where smoothing begins to be a serious issue (Rodriguez 2008). This technique is applied to winds derived from the Modern Era Retrospective-Analysis For Research And Applications (MERRA; Bosilovich et al. 2008) surface pressures.

A key consideration for makers of gridded data sets is determining the value of tuning parameters related to smoothing. In the case of our objective analysis technique (adapted from Pegion et al. 2000), the weights are tuned through cross validation (Wahba and Wendelberger 1980). Such tuning is done by removing a large block of data, and tuning the weights so that the objectively analyzed data at the center of the removed data is a good match to the data from the same region (Pegion et al. 2000). The size of this region was arbitrarily set at one grid cell, with data within ±10 grid cells being removed. It is likely that for most applications it would be better to use data that have been averaged over a slightly larger scale for the cross validation (reducing the noise issues). This averaging scale could be increased until it adversely impacts the resolution as seen in the plot of spectral density. This process likely to result in better tuned weights.

The application to weighting coefficients will not be examined herein. This study will show that high resolution SST data can be used to add finer scale information to vector wind fields that otherwise have resolution limited by smoothing.

II. DATA

Two data sets are used in this study: high resolution SSTs and sea level pressures. An overly smooth wind field is simulated by interpolating the MERRA sea level pressures (0.5 x 0.66°) to the grid spacing of the Reynolds GHRSST product (0.25 x 0.25°; Reynolds et al. 2007). A spline fit is used to greatly reduce spurious spatial derivatives. The magnitude of vector wind components is related to the pressure gradient; therefore, the vector wind is sensitive to spurious changes in the pressure field. The University of Washington Planetary Boundary Layer model (UWPBL) is used to find a field of vector winds based on the pressure or the pressure and the SSTs..

The time period of examination is February 2003. The MERRA data are hourly; however, only the data for 01Z are examined herein. This time step is consistent with that of the Reynolds SST product, which has a daily time step.

III. VECTOR WIND FIELDS

Two sets of vector wind fields are generated. One set ignores air temperature, and assumes that there is no surface temperature gradient. The reanalysis pressures are very smooth at the native scale: the interpolated pressure field certainly does not contain information on scales less that of the native pressure grid. The spectral density of these winds is shown as the black lines in figure 1, for latitudes of 55°N, 45°N, 30°N and 20°N. The influence of excessive smoothing is quite evident in the zonal component (left column) for 45 and 55°N, where there is a sharp increase in the rate of change of the log of spectral density with respect to the log of wavelength, at a wavelength of roughly 100km at 55°N, and roughly 200km at 45°N. Similar drops are seen in the other frames. At shorter wavelengths the curves become near horizontal (near zero slope) indicating a limiting spatial scale associated with white noise. At most latitudes the smoothing is a serious constraint on the effective resolution at roughly 200km.

The spectral density for the meridional vector component has a strange bump at around 200km wavelength (100km at 55°N). If there were substantial errors in interpolation, they are highly unlikely to be manifested at that wavelength. Consequently, these features are very likely found in the MERRA data set.

The GHRSST data are used, with the MERRA pressure data, to construct a baratropic, but non-isothermal, vector wind fields. It is assumed that the air temperature is equal to the SST. This assumption is unrealistic, but will result in many realistic air temperature gradients. The spectral densities for these wind vector components are shown as the red lines in Fig. 1. Changes in slope associated with smoothing are largely removed. The SST data are remarkably effective for adding information to the wind field.

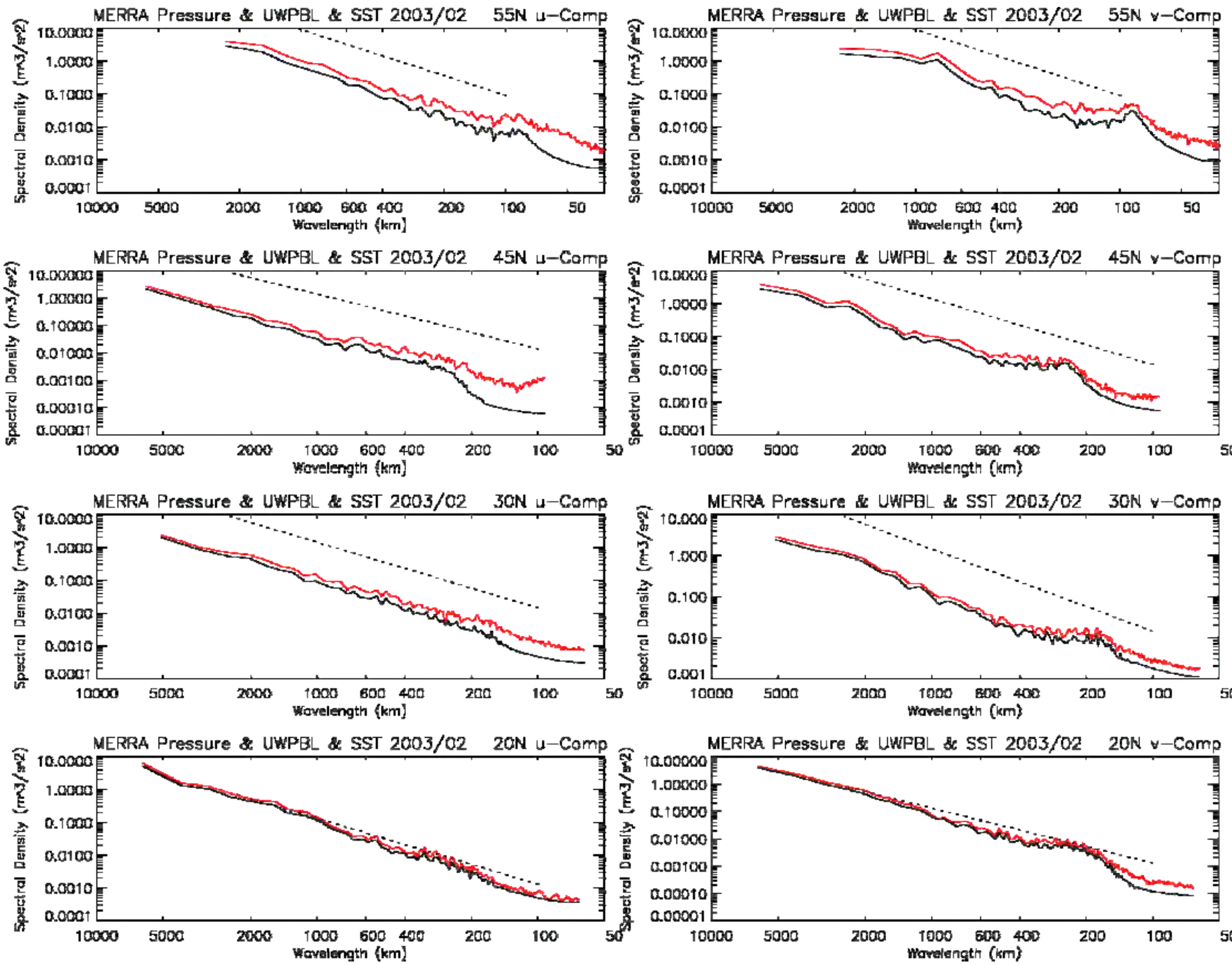

Fig. 1. Spectral density for zonal (left) and meridional (right) vector wind components at 55°N, 45°N, 30°N and 20°N. The black line assumes isothermal surface temperatures, and the red line assumes air temperature that are equal to the SSTs.

IV. Summary and Discussion

The finding that information from SSTs can be used to add realistic information to overly smooth vector wind fields suggests that SSTs would be similarly useful for the construction of satellite-based fields of gridded wind vectors. The method for addition this information is the physically-based UW PBL model. It remains to be seen if wind fields derived in this manner are consistent with the observed wind and SST features.

Acknowledgements: We thank Ryan Maue for extracting the MERRA surface pressures. This work was support by grants from NASA HQ and the NASA OVWST.

V. References

Atlas, R., R. N. Hoffman, S. C. Bloom, J. C. Jusem, and J. Ardizzone, 1996: A multiyear global surface wind velocity data set using SSM/I wind observations. *Bull. Amer. Meteor. Soc.*, **77,** 869–882.

Bosilovich, M., J. Chen, F. R. Robertson and R. F. Adler, 2008. Evaluation of Global Precipitation in Reanalyses. *J. Appl. Meteor. Clim.*, **47**, 2279–2299.DOI: 10.1175/2008JAMC1921.1.

Chin, TM and Milliff, RF and Large, WG, 1998: Basin-scale, high-wavenumber sea surface wind fields from a multiresolution analysis of scatterometer data. *Journal of Atmospheric and Oceanic Technology*, **15**, 741-763, doi:10.1175/1520-0426(1998)015<0741:BSHWSS>2.0.CO;2.

Liu, W.T. and Tang, W.Q. and Polito, P.S., 1998: NASA scatterometer provides global ocean-surface wind fields with more structures than numerical weather prediction. *Geophysical Research Letters*, **25**, 761-764, doi:10.1029/98GL00544

Morey, S. L., M. A. Bourassa, D. S. Dukhovskoy, and J. J. O'Brien, 2006: Modeling studies of the upper ocean response to a tropical storm. *Ocean Dynamics*, DOI: 10.1007/s10236-006-0085-y.

Pegion, P. J., M. A. Bourassa, D. M. Legler, and J. J. O'Brien, 2000: Objectively-derived daily "winds" from satellite scatterometer data. *Mon. Wea. Rev*., **128**, 3150–3168.

Reynolds, R. W., T. M. Smith, C. Liu, D. B. Chelton, K. S. Casey and M. G. Schlax, 2007: Daily High-resolution Blended Analyses for sea surface temperature. *J. Climate*, **20**, 5473-5496.

Rodriguez, E. 2008: personal communication. http://coaps.fsu.edu/scatterometry/meeting/docs/2008/lproducts/rodriguez.pdf

Ross, D. B., V. J. Cardone, J. Overland, R. D. McPherson, W. J. Pierson Jr., and T. Yu, 1985: Oceanic surface winds. Adv. Geophys., 27, 101-138.

Schlax, M. G., D. B. Chelton, and M. H. Freilich, 2001: Sampling errors in wind fields constructed from single and tandem scatterometer datasets. Journal of Atmospheric and Oceanic Technology, 18, 1014 1036, doi:10.1175/1520-0426(2001)018<1014:SEIWFC>2.0.CO;2.

Wahba, G., and J. Wendelberger, 1980: Some new mathematical methods for variational objective analysis using splines and cross-validation. Mon. Wea. Rev., 108, 1122-1143.

Yu, L., and R. A. Weller, 2007: Objectively analyzed air-sea heat fluxes for the global ice-free oceans (1981-2005). *Bull. Amer. Meteor. Soc.*, **88**, 527-539.

Use of New SST Products in the CLIvar MOde Water Dynamic Experiment (CLIMODE)

Suzanne Dickinson, Kate Edwards and Kathryn A. Kelly
Applied Physics Lab, University of Washington, Seattle, WA 98105 USA

Introduction

The CLIvar MOde Water Dynamic Experiment (CLIMODE) was conducted in the Northwest Atlantic to study the thermodynamics of the subtropical mode water associated with the Gulf Stream. A tethered mooring placed in the active region of the SST front, (38N, 295W) collected data, as did six research cruises and a drifting buoy.

The mooring data, a 14-month time series over two winters, contains hourly oceanic and atmospheric data, including sea surface temperature (SST). The SST data, which were measured at a depth of 80cm and averaged to daily for this study, are plotted in Figure 1 (below).

The activity in the SST signal shows that the Gulf Stream is initially north of the mooring (Nov05-Jan05), meanders south of the mooring during the spring of 2006 and meanders back north of the mooring in May 2006.

Comparison to GHRSST Products

We compare these mooring data to four GHRSST daily L-4 products and the AMSR-fused product from Remote Sensing Systems. Two of the GHRSST products contain infrared satellite data only (NOAA/NCDC OISST-AVHRR [OISST(av)] and NOAA/NCEP RTG [RTG]) and two integrated microwave and infrared satellite data (NOAA/NCDC OISST-AVHRR+AMSR [OISST], and REMSS MW_IR [REMSS]). The statistical comparison of the gridded SST products to the mooring data is shown in Figure 2 (below).

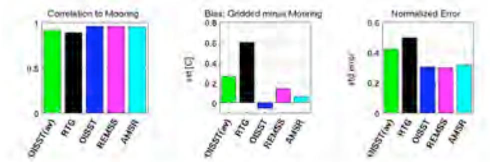

The correlations (left panel) are all high and significant. The biases (middle panel) show the infrared products are biased warm compared to the mooring data. The error (right panel) is normalized by the standard deviation of the mooring observations. The products containing microwave data have better statistics.

Figure 3 shows the Taylor diagram for the comparison, which considers both the correlation between two time series and their relative magnitudes. The statistic is plotted in polar coordinates, where $\theta=\cos^{-1}$(correlation), and R is the relative magnitude of the signals; gridded over observations. Normalized error is the distance to the red dot in Figure 3 (below). We see that

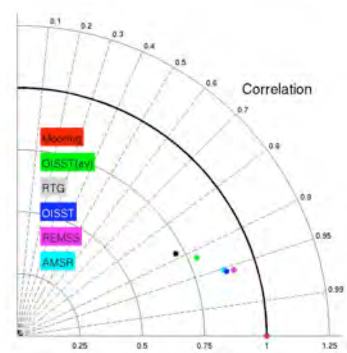

all the satellite based products have lower energy than the mooring data and that the products containing microwave data show improvement over the infrared data only.

Improved Fluxes

We use the COARE algorithm v3.0 (Couple Ocean Atmosphere Response Experiment) to calculate turbulent fluxes using variables from the NCEP Eta/NAM forecast model. These variables include sea level pressure, wind speed, air temperature and humidity, and sea surface temperature. The SST from Eta, comes from RTG. To take advantage of the improved SST products (including microwave data) in calculating better fluxes, we replace the Eta SST with that from OISST. In an effort to preserve the inherent coupling between the air and sea temperatures that exists due to air-sea interaction, we improve the Eta air temperature field with an empirical correction.

Figure 4 (below) shows the air temperature error (dT_{air}) plotted against the SST error dT_{sea}, where error is Eta minus mooring data.

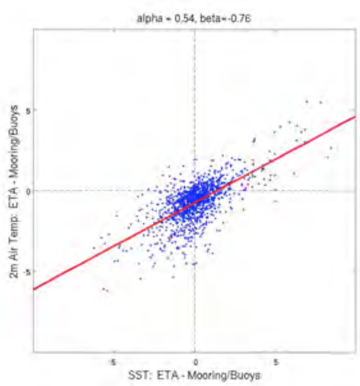

A least squares fit through the scatterplot gives a slope (alpha) of 0.54. This means with an SST error of 1°C, we have an air temperature error of about 0.5°C. We get a very similar slope if we use a dT_{sea} = Eta – OISST. We correct the Eta air temperature over the Gulf Stream region with the following equation:

$$T_{air\_corr}=T_{air\_Eta} - alpha*(T_{sea\_Eta} - T_{sea\_OISST}).$$

Figure 5 is a Taylor diagram comparing three sets of latent heat fluxes compared to the latent heat flux calculated with the mooring data and the COARE algorithm. The green dot shows the Taylor statistic for the fluxes computed with the Eta algorithm. The magenta dot shows that for the Eta variables (sea level pressure, humidity, wind speed, air and sea temperatures) run through the ÇOARE algorithm. Although the energy is reduced (using the COARE algorithm), the correlation is increased and the error goes down. Eta variables with the OISST for SST and the improved Eta air temperature, run through the COARE algorithm, results in the blue dot in Figure 5. We see another decrease in error, and a little more energy when compare to the fluxes computed at the mooring.

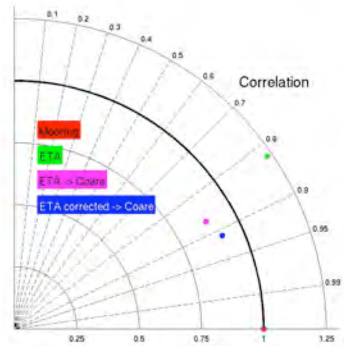

GHRSST Products Measuring Outcrop Area

Figure 6 (below) shows the March 2006 SST mean from OISST.

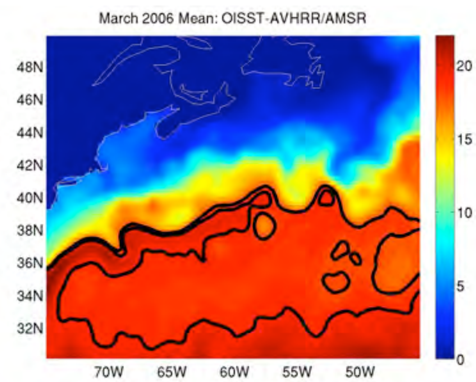

The 18°C and 19°C contours are shown to indicate outcrop area over the subtropical mode water, south of the Gulf Stream.

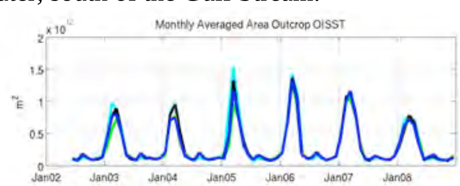

The monthly averages of outcrop are plotted in Figure 7, for OISST (blue), RTG (black), OISST infrared only (green) and AMSR-fused (cyan), for the time period June, 2002 through 2008. The interannual signal of maximum outcrop area in the spring is quite evident. The errors of the outcrop area between the different products, normalized by the variance of the OISST, are about 10-20%. This means we can distinguish the interannual signal of outcrop area. Outcrop area is a parameterization of the stratification of the mode water, which is a deep isothermal layer of 18°C in the Atlantic Ocean.

Impact of using merged regional operational L3 in the operational Meteo-France regional Aladin model to forecast Mediterranean convective events

Françoise Orain(CMS/MF), Françoise Taillefer (CNRM/MF), Pierre LeBorgne(CMS/MF), Hervé Roquet(CMS/MF)
Contact :francoise.orain@meteo.fr

Forecasting convective events in the Mediterranean sea area is important. In Southern France, for instance, the "Cevenol events" are responsible of flash floods and generate casualties and a lot of damage. We investigate the potential benefit of satellite SST to meteorological and oceanographic models in this context. This study is also a contribution to the Hymex project (2011).
SST plays an obvious role in creating the convection conditions but satellite data have been so far difficult to assimilate in practice.
A method to insert the ("supercollated") L3 SST data from the Mersea project in the Meteo-France operational surface data assimilation has been developed. The fine scale ALADIN model has been used to test the impact of satellite SST directly within the usual operational modeling at Meteo France .

The presentation will include a short description of the Mersea L3 products, a presentation of the assimilation processing and the main characteristics of the ALADIN forecast model.

The convective case of 29 September 2007 will be presented (comparison of several current analysis) and analyzed .
The impact of L3 products on latent heat fluxes, Cape (Convective available potential energy), sensible heat flux and precipitations will be commented .

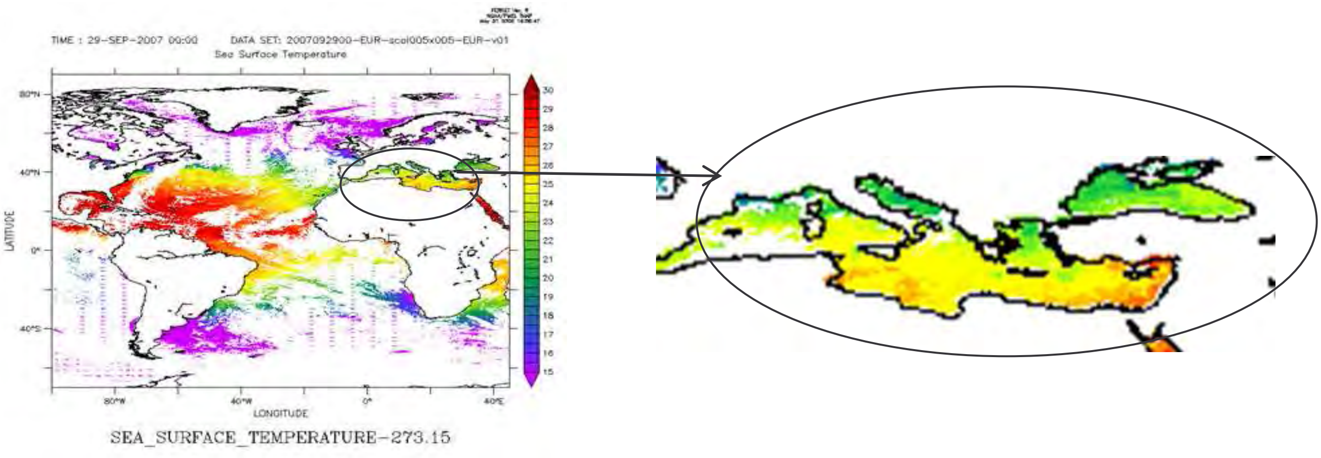

Fig1 L3 (Mersea 5 km °C) on the 29/09/2007 over the Mediterranean sea

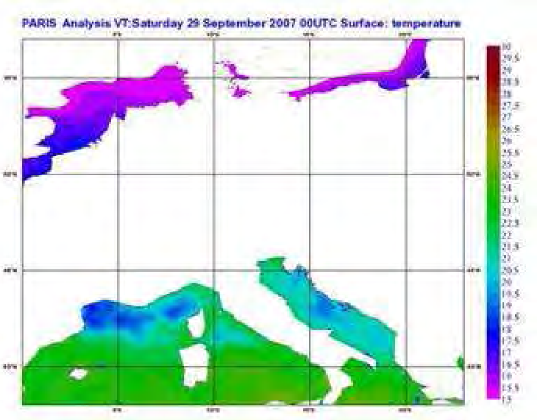

Fig 2
Canari/Aladin Operational
Analysis using Mersea L3

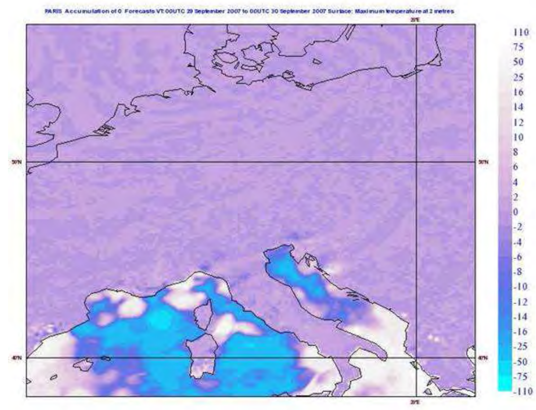

Fig3
Aladin 24 H forecast Latent Heat flux
for the 30/09/2007

Application of MISST L4p analyses product at the NOAA Ocean Prediction Center

Joseph Sienkiewicz, Robert Daniels, and Ming Ji

The NOAA Ocean Prediction Center issues operational marine weather warnings and forecasts of winds and waves for high seas area in North Pacific and North Atlantic oceans and off shore regions adjacent to the U.S. High resolution sea surface temperature analysis is an important tool for forecasters to determine factors such as the location and strength of the Gulf Stream, associated eddies, and thermal features such as the shelf break front. In winter, frequent heavy cloud cover the extratropical ocean resulting in the loss of SST observations by IR sensors for extended periods. Techniques using a combination of IR and microwave SST observations have demonstrated a superior capability to produce much improved SST coverage. OPC introduced a L4p analysis product (Reynolds, et al., 2007) into marine forecast operations in Fall, 2007.

The MISST has been available to the OPC for over one year. In this paper we will discuss the various uses of the MISST by the OPC such as: the evaluation of the Navy Coastal Ocean Model (NCOM) and NCEP Real Time Ocean Forecast System Atlantic (RT_OFS_ATL), an assessment of low level atmospheric stratification, the generation of freezing spray guidance, and tracking of ocean features.

NOAA CORAL REEF WATCH'S APPLICATION OF SATELLITE SEA SURFACE TEMPERATURE DATA IN OPERATIONAL NEAR-REAL-TIME GLOBAL MONITORING AND EXPERIMENTAL OUTLOOK OF CORAL HEALTH AND POTENTIAL APPLICATION OF GHRSST

Gang Liu[(1)], Tyler R. L. Christensen[(1)], C. Mark Eakin[(2)], Scott F. Heron[(3)], Jessica A. Morgan[(1)], Britt-Anne A. Parker[(1)], William J. Skirving[(3)], Alan E. Strong[(2)]

[(1)] *IMSG at NOAA Coral Reef Watch, 1335 East West Hwy, Silver Spring, MD 20910, USA, Email: Gang.Liu@noaa.gov*
[(2)] *NOAA Coral Reef Watch, 1335 East West Hwy, Silver Spring, MD 20910, USA*
[(3)] *NOAA Coral Reef Watch, 675 Ross River Rd, Townsville, Australia*

ABSTRACT

NOAA Coral Reef Watch (CRW) has developed a product suite using global satellite and model data to provide daily monitoring and forecasting of coral bleaching and other coral reef environmental conditions. Currently, NOAA/NESDIS operational 0.5-degree (50-km) AVHRR sea surface temperature (SST) data are used for near-real-time monitoring of thermal stress that can cause coral bleaching. The NOAA Reynolds and Smith Optimum Interpolation SST (OISST) analysis that includes both *in situ* and satellite SSTs is used to train and initialize forecast models used for producing the bleaching outlook. We are transitioning to using recently implemented NOAA/NESDIS operational AVHRR Clear-Sky Processor for Oceans (ACSPO) SST and POES-GOES Blended SST with higher data density and increased spatial and temporal resolutions. The availability of the Group for High-Resolution SST (GHRSST) data, as a new generation of uniformly processed high-resolution satellite SST data, especially through inclusion of microwave-based observations that penetrate clouds, may aid CRW's development of enhanced products for monitoring and management of global coral reef ecosystems.

1. INTRODUCTION

Over the past few decades, climate change related mass coral bleaching has become a major contributor to the worldwide deterioration of coral reef ecosystems (1,2). Most reef-forming corals contain symbiotic microscopic algae within their tissues (3), with the photosynthetic pigments of the algae providing the colors seen in healthy host corals. Under certain environmental stresses these algae can be expelled by the host corals, revealing their white calcium carbonate skeleton through the translucent coral tissue and leaving the affected coral colonies stark white or pale. This phenomenon is commonly known as "coral bleaching" (4). Coral bleaching is often caused by ambient water temperatures that exceed the coral's tolerance level (5,6). Bleaching reduces the coral's growth and reproductive capacity (1) and weakens the coral's ability to fight disease (7,8). Prolonged thermal stress often leads to the death of the corals (1,9). Severe bleaching events have dramatic long-term ecological and social impacts (10,11,12). Even under favorable conditions, it can take many years for severely bleached reefs to recover (12). Mass bleaching events may even involve entire reef systems and geographic realms.

In response to critical scientific and management needs for improved understanding, monitoring, and prediction of coral bleaching, NOAA CRW has worked since 1997 to develop and deliver a suite of global satellite near-real-time coral bleaching monitoring products and a seasonal tropical bleaching outlook product, that rely on satellite SST measurements. With the capability of synoptic views of the global oceans in near-real-time and the ability to monitor remote reef areas, CRW's products have become widely and successfully used by resource managers and scientists around the world (13). CRW's products are available in multiple graphic and data formats at our website (http://coralreefwatch.noaa.gov).

2. SST-BASED PRIMARY PRODUCTS

CRW's primary near-real-time operational satellite products include twice-weekly 50-km global Coral Bleaching HotSpots (Fig. 1) and accumulated thermal stress Degree Heating Weeks (DHW) (Fig. 2) (13,14,15,16). The Coral Bleaching HotSpot measures the intensity of bleaching thermal stress as the difference between the observed SST at a grid point and the climatologically averaged temperature for the warmest month. Integrating both the intensity and duration of thermal stress, the Degree Heating Week (DHW) accumulates HotSpot values of ≥1.0 ºC during the prior 12 weeks to provide a stress index that has been a good predictor of the severity of bleaching. Based on bleaching reports and feedback from our collaborators in the field, our data have shown that DHW of 4 ºC-weeks is typically related to significant coral bleaching, and that 8 ºC-weeks or above is typically related to observed widespread severe bleaching and observed mortality (13). These products are presently being updated twice-weekly using NOAA/NESDIS operational 50-km composite satellite nighttime AVHRR SST data. Since 1997, these products have been successful in providing a short-term prediction of mass coral bleaching episodes around the globe, including the record-breaking 2002 Great barrier Reef mass coral bleaching event, record-breaking 2002 Northwestern Hawaiian Islands mass coral bleaching event, and record-breaking 2005 Caribbean mass coral bleaching event (2,13,15).

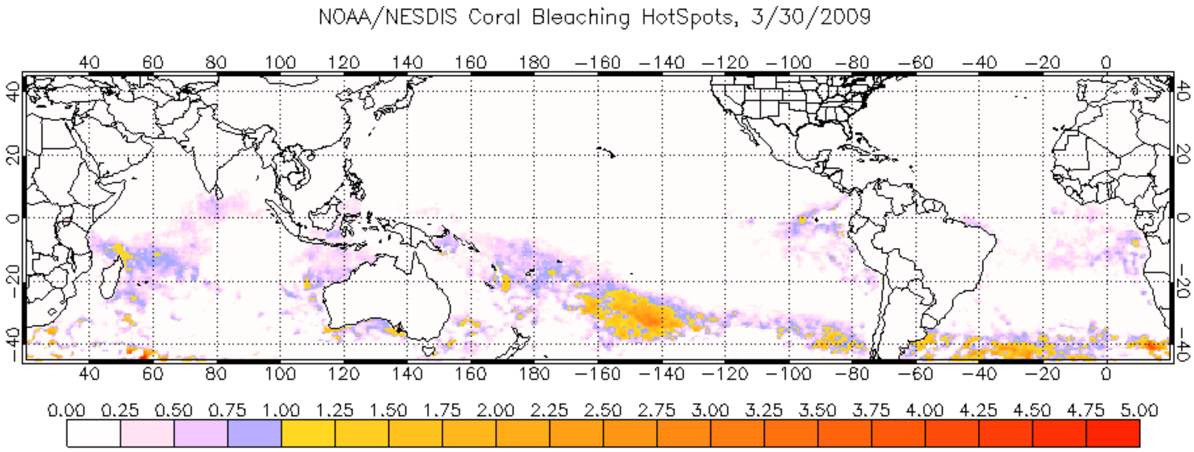

Figure 1. CRW's operational twice-weekly near-real-time satellite 50-km coral bleaching HotSpot chart of March 30, 2009.

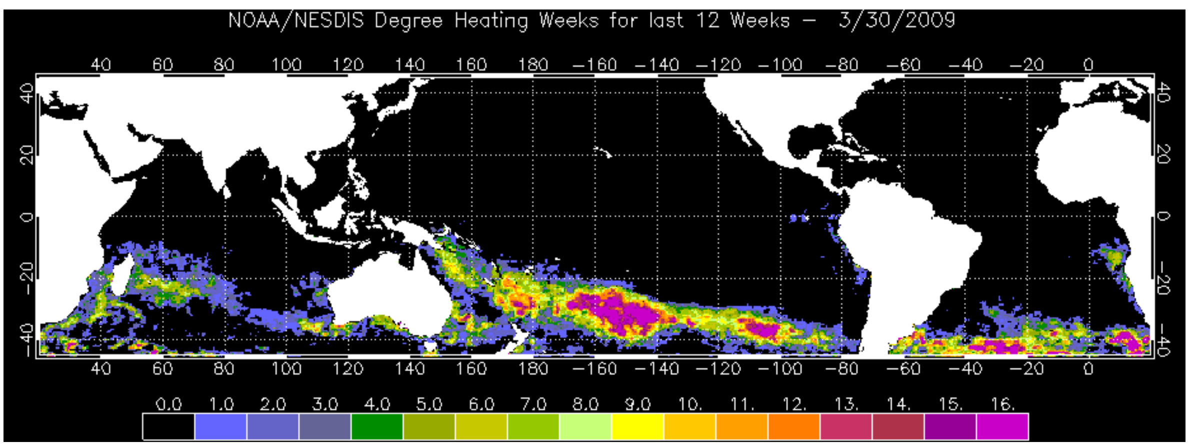

Figure 2. CRW's operational twice-weekly near-real-time satellite 50-km coral bleaching Degree Heating Week chart of March 30, 2009.

The global HotSpot and DHW products are further customized at the pixel level to provide detailed near-real-time thermal stress information for about 190 reef sites around the globe, called Coral Bleaching Virtual Stations. The Virtual Station product provides a summary of CRW products for the pixel associated with each of the stations. Based on the values of HotSpot and DHW at these stations, CRW's Satellite Bleaching Alert System categorizes the bleaching thermal stress into five predefined levels (No Stress, Bleaching Watch, Bleaching Warning, Bleaching Alert Level 1, and Bleaching Alert Level 2) and automatically alerts subscribers of any changes in thermal stress level at these stations.

An experimental seasonal tropical coral bleaching outlook system was developed by CRW in collaboration with the NOAA Physical Sciences Division of the NOAA's Earth System Research Laboratory (ESRL). Since 2008, updated on a weekly basis, it has been providing coral reef managers and researchers critical information on the potential for large-scale bleaching thermal stress events weeks to months in advance (Fig. 3). The outlook covers the tropical latitudes between 30ºS and 30ºN at 2-degree weekly resolution. The system uses an SST prediction model based on NOAA's Linear Inverse Model (LIM) (17,18,19) and a bleaching thermal stress model based on the HotSpot and DHW algorithms similar to those used in CRW's HotSpot and DHW near-real-time monitoring described above. The NOAA weekly 1-degree Reynolds and Smith Optimum Interpolation SST (OISST) analysis (20,21) was used to train the model and is used to provide the initial conditions for producing the SST prediction.

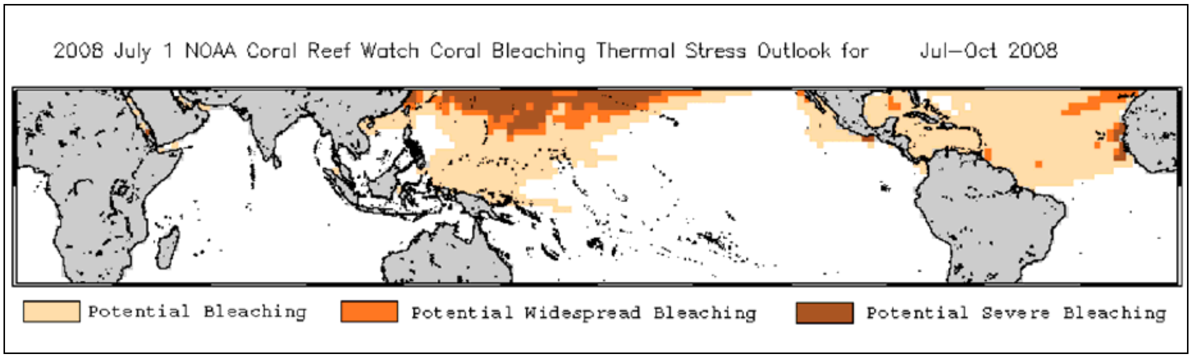

Figure 3: CRW's seasonal bleaching outlook for July-October 2008 produced on July 1, 2008. Based on the predicted thermal stress in terms of HotSpot and DHW prediction, three levels of bleaching potential are defined as Potential Bleaching (light orange), Potential Widespread Bleaching (orange), and Potential Severe Bleaching (dark brown).

3. PLAN FOR FUTURE IMPROVEMENT

CRW is developing improved monitoring products using recently implemented operational NOAA/NESDIS AVHRR Clear-Sky Processor for Oceans (ACSPO) SST and POES-GOES Blended SST data. These new SST data provide increased spatial and temporal resolutions and higher density SST data derived from multiple satellites and multiple sensors. We will soon transition to these new products. Hopefully, NOAA/NESDIS will develop an operational blended product that includes microwave-based SST data to penetrate the persistent cloud cover common in many (tropical) coral reef regions. The 4-km NOAA/NASA Pathfinder SST data set is an internally consistent climate data record that, although not produced in a near-real-time fashion, has been used extensively by CRW in product development, evaluation, validation, and hindcasting.

The GHRSST project created in 2002 to address an emerging need for accurate high resolution SST products required by operational ocean and atmospheric forecasting systems aims to provide the best quality SST data for applications in short, medium and decadal/climate time scales in the most cost effective and efficient manner through international collaboration and scientific innovation. GHRSST has now developed into a truly international project with a growing international user community testing and applying GHRSST data products and services within scientific projects and operational systems in real time. The availability of the GHRSST data stream, as a new generation of uniformly processed satellite SST data and global high-resolution SST products, especially through inclusion of microwave-based observations that penetrate clouds, may aid CRW's development of a new generation of products for improved monitoring and management of global coral reef ecosystems.

4. ACKNOWLEDGEMENTS

This project was funded by NOAA's Coral Reef Conservation Program (CRCP) and NOAA Climate Program Office's Sectoral Applications Research Program (SARP). The manuscript contents are solely the opinions of the authors and do not constitute a statement of policy, decision, or position on behalf of NOAA or the US Government.

5. REFERENCES

1. O. Hoegh-Guldberg, "Coral bleaching, climate change and the future of the world's coral reefs", *Rev. Mar. Freshw. Res.*, vol. 50, pp839-866, 1999.

2. J. K. Oliver, R. Berkelmans and C. M. Eakin, "Coral bleaching in space and time", in: M. J. H. van Oppen, J. M. Lough (eds.), Coral Bleaching, Ecological Studies 205, in press.
3. C. M. Yonge and A. G. Nicholls, "Studies on the physiology of the zooxanthellae", Science Report, GBR Exp., 1928-29, vol. 1, pp135-176, 1931.
4. R. Berkelmans and B. L. Willis, "Seasonal and local spatial patterns in the upper thermal limits of corals on the inshore central Great Barrier Reef", *Coral Reefs*, vol. 18, pp219-228, 1999.
5. P. W. Glynn and L. D. D'Croz, "Experimental evidence for high temperature stress as the cause of El Niño-coincident coral mortality", *Coral Reefs*, vol. 8, pp181-191, 1990.
6. M. P. Lesser, W. R. Stochaj, D. W. Tapley and J. M. Shiek, "Bleaching in coral reef anthozoans: effects of irradiance, ultraviolet radiation, and temperature on the activities of protective enzymes against active oxygen", *Coral Reefs*, vol. 8, pp225-232, 1990.
7. J. M. Cervino, T. J. Goreau, R. I. Hayes, L. Kaufman, I. Nagelkerken, K. Paterson, J. W. Porter, G. W. Smith and C. Quirolo, "Coral disease", *Science*, vol. 280, pp499, 1998.
8. L. L. Richardson, W. M. Goldberg, K. Kuta, R. B. Aronson, G. W. Smith, K. B. Ritchie, J. C. Halas, J. S. Feingold and S. L. Miller, "Florida's mystery coral-killer identified", *Nature*, vol. 392, pp557-558, 1998.
9. C. Wilkinson, O. Linden, H. Cesar, G. Hodgson, J. Rubens and A. E. Strong, "Ecological and socioeconomic impacts of 1998 coral mortality in the ocean: An ENSO impact and a warning of future change?" *AMBIO*, vol. 28(2), pp188-196, 1999.
10. J. L. Munro, "The scope of tropical reef fisheries and their management", in: Polunin NVC, Roberts CM (eds), Reef fisheries, Chapman and Hall, London, pp 1-14, 1996.
11. R. Berkelmans and J. K. Oliver, "Large scale bleaching of corals on the Great Barrier Reef", *Coral Reefs*, vol .18, pp55-60, 1999.
12. T. J. Done, "Coral community adaptability to environmental change at the scales of regions, reefs, and reef zones", *American Zoologist*, vol. 39, pp66-79, 1999.
13. G. Liu, A. E. Strong, W. Skirving and L. F. Arzayus, "Overview of NOAA Coral Reef Watch Program's near-real time global satellite coral bleaching monitoring activities", Proc. 10th Int Coral Reef Symp, Okinawa, Japan, pp1783-1793, 2006.
14. W. J. Skirving, A. E. Strong, G. Liu, C. Liu, F. Arzayus, J. Sapper and E. Bayler, "Extreme events and perturbations of coastal ecosystems: Sea surface temperature change and coral bleaching", in L.L. Richardson and E.F. LeDrew (Co-Eds), Remote Sensing of Aquatic Coastal Ecosystem Processes, Kluwer publishers, 2006.
15. G. Liu, W. Skirving and A. E. Strong, "Remote sensing of sea surface temperatures during 2002 Barrier Reef coral bleaching", *EOS*, vol. 84(15), pp137-144, 2003.
16. A. E. Strong, C. S. Barrientos, C. Duda and J. Sapper, "Improved satellite techniques for monitoring coral reef bleaching", Proc. 8th Int Coral Reef Symp, Panama City, Panama, pp1495-1498, 1997.
17. C. Penland and L. Matrosova, "Prediction of tropical Atlantic sea surface temperatures using linear inverse modeling", *J. Climate*, vol. 11, pp483–496, 1998.
18. C. Penland and P. D. Sardeshmukh, "The optimal growth of tropical sea surface temperature anomalies", *J. Climate*, vol. 8, pp1999–2024, 1995.
19. C. Penland, "Random forcing and forecasting using principal oscillation pattern analysis", *Mon. Wea. Rev.*, vol. 117, pp2165–2185, 1989.
20. R. W. Reynolds, N. A. Rayner, T. M. Smith, D. C. Stokes and W Wang, "An improved in situ and satellite SST analysis for climate", *J. Climate*, vol. 16, pp1609-1625, 2002.
21. R. W. Reynolds and T. M. Smith, "Improved global sea surface temperature analyses using optimum interpolation", *J. Climate*, vol. 7, pp929–948, 1994.

INTEGRATION OF SST AND OTHER DATA FOR ECOLOGICAL FORECASTING ON CORAL REEFS

Lewis J. Gramer[(1)], Dr. James C. Hendee[(2)], Dr. Chuan Min Hu [(3)]

[(1)] Cooperative Institute for Marine and Atmospheric Studies, University of Miami, Miami, FL 33149 (USA), Email: lew.gramer@noaa.gov
[(2)] NOAA Atlantic Oceanographic and Meteorological Laboratory, Miami, FL 33149 (USA), Email: jim.hendee@noaa.gov
[(3)] Institute for Marine Remote Sensing, University of South Florida, St. Petersburg, FL 33701 (USA), Email: hu@marine.usf.edu

ABSTRACT

A technique has been developed for evaluating environmental data integrated from multiple *in situ* and remote sensors in near real-time, producing forecasts of likely ecological impact (*ecoforecasts*) based on those data. The U. S. National Oceanic and Atmospheric Administration (NOAA) has applied this technique to forecast coral bleaching – the expulsion of symbiotic algae from the tissue of Scleractinian corals, potentially leading to coral mortality – at monitoring sites around the world. Recent successful bleaching ecoforecasts using this technique will be presented that utilize two distinct high-resolution satellite Sea Surface Temperature (SST) products – one synoptic and one optimally interpolated – both of which provide useful data on the shallow water thermal environment of coral reefs in remote, difficult-to-monitor sites. The biological field observations used to validate these ecoforecasts will also be briefly described.

1. BACKGROUND

Near real-time assessment of coral reef ecosystems implies the acquisition of precision data and observations appropriate for answering questions about the response of multiple organisms to physical and other environmental stimuli. As a part of the Integrated Coral Observing Network (ICON 2009) project at the National Oceanic and Atmospheric Administration's (NOAA's) Atlantic Oceanographic and Meteorological Laboratory (AOML), we model marine organismal and ecosystem response to the physical environment using an approach called heuristic programming. In this approach, time series for physical data at a specific reef site are evaluated to generate parameters ("fuzzy values") framed in subjective terms; ranges for these parameters are defined numerically by comparing the distribution of historical data with published research and expert opinion on past ecosystem response to that physical variable (Hendee et al. 2001; Hendee et al. 2007; Gramer et al. 2009; Hu et al. 2009).

These parameters taken as a whole are designed to match research with our best understanding of the process in question. The modeled organismal response is called an ecological forecast, or ***ecoforecast***, and the relative likelihood and intensity of that response is reflected in a rising numerical value called a Stimulus/Response Index (S/RI) calculated from the appropriate fuzzy values. A hypothetical example might incorporate research linking sea temperature with the coordinated spawning of a particular reef species *S*: If a time series of daily average sea temperature for a specific reef site is categorized with a fuzzy value of '*conducive-to-S-spawning*', relative to published research on that spawning behavior – and relative to local conditions at the site – then an ecoforecast for spawning of that species would be generated automatically for the site. (For the reproductive behavior of real organisms, of course, many other physical criteria besides sea temperature might come into play, e.g., lunar phase, photo-period, tides or local circulation, etc. In the heuristic approach, all appropriate combinations of these stimuli would be modeled.) This approach to ecosystem modeling requires: a) highly robust instrumentation (*in situ*, satellite, or other) producing high quality data for long periods, and reporting that data in near real-time, b) a basic understanding of the ecosystem process or behavior being modeled, and, c) knowledge about approximate threshold levels for both single and synergistically-acting environmental factors that elicit the phenomenon in question.

One significant response of the reef ecosystem to stressors is *coral bleaching*. This term is used here to refer to the expulsion of symbiotic microalgae (*zooxanthellae*) from the tissue of individual coral organisms, and in particular those hard coral species that are responsible for the structural development and stability of coral reefs. Without these photosynthetic endosymbionts, corals are unable to sustain the energy-intensive calcification process that is responsible for much of reef growth. The expulsion of the colored primary producer also renders coral tissue transparent, resulting in the visible paling or "bleaching" of a reef.

Bleaching has been frequently observed to coincide with extremes of sea temperature (Baker et al. 2008) and incident light (Dunne and Brown 2001; McClanahan et al. 2007a), as well as periods of high residence time and reduced ocean circulation at very small scales within a reef system (Nakamura and van Woesik 2001). When it occurs simultaneously in many individuals within a coral community for an extended period, bleaching may precede mass coral mortality, cessation of reef growth, and ultimately the destruction of sections of reef due to physical and biological processes such as wave action, biological and biochemical erosion, and human degradation.

2. CURRENT RESEARCH

The ICON project has had success to date in modeling observed coral bleaching and other ecological responses based on an integrated data stream consisting of sea temperature, incident irradiance, mean wind speed and other *in situ* variables (Hendee et al. 2007; Gramer et al. 2009; Manzello et al. 2009). One problem with applying heuristic programming to broader studies of coral bleaching response in particular, however, is the paucity of high quality *in situ* data for many ecologically imperiled or sensitive reef sites around the world. Coral reef environments may be geographically remote, not permitting frequent site visits by trained personnel; at the same time, these sites are often subject to vagaries of both the open ocean (wave action, shipping) and near-shore coastal waters (extreme bio-fouling, marine debris, vandalism and theft, as well as extreme events like tropical cyclones). The result is that the costs of extending a program of effective near real-time *in situ* physical monitoring to all reefs currently under protection and management within just the U.S. and territorial waters would be financially prohibitive.

Remote sensing data for Sea Surface Temperature (SST), together with SST climatology, Degree-Heating Weeks (DHW) and other products derived from them (see e.g., CRW 2009), have shown some efficacy for modeling and predicting large-scale bleaching events – for example, those affecting an entire region or system of reefs, such as past mass bleaching events in the Great Barrier Reef (Liu et al. 2003; Berkelmans et al. 2004), Western Indian Ocean (McClanahan et al. 2007b), or the Caribbean Sea and elsewhere (Gleeson and Strong 1995; Strong et al. 2004). However the SST data products that have served as indicators for these mass-bleaching events may lack both the spatio-temporal resolution and coverage over shallow near-shore waters necessary to effectively model differences in bleaching response between distinct sub-regions of a reef system (Manzello et al. 2007; Hu et al. 2009), or between hard coral species. Furthermore, the ability of other environmental variables like incident light to elicit the bleaching response is an area of active research (Dunne and Brown 2001; McClanahan et al. 2007a; Maina et al. 2008). For sites where *in situ* monitoring is not being done, remote sensing data on such physical variables have been either lacking or of insufficient spatial and time resolution.

The ICON project is therefore collaborating with remote sensing researchers within both academia and the private sector to produce satellite SST and other data products with spatial and temporal resolution, shallow-water coverage, and with a timeliness that is sufficient to such modeling. The expected outcome of these collaborations will be reliable heuristic forecasts of the bleaching response over mid- to smaller-scale coral ecosystems, at both geographically remote and more accessible reef sites around the world. Optimally interpolated SST data products at 9km resolution (Remote Sensing Systems, Inc.; REMSS 2009) have been integrated in time and space with other *in situ* and remote sensing data at over 120 individual reef sites throughout the Caribbean Sea, Florida waters, Pacific Ocean, and the central and eastern Indian Ocean; while synoptic gridded SST and chlorophyll *a* concentration at 1 km resolution including extreme shallow water coverage (University of South Florida; USF 2009) have been integrated at sites in the Caribbean Sea and Florida Reef Tract. Promising recent results of this research will be discussed, including analysis of small-scale bleaching events in the Florida Reef Tract during the summers of both 2005 and 2008 using the 1km SST product (see Fig. 1), and use of the 9km SST product in March of 2009 to successfully forecast distinct patterns of partial bleaching between two fringing reefs in American Samoa – one near the village of Alofau on the island of Tutuila and the other off the small island of Aunu’u – which lie within 10km of one another (see Fig. 2).

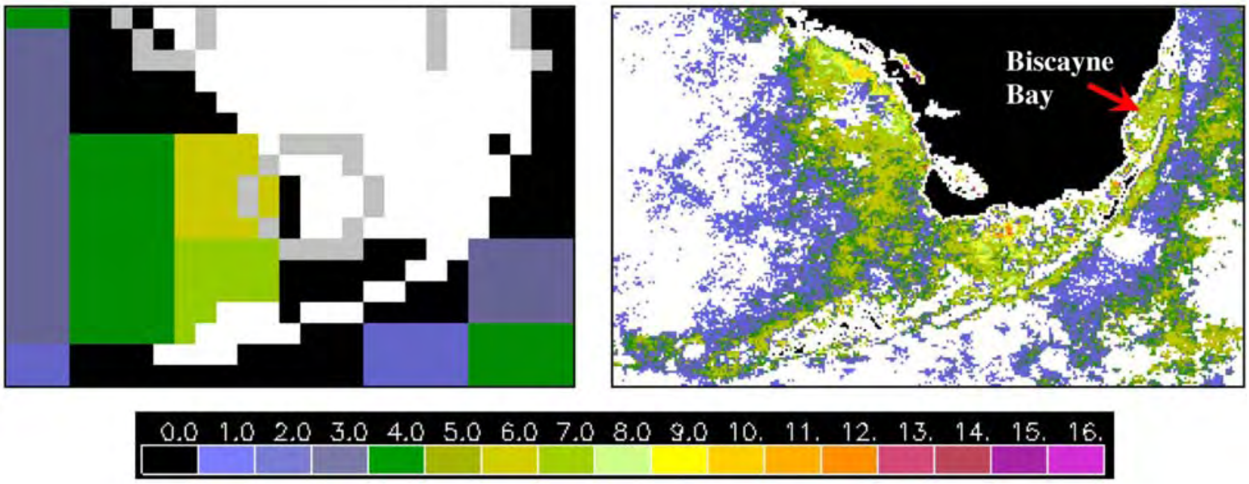

Figure 1. Comparison of (left) existing NOAA/NESDIS 50-km Degree-Heating Weeks (DHW) product and (right) USF/ICON equivalent 1-km DHW product for the 3-day period ending on August 20, 2005. Land mask colors are reversed between the images; areas of zero DHW (i.e., minimal threat of coral bleaching) are also shown as black in the NOAA/NESDIS image, and as white in the USF/ICON image. Figure from Hu et al. (2009), their Fig. 9.

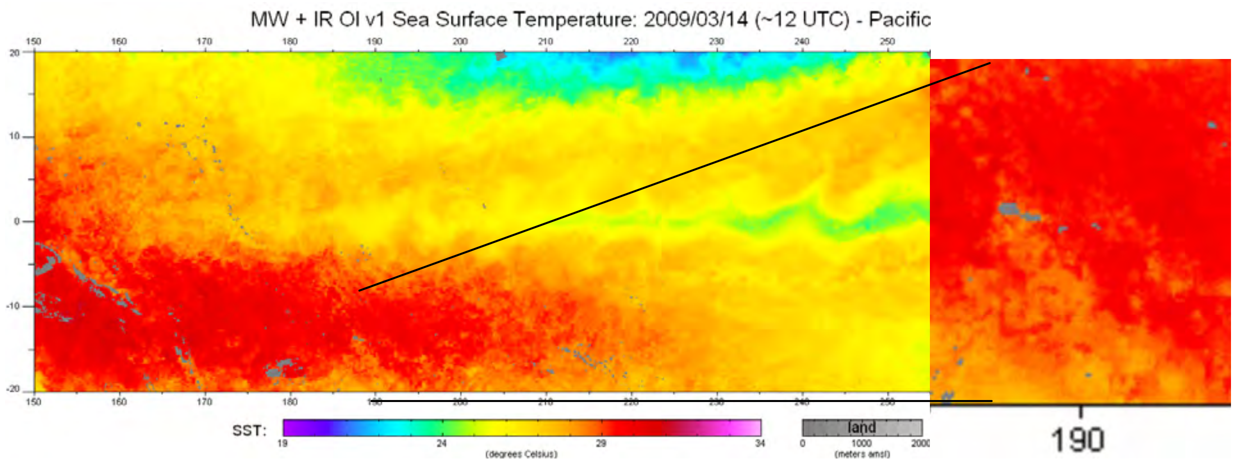

Figure 2. Optimally interpolated, blended microwave and infrared, 9km-resolution Sea Surface Temperature field (MW+IR OI SST) for tropical Pacific on March 14, 2009 (left), with blow-up of the same image showing region of warmer surface water to the north and west of American Samoa (right). Island land masks appear grey on both panels; American Samoan island pair of Tutuila and Aunu'u are shown just to the left of, and island pair of Ofu and Olosega are shown just to the right of center in the right panel (approximate latitude 14.2S, longitude 190E). The somewhat larger land group to the upper left of Tutuila/Aunu'u is the sovereign state of Samoa. Image and data courtesy of Remote Sensing Systems, Inc., http://www.remss.com/sst/sst_data_daily.html.

3. REFERENCES

ICON (2009) National Oceanic and Atmospheric Administration Integrated Coral Observing Network (ICON) Web site, accessed May 2009. http://ecoforecast.coral.noaa.gov.

CRW (2009) NOAA National Environmental Satellite, Data, and Information Service Coral Reef Watch (CRW) Web site, accessed May 2009. http://coralreefwatch.noaa.gov.

REMSS (2009) Remote Sensing Systems, Inc. Web site, accessed May 2009. http://www.remss.com.

USF (2009) University of South Florida Institute for Marine Remote Sensing MODIS Web site, accessed May 2009. http://modis.marine.usf.edu.

Baker AC, Glynn PW, Riegl B (2008) Climate change and coral reef bleaching: An ecological assessment of long-term impacts, recovery trends and future outlook. Estuarine Coastal and Shelf Science 80:435-471

Berkelmans R, De'ath G, Kininmonth S, Skirving WJ (2004) A comparison of the 1998 and 2002 coral bleaching events on the Great Barrier Reef: spatial correlation, patterns, and predictions. Coral Reefs 23:74-83

Dunne RP, Brown BE (2001) The influence of solar radiation on bleaching of shallow water reef corals in the Andaman Sea, 1993-1998. Coral Reefs 20:201-210

Gleeson MW, Strong AE (1995) APPLYING MCSST TO CORAL-REEF BLEACHING:151-154

Gramer LJ, Johns EM, Hendee JC, Hu C (2009) Characterization of biologically significant hydrodynamic anomalies on the Florida Reef Tract. In: Dodge R (ed) Proceedings - 11th International Coral Reef Symposium, Ft. Lauderdale, FL 5 pp.

Hendee J, Gramer L, Kleypas J, Manzello D, Jankulak M, Langdon C (2007) The Integrated Coral Observing Network: Sensor Solutions for Sensitive Sites. ISSNIP: The Third International Conference on Intelligent Sensors, Sensor Networks and Information Processing:669-673

Hendee JC, Mueller E, Humphrey C, Moore T (2001) A data-driven expert system for producing coral bleaching alerts at Sombrero Reef in the Florida Keys, USA. Bulletin of Marine Science 69:673-684

Hu CM, Muller-Karger F, Murch B, Myhre D, Taylor J, Luerssen R, Moses C, Zhang CY, Gramer L, Hendee J (2009) Building an automated integrated observing system to detect Sea Surface Temperature anomaly events in the Florida Keys. IEEE TRANSACTIONS ON GEOSCIENCE AND REMOTE SENSING (in press)

Liu G, Strong A, Skirving W (2003) Remote sensing of sea surface temperature during the 2002 (Great) Barrier Reef coral bleaching. EOS Trans AGU 84:137-144

Maina J, McClanahan TR, Venus V (2008) Meso-scale modelling of coral's susceptibility to environmental stress using remotely sensed data: Reply to comments by Dunne (2008). Ecological Modelling 218:192-194

Manzello D, Warner M, Stabenau E, Hendee J, Lesser M, Jankulak M (2009) Remote monitoring of chlorophyll fluorescence in two reef corals during the 2005 bleaching event at Lee Stocking Island, Bahamas. Coral Reefs 28:209-214

Manzello DP, Berkelmans R, Hendee JC (2007) Coral bleaching indices and thresholds for the Florida Reef Tract, Bahamas, and St. Croix, US Virgin Islands. Marine Pollution Bulletin 54:1923-1931

McClanahan TR, Ateweberhan M, Muhando CA, Maina J, Mohammed MS (2007a) Effects of climate and seawater temperature variation on coral bleaching and mortality. Ecological Monographs 77:503-525

McClanahan TR, Ateweberhan M, Sebastian CR, Graham NAJ, Wilson SK, Bruggemann JH, Guillaume MMM (2007b) Predictability of coral bleaching from synoptic satellite and *in situ* temperature observations. Coral Reefs 26:695-701

Nakamura T, van Woesik R (2001) Water-flow rates and passive diffusion partially explain differential survival of corals during the 1998 bleaching event. Marine Ecology-Progress Series 212:301-304

Strong AE, Liu G, Meyer J, Hendee JC, Sasko D (2004) Coral reef Watch 2002. Bulletin of Marine Science 75:259-268

USE OF SST AND SEA-ICE DATA IN OPERATIONAL ANALYSIS AND ASSIMILATION SYSTEMS AT THE UK MET OFFICE.

Matt Martin[1], Jonah Roberts-Jones[1], Daniel Lea[1], John Stark and Craig Donlon[2].

[1] National Centre for Ocean Forecasting, Met Office, FitzRoy Road, Exeter, (United Kingdom),
[2] ESA/ESTEC, Keplerlaan 1, 2201 AZ Noordwijk, The Netherlands
Emai : matthew.martin@metoffice.gov.uk

ABSTRACT

Sea surface temperature and sea-ice data are used in a number of operational systems at the UK Met Office. This paper provides a brief description of two of these, namely the OSTIA and FOAM systems, and shows an example of an inter-comparison between the two.

1. INTRODUCTION

A number of operational systems run at the UK Met Office require an accurate estimate of the global sea surface temperature (SST) and sea-ice fields on a daily basis. These include the numerical weather prediction (NWP) systems as well as the ocean modelling systems for short and long range forecasting. In order to meet the SST requirements of the NWP system, and for a range of other applications, an objective analysis system was set up called the Operational SST and Sea Ice Analysis system (OSTIA). This system takes in the data from a number of data sources (satellite and in situ) and produces a global high resolution SST and sea-ice analysis.

The short-range ocean forecasting system and the seasonal coupled ocean-atmosphere forecasting systems also make use of SST and sea-ice data to initialise their forecasts. New versions of these systems have been developed recently with a number of major developments, including the use of some of the techniques and data which are used in OSTIA.

This paper presents a brief overview of OSTIA together with a description of the use of SST and sea-ice data in the ocean forecasting systems. Both the short-range and seasonal forecasting systems use the same techniques to initialise the ocean model, so only the short-range system is described here.

2. THE OSTIA SYSTEM

The OSTIA system has been running operationally at the UK Met Office since November 2006. The output is a daily global coverage combined SST and sea-ice concentration product on a 1/20° (~6km) grid, based on measurements from several satellite and in situ SST data sets. OSTIA uses SST data in the common format developed by GHRSST and makes use of the uncertainty estimates and auxiliary fields as part of the quality control and analysis procedure. Satellite derived sea ice products from the EUMETSAT Ocean and Sea Ice Satellite application Facility (OSI-SAF) provide sea-ice concentration and edge data to the analysis system. After quality control of the SST observations, a bias correction is performed using AATSR data as a key component. To provide the final SST analysis, a multi-scale optimal interpolation (OI) is performed using the previous analysis as the basis for a first guess field.

3. ASSIMILATION OF SST IN FOAM

The Forecasting Ocean Assimilation Model (FOAM) system is a deep ocean forecasting system which is run daily in the operational suite at the UK Met Office producing analyses and 5-day forecasts of three-dimensional temperature, salinity, currents and sea-ice variables. The model is driven by six-hourly surface fluxes from the Met Office's Numerical Weather Prediction (NWP) system. The model configurations include a global 1/4° resolution configuration with nested 1/12° resolution regional configurations in the North Atlantic, Mediterranean and Indian Ocean. All these configurations assimilate in situ and satellite SST data, satellite altimeter sea surface height data, in situ temperature and salinity profile data, and sea-ice concentration data using an optimal interpolation type method. The model used in the FOAM system has recently been changed to NEMO, and a new version of FOAM was implemented operationally in December 2008, with a number of improvements to the data assimilation.

FOAM assimilates the AATSR, AMSR-E and AVHRR data (from NOAA and MetOp satellites) together with the in situ SST data. The satellite observations are superobbed by calculating the median of all observations of a particular type within a 13km radius. The model counterparts of these observations are calculated during a one-day model run in a first-guess-at-appropriate-time (FGAT) scheme. The observations undergo a bias correction which uses the AATSR and in situ data as reference data, using the same scheme as OSTIA. The bias corrected observations and their model counterparts are then used in an OI-type scheme in order to produce two-dimensional SST increments. The one-day model run is then re-integrated with the addition of these SST increments throughout the mixed layer of the model using an incremental analysis updating (IAU) scheme. This same procedure is performed for each of the model configurations.

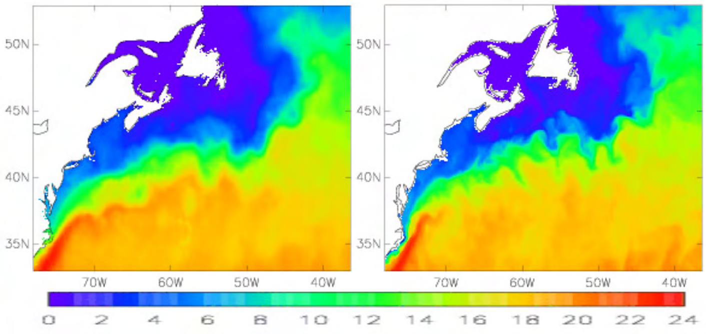

Figure 1: Plots comparing monthly mean SST fields for OSTIA (left) and the FOAM North Atlantic 1/12˚ model (right) in the vicinity of the Gulf Stream for March 2006.

A number of hindcasts have been run with the FOAM system and the results have been compared to both OSTIA, and assimilated and independent observations. An example of a comparison between the FOAM 1/12˚ North Atlantic model and OSTIA is shown in Figure 1. These monthly mean plots show that the large scale features are similar between the two systems. However, the FOAM system clearly resolves smaller scale features than OSTIA, even though the resolution of the OSTIA grid is higher, due to the inclusion of the ocean model. Work to improve the resolution of features within the OSTIA system is now beginning.

Towards the utilization of GHRSST data for improving estimates of the global ocean circulation

D. Menemenlis[1], H. Zhang[1], G. Forget[2], P. Heimbach[2], and C. Hill[2]
[1]*Jet Propulsion Laboratory, California Institute of Technology, Pasadena, USA;*
[2]*Massachusetts Institute of Technology, Cambridge, USA*

The Estimating the Circulation and Climate of the Ocean, Phase II (ECCO2) project, aims to produce a best-possible, global, time-evolving synthesis of most available ocean and sea-ice data at a resolution that admits ocean eddies. A first ECCO2 synthesis for the period 1992–2002 has been obtained using a Green's Function approach to estimate initial temperature and salinity conditions, surface boundary conditions, and several empirical ocean and sea ice model parameters. Data constraints include altimetry, gravity, drifter, hydrography, and observations of sea-ice. Although the control space is small (~80 parameters have been calibrated), this first global-ocean and sea ice data synthesis substantially reduces large-scale biases and drifts of the model relative to observations and to the baseline integration. A second ECCO2 synthesis is being obtained during the ARGO-rich period (2004–present) using the adjoint method, which permits a much larger number of control parameters to be estimated. This paper describes first efforts towards the utilization of Group for High Resolution Sea Surface Temperature (GHRSST) data as constraints for this adjoint-model-based optimization. Initial GHRSST data constraints come from the REMS L2P AMSR-E data product. We will discuss issues related to utilization of the REMS data, including the diurnal amplitude, and we will present status and future plans for the adjoint-method-based optimization.

Application of satellite derived Sea Surface Temperature fields along the Delmarva region.

Ajoy Kumar and Justin Gilchrist[1]

[1]Millersville University of Pennsylvania

1. Abstract

Satellite data, especially high resolution sea surface temperature (SST) fields, have a strong influence on the air-sea interaction and the seasonal heating of the water column. In Delmarva, a region between the Chesapeake Bay and the Delaware Bay, along the Eastern Shore, heating and cooling have known to cause strong summer stratification and winter mixed regimes. Understanding the strength and timing of the heat fluxes can improve our understanding of the water column physics, nutrient availability and biology of this region.

2. Introduction

The Delmarva coastal region periodically comes under the influence of both the Chesapeake Bay and Delaware Bay fluxes of fresh water, sediments and nutrient load. The importance of these fluxes and its strong influence of the adjacent coastal margin ecosystems have resulted in two large interdisciplinary programs within the last few years. The Bio-physical Interaction in Ocean Margin Ecosystems (BIOME) program consists of four cruises collecting optical, biological and chemical data. The Coastal Ocean Bio-optical buoy (COBY) program has resulted in a large number of monthly transects across the coastal margins (Fig. 1). Simultaneously, coastal ocean surface currents from High Frequency (HF) Radars and in-water column currents from ADCP have been collected in this region. In this study, we show some of the early results of our analysis of this large data set.

Satellite data complements the *in situ* observations and helps to give a different temporal and spatial perspective. SST data are specifically important for two reasons: i) to calculate the heat flux and hence understand the seasonal heating of the water column and formation of a strong thermocline and ii) to help identify large scale features like warm and cold core eddies, shelf-slope frontal features and presence of Gulf Stream discharge water over the shelf and slope region. In this study we have used the ~ 6km weekly Coastwatch SST product along with the above data sets to describe the seasonal progression of the water column and the creation and eventual destruction of the stratification regime.

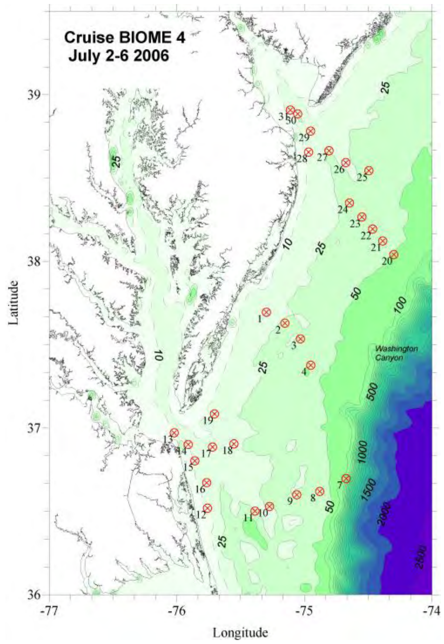

Fig.1: Map showing the BIOME cruise locations and bathymetry of the Delmarva region. The figure was made available to us by Dr. Julie Ambler and Jose Blanco.

3. Data Analysis

Compilation and analysis of the all weekly SST images from the Coastwatch program show a number of unique features. The presence of warm core eddies (Fig. 2), the onshore veering of the Gulf Stream and seasonal movements of the shelf-slope front have been documented. The extent and frequency of the presence of Gulf Stream discharge water on the shelf region have also been clearly identified. The SST images will also help in the estimation of heat fluxes and the timing and strength of the stratification regime (Fig. 3). Heat transports in this region are estimated using near surface ADCP velocities from ADCP data and temperature cross-sections (Fig. 4). The correlation between the above heat and other fluxes and the nutrient fluxes provide strong physical evidence to the distribution and biomass of different species of phytoplankton and zooplankton identified in the Delmarva region.

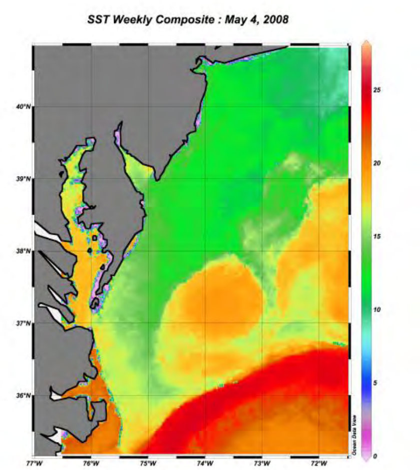

Fig.2: SST image showing the presence of warm core eddy and entrained Gulf Stream water on the shelf region.

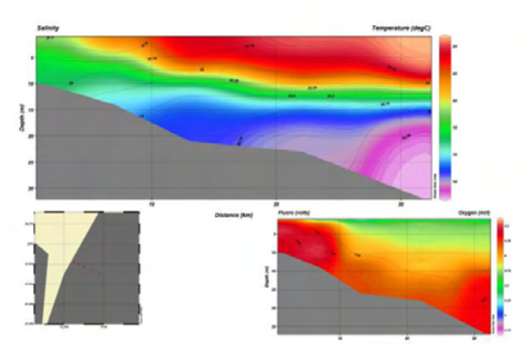

Fig. 3: The crossection of temperature, salinity, fluorescence and oxygen during the summer.

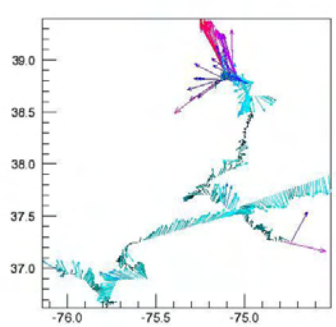

Fig.4 shows the near surface current vectors computed from ADCP data.

4. Result

Our initial results have also identified low oxygen regions in the continental margins off Delmarva. The strength and area of the above low oxygen zones appear to be related to the seasonal changes of the water column described above. This observation has important implications to the phytoplankton, zooplankton and benthic marine organisms of the region.

5. References:

1. Moisan, T.A.; Atkinson, L.P.; Blanco, J.L.; Boicourt, W.; Hooker, S.; Maldnen, C.; Moisan, J.R.; Mannino, A.; Mitra, M.; Mulholland, M.; Nolan, J.; Russ, M.; Swift, R.W.; Tester, P.A. Bio-physical Interactions in Ocean Margin Ecosystems (BIOME): understanding coastal dynamics in the Southern Mid-Atlantic BightOCEANS, 2005. Proceedings of MTS/IEEE Volume , Issue , 2005 Page(s): 2830 - 2837 Vol. 3
2. NASA Coastal Observations: http://phytoplankton.gsfc.nasa.gov

Investigating the Structure of the Coastal Ocean using HF Radar and Remotely Sensed Sea Surface Temperature

Chris Halle[(1)], **John Largier**[(1)]

(1) Bodega Marine Laboratory, Univ. of California, Davis, Bodega Bay, California, (United States)
Email : cmhalle@ucdavis.edu

ABSTRACT

High frequency radar systems (HF Radar) along the coast of California provide hourly maps of surface currents in the coastal ocean, from the coast out to 50 – 150 km offshore. These current estimates are used to derive surface convergence / divergence probability maps for the region just south of the Point Arena "upwelling center". Because the HF Radar is unaffected by clouds, the HF Radar probability maps have the potential for augmenting the large-scale frontal maps obtained from satellite sea-surface temperature (SST) estimates. Slight updates to the HF Radar algorithms should provide more reliable hourly "feature" maps. In the future, comparisons of the HF Radar convergence maps with the satellite SST maps should aid in continued investigation of coastal dynamics, as well as providing insight into the linkages between the "rapidly" changing coastal ocean and the open sea.

1. INTRODUCTION

Under the auspices of the Coastal Ocean Currents Monitoring program (COCMP), the state of California has installed a network of HF Radar stations along the coast (Figure 1). The program built upon existing stations at Bodega Marine Lab and Monterey Bay. Complete coverage of central California was achieved in mid-2006. The major goals of the system include the delivery of real-time products of use to managers (e.g., real-time tracking of oil spills), and enhancing long-term understanding of the coastal ocean (e.g., quantifying the connectivity between Marine Protected Areas) [e.g., Kamer, 2009, Kaplan, et. al., 2009].

The network is comprised of stations that record at different spatial resolutions: long-range (~ 5km), standard-range (~ 2km), and short-range (~ 300m). The standard- and long-range systems are mainly used to map the coastal ocean currents. Short-range systems are used in bays.

Each radar system measures the component of the surface current toward or away from the radar. At least two radar systems with overlapping coverage areas are required to obtain vector estimates of sea-surface currents for a given region. The systems as a whole are configured to record hourly.

This initial study is aimed at obtaining convergence / divergence maps for a small portion of this region using the current estimates provided by the radar systems. Relating convergences ("fronts") to environmental conditions is useful in the context of understanding the influence of fronts and frontal movement on marine populations, including seabirds [e.g., Moore and Abbott, 2002, Thorpe, et. al., 2002, Yen, et. al., 2006]. In addition, convergence and divergence maps can aid in quantifying near-coastal processes such as upwelling. Evidence suggests that at least some of the time, a jet, originating as a point source behind capes, is established during upwelling. This contrasts with canonical "upwelling front" that parallels the coast [e.g., Barth, et. al., 2000, Roughan, et. al., 2006].

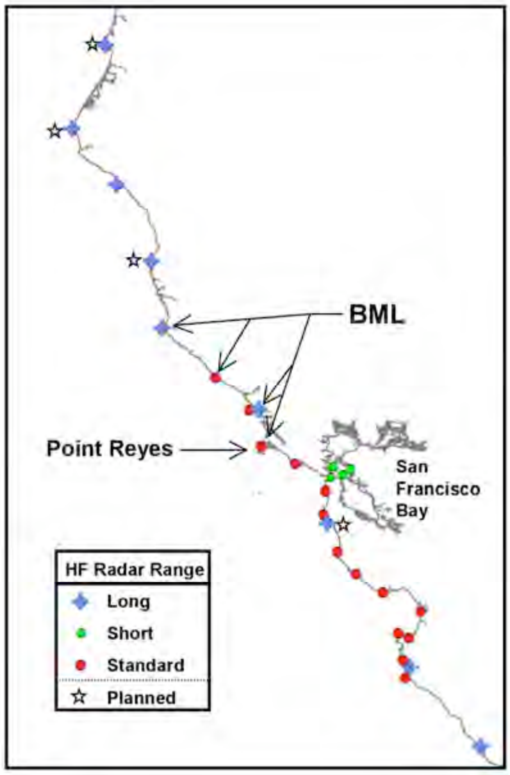

Figure 1 Central and Northern California HF Radar network. Bodega Marine Laboratory operates five of the HF Radar sites. Figure adapted from the COCMP quarterly report [Kamer, 2009, figure A-1].

2. SURFACE CURRENT MAPPING OFFSHORE BODEGA MARINE LABORATORY

We restrict our analysis here to the region offshore Bodega Marine Laboratory (Figure 1). The systems operated by BML consist of two long-range and three standard-range radar systems. For this initial investigation, we adopt the simplistic ad-hoc procedure of obtaining surface currents separately from the long-range and standard range systems. Standard processing techniques are used to ensure reliable estimates of surface currents [e.g., Chapman and Graber, 1997, Kaplan et. al., 2005, Halle and Largier, 2008].

Hourly surface current maps are formed by interpolating the long-range surface current estimates to a higher spatial resolution, and combining these with the standard-range estimates. Long- and standard- range currents at each location in the region of overlap are averaged. Currents at locations outside of the overlap are set to the appropriate standard- or long- range system estimates.

3. SURFACE CURRENT MAPS

Surface current maps offshore BML are presented in Figure 2. Three-day averages are shown, superimposed on three-day composites of SST measured from AVHRR (National Oceanic and Atmospheric Administration, 2008, http://coastwatch.pfel.noaa.gov/). Panel (a) is associated with relaxation (low-wind) conditions, and low-speed or northward surface currents over much of the domain. Panel (b) is taken from a time of high-downcoast (upwelling-favorable) winds, with strong southward currents. The beginning of a potential recirculation is evident as a perturbation between warmer oceanic waters and the colder near-coastal environment.

Coverage during relaxation conditions is reduced compared to upwelling conditions. This is presumably due to a more quiescent wave environment resulting from the very light winds during relaxation events. The HF Radar signal scatters off the ambient wave field [Halle and Largier, 2008].

Satellite SST coverage is particularly good during this relaxation / upwelling cycle in early October 2008. Several days can often elapse between glimpses of the ocean surface. In spite of the generally excellent coverage, however, gaps in the satellite SST estimates can be clearly seen in panel (a).

4. CONVERGENCE / DIVERGENCE PATTERNS

Divergences are defined using the surface currents:

$$div = du/dx + dv/dy, \quad (1)$$

where: div is the surface current divergence,
u is the eastward component of velocity,
and v is the northward velocity component.

Three-day averages of hourly surface current divergence are presented for the same relaxation and upwelling periods as the mean flow pictures (Figures 3a and 3b). The convergences / divergences tend to be fairly low during relaxation. The split of the jet around the "recirculation" feature during upwelling is associated with a rather strong convergence. A fairly strong divergence can be seen below the split.

The somewhat large "smoothed" region just outside the bounds of the standard-range radar coverage (for example, near 123° 40" W) may be partially artificial. Although some reduced variability as one moves away from the coast might be expected, much the smoothing may be due to the rather simple scheme used for gap filling and merging the radar data.

Radial "stripes" are artifacts associated with the measurement system. For example, the high divergence in the region labelled "possible artifact" is presumably due to the direction finding algorithm associated with a particular radar installation. Under certain conditions, the algorithm can "misplace" the velocity measurement in space enough to significantly influence the resulting divergence estimates.

Not all radial features are associated with artifacts. For example, the flow field of the jet near the coast (Figure 3b, labelled "real convergence") is associated with a strong convergence that is radial in shape, but makes sense when compared to the mean flow picture of Figure 2b. This feature is wider than a simple radial spoke. Separating real features from artifacts can be difficult when the dominant flow features are aligned radially with the radar installations.

Adapting the methodology used for frontal detection by satellite SST [e.g., Belkin and Cornillon, 2003, Breaker, 2004, Legeckis, et. al., 2002, Ullman and Cornillon, 2000], we present the probability of detecting strong convergence / divergence features in Figure 4. In this presentation, a probability of –100% (+100%) indicates a constant convergence (divergence). "Strong" is somewhat arbitrarily defined as 1×10^{-5} /s, and is large enough to stand out in individual hourly snapshots.

A few radial spoke artifacts are particularly clear in this presentation. The overall patterns, however, appear robust and reflect what one might expect. In particular, the area labelled "real convergence" in Figure 3b seems to be a typical area of convergence during upwelling (Figure 4b). The area of strong divergence just below is associated with the spread of the along-coast jet and offshore transport.

One limitation of this presentation is that it smooths over features that evolve. For example, the meander in Figure 2b often develops into a recirculation that travels toward the coast [Halle and Largier, 2008]. An area associated with both convergence and divergence during the analysis period will average toward a probability of zero. The analysis periods should be shortened to capture such evolving features.

5. CONCLUSIONS

HF Radar can be an effective tool in describing the convergence / divergence field in the coastal ocean. Some slight adjustments need to be made to the method of calculation. These include: (1) upgrading the "gap-filling" algorithm, and (2) identifying and removing radial artifacts. The simplest means of doing this last may be to use a series of probability maps (Figure 4) to identify the regions associated with artifacts and then consistently remove those regions after processing.

Producing hourly "frontal" maps will also require a careful analysis of the measurement system noise levels. For example, if two nearby locations (~ 2 km apart) measured by the standard range system are associated with a relative current speed difference, or error, of 5 cm/s, the associated divergence is ~ 2.5×10^{-5} /s. This (overestimate of) the noise level will set the feature detection limit.

Finally, the combined use of the HF Radar and sea surface temperature maps should help to validate both systems near the coast, and provide continued insight into the dynamics associated with this important upwelling region. The wide field of view afforded by the satellite is particularly useful for illustrating links between the coastal and open ocean, while the higher resolution, continuous snapshots provided by the HF Radar allow detailed investigation of near-coastal features.

6. REFERENCES

1. Barth, J.A., S.D. Pierce, and R.L. Smith (2000), A separating coastal upwelling jet at Cape Blanco, Oregon, and its connection to the California Current System, *Deep Sea Res., Part II, Topical Studies in Oceanography*, Vol. 47, 783-810.
2. Belkin, I., and P. Cornillon (2003), SST Fronts of the Pacific coastal and marginal seas, *Pacific Oceanography, Vol. 1 (No.2),* 90-113.
3. Breaker, L. (2004), Ocean fronts off California: a new product from GOES satellite data, *Coastal Ocean Research (Sea Grant Report),* R/CZ-181: 3.1.2002–2.28.2005.
4. Chapman, R. D., and H. C. Graber (1997), Validation of HF radar measurements, *Oceanography*, *10*(2), 76-79.
5. Halle, C.M., and J. Largier (2008), *Patterns of Surface Currents Near the Point Arena Upwelling Region as Revealed by Long Range HF Radar*, Radiowave Oceanography Workshop Proceedings, April 2008.
6. Kamer, Krista (editor) (2009), Year Four Progress Report Three (PR3 2008): Coastal Ocean Currents Monitoring Program – Northern and Central California (COCMP-NC), Contract #04-034, Project Period of Performance: 1 January, 2008-31 December 2008, Reporting Period: 1 July, 2008-30 September 2008.
7. Kaplan, D., C. Halle, J. Paduan, J. Largier (2009), Surface currents during anomalous upwelling seasons off central California, in review.
8. Kaplan, D.M., J. Largier, and L.W. Botsford (2005), HF radar observations of surface circulation off Bodega Bay (northern California, USA), *J. Geophys. Res., 110,* C10020, doi:10.1029/2005JC002959.
9. Legeckis, R., C. Brown, and Paul Chang (2002), Geostationary satellites reveal motions of ocean surface fronts, *J. Mar. Syst., 37,* 3-15.
10. Moore, J., and M. Abbott (2002), Surface chlorophyll concentrations in relation to the Antarctic Polar Front: seasonal and spatial patterns from satellite observations, *Jour. Marine Systems*, *37*, 69-86.
11. Roughan, M., N. Garfield, J. Largier, E. Dever, C. Dorman, D. Peterson, and J. Dorman (2006), Transport and retention in an upwelling region: The role of across-shelf structure, *Deep Sea Res., Part II, Topical Studies in Oceanography*, Vol. 53, pp 2931-2955.
12. Thorpe S., K. Heywood, M. Brandon, D. Stevens (2002), Variability of the southern Antarctic Circumpolar Current Front north of South Georgia, *Jour. Marine Systems*, *37*, 87-105.
13. Ullman, D., and P. Cornillon (2000), Evaluation of Front Detection Methods for Satellite-Derived SST Data Using In Situ Observations, *J. Atmos. Ocean. Technol.*, *17*, 1667-1675.

14. Yen, P.P.W., W.J. Sydeman, S.J. Bograd, and K.D. Hyrenbach (2006), Spring-time distributions of migratory marine birds in the southern California Current: Oceanic eddy associations and coastal habitat hotspots over 17 years, *Deep Sea Res., Part II, Topical Studies in Oceanography*, Vol. 53, pp 399-418, doi: 10.1016/j.dsr2.2006.01.013

Acknowledgements:

This study was supported by the California Coastal Conservancy as part of the Coastal Ocean Currents Monitoring Program (COCMP). The authors thank Deedee Shideler and Marcel Losekoot for the maintenance of the HF radar systems and for providing the current data. Chelle Gentemann helped with illuminating discussions. The HF Radar maps were generated using the m_map toolbox (Pawlowicz, 2007, available for download at http://www.eos.ubc.ca/~rich/).

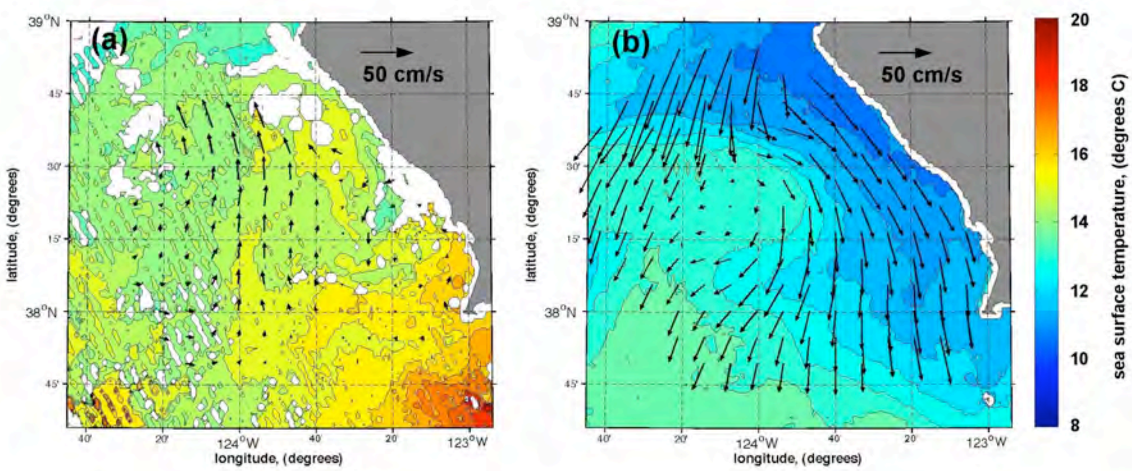

Figure 2. *Three-day averaged surface currents on (a) 1 October 2008 (relaxation conditions), and (b) 10 October 2008 (upwelling conditions). Sea surface temperature is obtained from AVHRR and provided by CoastWatch (National Oceanic and Atmospheric Administration, 2008, http://coastwatch.pfel.noaa.gov/). The surface currents are spatially averaged to 10 km resolution for clarity prior to presentation in this figure.*

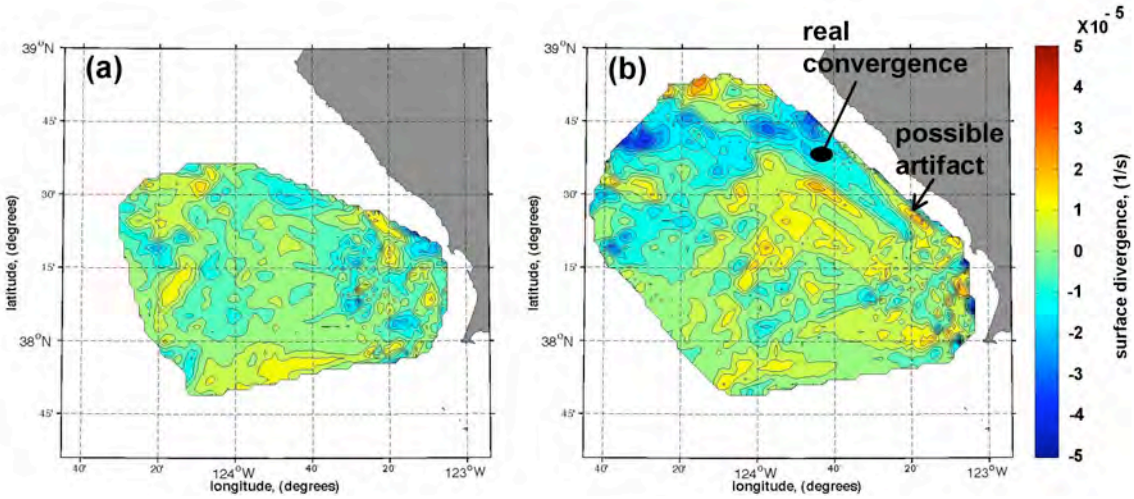

Figure 3. *Three-day averaged surface current divergence on (a) 1 October 2008 (relaxation conditions), and (b) 10 October 2008 (upwelling conditions). The high divergence radial spoke labelled "possible artifact" is due to the processing inherent to the radar measurement system. The radial feature labelled "real convergence" results from the bending / splitting of the upwelling jet. Please refer to the text for more explanation.*

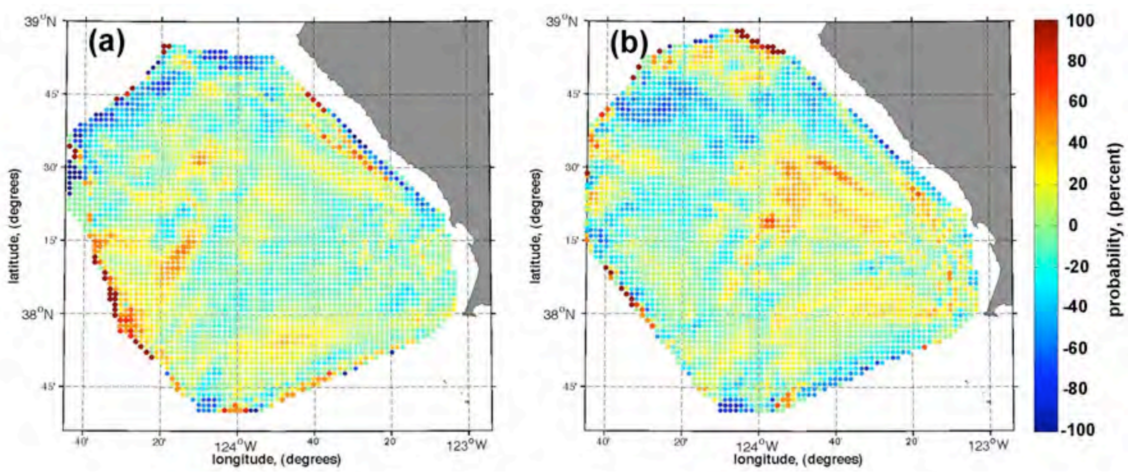

Figure 4. *Probability of detecting strong hourly convergences and divergences during (a) the relaxation conditions of 26 September through 6 October 2008, and (b) the upwellling favorable conditions of .7 October through 13 October 2008. A probability of 100 percent (minus 100 percent) indicates a consistently strong divergence (convergence). "Strong" is defined here as a convergence or divergence with an absolute value greater than 1x10^{-5} /s.*

A PELAGIC HABITAT ANALYSIS MODULE FOR TUNA OF THE EASTERN TROPICAL PACIFIC

Dale Kiefer, Daniel Harrison, Timothy Lam, Frank O'Brien[(1)], Michael Hinton[(2)], Ed Armstrong[(3)]

[(1)] *System Science Applications, P.O. 1589, Pacific Palisades, CA 90272, (USA), Email: kiefer@runeasy.com*

[(2)] *Interamerica Tropical Tuna Commission, La Jolla, CA , (USA), Email: mhinton@iattc.org*

[(3)] *Jet Propulsion Laboratory, 4800 Oak Grove Drive, Pasadena, CA 91109-8099 (USA), Email:Edward.M.Armstrong@jpl.nasa.gov*

ABSTRACT

We have begun development of a pelagic habitat information system that is designed to map the habitat of marine pelagic species. This information system integrates commercial fisheries data and scientific surveys of species distribution with satellite imagery and circulation models to identify physical and biological parameters that determine a specie's distribution. We first applied this software to define the habitat of tuna of the Eastern Pacific Ocean. Our analyses clearly shows that the distribution of yellowfin, bigeye, and skipjack tuna are determined to a large extent by the distribution of sea surface temperature and chlorophyll concentration. In addition we found that ENSO plays a large role in determining both the distribution of the adult population and the rate of recruitment of juveniles to the adult population.

1. INTRODUCTION

Classical assessment of the sustainable exploitation of a commercial stock of fish is largely based upon data from the fleet. The total catch and catch per unit effort provide an estimate of the size and distribution of the adult population and measurements of the age structure of the catch provides estimates of the rates of recruitment of juveniles to the adult population. Recently, national and international agencies have requested a more ecological approach to managing fisheries and other marine resources. With support from NASA's Decision Support Program we have begun development of a "Pelagic Habitat Analysis Module". The goal of this work is to improve stock assessment by integrating classical fishery data with environmental information. Specifically, PHAM is an application of the EASy geographical information system by which one can merge fisheries data, satellite imagery, output from a global circulation model, and statistical algorithms to characterize and map the habitat of pelagic species. Such information along with supporting information on recruitment can then be introduced into existing stock assessment models.

Here we describe our first application, the mapping of the habitat and recruitment variability of the tuna of the Eastern Pacific Ocean.

2. OVERVIEW OF TUNA MAPPING IN THE EASTERN PACIFIC OCEAN

The Pelagic Pelagic Habitat Analysis Module (PHAM) is a development of the Environmental Analysis System (EASy), a geographic information system that has been specifically designed for marine applications (www.runeasy.com). EASy is a 4-dimensional (latitude, longitude, depth, and time) that runs on either Windows desktops or on servers, where the application can be run interactively over the Internet.

The PHAM-tuna application contains records of the distribution of fish catch and age structure of bigeye, *Thynnus obesus*, skipjack, *Katsuwonus pelamis*, and yellowfin, *Thunnus albacares* ,tuna from 1975 to present. This data was provided by the Interamerican Tropical Tuna Commission. The fishery deploys both long lines and purse seines. The fishery also supports it purse seining with fish aggregation devices of varying sophistication.

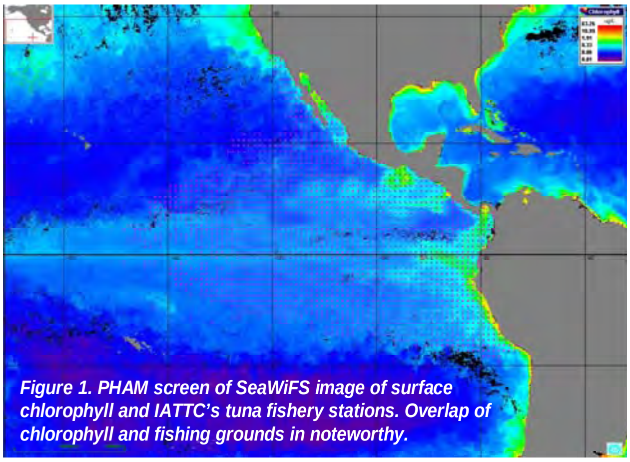

Figure 1. PHAM screen of SeaWiFS image of surface chlorophyll and IATTC's tuna fishery stations. Overlap of chlorophyll and fishing grounds in noteworthy.

Figure 1 shows the IATTC grid (1X1 degree) of sampling sites superimposed on an image of sea surface chlorophyll. The overlap between intermediate concentrations of chlorophyll and the grid of fishing effort is remarkable.

The application also contains GHRSST and AVHRR imagery of SST, CZCS and SEAWiFS imagery of the concentration of chlorophyll within the surface mixed layer, and AVISO sea surface height. It also contains output from the ECCO-2 global circulation model, which can be displayed dynamically at any selected depth. The circulation field can be seeded with tracer particles at any location in order to track water movement from sources such as spawning sites. Finally, the application contains a number of graphical and statistical tools such as unbalanced ANOVA, polynomial regression analysis, histograms, and soon code for empirical orthogonal function analyses. These tools allow rapid integration and analysis of a specie's habitat. Our initial tests of the application are described below.

2. RESULTS

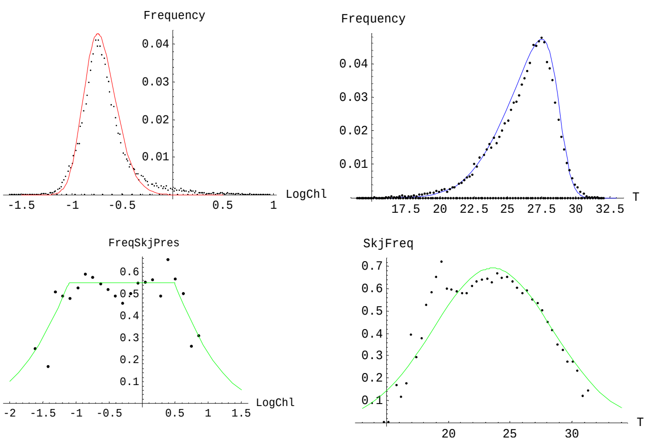

Figure 2. Upper panel. The frequency distribution of CZCS and SEAWiFS log chlorophyll concentration and GHRSST temperature at tuna fishing sites, and our fits of skewed normal functions to the data. Lower panel. The frequency with which fisherman caught skipjack at fishing sites where remotely sensed chlorophyll (left) and temperature (right) were recorded.

Figures 2 and 3 shows our approach to integrating sea surface temperature and chlorophyll imagery with data from the tuna fishery data. The upper panel of figure 1 shows the distribution of chlorophyll concentration (left) and the temperature at the sea surface at grid points where fishing occurred. The data points show the frequency that fishing occurred as a function of the value of log chlorophyll as recorded from CZCS or SEAWiFS imagery and temperature as recorded from AVHRR or GHRSST imagery. The curves are best fits to the data for a skewed normal distribution. We see from the figure that fishing occurred most frequently in waters where the concentration of chlorophyll within the mixed layer was 0.16 ug/l and the surface temperature was 27.6 ^{o}C.

The lower panel shows the frequency with which the fisherman caught skipjack tuna at a grid point vs the log of the chlorophyll concentration (left) or temperature (right) at that grid point. The best fits to the skewed normal function are also shown. We see that the fisherman caught skipjack with a frequency of about 0.6 over a broad range of chlorophyll concentrations. In order to fit the skewed normal distribution to this relationship we set an upper threshold of 0.6 to the predicted frequency. Variations in the frequency of catch with temperature fit better the skewed normal distribution.

We then formulated a function to predict the frequency with which fisherman catch skipjack as a function of both temperature and chlorophyll. This function has the form of the product of the function for predicting the frequency of catch for temperature alone (left hand side of the lower panel in figure 2) and the function for predicting the frequency of catch for log chlorophyll alone (right hand side of the lower panel in figure 2). The values for the coefficients of this function were once again obtained by searching for values of the coefficients that provide the best fit to the data. A graph of this function is shown in the upper panel of figure 3, and a plot of the predicted frequencies of catch and the observed frequencies are shown in the lower panel (We expect much closer agreement when we complete the tuning.)

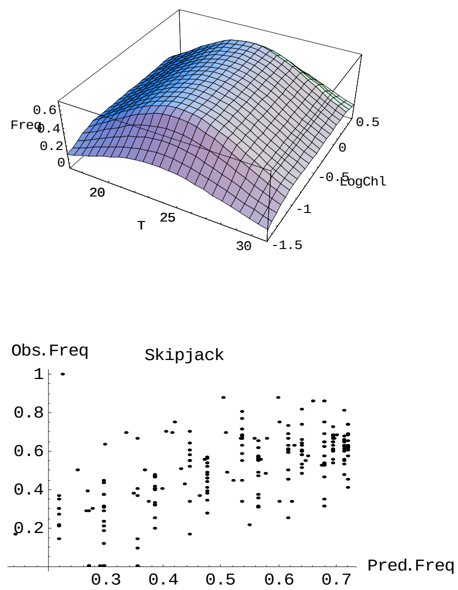

Figure 3. Upper panel. 3-dimensional plot of the function describing the frequency with which skipjack are caught at a given temperature and log chlorophyll concentration. Lower panel. Plot of observed catch frequencies and predicted frequencies.

Figures 4 and 5 show a second analysis using the PHAM-tuna application- the impact of ENSO variations on the recruitment of tuna of the Eastern Pacific Ocean. Here we subjected the time series from 1985 to 2007 of GHRSST imagery of the region to an EOF analysis and then compared the times series of variability in the temporal expansion coefficients of the modes with both the time series for the Southern Oscillation Index (SOI) and the time series of recruitment for our 3 species of tuna. This comparison clearly revealed that:

- The temporal expansion coefficients of both GHRSST modes 2 and 3 closely track the SOI.
- The time series of recruitment calculated from IAATC's stock assessment model for all 3 species track each other well.
- Large variations in the time series of recruitment calculated from IAATC's stock assessment model for all 3 species appear to be driven by large variations in the temporal expansion coefficient of GHRSST modes 2 and 3.

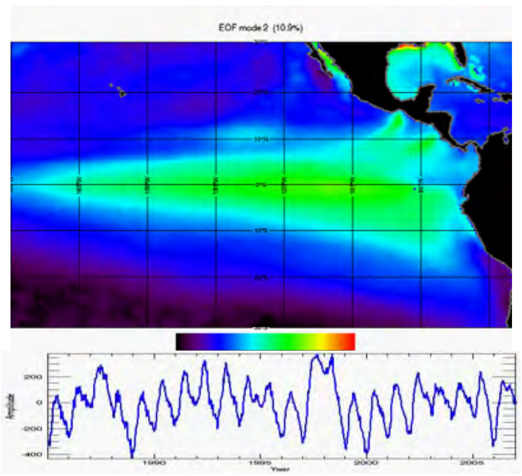

Figure 4. The 2nd EOF mode (upper) and it temporal expansion coefficient (lower) for the GHRSST time series for eastern Pacific. The mode "catches" temperature shifts caused by El NINO and La NINA events.

Figure 4 displays both the 2nd EOF mode of weekly GHRSST imagery and its temporal expansion coefficient. The El Nino of 1987,1992-93, and 1997-98 are expressed as maxima in the expansion coefficient, and the La Nina of 1989, 1999, and 2000 are expressed as minima.

The upper panel in Figure 5 displays the time series for the Southern Oscillation Index and the temporal expansion coefficient for the 3rd EOF mode of weekly GHRSST imagery. The co-variation between the time series is excellent as is the co-variation between the 3rd EOF expansion coefficient and SOI series. Obviously, the coupling between the ocean and atmosphere is tight and without significant lag.

The lower panel of figure 5 displays the time series of skipjack recruitment and the expansion coefficient of EOF mode 2. Although the co-variation between the two time series is not strong, it is clear that large swings in ENSO elicit a response in recruitment. Thus, the large swings in the temporal expansion coefficient that occurred between 1986 and 1989 and between 1997 and 99 drove large swings in recruitment.

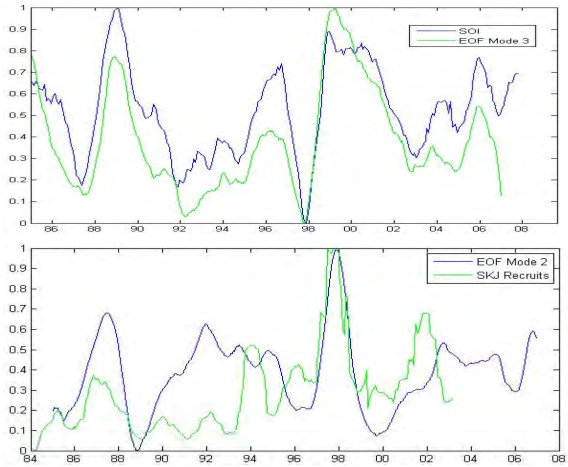

Figure 5. Upper Panel. The temporal expansion coefficient for mode 2 closely tracks the Southern Oscillation Index. Lower Panel. The temporal expansion coefficients for mode 2 track the recruitment of skipjack as well as the bigeye and yellowfin tuna.

3. CONCLUSION

Although our work on the Pelagic Habitat Analysis has just begun, we feel that the results so far indicate that the software will likely become a useful tool for ecosystem-based management of pelagic fisheries.

SST WARM SPOTS IN THE ARCTIC

Steinar Eastwood[(1)], Pierre LeBorgne[(2)], Sonia Pere[(2)], David Poulter[(3)]

[(1)] Norwegian Meteorological Institute, email : s.eastwood@met.no
[(2)] Centre de Météorologie Spatiale, Météo-France
[(3)] Southampton Oceanography Center (United Kingdom)

ABSTRACT

Sea surface skin-to-bulk temperature differences due to diurnal variability is well known, and the formation of surface warm spots in areas with low wind is well documented at low and mid latitudes. Less attention has been given to high latitudes. In the context of the EUMETSAT OSI SAF studies have been initiated to document the occurrence of such warm spots in the Arctic, using different GHRSST SST data products. This paper shows that such warm spots do form in the Arctic as well.

1. INTRODUCTION

The increasing attention on climate change has brought more focus on sea ice and SST in the Arctic. Special attention was also given to the Arctic during the validation of the new global METOP AVHRR SST product produced by the EUMETSAT Ocean and Sea Ice Satellite Application Facility (OSI SAF). At CMS, Meteo-France, it was discovered that these SST fields have a warm bias during summer months in the Arctic. This warm bias was evident in the Norwegian, Greenland and Barents Seas, areas that have been well covered with drifting buoys since autumn 2007 due to the Poleward drifter project. By closer look, the team at Meteo-France also discovered occurrences of what looked like typical sea surface warm spots.

Sea surface temperature warm spots are well know and documented from warmer seas. Less attention has been given to the occurrence of such at high latitudes. To study this further, the formation of such warm spots in the Arctic has been investigated by the OSI SAF using the METOP AVHRR SST product together with other GHRSST SST data products, as well as in situ drifting and moored buoy data. Theoretical confirmation has been sought using fine scale turbulence modelling on some of the observed cases.

In this paper we present the first results of these studies.

Seasonal to decadal variability of the SST front off the Peruvian coast: connection with the intraseasonal equatorial Kelvin wave activity

Purca S.*, B. Dewitte, D. Correa, B. Giese and J. Vazquez

* Esquina Gamarra y Gral. Valle S/N. Chucuito. Callao-Peru. Phone:+51-1-6250836. Fax:+51-1-4296069

The upwelling of Peru is experiencing a significant variability at a wide range of frequencies owned to a large extent to its connection with the equatorial region. In particular, the El Niño Southern Oscillation (ENSO) can have drastic societal impacts for Peru. Besides ENSO, the intraseasonal variability, as the form of equatorial Kelvin waves can significantly modify the regional environment because those tend to be trapped along the coast. In this study, the link between equatorial variability and the regional SST variability (3°S-18°S; coast to 100 km off shore) is investigated by means of historical satellite and *in situ* data (IMARPE coastal stations). As a first step the in situ data are confronted to the satellite data over the overlapping period (1985-2006), which reveals a good agreement between both data sets for the dominant statistical variability modes. The high-resolution (4km) satellite data Sea Surface Temperature Pilot Project (GHRSST-PP) available from the Global Ocean Data Assimilation Experiment (GODAE) allows for documenting the SST front associated with the narrowly extended coastal upwelling, which is not the case for the historical data from the IMARPE cruises (1950-2006). Statistical analysis of the satellite data combined with the in situ data suggests that this front experienced cross-shore displacement at seasonal to decadal timescales, which provides an index of upwelling variability at low frequency. Second, the equatorial Kelvin waves are estimated from a modal decomposition of the SODA Reanalysis and indices of the low frequency modulation of the intraseasonal Kelvin wave activity are derived. The analysis indicates that those indices are significantly correlated to the interannual and decadal modes of SST along the coast, which suggests that the decadal mode along the coast of Peru can results from a residual effect of the intraseasonal equatorial Kelvin wave activity. Our results illustrate the specificity of the response of the Peru coastal system to the equatorial Kelvin waves and the importance of energy upscale associated to this forcing at the regional scale.

Mesoscale and Submesoscale Eddies Detected from GHRSST Product

Changming Dong,
IGPP, UCLA
Email: cdong@atmos.ucla.edu

Francesco Nencioli,
OPL, UCSB

Tim Mavor,
NOAA/NESDIS/ORA

==

ABSTRACT

The GHRSST products possess unprecedented high resolution information of oceans, in which mesoscale and submesoscale variation in the SST can be well revealed. In this study, a new algorithm is developed to detect mesoscale and submesoscale eddies from high-resolution SST data. In the first step, a Canny edge-detection scheme is applied to the SST data to generate the SST longitudinal and latitudinal gradients; in the second step, a newly-developed algorithm, Vector Geometry Eddy Detector Algorithm (VeGEDA) is applied to the SST gradient; and in the third step eddies trajectories are tracked (this is also included in VeGEDA. The algorithm is being applied to the eddy-rich regions and then to global oceans. Eddy data detected from the GHRSST data will be released on online.

1. Introduction

As early as 1978, Legeckis (1978) started to use environmental satellites-observed SST images to study SST fronts. Recently, Castelao et al (2006) estimated the locations of the SST fronts and filaments in the California Current System by using the 5km resolution SST data from the Geostationary Operational Environmental Satellite (GEOS), in which an edge-detection algorithm (Canny, 1986) is applied to the identification of SST fronts. Using a multi-image edge detection algorithm (Cayula and Cornillon, 1995) to a time series of the 9.3 km resolution AVHRR/Pathfinder SST imagery, Ullman et al (2007) investigated the subtropical frontal zone in the North Atlantic Ocean, in which "all-pixel" fields were elected for use rather than the cloud-masked "best" field (Cayula and Cornillon, 1996). In this study, we investigate activities of mesoscale and submesoscale eddies using the high-resolution GHRSST product.

2. Multiple-scale Variation in GHRSST

The GHRSST product includes multiple-resolution real-time SST data from multiple satellites. Due to cloud cover and other error sources, missing data points are presented in satellite-observed SST. To make use of all available SST resources, we are developing an Optimum Interpolation approach to merge the multiple-satellite SST data by removing missed data. Chao et al (2009) developed 2D-Var to blend multiple satellites data with in-situ observations to produce a global 1km SST product with missed data filled. The data provided by Yi Chao's group are used in this study.

To analyze the multiple scales that characterize the SST, spatial spectrum analysis is applied to the SST gradient data. An example in Fig. 1 shows that the submesoscale mesoscale variations is well separated.

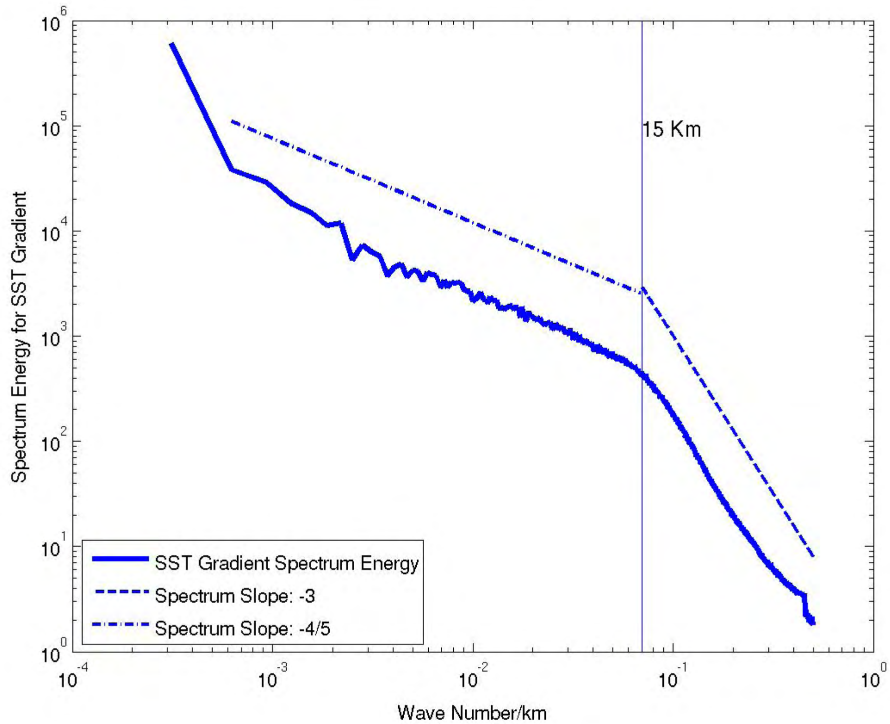

Fig. 1 The Spectrum Analysis for a sampled SST gradient in eastern Pacific Ocean on April 28, 2009. The 1km-resoution blended SST data are provided by Yi Chao, JPL, which can be viewed online ourocean.jpl.nasa.gov/SST. The methodology can be referred to Chao et al (2009).

3. Eddy Detection from GHRSST

We developed an algorithm to automatically detect mesoscale and submesoscale eddies from the high-resolution SST data. There are three steps for the algorithm:

Step I: Apply a Canny edge-detection algorithm to calculate SST gradients

Step II: Apply the Vector Geometry Eddy Detector Algorith (VeGEDA) we recently developed (Nencioli et al, 2009, Dong et al, 2009a) to the SST gradient field to detect mescoscale and submesoscale eddies from the high-resolution SST.

Step III: Track eddy trajectories, which is also part of VeGEDA.

Fig. 2 shows an example of eddies detected from a snapshot of SST data on the eastern Pacific Ocean from blended 1km SST data (Yi et al, 20009).

The SST-eddy detection scheme provides several parameters for detected eddies, such as locations, sizes, signs, intensities, shapes and so on, and also can track eddies trajectories and monitor eddies evolution. Details about the scheme can be found Dong et al (2009b**)**

4. Discussions

Strictly to say, eddies detected from SST are centers of warm (cold) water masses and features associated with them. It is an arguable question if such warm (cold) water masses are anticyclonic (cyclonic) eddies. Such confirmation can not be done using SST data only and it must be analyzed along with other variables such as velocity, sea surface height, and so on. Solutions from numerical models represent one option (Dong (2009b). In Dong et al (2009a), surface drifter trajectory data were used to confirm cold water ring was associated with a cyclonic eddy, however it is still a challenging topic for general application.

Acknowledgements:

The project is supported by the NASA (Grant NNX08AI84G). Jorge Vazquez and Ed Armstrong provided CD the historical GHRSST data and aided in processing the

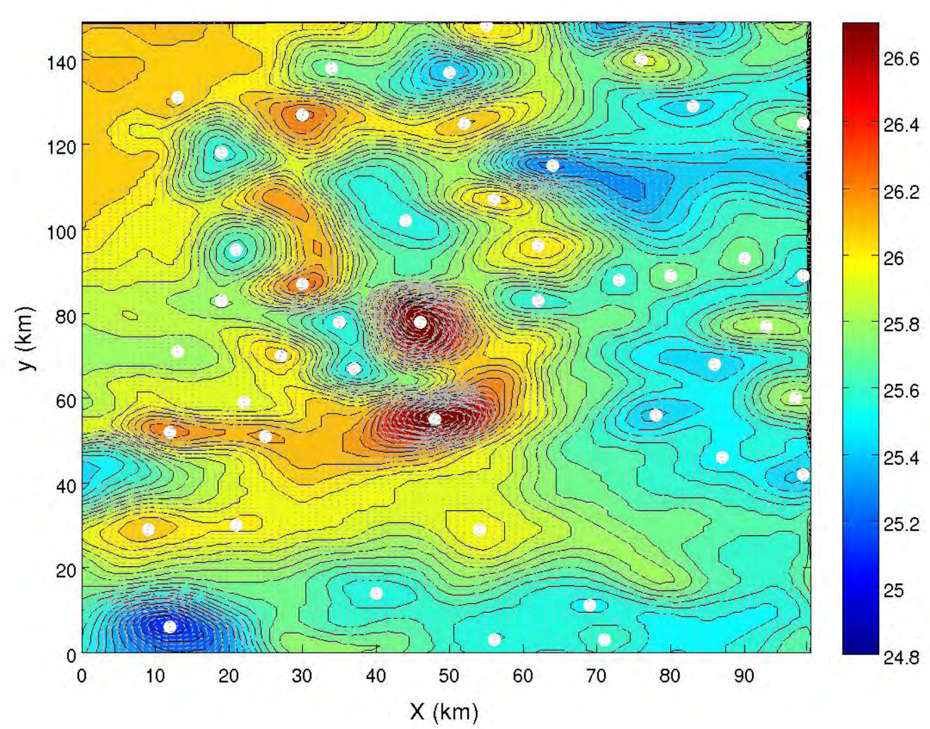

Fig. 2 An example for eddies detected from SST data by VeGETA. The color contours are SST, vectors are (Ux,Vy)=(Ty,-Tx), the white dots are identified eddies' centers. The SST data is the same as that used in Fig. 1.

GRFSST data. Yi Chao and Banyang Tang provided CD their beta-version global mapped 1km resolution SST product Pablo Sangra and Des Barton from Spain are collaborators of the project, who share their field experiments data along the Eastern Atlantic Oceanic Upwelling Zone and Gran Canary Island Wakes with the project.

References:

Canny, J, 1986: A computational approach to edge-detection, *IEEE Trans Patt. Anal. Mach. Intell*., **6**, 679-698.

Castelao R.M., T.P. Mavor, J. A. Barth, and L. C. Breaker, 2006, Sea surface temperature fronts in the California Current System from geostationary satellite observations, *J. Geophys. Res.*, ***11***, C09026, doi:10.1029/2006JC003541.

Cayula, J.-F., and P. Cornillon, 1995, Multi-image edge detection for SST images, *J. Atmos. Oceanic. Technol.*, **12**, 821-829.

Cayula, J.F. and P. Cornillon, 1996, Cloud detection from a sequence of SST image, *Remote Sens. Environ.*, **55**, 80-88.

Chao, Y., Z. Li, J. Farrara, P. Huang, 2009, Blending sea surface temperatures from multiple satellites and in-situ observations for coastal oceans, J. Atmos. Ocean. Tech., in press.

Dong, C., T. Mavor, F. Nencioli, S. Jiang, Y Uchiyama, J. McWilliams, T. Dickey, M. Ondrusek, D. Dennis, H. Zhang: 2009a, An eddy observed in lee side of Lanai Island Hawaii,submitted to *J. Geophy s. Res.*

Dong, C. et al, 2009b: Mesoscale and submesoscale eddies detection from high-resolution SST data, in preparation.

Legeckis, R., 1978: A survey of worldwide sea surface temperature fronts detected by environmental satellites, *J. Geophys. Res.*, **83**, 4501-4522.

Nencioli, F, C. Dong and T. Dickey, 2009 Mesoscale and submesoscale eddies in Southern California Bight: An eddy algorithm and its application to high-resolution numerical model product, submitted to *J. Atmos. Oceanic. Tech.*

Ullman, D. S., ,and P. C. Cornillon, 1999: Satellite-derived sea surface temperature fronts on the continental shelf off the northeast U.S. coast, *J. Geophys. Res.*, **104**, 23,459-23,478

Ullman, D.S, P.C. Cornillon, and Z. Shan, 2007, On the characteristics of subtropical fronts in the North Atlantic, *J. Geophys. Res*.,**112**,C01010,doi:10.1029/2006JC003601.

An Atlas of SST Fronts in the North and South Altantic

Peter Cornillon, Graduate School of Oceanography, University of Rhode Island, Narragansett, RI, 02874, USA (pcornillon@me.com)
and
Pierre Le Borgne, Centre de Météorologie Spatiale, Météo-France, Lannion, 22307, France (Pierre.LeBorgne@meteo.fr)

The objective of this project is to produce an atlas of sea surface temperature (SST) fronts for the North and South Atlantic basins based on geosynchronous satellite data. To this end, we used all hourly SST fields from the Spinning Enhanced Visible and Infra-Red Imager (SEVIRI) of the Meteosat Second Generation (MSG) geostationary satellites 8 and 9 and the Geostationary Operational Environmental Satellite (GOES) 8 and 12 Imagers, available at the Centre de Météorologie Spatiale of Météo-France. These data were obtained from the EUMESTSAT's Ocean and Sea Ice Satellite Application Facility (OSI SAF) processing chain. The SST fields are available in both a "Standard Projection" – a Platte-Carre projection, rectangular in latitude and longitude, with a grid spacing of 0.05° – and a "SpaceView Projection" – the Earth as seen by the geosynchronous satellite. The grid spacing of the SpaceView projection is based on the angular spacing of samples as seen from the sensor and varies substantially in kilometers or degrees of latitude and longitude over the image with a minimum spacing of a bit over 3km at nadir. Minor variations in the Earth as seen by the satellite in the SpaceView projection – due to pointing and orbital anomalies – are corrected so that all fields are available on the same grid. The GOES archive extends from 20 February 2001 through 14 December 2008 and the MSG archive extends from 12 June 2003 through 31 December 2008 although coverage during the first several months of the latter is sparse.

Two different approaches to edge detection have been undertaken. One is based on the Sobel gradient operator and the other on the Cayula-Cornillon edge detection algorithm (Cayula and Cornillon, 1992; 1995). These algorithms are complimentary in that they address the location of SST fronts from two different perspectives. The Sobel gradient operator is a local operator determining SST gradients based on the SST field in 3x3 pixel blocks. The Cayula-Cornillon edge detector (CC95 henceforth) operates on 32x32 pixel histograms with fronts based on differences in populations in the histograms; i.e., it defines fronts based on the separation of water masses rather than on SST gradients.

Prior to processing the entire time series, in excess of 47,000 MSG images and 65,000 GOES images, we addressed three questions – which projection, which variable and how often - with regard to which fields to process. Based on fronts found for the October 2007-September 2008 time frame using CC95 we concluded the following:

1. *Which projection, the Standard Projection or the SpaceView projection?* We elected to use the SpaceView projection. Not only does this provide the highest spatial coverage but, more importantly, also avoids spurious fronts due to regridding near the edges of coverage.
2. *Which variable, SST or brightness temperatures?* Although our first thought was that using brightness temperatures would provide for a more accurate detection of fronts, the smoothing associated with the derivation of the SST fields together with the use of multiple channels lead to fewer false fronts without a substantial loss of actual fronts. We therefore decided to use SST fields.
3. *How often*, *at the full temporal resolution of the sensor (20 minutes for GOES and 15 minutes for MSG), hourly or daily?* In order to facilitate combining MSG and GOES data while obtaining the highest temporal resolution, we decided to use hourly data.

We have now processed all 113,000+ images via both algorithms and are beginning to generate atlases based on the resulting frontal data sets. These will be discussed in the presentation.

References

Cayula, J.-F. and P. Cornillon, 1992, Edge detection algorithm for SST images, J. Atmos. Oceanic Technol., 9, 67-80.

Cayula, J.-F. and P. Cornillon, 1995, Multi-Image Edge Detection for SST Images, J. Atmos. Oceanic Technol., 12, 821-829.

Detection of Rossby Waves in SST and Salinity

Bulusu Subrahmanyam(1), David M. Heffner(2), David Cromwell(3), and Jay F. Shriver(4)

[1]*Marine Science Program & Dept. of Geological Sciences, University of South Carolina, Columbia, SC 29205, USA.* (E-mail: sbulusu@geol.sc.edu)
[2]*Dept. of Geological Sciences, University of South Carolina, Columbia, SC 29205, USA.*
[3]*Ocean Observing and Climate Research Group, National Oceanography Centre, Southampton, S014 3ZH, UK*
[4]*Naval Research Laboratory, Stennis Space Center, Mississippi, USA*

ABSTRACT

Rossby waves are difficult to detect with *in situ* methods. In this study we show Rossby waves in Sea Surface Temperature data from the Global High-Resolution Sea Surface Temperature Pilot Project (GHRSST-PP), and salinity from 1/12° global HYbrid Coordinate Ocean Model (HYCOM) simulations in the Indian Ocean. In this study we are using HYCOM sea surface salinity (SSS) simulations as a proxy for the awaited SSS data from satellites. The first three baroclinic modes of the Rossby waves are inferred from the Fast Fourier Transform (FFT), and two-dimensional Radon Transform (2D RT). Wavelet Transforms of these multi-parameters from satellite observations and model simulations help to discriminate between the annual and semi-annual signal of these Rossby waves. This comprehensive study reveals the surface signature of Rossby waves in sea surface salinity anomalies is likely to be between 0.05-0.3 in the South Indian Ocean.

1. INTRODUCTION

The purpose of this study is to demonstrate that Rossby waves can be observed in SSS. Up until this point, nobody has shown that Rossby waves can be seen in SSS at least in the Indian Ocean, largely because there is currently no easy way to acquire basin wide salinity data. For the first time, Heffner et al. (2008) and Subrahmanyam et al., (2009) demonstrated that Rossby waves can be identified in the sea surface salinity (SSS) signal, using HYbrid Coordinate Ocean Model (HYCOM) simulations as a proxy for the awaited SSS data. Satellite measurements of SST using passive (infrared) and active (microwave) radiometers have been available since the 1970s, but as of the writing of this paper, no methods are available for measuring SSS from a satellite, although there are two planned satellite missions – Aquarius and SMOS. The European Space Agency's (ESA) Soil Moisture and Ocean Salinity (SMOS) mission has been designed to observe soil moisture over the Earth's landmasses and salinity over the oceans. The SMOS satellite launch is scheduled for 2009. Aquarius/SAC-D is a space mission developed by NASA and the Space Agency of Argentina (Comisión Nacional de Actividades Espaciales, CONAE), which is planning to launch in 2010.

2. METHODOLOGY & ANALYSIS

Sea Surface Temperature (SST) data from the GODAE High Resolution Sea Surface Temperature Pilot Project (GHRSST-PP) product of Operational SST and sea Ice Analysis (OSTIA) Level-4 data with a spatial resolution of ¼° and daily temporal resolution was obtained from the National Centre for Ocean Forecasting. In this study we use global HYbrid Coordinate Ocean Model (HYCOM) simulations with 1/12° horizontal resolution (~7 km at mid-latitudes) and 32 hybrid layers in the vertical.

Longitude/Time (L/T) plots of GHRSST, and the HYCOM simulations (SST, SSS) were plotted at 10°S and 20°S on the same temporal (10-day) spacing and same spatial (0.5° x 0.5°) resolution. All of these parameters were detrended in time and space by subtracting the 4-year mean for each point, and then subtracting the longitudinal mean (at a given time) for each point in order to remove seasonal and spatial trends. The zonal gradients of the detrended (anomaly) data were taken by subtracting the value at each point from the point on the left (west) and dividing by the spatial resolution in kilometers (to get a gradient in kilometers).

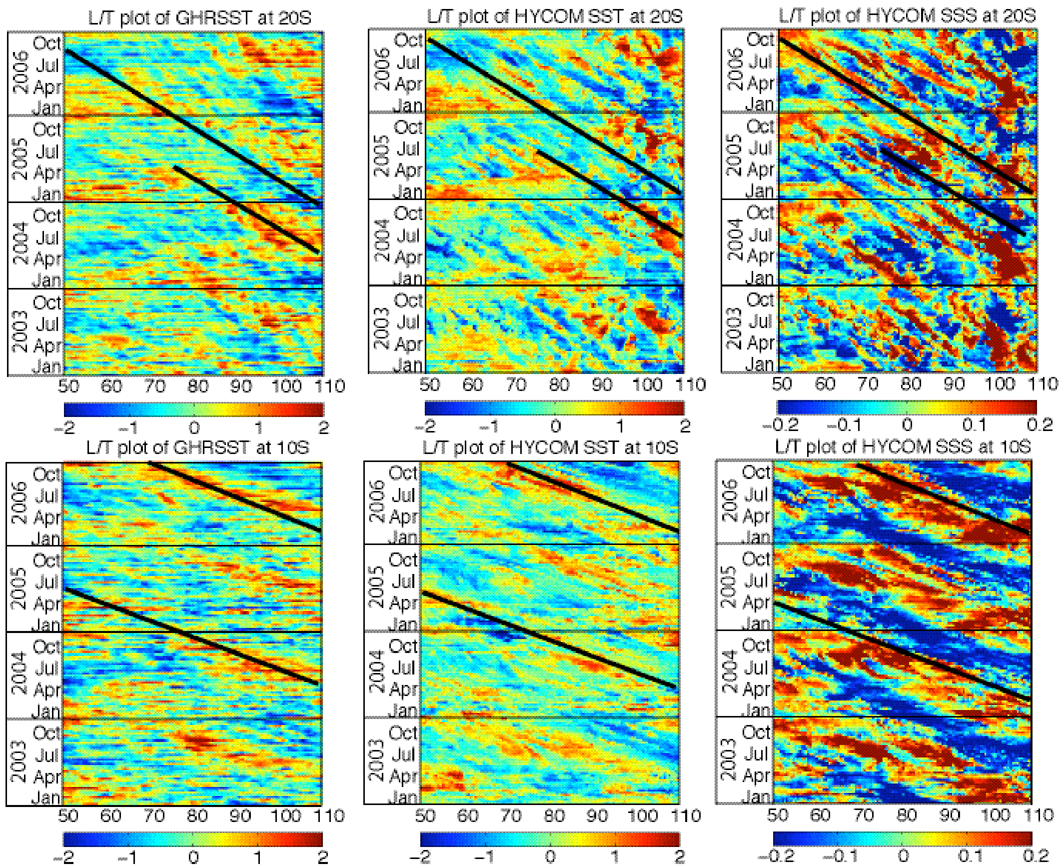

Figure 1. Longitude-time plots at 20ºS of GHRSTT anomalies, HYCOM SST and SSS anomalies (Top Panel). Bottom panel is for 10°S. The solid lines represent Rossby wave propagation.

3. CONCLUSIONS

Future salinity missions, notably ESA's Soil Moisture and Ocean Salinity (SMOS) and joint U.S. and Argentina Aquarius missions, will open a new era in Rossby wave studies using high spatial and temporal coverage of satellite-derived salinity. Rossby wave amplitudes in HYCOM SSS have a range of 0.05 – 0.3 which demonstrates that these satellite missions should be able to resolve Rossby waves in SSS at some latitudes. GHRSST showed a surface amplitude range in SST between 0.45-0.57C, whereas HYCOM SST amplitudes are between 0.33-0.62°C. We believe GHRSST along with SSS from satellites will be very useful to understand Rossby wave and ocean dynamics.

4. REFERENCES

Heffner, D.M., **B. Subrahmanyam**, J.F. Shriver, and J.F. Blundell (2008). Indian Ocean Rossby waves detected in HYCOM sea surface salinity , Geophys. Res. Lett., 35, L03605, doi:10.1029/2007GL032760.

Subrahmanyam, B., D.M. Heffner, D. Cromwell, J.F. Shriver, (2009). Detection of Rossby Waves in Mult-parameters in Multi-mission Satellite Observations and HYCOM simulations in the Indian Ocean, *Remote Sensing of Environment* , 113, 1293-1303.

GHRSST AND ECCO2: SST VARIABILITY AND OCEAN SURFACE CURRENTS FROM SATELLITE OBSERVATIONS AND A HIGH RESOLUTION OCEAN MODEL.

Holger Brix[(1)], Dimitris Menemenlis[(2)], Jorge Vazquez[(2)], Edward M. Armstrong[(2)], and David F. Moroni[(2)]

[(1)] *University of California, Los Angeles, CA, Email: hbrix@ucla.edu,*
[(2)] *Jet Propulsion Laboratory, California Institute of Technology, Pasadena, CA*

ABSTRACT

Mesoscale eddies transport the biggest part of the kinetic energy contained in ocean currents. While satellite altimetry can give us an estimate of the propagation velocity of these dynamics, either being Rossby wave speed or eddy propagation speed, we are limited by the spatial resolution of the available satellite products. Numerous sea surface temperature (SST) products, as provided through GHRSST, are available with high spatial resolution and historic records dating several decades back. Using these SST products as an alternative way to estimate (geostrophic) ocean surface velocity fields would give us an important tool for improving ocean models and historic ocean and climate simulations.

Advection, mixing, air-sea exchange processes, and diffusion determine SST variability. Despite this variety of processes influencing SST it is striking how SST images can resemble (dynamically driven) eddy structures (see Fig. 1) and how animated sequences of SST images show the development and propagation of mesoscale features. We investigate results from a high resolution ocean model (Estimating the Circulation and Climate of the Ocean, Phase II: ECCO2) simulation that provides us with values for sea surface height (SSH), SST, and (total and geostrophic) velocities on a ¼ degree grid. In a first step we compute the propagation speed of eddies from SSH fields applying a space-time lagged correlation analysis similar to the maximum cross correlation method applied by Fu (2006). This method computes the correlations between SSH anomalies (time mean removed) at a given point with all neighboring SSH anomalies at various time legs and allows us to determine estimates of the speed and direction of maximum correlations as the anomalies move in space and time.

We compare these results to velocity fields determined with the same method from model SST data and geostrophic velocities directly available from the model runs. While SST is influenced by a multitude of processes and SST-derived velocity fields are therefore likely to be noisier than SSH-derived fields, we do expect to be able to identify regions/spatial scales where SST data can be used to estimate eddy propagation velocities.

In a second step, we will analyze GHRSST data products with the aforementioned maximum cross correlation method. Do the same constraints (spatially and possibly temporally) that are valid for the model hold for the satellite data? In the long term, these results can serve to improve our knowledge of geostrophic ocean circulation fields and therefore the constraints we need to impose on ocean models for an optimum representation of dynamic processes.

REFERENCE:

Fu, L.-L. (2006), Pathways of eddies in the South Atlantic Ocean revealed from satellite altimeter observations, Geophys. Res. Lett., 33, L14610, doi:10.1029/2006GL026245.

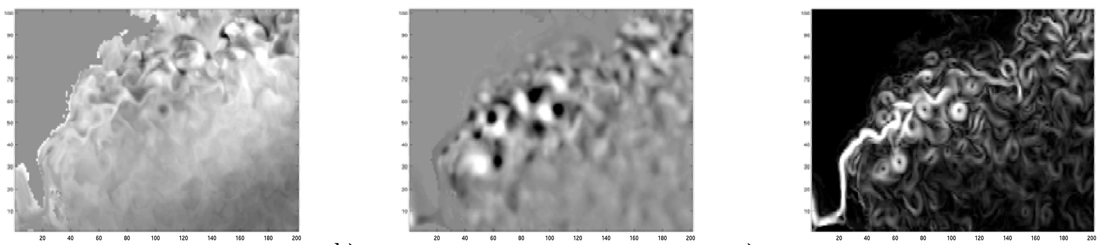

a) b) c)

Figure 1. Results from an ECCO2 model run showing a) sea surface temperature, b) sea surface height, and c) current speed in the top layer. The depicted region is off the U.S. East Coast.

USING GHRSST L4 PRODUCTS TO CALCULATE BULK AIR-SEA HEAT FLUXES.

C. D. Jeffery[1]

[1] *NOAA National Oceanographic Data Center, Silver Spring, MD (USA),*
Email: christopher.d.jeffery@noaa.gov

ABSTRACT

High resolution SST analyses are combined with other satellite-based meteorological variables to calculate daily global latent and sensible heat fluxes for 2006, using the NOAA-COARE 3.0 bulk flux aerodynamic algorithm. Air-sea fluxes from two GHRSST (Group for High Resolution Sea Surface Temperature) L4 products (NCDC and RSS) are examined; these show differences of up to 15% caused by SST. These are also compared with equivalent OAFlux estimates, revealing large biases in the sensible heat flux likely due to different input air temperatures used in the flux calculation.

1. INTRODUCTION

Ocean-atmosphere heat exchange occurs via solar and longwave radiation, conductive and convective transfer (sensible heat), and by evaporation (latent heat). The resulting net heat flux is a key variable for climate studies. However direct observations are sparse, thus we rely on bulk parameterization of the air-sea fluxes as functions of surface meteorological variables. Whilst sources for flux-related variables include marine surface weather reports from voluntary observing ships and atmospheric reanalyses from numerical weather predication (NWP) centers, comprehensive global coverage is only possible from an analysis incorporating satellite measurements. With advances being made in the retrieval of air temperature and humidity from space, it is now possible to produce fluxes using only satellite-derived parameters. We aim to produce global air-sea heat fluxes using GHRSST L4 products and other satellite-derived meteorological parameters. Intercomparison of the SST products and the subsequently calculated fluxes will feed back into their processing and development, and provide the opportunity to improve the current state of knowledge.

2. COARE 3.0 BULK FLUX ALGORITHM

The NOAA-COARE 3.0 parameterization [Fairall et al., 1996] is selected on the basis of a comparative study of 12 bulk aerodynamic algorithms for computing ocean surface turbulent fluxes [Brunke et al., 2003]. The algorithm also includes subroutines to account for the effect of the cool-skin and warm surface layer. However, the effect of diurnal warm layer is not included at present. Four independent meteorological variables are required to calculate latent and sensible heat fluxes. These are: wind speed (U); air temperature (T_a); air humidity (q_a) and sea surface temperature (T_s). Including shortwave (Q_{sw}) and longwave radiation (Q_{lw}) allows the net heat flux (Q_{net}) to be estimated.

3. DATA

Satellite based datasets are used for the independent variables required by the algorithm. Blended Seawinds data from NCDC [Zhang et al., 2006] is used for U. Experimental products being developed at NCDC, derived from the AMSU brightness temperatures onboard NOAA POES are used for q_a and T_a [Shi and Zang, 2008]. In the case of T_s, multiple GHRSST L4 products are used with the aim of comparing fluxes based on different SST analyses. Finally, Q_{sw} and Q_{lw} are obtained from the international satellite cloud climatology project (ISCCP) surface flux dataset. The input data are regridded onto a daily 1°x1° global grid.

4. SST DIFFERENCES

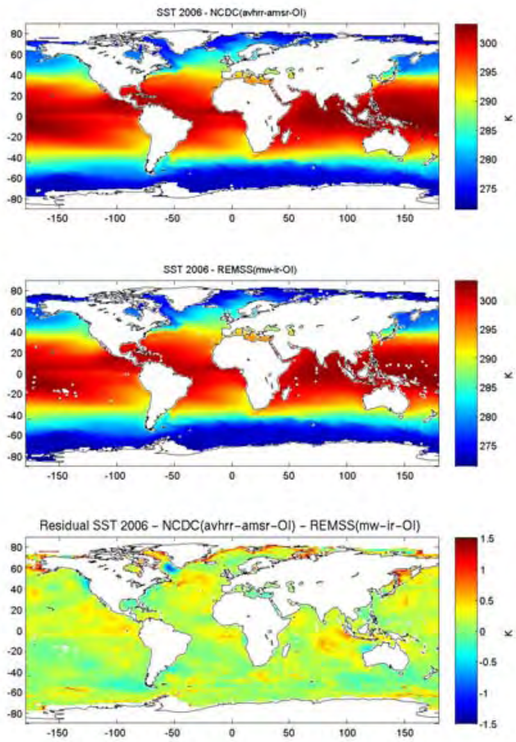

Figure 1. NCDC and RSS 1°x1° yearly average SST analyses for 2006, and the residual difference between them [K].

Two GHRSST L4 products for 2006 and the yearly average difference between them are shown in Figure 1 -AVHRR_AMSR_OI (hereafter NCDC) and MW_IR_OI (hereafter RSS). Extreme differences of up to 1.5 K between the SST analyses are observed resulting from input data and differences in processing.

5. AIR-SEA HEAT FLUXES

Preliminary results consisting of 1°x1°, daily, latent and sensible heat fluxes for 2006 are calculated using the COARE 3.0 bulk flux algorithm (Figure 2). Surface radiation fluxes from ISCCP are also combined to estimate the net heat flux. So far, two GHRSST L4 datasets (NCDC and RSS) have been processed and heat fluxes calculated:

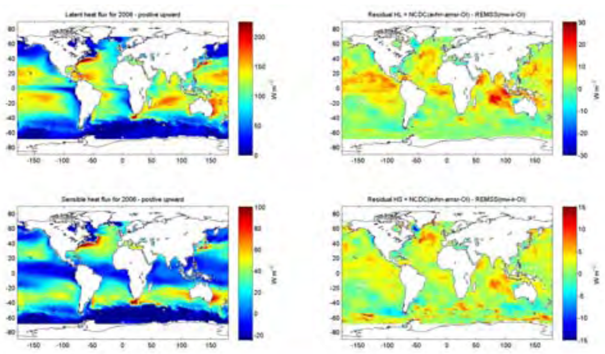

Figure 2. Latent and sensible heat fluxes calculated using COARE 3.0 and NCDC SST [W m^{-2}] (Left). Difference between latent and sensible heat fluxes [W m^{-2}] calculated using NCDC SST and RSS SST (Right).

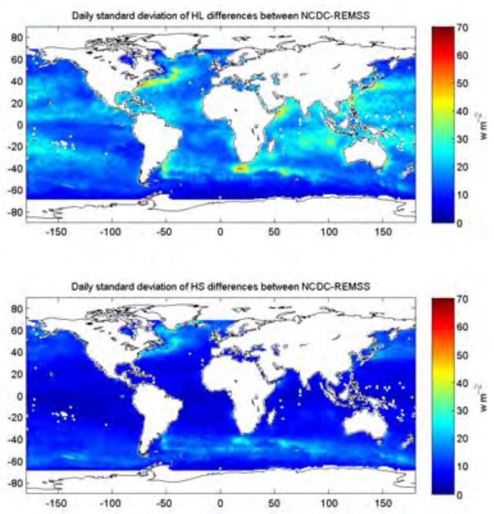

Figure 3. Daily standard deviation of Latent (top) and Sensible (bottom) heat fluxes [W m^{-2}] when calculated using NCDC and RSS SST analysis products.

Figure 3 shows the daily standard deviation of latent and sensible heat fluxes between the NCDC and RSS fluxes. Extremes of up to 70 W m^{-2} are present in the latent heat fluxes and up to 25 W m^{-2} in the sensible heat fluxes, this is approximately 15% of the total.

6. INITIAL COMPARISON WITH OAFLUX

NCDC and RSS fluxes for 2006 are compared with the equivalent latent and sensible heat fluxes from OAFlux (http://oaflux.whoi.edu/) (Figure 4). Latent heat fluxes compare well, but the sensible heat fluxes contain significant biases, with spatial patterns matching those of ΔT_a (where ΔT_a = NCDC T_a – OAFlux T_a).

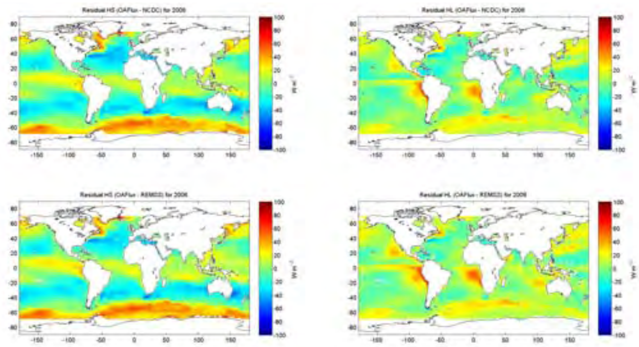

Figure 4. Top Left – Residual Sensible heat flux (OAFlux-NCDC), Bottom Left – Residual Sensible heat flux (OAFlux-RSS). Top Right – Residual Latent heat flux (OAFlux-NCDC), Bottom right - Residual Latent heat flux (OAFlux-RSS) [W m^{-2}].

7. CONCLUSIONS

Differences of up to 15% in certain regions are observed in the annual average latent and sensible heat fluxes as a result of discrepancies between the global SST analysis products. In addition, comparisons with OAFlux latent and sensible heat fluxes reveal large biases in NCDC and RSS sensible heat fluxes due to differences in input T_a. This may be a result of OAFlux using NWP data. Future work aims to address the T_a issue and calculate fluxes for additional GHRSST L2(P)/L4 datasets.

8. REFERENCES

Brunke, M. A., Fairall, C. W., Zeng, X., Eymard, L., and Curry, J. A. 2003: Which bulk aerodynamic algorithms are least problematic in computing ocean surface turbulent fluxes? Journal of Climate, 16, 619-635.

Fairall, C. W., Bradley, E. F., Rogers, D. P., Edson, J. B., and Young, G. S. 1996: Bulk parameterization of air-sea fluxes for Tropical Ocean-Global Atmosphere Coupled-Ocean Atmosphere Response Experiment. J. Geophys. Res., 101 (C2), 3747-3764.

Shi, L., and Zhang, H.-M. 2008: Sea surface air temperature and humidity retrievals based on AMSU measurement. 16th Conference on Satellite Meteorology and Oceanography. Fifth Annual Symposium on Future Operational Environmental Satellite Systems-NPOESS and GOES-R.

Zhang, H.-M., Bates, J. J., and Reynolds, R. W. 2006: Assessment of composite global sampling: Sea surface wind speed. Geophysical Research Letters, 33, L17714, doi:10.1029/2006GL027086.

DIURNAL VARIABILITY ANALYSIS FOR GHRSST PRODUCTS.

Christopher J. Merchant[1], Mark J. Filipiak[1]

and the Diurnal Variability Working Group

[1] *University of Edinburgh, Edinburgh, (United Kingdom), Email : c.merchant@ed.ac.uk*

ABSTRACT

The diurnal cycle of sea surface temperature is of intrinsic scientific interest, modulating air-sea fluxes and is a source of discrepancy between satellite observations of sea surface temperature (SST). The objective of diurnal variability analysis has been proposed by the GHRSST diurnal variability working group. This objective is elucidated, and some early results towards the goal presented.

1. INTRODUCTION

The diurnal cycle of sea surface temperature is of intrinsic scientific interest, modulating air-sea fluxes [e.g., 1] and is a source of discrepancy between satellite observations of sea surface temperature (SST). It has long been an aspiration of GHRSST to have a field estimating the diurnal increment in SST (dSST) available routinely within L2P.

The Diurnal Variability Working Group (DVWG) of GHRSST has had a series of 5 working group meetings between November 2006 and February 2009. As chair of the DVWG during this interval, Merchant wants to acknowledge the commitment and enthusiasm of the core group of the DVWG and those who have participated peripherally. Despite no core funding for the work of the group, significant progress has been made through the willingness of the participating scientists.

Progress has been made in modelling the relationships of dSST to the fundamental drivers of the diurnal cycle: the diurnal cycle of net heating at the air-sea interface, principally associated with the daily cycle of solar insolation, and wind driven mixing.

2. THE NEED FOR DV ANALYSIS

The working group has noted that there are two types of estimate of dSST available: (1) observational estimates based on the different between the SST observed by satellite at a given time and place and the SST previously observed (or analysed) for that time and place before the daily warming cycle; (2) model based estimates, driven by some knowledge of the state of the wind and insolation.

Geostationary sensors are useful in providing a dSST that is very closely related to the theoretical conceptualisation of dSST as the difference between the sub-skin temperature and the foundation temperature [2]. This is achieved by subtracting from the SST observed at some time, h, during the day, the SST observed during the "pre-dawn" interval (say, local midnight to dawn) when diurnally-induced stratification is assumed to be small. Such an estimate is restricted to where skies are clear both during part of the pre-dawn interval and during the day. More spatial completeness can be achieved by using a midnight or predawn analyzed SST, at the cost of folding analysis errors into the dSST.

Sensors on polar orbiting platforms are, outside of the very high latitudes, restricted to differences of SST ~12 hours apart. Using such differences as dSST estimates is prone to rather more error than a difference to a pre-dawn SST, but on the other hand the relative spatial completeness of microwave SSTs in particular means that a very informative field of estimated dSST is available daily.

Both empirical and physically-based models have made progress in recent years. Convergence between such models over a wide range of forcing situations has been a priority of the DVWG, and a formal assessment is now under-way.

Model dSSTs suffer from both model errors and errors due to the fields used to force them. Compared to the observational estimates, their advantage is that estimates can be spatially complete and predictive for any time, given suitable forecast fields.

In short, observational SSTs give spatially incomplete "snapshot" estimates of dSST with some error that depends on both the observation error and the error in the pre-dawn estimate; model SSTs given spatially compete fields with different errors.

The vision of the DVWG has therefore been to centres/systems for diurnal variability analysis (DVA) in real time, such that generators of L2P are able to draw on the analyses routinely to associated dSST with their L2P products.

3. EXPERIMENTAL DVA

Experiments in diurnal variability analysis are in early stages. This paper gives early results of one approach under development at University of Edinburgh in collaboration with Pierre Le Borgne of Meteo-France, but the strength of the DVWG is that a diversity of approaches will be taken across the group as a whole.

For details of the model used, see the poster by Mark Filipiak. The model is designed for use with NWP data, specifically ECMWF. ECMWF fields of (i) maximum wind, w_{max}, from the time when net heating at the surface becomes positive into the ocean, and (ii) the integrated positive heating, Q_{int}, from that same time. These fields are calculated from ECMWF 6 hourly forecast or analysis fields. The dSST response is based on SEVIRI observational dSSTs (referenced to pre-dawn SSTs).

The model dSST and 2 pm local time is shown as Fig 1a. The observation dSST at 2 pm is Fig 1b, although note that all under-cloud areas in the latter panel are set to zero. It is clear that dSSTs are somewhat underestimate in some locations in the model, and overestimated elsewhere, relative to the SEVIRI-based difference. Both have errors.

The analysis method is to solve for the w_{max} and Q_{int} that best explain the model and observational estimates given their respective errors, where both dSSTs are available. Where no observational dSST is available because of cloud, nearby observational estimates are used with increasing error according to a selected length scale. Beyond that length scale, the model estimate alone is available.

The analyzed field at 2 pm is shown as Fig 1c.

The observations added to the model at 2 pm have the capacity, without using any observations at other times, to improve the agreement between model and observation (M-O) at earlier and later hours, as shown by the statistics in Table 1. Mean M-O is reduced towards zero, standard deviation of M-O is reduced to ~0.25 K and correlations of M-O are improved. This is achieved by propagating the adjusted solutions for w_{max} and Q_{int} in time through the day. The ability to do this is a key advantage of doing the analysis in forcing space rather than analysing the dSST directly.

Analysis of observations into the model at only 2 pm thus improves the estimate of DV significantly between 11 am and 5 pm inclusive. This suggests a framework in which irregular snap-shots of dSST from, say, a few polar orbiting sensors can improve the dSST estimate throughout the day.

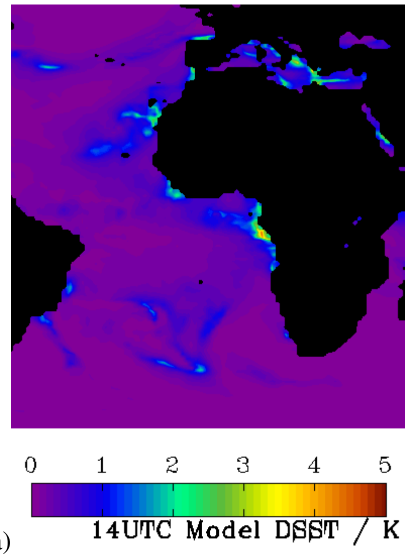

(a)

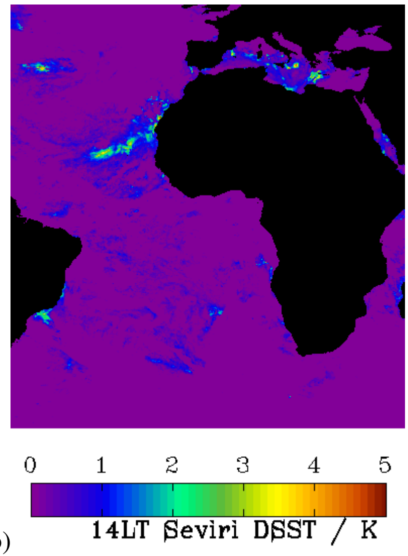

(b)

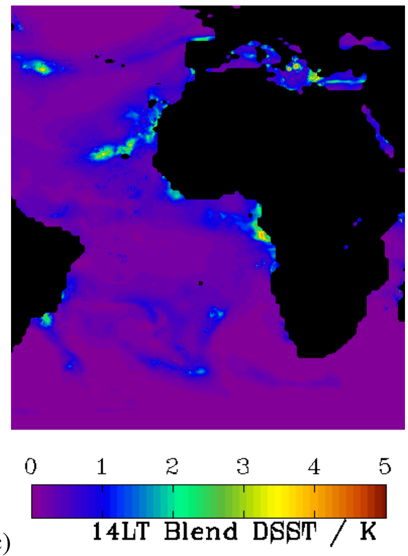

(c)

Fig 1 (previous page). (a) Model of dSST based on NWP fields. (b) Observations of dSST from SEVIRI (where cloudy, set to zero). (c) Experimental blend ("diurnal variability analysis") of model and observational estimates.

Time / local hour	SD(M-O) / K	Correlation M v O
11	0.27 (0.32)	0.62 (0.45)
12	0.26 (0.38)	0.74 (0.51)
13	0.26 (0.40)	0.84 (0.52)
14	Analysis hour.	
15	0.25 (0.40)	0.87 (0.62)
16	0.26 (0.37)	0.83 (0.62)
17	0.25 (0.34)	0.81 (0.63)

Table 1. Statistics of Model minus Observation dSST with analysis of Observations at 14 h LT and, in parentheses, without analysis of Observations at 14 h LT.

4. CONCLUSION

Routine diurnal variability analysis is an objective of the DVWG activities, and early experiments show promise.

5. REFERENCES

1. Kettle, H., C. J. Merchant, C. D. Jeffrey, M. J. Filipiak, and C. L. Gentemann (2009), The impact of diurnal variability in sea surface temperature on the atlantic air-sea CO2 flux, Atmos. Chem. Phys., 9, 529-541.

2. Donlon C, I Robinson, K Casey, J Vasquez, E Armstrong, C Gentemann, D May, P LeBorgne, J Piolle, I Barton, H Beggs, D J S Poulter, C J Merchant, A Bingham, S Heinz, A Harris, G. Wick, B. Emery, A Stuart-Menteth, P. Minnett, B Evans, D Llewellyn-Jones, C Mutlow, R Reynolds, H Kawamura and N Rayner (2007), The Global Ocean Data Assimilation Experiment (GODAE) High Resolution Sea Surface Temperature Pilot Project (GHRSST-PP), Bull. Am. Met. Soc, 88 (8), 1197-1213.

MULTI-SATELLITE MEASUREMENTS OF LARGE DIURNAL WARMING EVENTS.

Chelle L. Gentemann[(1)] , Peter J. Minnett[(2)], Pierre Le Borgne[(3)], Christopher J. Merchant[(4)]

[(1)] *Remote Sensing Systems 438 First St. #200, Santa Rosa, CA, (United States), Email :gentemann@remss.com;*
[(2)] *University of Miami, 4600 Rickenbacker Cswy, Miami FL, (United States), Email: pminnet@rsmas.miami.edu;*
[(3)] *Météo-France, Avenue de Lorraine, Lannion Cedex, (France), Email : pierre.leborgne@meteo.fr;*
[(4)] *University of Edinburgh, Mayfield Rd., Edinburgh, (United Kingdom), Email: c.merchant@ed.ac.uk*

ABSTRACT

Diurnal warming events between 5 and 7 K, spatially coherent over large areas (~1000 km), are observed in independent satellite measurements of ocean surface temperature. The majority of the large events occurred in the extra-tropics. Given sufficient heating (from solar radiation), the location and magnitude of these events appears to be primarily determined by large-scale wind patterns. The amplitude of the measured diurnal heating scales inversely with the spatial resolution of the different sensors used in this study. These results indicate that predictions of peak diurnal warming using wind speeds with a 25 km spatial resolution available from satellite sensors and those with 50-100 km resolution from Numerical Weather Prediction models may have underestimated warming. Thus, the use of these winds in modeling diurnal effects will be limited in accuracy by both the temporal and spatial resolution of the wind fields.

1. INTRODUCTION

About half of the solar energy reaching the surface of the earth is absorbed by the top 10 m of ocean, often resulting in formation of a diurnal thermocline. The existence of this diurnal warm layer was first described in 1942 (Sverdrup et al.), and has been studied extensively since. Surface temperature deviations greater than 3.0 K, referenced to the foundation temperature (the subsurface temperature below the diurnal thermocline), have been shown (Gentemann and Minnett, 2008;Merchant et al., 2008;Minnett, 2003). These large diurnal events have generally been viewed as isolated occurrences. In this paper, we use independent satellite measurements to verify the existence of large diurnal warming events and examine their spatial and temporal distributions.

2. DATA

Three independent satellite datasets were used to investigate large diurnal warming events. The AQUA satellite carries both the Advanced Microwave Scanning Radiometer - Earth Observing System (AMSR-E) and the Moderate Resolution Imaging Spectroradiometer (MODIS), providing independent contemporaneous microwave (MW) and infrared (IR) measurements. The AQUA satellite was launched in May 2002 into a polar, sun-synchronous orbit, with a LECT (Local Equator Crossing Time) of 1:30 AM/PM. Over much of the Atlantic Ocean, the geostationary METEOSAT-8 Second Generation (MSG) Spinning Enhanced Visible and Infrared Imager (SEVIRI) provides hourly data. While both MODIS and SEVIRI measure IR radiances, the SEVIRI instrument and viewing geometry is different than MODIS and is therefore independent.

A) Day night difference: The geostationary SEVIRI and polar-orbiting MODIS and AMSR-E have different sampling characteristics. In most regions, the propagation of SST features introduces a relatively small effect and the day-night difference is primarily due to diurnal warming. The location of valid data changes from day to night due to clouds, rain, or location of gaps between successive orbits (swath gaps). To preserve all the daytime measurements, it is important to have a night-time data set with as few missing data as possible. The nighttime SST field for the geostationary sensor, SEVIRI, is an average of all valid data between midnight and 6:00 LMT. For the polar orbiters (MODIS and AMSR-E), nighttime data are the same day descending orbits. Where same-day nighttime data were missing, valid nighttime data from the previous or following day were used.

B) Wind speed: Since it has been shown that diurnal variability is sensitive to wind speed variations, it is important to examine the connection between day-night SST differences and collocated wind speeds. The 6-hourly, 25 km, NASA Cross-Calibrated Multi-Platform (CCMP) winds, a global variational analysis of wind speed (Atlas et al., 1996), are linearly interpolated onto hourly, 2.2 km maps for this study.

3. DIURNAL WARMING OCCURANCE

The Probability Density Functions (PDFs) of SEVIRI ΔT_{dw} at 14:00 LMT for (A) different wind speeds and (B) after averaging to different spatial resolutions are shown in Figure 1. Figure 1A shows that low wind speeds are associated with significant diurnal warming. The distribution peak shifts towards zero and narrows as wind speeds increase. The lowest wind speed class (<1ms-1) has the highest probability of diurnal events over 1.0 K (60.2%), with the probability of large events decreasing smoothly with increasing wind speed.

Although not common, the figure clearly demonstrates that events over 4 K occur. The probability of a diurnal warming event larger than 5 K is 0.5%, 4 K is 3.5%, and 3 K is 14.6% at wind speeds less than 1 ms-1. Variability in diurnal warming is directly related to wind speed, variability in insolation, and variability in wind speed prior to 14:00 LMT SEVIRI measurement. The larger diurnal events likely had low wind speeds for several hours prior to 14:00 LMT, while the smaller diurnal events may have had higher or more variable wind speeds. Figure 1B shows the effect of spatial resolution on the probability of diurnal warming, for wind speeds less than 3 ms-1. As the spatial resolution decreases, the probability of diurnal heating > 2 K decreases, while the probability of smaller diurnal events, < 2 K, increases. The effect is largest for the lowest spatial resolution. These results clearly demonstrate that spatial resolution will affect measurement of diurnal warming. In the next section several diurnal events are studied using satellite measurements of diurnal warming at different spatial resolutions.

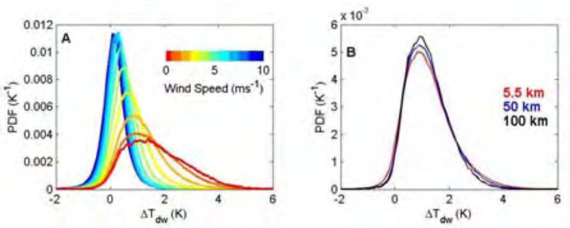

Figure 1. Figure 1. A) PDF of the SEVIRI day (14:00 LMT) minus night SST difference, ΔTdw, for different wind speeds. B) PDF of ΔTdw for wind speeds <3 ms-1 at different spatial resolutions. As averaging increases, the probability of diurnal events <2 K increases while the probability of larger diurnal events decreases.

4. MULTI-SENSOR SATELLITE RETREIVALS OF DIURNAL WARMING

The SEVIRI day-night differences were examined for spatially coherent large positive differences over 5 K. 595 events were found (Figure 2). Low wind speeds occur more frequently where large diurnal warm events were also found, except in the Tropics where two regions off Africa show frequent low winds, but no large events. Near Angola, cloud cover prevented retrieval of IR SSTs during low wind events. The West African area is known to have aerosol biasing (which cools the IR SSTs) and this may have masked and reduced large warming events. Images of the daily diurnal events are available as auxiliary materials . Once these large events were identified in the SEVIRI data, verification using other sensors was completed. The IR and MW SST retrievals are independent and have different error sources. The primary errors in IR SST retrievals are due to undetected clouds, atmospheric aerosols, and anomalous temperature and

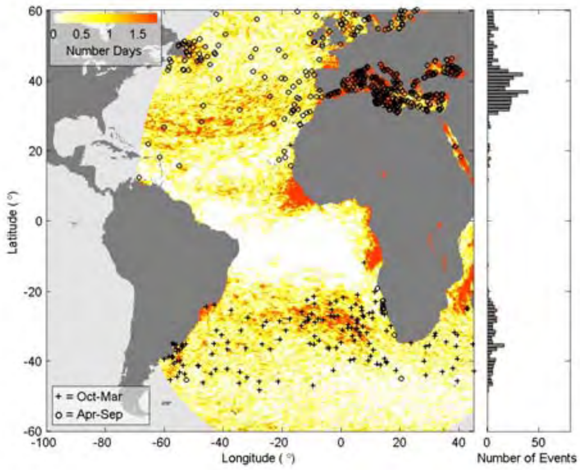

Figure 2. Location of diurnal events over 5 K (black '+' and 'o'). Events generally occur in the boreal(austral) summer. The background color shows the days in a year (on average) that wind speed was < 1 ms-1 at 14:00 LMT.

water vapor distributions in the atmosphere. The primary errors in MW SSTs are due to calibration errors, high surface wind speeds, near-land side lobe contamination, undetected rain, and satellite attitude errors. Since the sources of errors are independent, coincident observations of similar phenomena lend credibility to the accuracy of the observed behavior. Here MW and IR SSTs are used to examine large diurnal events in the Atlantic Ocean with examples shown in Figures 3. MODIS and SEVIRI are less complete than AMSR-E due to cloud cover. There are coherent patterns of missing data, most pronounced in the AMSR-E fields, due to gaps between measurements from adjacent orbits. MODIS has a wider swath than AMSR-E and therefore, the gaps between swaths are less apparent in the MODIS SST fields.

5. CONCLUSION

Understanding of diurnal warming at the ocean surface is important for improving our estimates of air-sea heat and gas fluxes, optimal assimilation of satellite SST data into analysis systems for weather, ocean state and climate forecasts. Measurements from three satellites show large diurnal heating events extending over large areas. The large diurnal heating signals were found where low winds and high surface insolation occurred in concert. The results presented here indicate a strong dependence of the measured diurnal peak on sensor type, likely due to the sensor's spatial resolution; the probability of measuring diurnal events over 2 K decreases with decreasing spatial resolution. This is the first study to directly compare measurements of diurnal warming events detected using the three main types of spacecraft sensors used to derive SST: infrared and microwave radiometers from polar-orbiters, and an infrared radiometer in geosynchronous orbit. The large

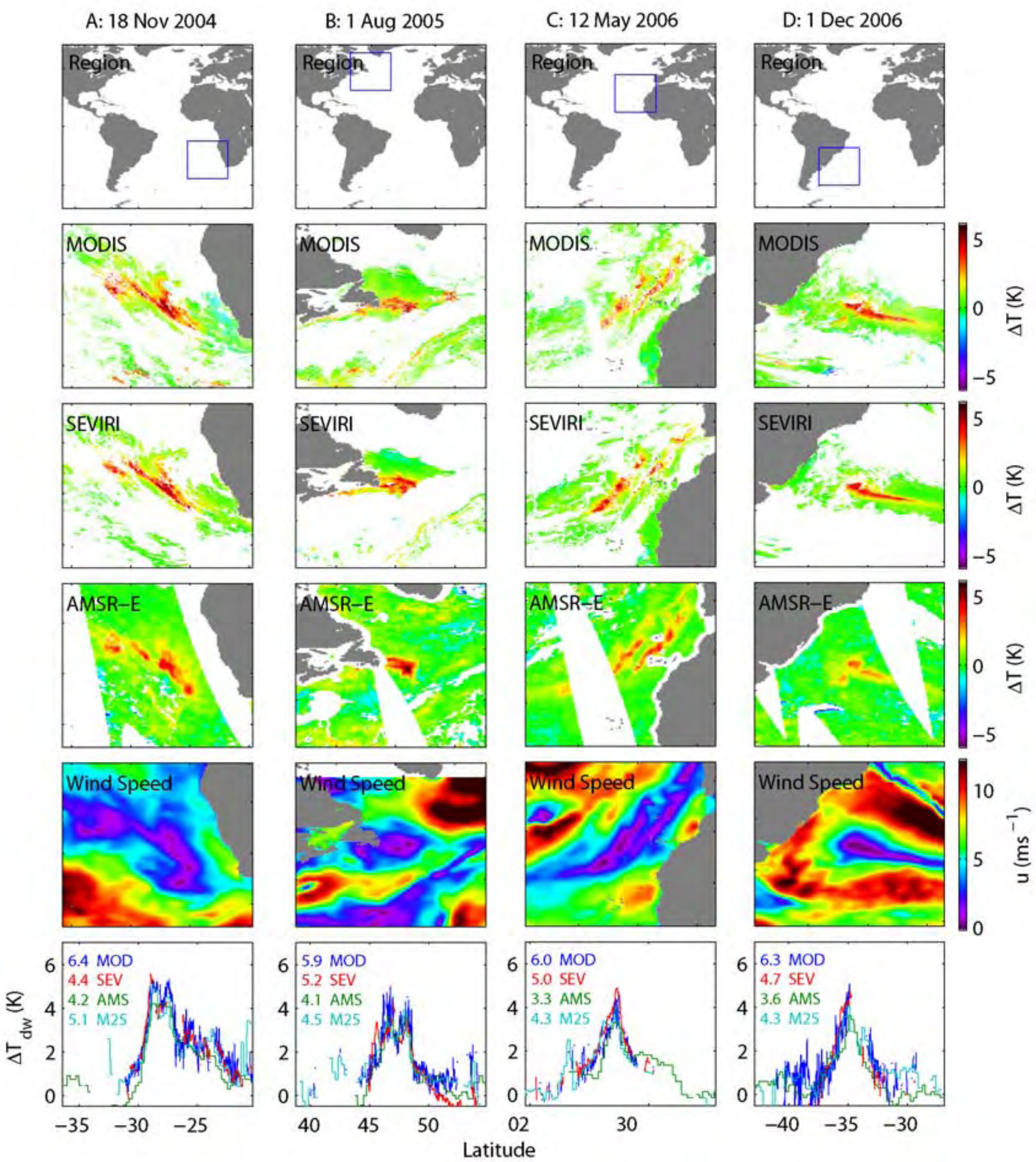

Figure 3. Figure 3. Multiple satellite measurement of diurnal warming events. The panels (from top to bottom) indicate the location of the areas for which the SSTs are shown, MODIS ΔTdw at 2 km spatial resolution, SEVIRI ΔTdw at 5.5 km, AMSR-E ΔTdw at 25 km, CCMP wind speeds, and the meridional cross-section of SSTs from each sensor through the center of the area, with the numbers giving the peak amplitudes, colored by the data source: MOD is MODIS; SEV is SEVIRI; AMS is AMSR-E, and M25 is MODIS cloud-free data averaged to a 25 km spatial resolution.

diurnal events are independently verified by these different sensors. Although, diurnal warming is frequently present in the Tropics, the observed large diurnal events (greater than 5 K) occurred in extra-tropical regions. These large diurnal events present a new challenge to understanding and modeling air-sea heat and gas fluxes accurately throughout the day.

6. REFERENCES

1. Gentemann, C. L. and P. J. Minnett (2008), Radiometric measurements of ocean surface thermal variability, Journal of Geophysical Research, 113, C08017, doi:10.1029/2007JC004540.

2. Merchant, C. J., M. J. Filipiak, P. Le Borgne, H. Roquet, E. Autret, J.-F. Piollé and S. Lavender (2008), Diurnal warm-layer events in the western Mediterranean and European shelf seas, Geophysical Research Letters, 35, L04601, doi:10.1029/2007GL033071.

3. Minnett, P. J. (2003), Radiometric measurements of the sea-surface skin temperature - the competing roles of the diurnal thermocline and the cool skin, International Journal of Remote Sensing, 24, 5033-5047.

4. Sverdrup, H. U., M. W. Johnson and R. H. Fleming, The Oceans: Their Physics, Chemistry, and General Biology, Prentice-Hall, Englewood Cliff, NJ, 1942.

ENHANCING SHIP OF OPPORTUNITY SEA SURFACE TEMPERATURE OBSERVATIONS IN THE AUSTRALIAN REGION

Helen Beggs(1), Ruslan Verein(1), Hiski Kippo(2), Mark Underwood(3), Ian Barton(3), Craig Steinberg(4), Eric Schulz(1), Ross Hibbins(5), Alan Thomas(5) and Graeme Ball(5)

(1) Centre for Australian Weather and Climate Research, Bureau of Meteorology, Melbourne, Australia,
Email: h.beggs@bom.gov.au,
(2) CSIRO Marine and Atmospheric Research, Perth, Australia,
(3) CSIRO Marine and Atmospheric Research, Hobart, Australia,
(4) Australian Institute of Marine Science, Townsville, Australia,
(5) Bureau of Meteorology, Melbourne, Australia.

1. INTRODUCTION

Remotely sensed sea surface temperature (SST) data are important inputs to ocean, numerical weather prediction, seasonal and climate models. In order to improve calibration and validation of satellite SST in the Australian region, there is a need for high quality in situ SST observations with greater timeliness, spatial and temporal coverage than is currently available. Regions particularly lacking in moored or drifting buoy observations are the Western Pacific Tropical Warm Pool region (Indonesia), close to the Australian coast (including Bass Strait) and the Southern Ocean (e.g. Figure 1).

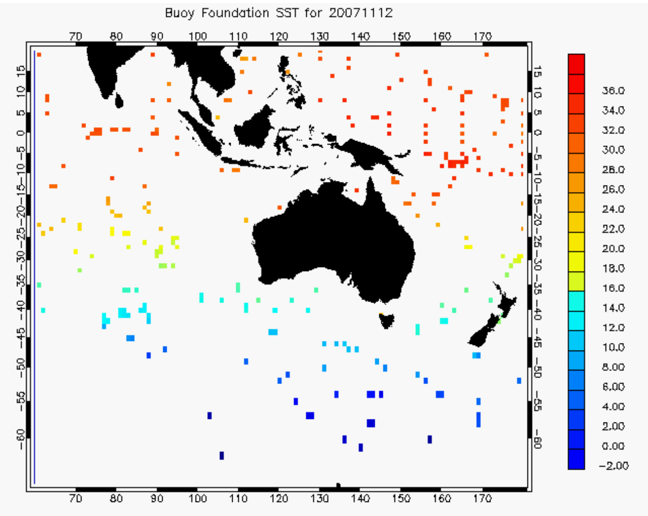

Figure 1. Drifting and moored buoy SST observations from the GTS for 12 November 2007 over the region 20°N to 65°S, 60°E to 180°E.

Typically, SST observations from the ships of opportunity program (SOOP) in the Australian region are either of uncertain accuracy or difficult to access in a timely manner, and have therefore not been used for near real-time validation of satellite SST observations. From 2008, the Integrated Marine Observing System (IMOS: http://www.imos.org.au) Project has enabled accurate, quality controlled, SST data to be supplied in near real-time (within 24 hours) from SOOPs and research vessels in the Australian region.

2. DATA STREAMS

There are eight vessels carrying automatic weather stations (AWS) that participate in the Australian Volunteer Observing Fleet (AVOF) program. Their routes include the Southern Ocean, coastal Australia, Bass Strait, North Pacific Ocean and the Tasman Sea. As part of the IMOS SOOP SST Sensors Sub-Facility, operated by the Bureau of Meteorology (Bureau), these AVOF vessels will be instrumented with hull-mounted temperature sensors (Sea Bird SBE 48), supplying high-quality bulk SST observations every one to three hours. There are also three passenger ferries taking SST measurements for CSIRO Marine and Atmospheric Research (Rottnest Island Ferry), the Australian Institute of Marine Science (AIMS) (Whitsunday Island to Hook Reef and Gladstone to Heron Island ferries in the Great Barrier Reef). In addition, there are near real-time SST data streams available from two Australian research vessels (RV Southern Surveyor and SRV Aurora Australis). In total, thirteen vessels by 2010 will contribute near real-time data to IMOS (see Table 1). All SST data are quality assured (see Section 3), placed in real-time on the Global Telecommunications System (GTS) and fed into the Bureau's near real-time satellite SST data validation system and operational regional and global SST analyses. The QC'd SST data are also available in netCDF SAMOS format (Rolph and Smith, 2005) via the IMOS data portal (http://bluenetdev.its.utas.edu.au). Figure 2 shows the tracks of ships providing IMOS SST data from 4 Feb 2008 to 29 April 2009 to the IMOS data portal and the GTS.

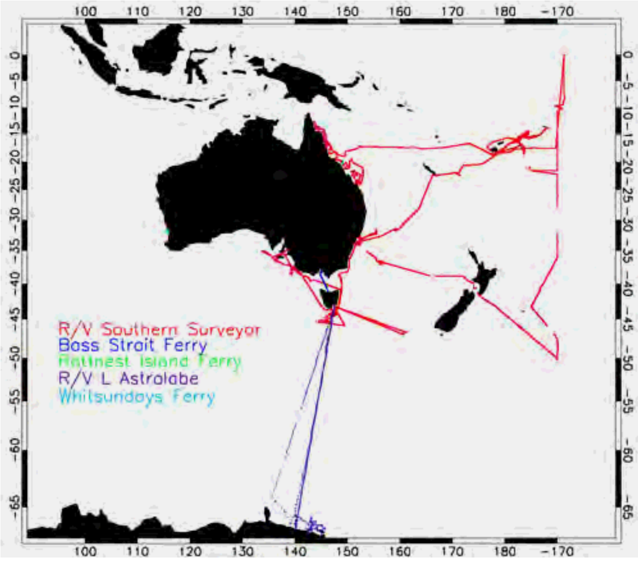

Figure 2. Locations of IMOS ship SST observations to 29 April 2009 from RV Southern Surveyor (red), Spirit of Tasmania II Ferry (indigo), MV SeaFlyte (Rottnest Island Ferry) (green), RV L'Astrolabe (purple) and MV Fantasea (Whitsundays Ferry) (Aqua).

3. QUALITY CONTROL AND VALIDATION

The IMOS ship SST quality control (QC) procedure is a fully automated process, and is based on the system developed by the Center for Ocean-Atmospheric Prediction Studies (COAPS), Florida State University, for the Shipboard Automated Meteorological and Oceanographic System Initiative (SAMOS: http://samos.coaps.fsu.edu), with small differences due to varying IMOS/Bureau requirements. The QC system flags data that fail to pass the following QC tests, in order of application:

- (i) Verify the existence of time, latitude and longitude data for every record;
- (ii) Flag data that are not within physically possible bounds;
- (iii) Flag non-sequential and/or duplicate times;
- (iv) Flag positions where the vessel is over land;
- (v) Flag vessel speeds that are unrealistic;
- (vi) Flag data that exceeds 3°C above/below the Bureau's most recent operational SST analysis (blended from satellite and in situ SST data either one or two days old).

Once any datum's flag is changed, it will not be altered further by any subsequent test.

In order to assess the accuracy of the largest of the initial IMOS ship SST datasets, the QC'd SBE 3 SST observations from the RV Southern Surveyor were compared against nighttime SST observations from the highly accurate Advanced Along Track Scanning Radiometer (AATSR) on the EnviSat polar-orbiting satellite for the period 1 March to 31 August 2008 (Table 2). For the study, the 10 arcmin averaged, Meteo Product skin (~10 µm depth) SST observations from AATSR were converted to subskin SST using the Donlon et al. (2002) empirical cool skin correction algorithms and the Bureau's operational, 0.375° resolution, Numerical Weather Prediction model surface wind fields. The same night-time, AATSR subskin SST observations were compared with collocated, night-time, subskin SST observations from drifting and moored buoys over a similar region and six month period. The results of the three-way comparison indicated that the RV Southern Surveyor SBE 3 SST observations were an average 0.1°C warmer than buoy SSTs, and the SBE 3 SSTs exhibited 0.1°C lower standard deviation error than buoys when compared with AATSR SSTs. A similar study of the SBE 48 SST from MV Spirit of Tasmania II showed that over the period 10 December 2008 to 29 April 2009 the ship SST measurements were an average 0.14°C warmer than the AATSR subskin SSTs with a standard deviation of 0.30°C. The AATSR subskin SSTs over the same period were 0.02°C cooler than night-time buoy SST with a standard deviation of 0.38°C. Both the RV Southern Surveyor and MV Spirit of Tasmania II SST data streams should therefore prove very useful for validating/calibrating satellite SST.

4. HULL-CONTACT SENSOR TESTS

Two SBE 48 hull-contact temperature sensors have been tested in the Bureau's sensor calibration lab and one installed on the RV Southern Surveyor (Figure 3) for comparison tests with the SBE 3 calibrated thermistor installed in the thermosalinograph water intake. The SBE 48 was attached using magnets to the exterior steel hull at a depth of approximately 3 m below the water line and approximately 20 m aft of the bow. The SBE 48 was located approximately 3.5 m to port of the SBE 3 sensor and approximately 2 m higher up on the hull plating. Thermal contact between the SBE 48 heat sink and the ship's hull was achieved by the use of contact grease with a high thermal conductivity. A two dimensional thermal analysis of the installation by CSIRO indicated that the ratio of the face area of the SBE 48 thermal sink in relation to the thickness of the hull affects the conduction of heat to the SBE 48 temperature sensor from the adjacent hull region. It was proposed that the effect of the hull thickness (in this case 0.025 m) can be reduced by placing insulating material around the SBE 48 housing extending to a distance from the sensor element of at least 10 times the hull thickness.

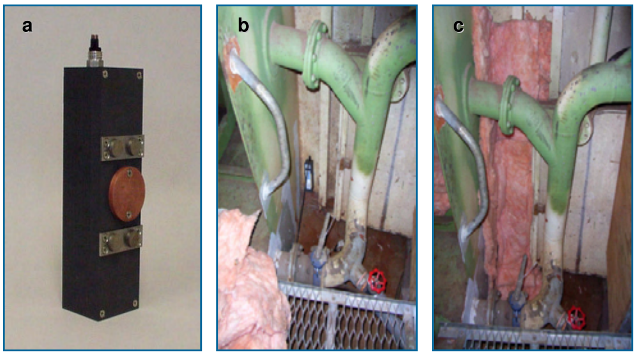

Figure 3. The Sea Bird SBE 48 Hull Contact Temperature Sensor (a) showing the thermal sink (red disk) and four magnets, (b) installed against the exterior hull of the RV Southern Surveyor next to the grey water tank, and (c) covered with "Pink Batt" ceiling insulation.

The SBE 48 sensor housing and surrounding hull was insulated on 27 July 2008 at 0300 UTC using three layers of Bradford "Pink Batt" R2.5 ceiling insulation covering the sensor and surrounding hull to an approximate thickness of 270 mm and a minimum distance of 0.25 m from the sensor (Figure 3(c)). The results presented here are for the cruise commencing 24 July 2008 at 16.6°S, 145.8°E and finishing on 11 August 2008 at 23.8°S, 151.6°E. Prior to insulation (for the period 24 to 27 July 2008), the SBE 48 temperature was on average 0.28°C warmer than the SBE 3 temperature, with a standard deviation of 0.14°C. After insulation (for the period 27 July to 11 August 2008), the average offset was 0.19°C with a standard deviation of 0.12°C. The majority of the error occurred during periods when the water mass exhibited sharp thermal gradients. In water masses with low thermal gradients the average offset was approximately 0.15°C.

An example of the sensor comparison after insulation is presented in Figure 4 for the transect between 2 August 2008 00 UTC, 18.4°S, 147.8°E and 6 August 2008 00 UTC, 21.8°S, 152.9°E. The SBE 48 temperatures exhibited less short term fluctuation compared to the thermosalinograph water intake SBE 3 temperatures, as expected from measurements of SST integrated over a ship's hull.

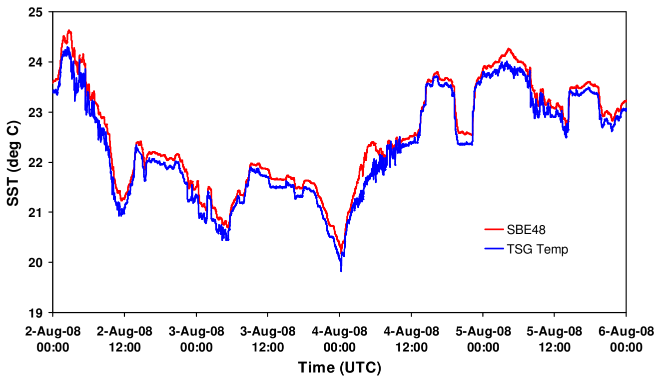

Figure 4. Example of the RV Southern Surveyor SST sensor comparison results after insulation of the hull-contact sensor. The SBE 48 hull-contact temperatures are shown in red and the SBE 3 temperatures in blue.

Although the RV Southern Surveyor has a particularly thick steel hull of 25 mm, and the positioning of the SBE 48 surrounded by black water pipes and hull ribs was far from ideal, this study indicates that the SBE 48 is capable of providing ship SST observations of sufficiently accurate for satellite SST validation and possible calibration. If the SBE 48 has good thermal contact with the hull, is positioned well below the water line away from on-ship heat sources, and the sensor and surrounding hull is sufficiently insulated from the interior ship's atmosphere, the hull-contact sensor should provide a bulk sea surface temperature measurement of comparable accuracy to thermosalinograph water intake temperatures, albeit possibly biased slightly warm. Further comparison tests are planned for the SBE 48 sensor on vessels with thinner hulls and wider spaced hull ribs.

5. CONCLUSIONS

During 2008, as part of the IMOS project, new streams of high quality, near real-time, SST observations from four vessels in the Australian region have become available on the GTS and the IMOS data portal. During 2009 and 2010, new data streams from a further nine Australian vessels will be added to the project.

Initial assessment of data from two of the temperature sensors (SBE 3 on RV Southern Surveyor and SBE 48 on MV Spirit of Tasmania II) using a three-way comparison between ship SST, AATSR ATS_MET_2P SST and drifting and moored buoy SST indicates comparable or lower errors than those available from drifting buoys. Although further tests are required, it would appear that the new IMOS ship SST data streams are suitable for calibration and/or validation of satellite SST observations, thereby considerably increasing the spatial and temporal coverage of available validation data.

6. ACKNOWLEDGMENTS

The authors would like to thank Werenfrid Wimmer and Margaret Yelland (National Oceanographic Centre, Southampton) and Bill Emery (University of Colorado) for advice on hull-contact sensors; Shaun Smith (Florida State University) for documentation and software; and Martin Buggellen, Peter Kernabone, Stephen Thomas (CSIRO), Drew Mills (CSIRO) and Michael Mahoney (AIMS) for sensor installations. In particular, the authors acknowledge the support of the owners and crews of the Australian ships of opportunity, who make such an important contribution to operational marine meteorology, oceanography and research. The European Space Agency supplied the AATSR Meteo Product (ATS_MET_2P) files used in this study.

The work was supported by the Integrated Marine Observing System (IMOS) - an initiative of the Australian Government being conducted as part of the National Collaborative Research Infrastructure Strategy.

7. REFERENCES

Rolph, J. J. and S. R. Smith, 2005: SAMOS netCDF Code Manual for Quality Controlled Surface Meteorological Data (http://samos.coaps.fsu.edu/html/docs/samos_netcdf_manual.pdf)

Donlon, C. J., P. Minnett, C. Gentemann, T. J. Nightingale, I. J. Barton, B. Ward and J. Murray, 2002: Towards improved validation of satellite sea surface skin temperature measurements for Climate Research, *J. Climate*, **15**, No. 4, 353-369.

Vessel	Callsign	Data Start	SST Sensor	Sensor Depth (m)	Data Interval (minutes)	Data Uploaded to GTS
RV Southern Surveyor	VLHJ	4 Feb 2008	SBE 3	5.5	1 (averaged)	6 hourly (Trackobs)
MV SeaFlyte (Rottnest Is Ferry)	VHW5167	23 Sep 2008	SBE 38	0.1 - 0.5	1 (averaged)	daily (Trackobs)
RV L'Astrolabe	FHZI	30 Dec 2008	SBE 38	4	60 (instantaneous)	hourly
RSV Aurora Australis	VNAA		-	5	1 (averaged)	TBD (Trackobs)
MV Spirit of Tasmania II	VNSZ	10 Dec 2008	SBE 48	1.5 - 2	60 (instantaneous)	hourly
MV Reef Voyager (Heron Is Ferry)	-		TSG	-	TBD	TBD (Trackobs)
MV Fantasea (Whitsundays Ferry)	VJQ7467		EI4000.4ZL (radiometer)	0	1 (averaged)	TBD
			AD590	1.4	1 (instantaneous)	Daily (Trackobs)
MV Stadacona	C6FS9		SBE 48		180 (instantaneous)	3 hourly
MV Portland	VNAH		SBE 48		180 (instantaneous)	3 hourly
MV Pacific Sun	MNPJ3		SBE 48		180 (instantaneous)	3 hourly
MV Highland Chief	VROB		SBE 48		180 (instantaneous)	3 hourly
MV Iron Yandi	VNVR		SBE 48		180 (instantaneous)	3 hourly
MV ANL Yarunga	V2BJ5		SBE 48		180 (instantaneous)	3 hourly

Table 1. Details of vessels either currently providing or planned to supply QC'd SST data streams to IMOS and the GTS.

Observations collocated with nighttime AATSR SSTsubskin data	Matchup Period (hours)	Mean (°C)	St. Dev. (°C)	Number Matchups
Southern Surveyor SST	1	-0.19	0.15	519
Southern Surveyor SST	3	-0.28	0.19	1651
Southern Surveyor SST	24	-0.19	0.22	7739
Buoy SST	24	-0.08	0.32	2214

Table 2. Mean and standard deviation of satellite observations of nighttime AATSR (ATS_MET_2P) subskin SST minus collocated observations of (a) SST (at ~5.5 m depth) from the RV Southern Surveyor and (b) nighttime subskin SST observations from drifting and moored buoys over the region 60°E – 170°W, 20°N - 80°S for the period 1 March to 31 August 2008. Observations are considered "matched" if measured within same UTC calendar day and matchup period and centres of observations are separated by no more than half the resolution of the AATSR SST observation (1/12° latitude, 1/12° longitude).